ISSN 0915-6348

NATIONAL INSTITUTE FOR FUSION SCIENCE

Proceedings of 2nd International Workshop on Tritium Effects in Plasma Facing Components at Nagoya University, Symposion Hall, May 19-20, 1994

K. Morita, N. Noda (Ed.)

(Received - Aug. 11, 1994)

NIFS-PROC-19 Aug. 1994

RESEARCH REPORT
NIFS-PROC Series

NAGOYA, JAPAN

Proceedings

of

2nd International Workshop on Tritium Effects in Plasma Facing Components

Nagoya University, Symposion Hall

May 19 - 20, 1994

Edited by

K. Morita, Nagoya University

and

N. Noda, National Institute for Fusion Science

National Institute for Fusion Science, Nagoya

Keywords : tritium effects, plasma facing components
recycling, re-emission, inventory,
permeation, diffusion, trapping, detrapping,
recombination

TABLE OF CONTENTS

2nd International Workshop on Tritium Effects in Plasma Facing Components

Report on the Workshop held before the 11th PSI Conference
Nagoya, Japan
19-20 May, 1994

R. A. Causey
Advanced Materials Research Department, 8347
Sandia National Laboratories
Livermore, California
United States of America

K. Morita
Department of Crystalline Materials Science
School of Engineering
Nagoya University
Nagoya, Japan

The 2nd International Workshop on Tritium Effects in Plasma Facing Components was held at Nagoya University in Nagoya, Japan on 19 and 20 May, 1994. Reflecting the growing importance of tritium effects in fusion reactor materials, the number of participants increased from about 30 for the first workshop in Livermore, California to 46 for the present workshop. A total of 30 talks by participants from 9 different countries made this a very interesting workshop. The workshop was hosted by Professor K. Morita of Nagoya University and Dr. N. Noda of the National Institute for Fusion Science. Organization of the Workshop was assisted by Dr. R. Causey, Dr. E. Vietzke, Dr. C. Wu, and Dr. M. Yamawaki.

Approximately 1/3 of the talks discussed the migration and retention of tritium in graphite and other forms of carbon. This topic has more or less come to maturity with general agreement on most of the different aspects of tritium reactions with the carbon. At lower temperatures(<800K), a tritium plasma interacts with graphite by forming a saturated layer on the geometrical surface, by forming a codeposited layer of sputtered carbon and tritium in areas of net deposition, and by allowing tritium diffusion along pore surfaces fairly deep into the graphite. At higher temperatures(>800K), the principal reaction of tritium with carbon is intergranular diffusion with high energy trapping. If graphite is used in ITER, the main sources of tritium inventory will be codeposition of tritium with carbon in the cool areas surrounding the divertor and trapping at high energy sites created by neutron irradiation.

Because beryllium is now the reference plasma facing material for ITER, several presentations on the reaction of tritium with beryllium were presented. For beryllium the consistent theme is inconsistency. There is no agreement on the diffusivity, solubility, trapping, or surface recombination rate coefficient for tritium in beryllium. The oxide layer appears to be the principal reason for the differences in the data generated for the tritium interaction. It was agreed at the workshop that tritium retention in the ITER beryllium will not be as bad as it would have been for graphite, but the inventory may still reach the kilogram level.

There were also several presentations on tritium permeation through metals other than beryllium. These presentations varied from tritium superpermeability to tritium migration in thermal and electrical gradients.

The first talk of the workshop was presented by D. Mueller of the TFTR Group. He presented the most recent results of the DT operation in TFTR. After a few small glitches in the beginning, the use of tritium in this tokamak has gone very smoothly. Results show enhanced magnetic confinement of the tritium(greater than deuterium which is greater than protium). While the inventory of tritium in TFTR is steadily increasing with time, the invessel retention remains significantly below the imposed 1 gram limit. New records for fusion energy in controlled devices are being set almost on a weekly basis.

The workshop closed with a decision to definitely hold a 3rd workshop somewhere in Europe immediately before or after the 12th PSI. Preparing for DT operation in ITER will continue to make this an important workshop for the next several years.

Session 1

Results of TFTR D-T Experiments*

D. Mueller
and the TFTR Group
Princeton Plasma Physics Laboratory

The deuterium-tritium (D-T) experimental program on the Tokamak Fusion Test Reactor (TFTR) has begun. The initial phase of this program has achieved the goals of 1) demonstration of greater than 5 MW of fusion power, 2) measurement of escaping alpha particles, 3) testing of diagnostics for confined alpha particles and 4) the measurement of tritium transport. The total injected fraction of tritium used in the neutral beam injectors was increased from less than 2 % to 100 % for a series of discharges during this initial phase. The highest fusion power achieved in this phase was 6.2 MW. Comparisons of the D-T discharges with similar D-D shots indicate that plasmas with significant tritium content exhibit higher plasma stored energy (W_{tot}), ion and electron temperatures ($T_i(0)$ and $T_e(0)$) and energy confinement time (τ_E) than the D-D plasmas. With 30 MW of neutral beam heating power (10 MW D and 20 MW T), the W_{tot} rose from 4.2 to 4.7 MJ, $T_i(0)$: 27 $\rightarrow$ 37 keV, $T_e(0)$: 9.5$\rightarrow$10.3 keV and τ_E: 0.15 $\rightarrow$ 0.18 s. Measurements indicate that the tritium recycling at the plasma edge is quite low so that the tritium concentration in the plasma is lower than the tritium fraction of the neutral beams used to fuel the plasmas.

No instability behavior (eg. TAE modes or kinetic ballooning modes) which could be attributed to the presence of alpha particles was observed in the D-T discharges. The normalized Beta, β_N, of the D-T discharges was higher than that in the comparison D-D plasmas. The alpha particles appear to be well-confined and alpha-particle-loss measurements are consistent with no anomalous particle loss.

Detailed analysis is underway to ascertain the relative importance of the power deposition profile, tritium transport, tritium and deuterium recycling and alpha particle heating on the changes observed for the D-T plasmas. Preliminary analysis indicates an isotopic scaling in the energy confinement time.

The vacuum-vessel tritium decontamination of TFTR will be accomplished by He-O glow discharge cleaning. It is expected a few months of He-O glow will be sufficient to remove >10 μm of graphite from the internal hardware. Methods to measure the in-vessel tritium inventory are under investigation and are expected to be valuable to determine the end-point of He-O glow.

*Work Supported by U.S.D.O.E. Contract No. DE-AC02-76-CHO-3073

RESULTS OF TFTR D-T EXPERIMENTS*

by

D. Mueller
and the TFTR Group

Princeton University
Plasma Physics Laboratory

Presented at
2nd INTERNATIONAL WORKSHOP ON
TRITIUM EFFECTS IN PLASMA FACING
COMPONENTS

Nagoya University, Japan

May 19-20, 1994

*Work sponsored by U.S.D.O.E. Contract No.
DE-AC02-76-CH0-3073

TFTR Collaborations & Industrial Participants

TFTR

UNIVERSITIES
- Colorado School of Mines, Golden, CO
- Columbia University, New York, NY
- Cornell University, Ithaca, NY
- Courant Institute, New York University, New York, NY
- Georgia Institute of Technology, Atlanta, GA
- Massachusetts Institute of Technology, Cambridge, MA
- University of California, Los Angeles, CA
- University of California, San Diego, CA
- University of California, Irvine, CA
- University of Illinois, Urbana, IL
- University of Tokyo, Japan
- University of Wisconsin, Madison, WI

INDUSTRIES
- Burns and Roe Company, Oradell, NJ
- Canadian Fusion Fuels Technology Project, Canada
- Ebasco Services, Inc., New York, NY
- Fusion Physics and Technology, Inc., Torrance, CA
- General Physics Corporation, Columbia, MD
- Grumman Aerospace/Energy Systems Program, Bethpage, NY
- General Atomics, San Diego, CA
- Lodestar, Boulder, CO
- Radiation Science, Inc., Belmont, MA

LABORATORIES
- Environmental Measurement Laboratory, New York, NY
- Idaho National Engineering Laboratory, Idaho Falls, ID
- I.V. Kurchatov Institute of Atomic Energy, Russia
- Ioffe Physical-Technical Institute, Russia
- Japan Atomic Energy Research Institute, Japan
- JET Joint Undertaking, United Kingdom
- Lawrence Berkeley Laboratory, Berkeley, CA
- Lawrence Livermore National Laboratory, Livermore, CA
- Los Alamos National Laboratory, Los Alamos, NM
- Oak Ridge National Laboratory, Oak Ridge, TN
- Sandia National Laboratory, Albuquerque, NM and Livermore, CA
- Savannah River Plant, Aiken, SC

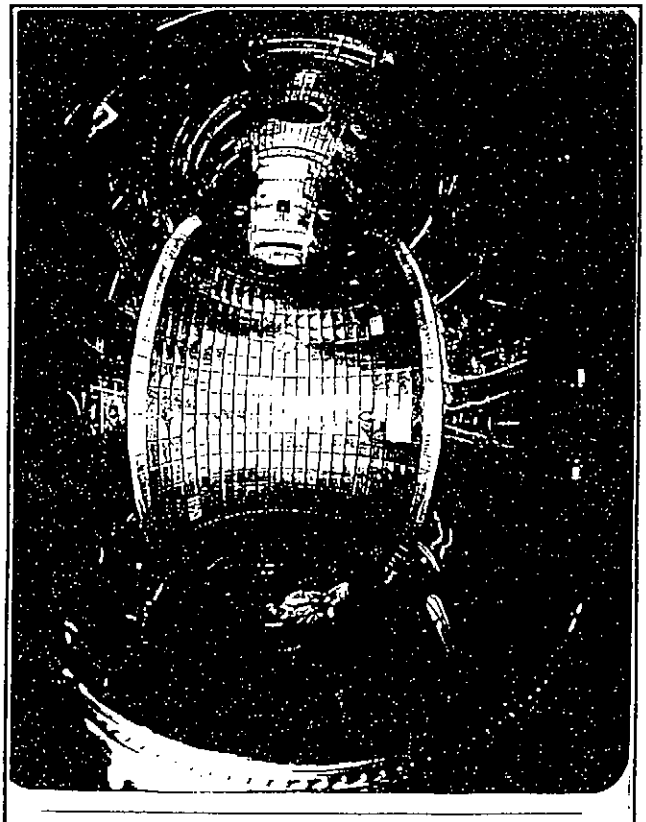

Why do D-T Plasmas on TFTR?

Energy Demonstration

- First clear demonstration of substantial amount of Magnetic Fusion Power (5 - 10 MW)
  - Phase I Goal: 5 MW
  - Phase 2 Goal: 10 MW

Potential Effects of Plasma

- Different mass for main plasma - isotope effects
- α-particles can be ≈ 10% of the central electron power balance i.e. alpha electron heating
- α-particles and or Tritium can influence plasma stability, e.g. JET X-event, or TAE modes

Opportunity for Transport Measurements

- Tritium Transport - Trace Tritium
- Energetic Alpha Particle Transport

Fusion Power of 6.2MW has been achieved on TFTR

TFTR

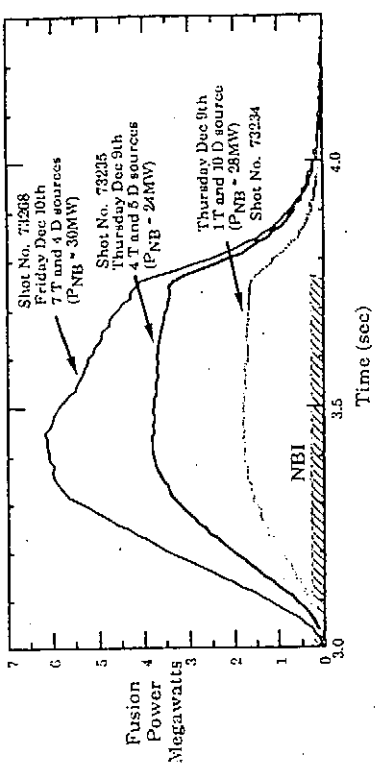

- We exceeded our December milestone of 5 MW of Fusion power

The TFTR plasmas are reproducible and reliable for comparison purposes

TFTR

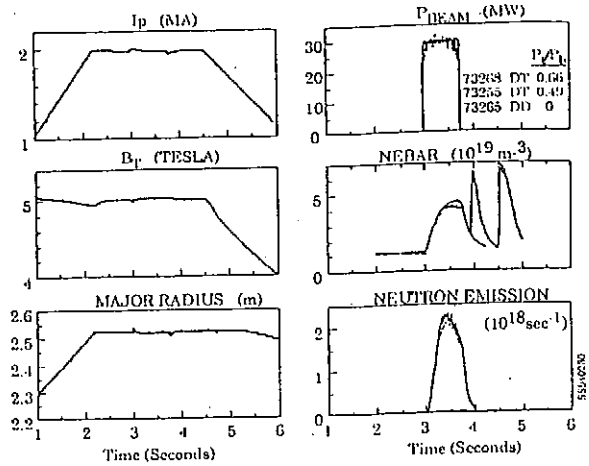

- A total of 55 plasmas of this type were obtained including 7 DT plasmas, 6 trace tritium plasmas, and 42 deuterium comparison plasmas.

Plasma Stored Energy Increased during D-T Operation

TFTR

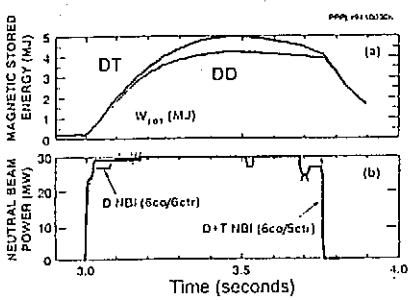

- τ_E increased from 150ms to 180ms
- $n_e(0)\, T_i(0)\, \tau_E$ increased from 3.4×10^{20} to 5.0×10^{20} m$^{-3} \cdot$ s $\cdot$ keV
- $n_i(0)\, T_i(0)\, \tau_E$ increased from 2.6×10^{20} to 3.8×10^{20} m$^{-3} \cdot$ s $\cdot$ keV

Electron and Ion Temperature Increased during D-T Operation

TFTR

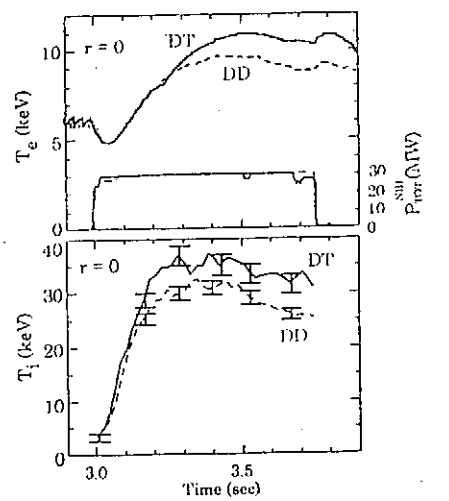

- Ion Temperature change on τ_E time-scale.
- Electron temperature change on alpha slowing down time-scale.
- Is this alpha heating or isotope scaling?

Ion Temperature Profile Measurements

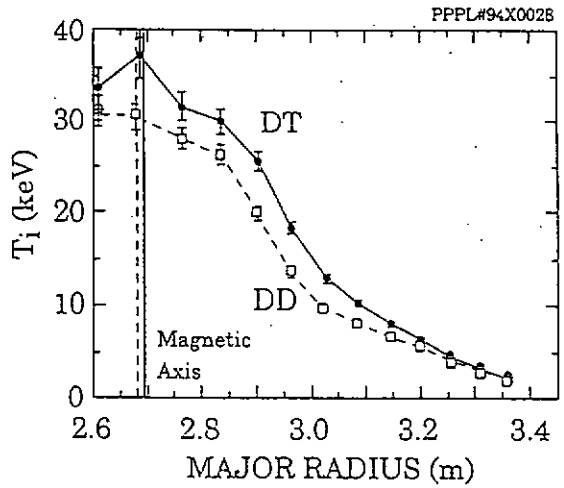

- χ_i decreases by up to a factor of 1.4

Change in Electron Temperature due to α-heating and Isotope Effects

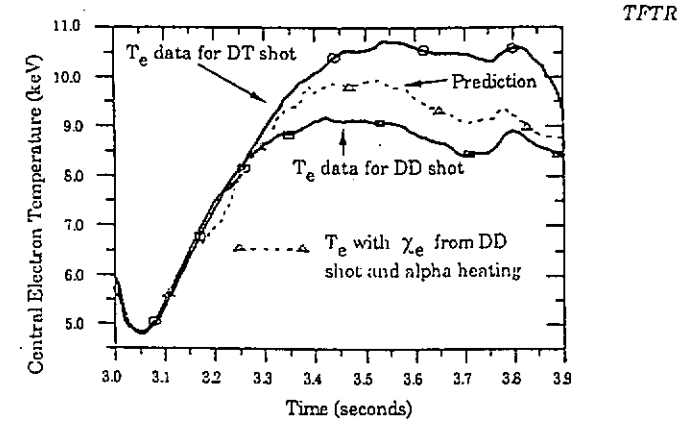

- Using the thermal electron diffusivity from the DD discharge, about half the increase in $T_e(0)$ can be attributed to α-heating.

Change in Electron Temperature due to α-heating and Isotope Effects

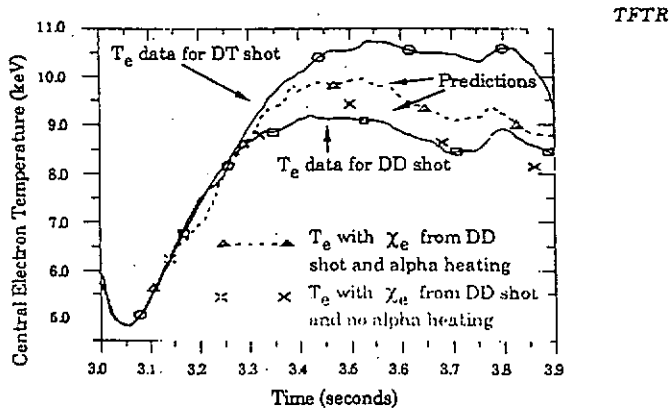

- Using the thermal electron diffusivity from the DD discharge, about half the increase in $T_e(0)$ can be attributed to α-heating.

Energy Confinement Time Improves with average Ion Mass in DT Plasmas

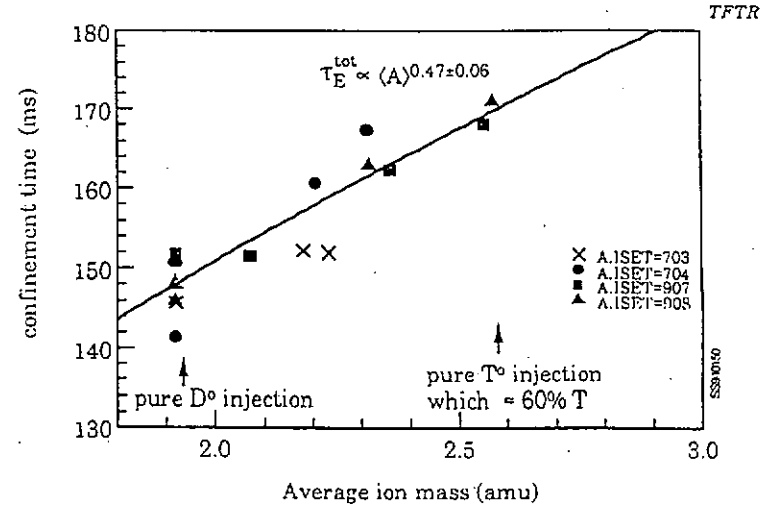

Loss of fast ions were significant in our DD experiments

TFTR

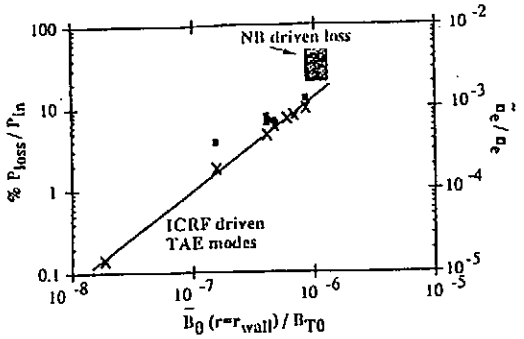

- TAE Instabilities Could Cause Loss of Self-Heating or Damage to the First Wall Components
- Will the alpha particles drive TAE modes unstable during DT operation?

DT versus DD Signals in 90º Detector

TFTR

D + D = He^3 (0.8 MeV) + n (2.5 MeV)

D + D = p (3 MeV) + T (1 MeV)

D + T = n (14 MeV) + α (3.5 MeV)

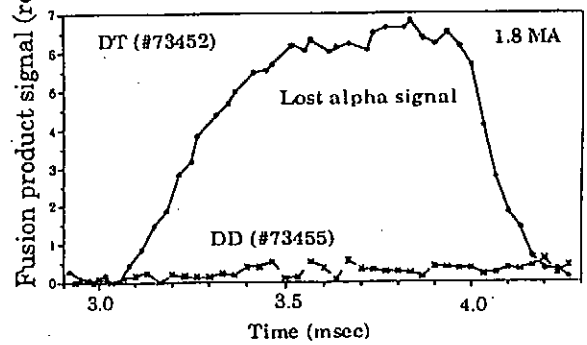

- Increase in fusion product signal for DT plasmas is due to α-particles
- α-particle signal is = correct on the basis of the detector responce

Escaping alpha flux is similar in magnitude to classical first orbit losses

TFTR

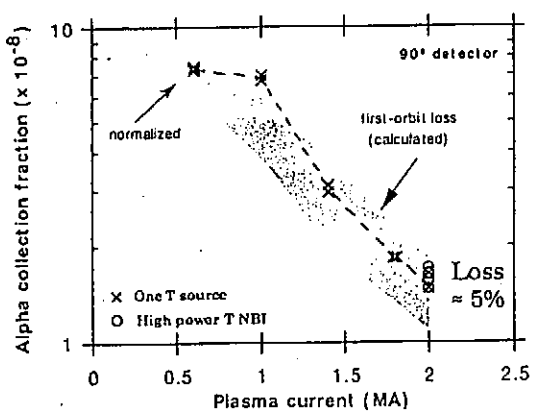

- Normalized to 0.6 MA since at low Ip, all trapped alphas escape
- Absolute calibration of detector in good agreement with model

Alpha loss does not increase with Fusion Power

TFTR

S. Zweben
D. Darrow

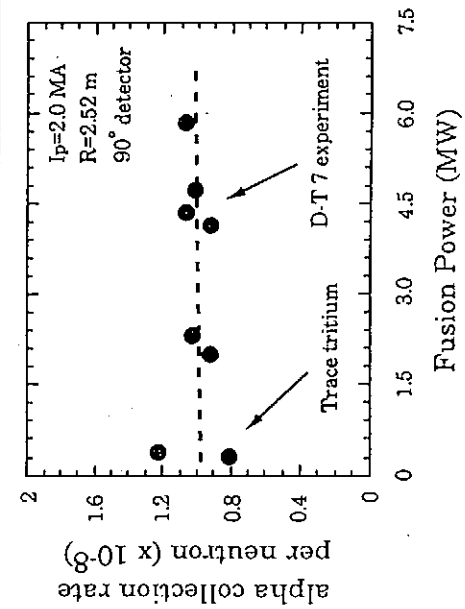

Influx of neutrals from the limiter affects fusion power production

TFTR

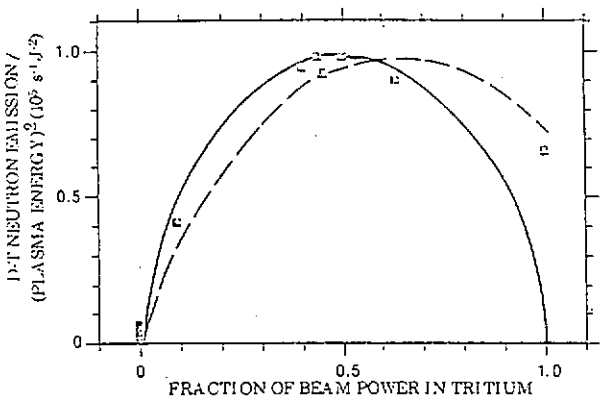

- Spectroscopic measurements show that influx of tritium neutrals from wall < 7% of the total hydrogenic influx

TRITIUM RECYCLING

- Tritium Balmer-alpha (Tα) emission measurements from TFTR plasmas were made, using a Fabry-Perot interferometer by C.H. Skinner et al.
- The Tα emission is near the Dα line (deuterium-alpha) and is blended with it.
- The Tα emission is a measure of the fueling of the plasma by tritium accumulated in the TFTR limiter.
- The Ta first became visible in a high power, tritium only neutral beam injection discharge at the level of
  Tα /(Hα +Dα +Tα) = 2%.
- Calculations by D. Ruzic and J. Kelly using the VFTRIM code predict that about 25% of the tritium incident on a deuterium-saturated graphite surface is reflected. Work is underway to understand the differences.

REFLECTED T / (REFLECTED PLUS SPUTTERED D + REFLECTED T)

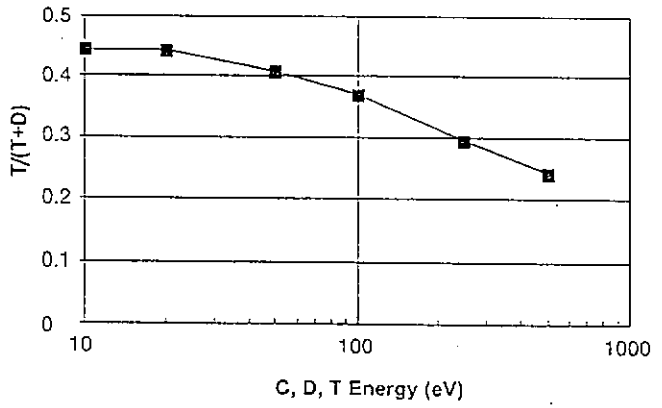

- Calculations using the VFTRIM code, a surface of 4/14 D and 10/14 C and D:T:C of 35:35:30 corresponding to a 50/50 DT plasma with Zeff=2.5 and C impurity.

D. Ruzic and J. Kelly , Univ of Ill.

Tritium-alpha simulation from Deuterium-alpha observations.

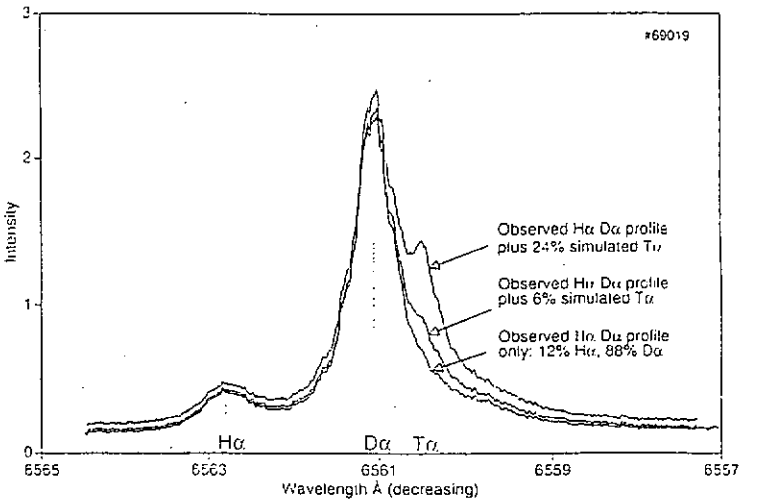

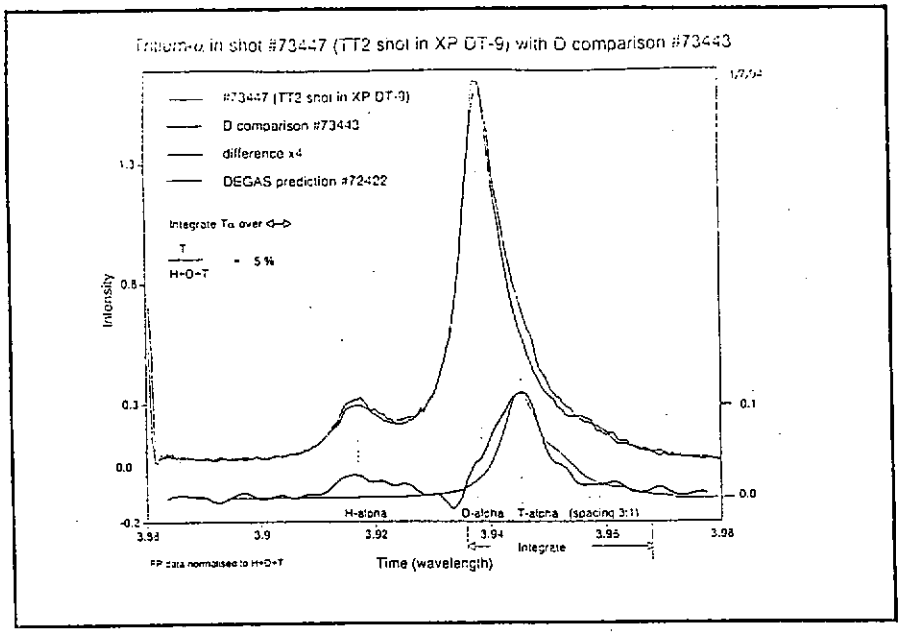

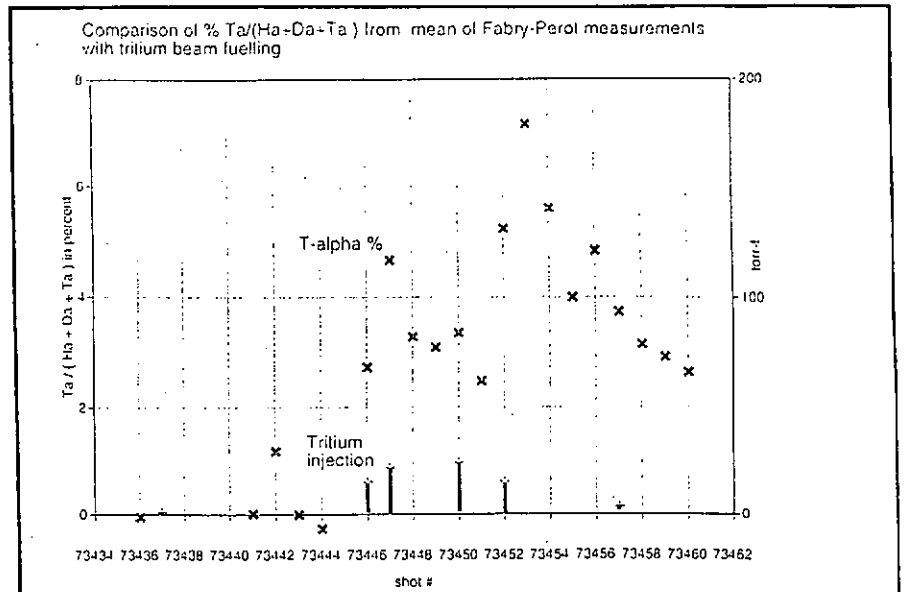

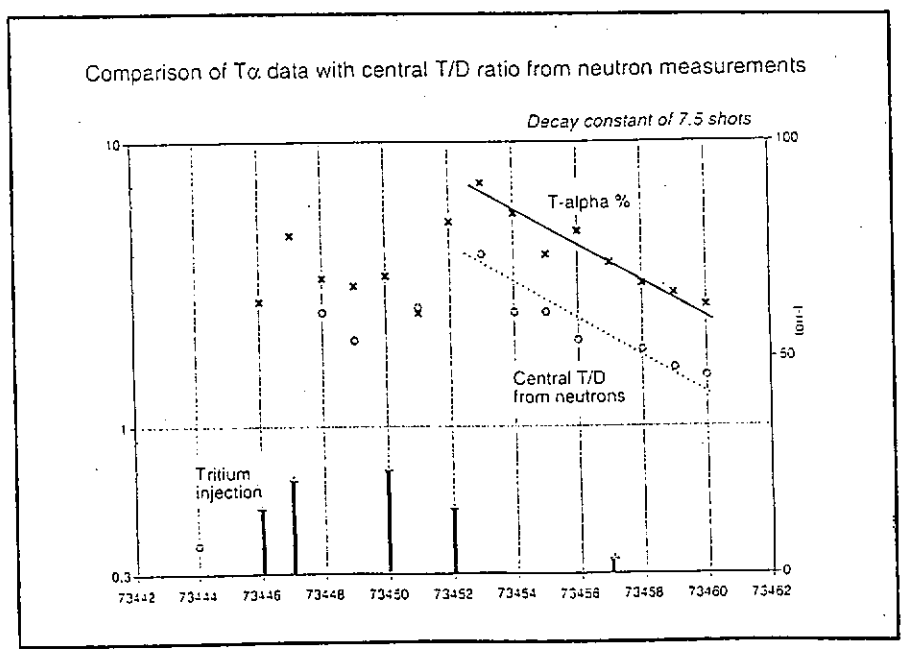

HELIUM-OXYGEN GLOW

- The tritium inventory in the TFTR vacuum vessel is limited by agreement to 20,000 Ci. This limit is expected to be reached near the end of TFTR's life.
- The tritium will reside mostly (70%) in regions of codeposition with carbon on the limiter tiles. This codeposited layer grows at the rate of approximately 40 A per neutral beam shot.
- Decommissioning and decontamination must reduce the in-vessel inventory for disposal.
- A Glow discharge in a 90% He, 10% O_2 mixture has been shown to be effective at removing carbon from surfaces.
- This technique has been used on TFTR twice. After the first, operation of TFTR was recovered following a boronization. The second,was followed by a vacuum opening.

INSTANTANEOUS CARBON REMOVAL RATE
BY He/O GDC

(Nov 12-16, 1992)

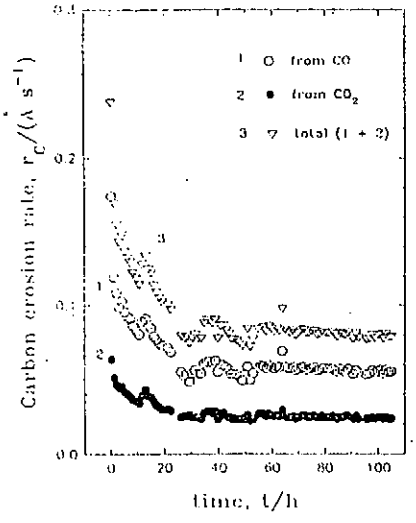

- EXPECTED THICKNESS OF CODEPOSITED LAYER IS
  ~ 3000 x 40 A = 1.2 x 10^5 A
- REMOVAL RATE – 0.05 A/s
  => 2.4 x 10^6 s, i.e. 28 DAYS NEEDED

MEASUREMENT OF TRITIUM INVENTORY

- *In situ* measurement of the tritium inventory in the TFTR vacuum vessel is important to permit compliance with the in-vessel limit, to provide guidance regarding the length of He-O glow required and to provide tritium inventory for disposal.
- The tritium is expected to be found distributed roughly:
  1/2 on carbon tile faces ≤ 10 μm
  1/4 in cracks between carbon tiles ≤ 10 μm
  1/4 on recessed metal walls ≤ 1 μm

spectrum of betas emitted from a tritium reference source (ref. 1) measured using an energy-resolving PIN diode detector

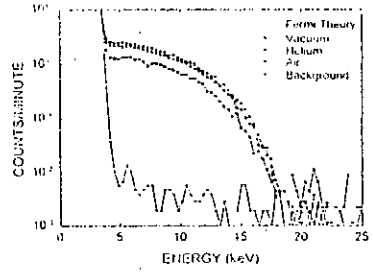

- Energy spectrum ~ unchanged by 1 μm of carbon

Tritium Betas from TFTR Walls

Assume tritium inventory =10,000 Ci (1/2 legal limit)

Assume all of this is on surface of wall (≤1μm deep)

Asssume uniform over =10^6 cm^2 (= whole vessel area)

Total beta emission:

==>> =4x10^{14} betas/sec (1 Ci = 3.6 x10^{10} disint/sec)

==>> =0.3 watts of beta energy (<E>=5.6 kev/beta)

Local beta emission:

==>> =4x10^8 beats/cm^2-sec emitted from wall

==>> =3x10^{-7} watts/cm^2 emitted from wall.

These averaged emission levels will most likely vary by at least an order-of-magnitude around the vessel wall, with higher levels on the inner carbon tile wall where the plasma-surface interaction has been largest.

MEASUREMENT OF TRITIUM INVENTORY

- Three non destructive techniques are being investigated.
- First, a Channel Electron Multiplier,CEM, to detect betas emitted from the surface. TFTR vertical and horizontal fields of ~ 100 G will be used to steer betas from wall to CEM detector inserted into TFTR.
- Second, ionization chamber method. Gas will be used to fill torus and e current collected on biased probe will be measured (e from e/i pairs produced by ionizing betas). Possible problem due to ~ 10 G stray field.
- Third, scintillating gas. Fill torus with scintillator gas and view with camera. Low light, but potentially good for imaging wall.
- Finally, after cessation of operation, core samples of the graphite limiter could be removed with a remote arm for *ex situ* analysis.

SUMMARY

- P_{fusion} ~ 5.2 MW with P_{α} ~ 1.2 MW
- Significant improvement in τ_E going from D-D to D-T
  - τ_E increased from 150 to 180 ms
  - Improved ion transport and possibly α-heating
- Escaping alpha particles in the 90 ° detector are well described by classical first orbit loss
  - No enhanced loss of alphas observed
- Significant fueling of plasma by wall neutrals
- He-O glow available for tritium removal
- Techniques for in-vessel tritium inventory measurement are available and under investigation

Status of the Tritium Plasma Experiment

R. A. Causey
Sandia National Laboratories

The recently upgraded Tritium Plasma Experiment (TPE) is being transferred to the Tritium System Test Assembly (TSTA) building at Las Alamos National Laboratory in New Mexico. The upgrade has increased the maximum 100eV triton flux from 10^{17} T/ $cm^2 \cdot s$ to 10^{19} T/ $cm^2 \cdot s$. The use of a LaB_6 cathode source in place of rf heating reduces the background tritium (or D + T) pressure signifantly. Vacuum conditions are also improved by the addition of a 2200 e/s turbomolecular punping system.

TPE should be operational in its new location by August or September of 1994. Experiments in support of ITER should begin shortly afterwards. The most important of these experiments is the direct measurement of tritium migration through a mock- up of the Be/ Cu duplex structure for the ITER divertor.

Because TPE is such a unique and important experimental device, collaborators from across the world are invited to join us in new experiments. Please contact Sandia National Laboratories in Livermore, California to arrange the joint research.

Status of the Tritium Plasma Experiment (TPE)

Rion A. Causey

Sandia National Laboratories
Livermore, California

Presented at:

2nd International Workshop on Tritium Effects in Plasma Facing Components

May 19-20

Nagoya University

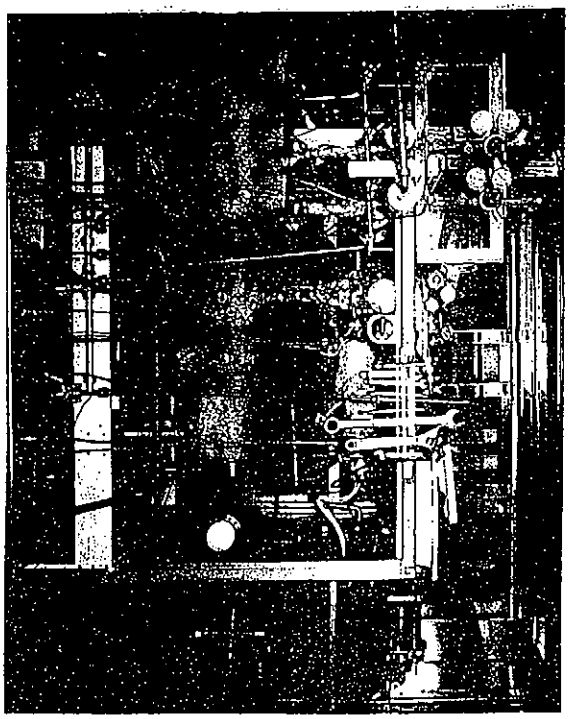

TRITIUM PLASMA EXPERIMENT

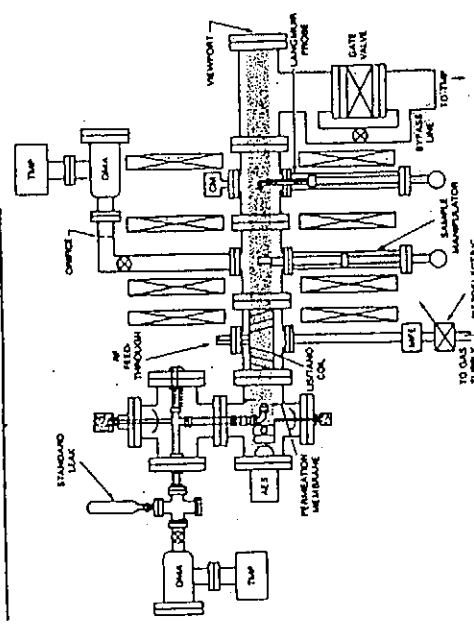

Schematic diagram of Tritium Plasma Experiment. AES = Auger electron spectrometer, QMA = quadrapole mass analyzer, TMP = turbomolecular pump, MTE = molecular bow sheaser, CM = capacitance manometer.

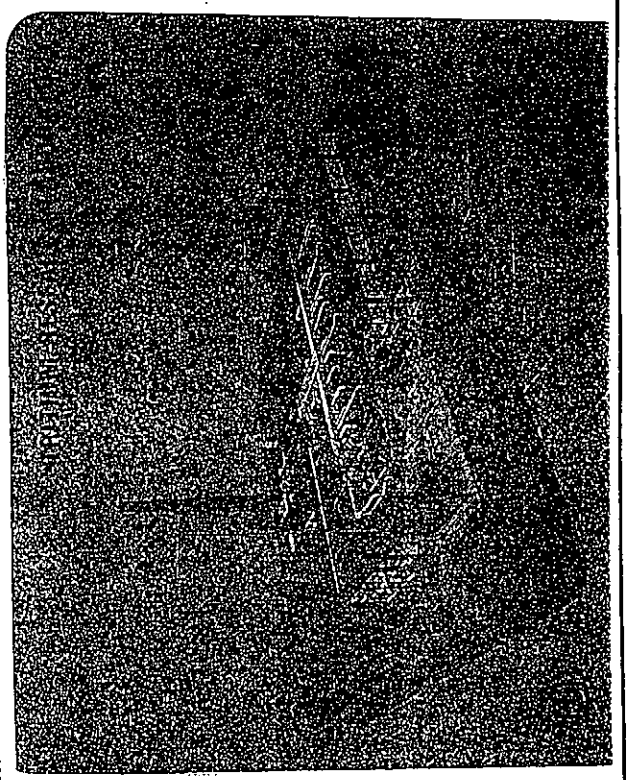

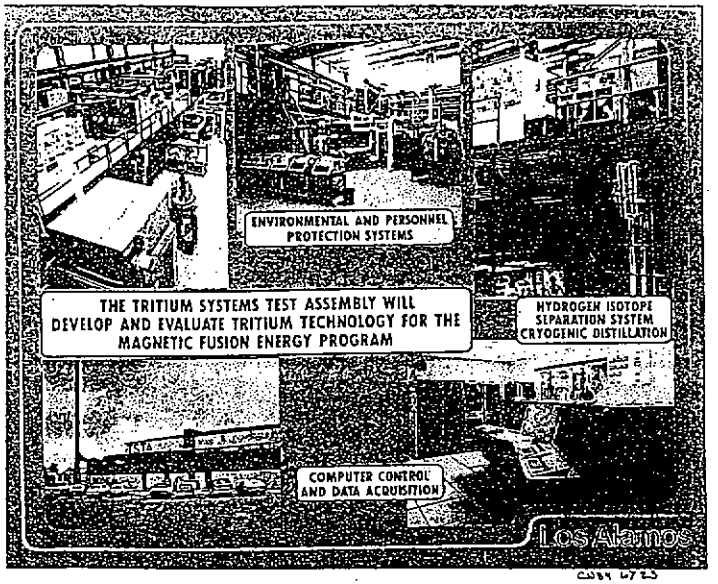

The Tritium Plasma Experiment (TPE) is a Unique Facility Devoted to Tritium-Material Interaction Studies

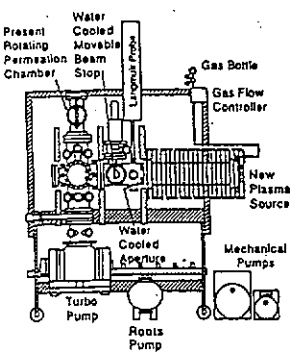

- Qualification of Materials for TFTR D-T Operation
- Insulator Tests for JET and TFTR
- Beryllium Studies for JET
- Tritium-Carbon Database
  - --Graphites
  - --Carbon/Carbon Composites
  - --Pyrolytic Graphite
- Tritium Release Studies (with INEL)
- In-Situ Tritium Removal Techniques
- Tritium Inventory in Neutron Irradiated Graphites and Beryllium for ITER
- Newly Upgraded to Duplicate Conditions Similar to that for the ITER Diverter

Sandia National Laboratories

The Tritium Plasma Experiment (TPE) is a Unique Facility Devoted to Tritium-Material Interaction Studies

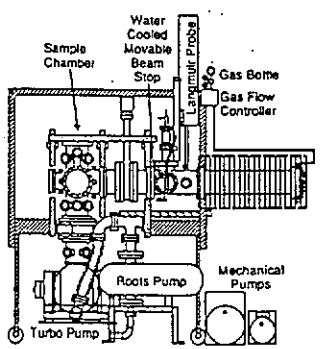

- TPE is presently being moved to the Tritium System Test Assembly (TSTA) at Los Alamos National Lab.
- It should be ready for operation in June 1994
- It is capable of delivering a 100 eV tritium ion flux of 10^{19} T/cm^2-s to a 5 cm diameter sample

Sandia National Laboratories

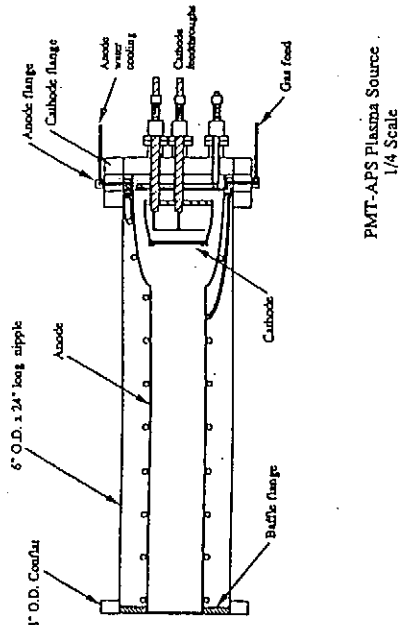

PMT-APS Plasma Source
1/4 Scale

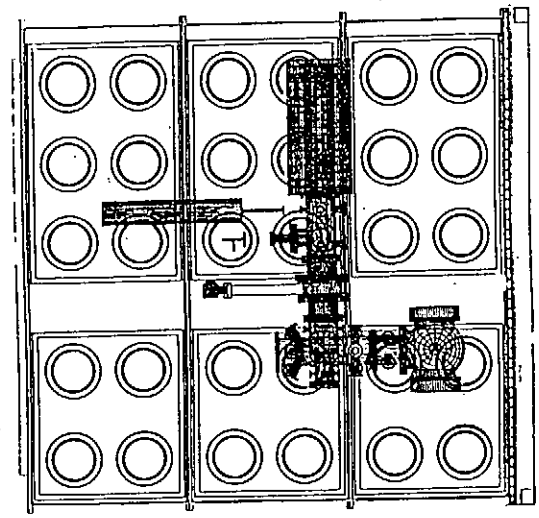

Future TPX Experiments

- Materials to be Tested: Beryllium, Copper, High-Z, New Carbon Composites, ITER Divertor Prototypes
- Properties to be Tested: Tritium Permeation, Tritium Retention and Trapping, Tritium Re-emission, and Soret Effect

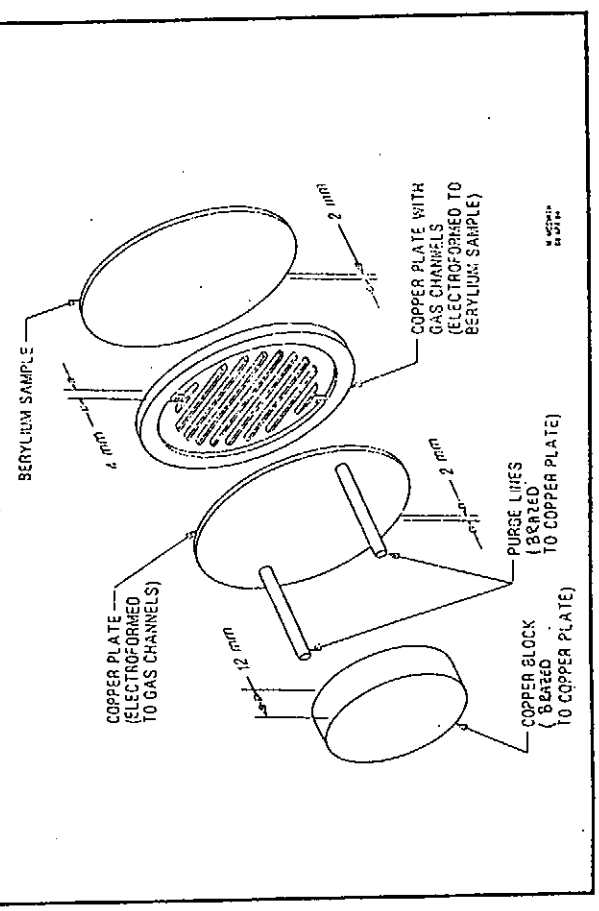

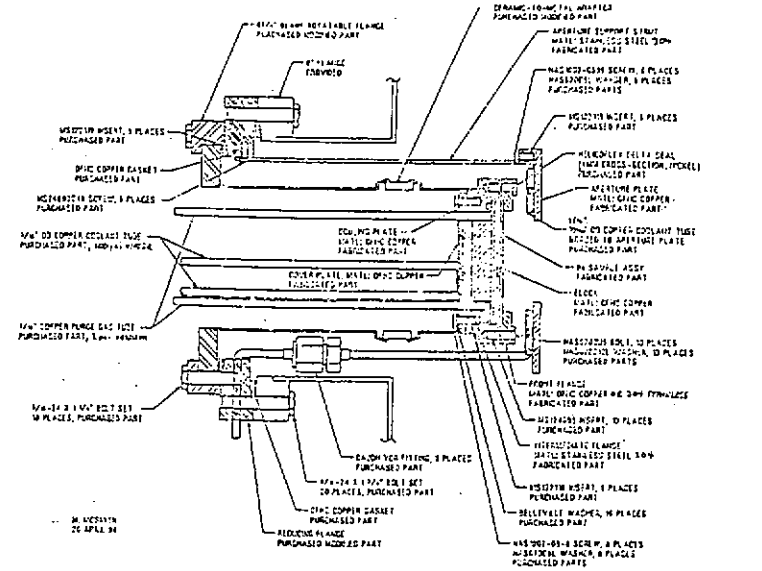

Summary

- The Tritium Plasma Experiment is expected to be back in operation by August or September of this year.
- Experiments on the retention and permeation of tritium in graphite and beryllium in support of ITER will begin soon after.
- We invite collaborators from all countries to come to Los Alamos and perform tritium experiments. Please begin by contacting me at Sandia National Laboratories.

Sandia National Laboratories

Fusion Research Programmes of Russian - Its Principles and Future.

A. Sherbak
Ministry of Science and Technical Policy of Russian Federation

Ministry of Science and Technical Policy of Russian Federation control about 40 state Scientific Programmes. The aim of each State Scientific Programme is a Realisation one of the modern scientific Priority. Control Scheme of State Scientific Programme is

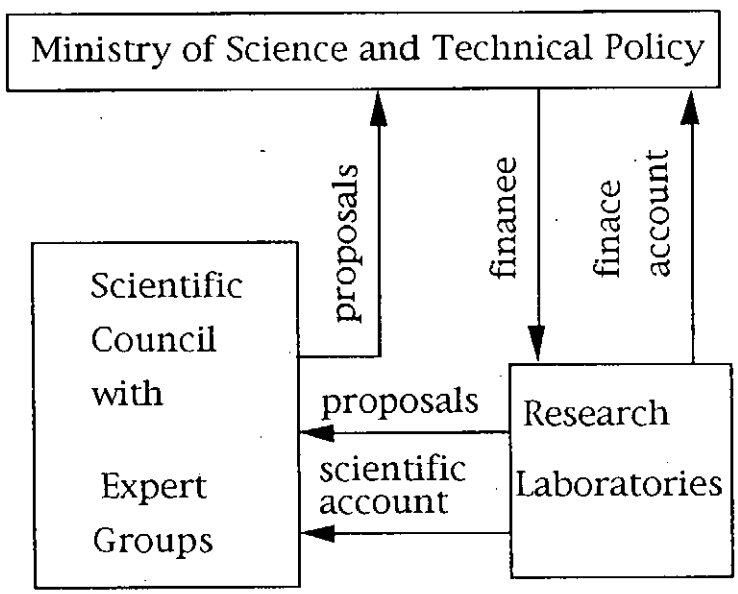

In these Programmes to take place a block fundamental physical programmes, These are :

1. Fundamental Nuclear Physics
2. Physics of High Energies
3. Synchrotonic Radiation
4. High Temperature Superconductivity
5. Nuclear Fusion and Plasma Processes
6. Fundamental Space Researches
7. Fundamental Metrology
8. Astronomy

The State Scientific Programme " Nuclear Fusion and Plasma Processes" was constructed in 1990 and its main Research Directions are :

1. Magnetic Confinement

- Tokamak : Kurchatov Inst., Moscow
  Triniti Inst., Troitsk
  Ioffe Inst., St- Peferburg
  High Temperature Inst., Moscow
- Mirror : Kurchatov Inst.
  Triniti Inst.
  Budker Inst., Novosibirsk
- Stellarator: Inst. of Physics, Moscow

2. Inertial Confinement

- Laser Fusion : Lebedev Inst., Moscow
  Inst. of Experimental Physics, Arsamas.
- Beam Fusion : Triniti Inst.

3. Fusion Researches in Higher School

7 Inst. in Moscow
3 Inst. in St.- Peterburg
2 Inst. in N. Novgorod
1 Inst. in Novosibirsk

4. Researches of ITER - programme (1991 - 1993)

Now(in 1994) these directions have a status of State Scientific Programme and Russian Ministry of Atomic Energy controls these Programme.

State Scientific Programme
"Nuclear Fusion and Plasma Processes"

Directions:

1. Magnetic Confinement
   - Tokamak: Kurchatov Inst., Moscow
     "Triniti" Inst., Troitsk
     Joffe Inst., St.-Peterburg
     Inst. of High Temperature, Moscow
   - Mirror: Kurchatov Inst.
     "Triniti" Inst.
     Budker Inst., Novosibirsk
   - Stellarator: Inst. of Fysics, Moscow
2. Inertial Confinement
   - Laser Fusion: Lebedev Inst., Moscow
     Inst. of Experimental Fysics, Arsamas
   - Beam Fusion: "Triniti" Inst.
3. Nuclear Fusion Researches in Higher School
   Moscow
   St.-Peterburg
   N. Novgorod
   Novosibirsk
4. ITER

State Scientific Programme
Ministry of Atomic Energy

Fusion Research Programs of Russia
- Its Principles and Future

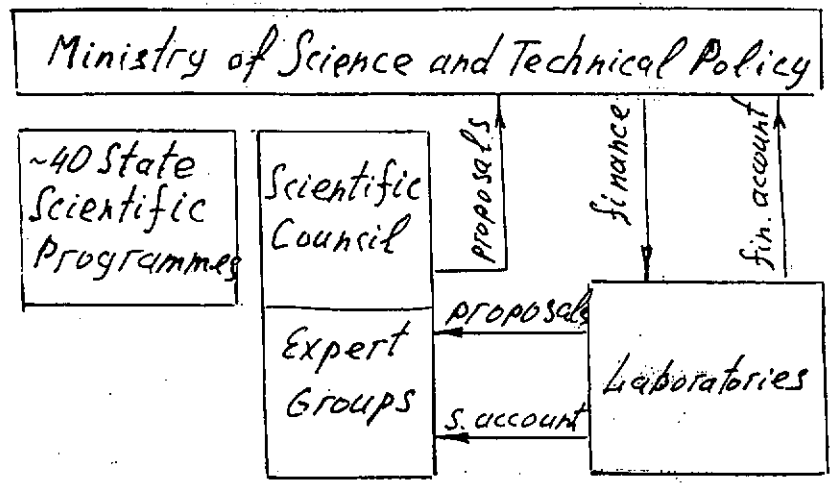

1. Fundamental Nuclear Fysics
2. Fysics of High Energy
3. Syncrotron Radiation
4. High Temperature Superconductivity
5. Nuclear Fusion and Plasma Processes
6. Fundamental Space Researches
7. Fundamental Metrology
8. Astronomy

Transport of Hydrocarbon in the Laboratory Plasma MAP (Materials And Plasma)

Satoru Tanaka, Seiji Matsuyama and Michio Yamawaki
Faculty of Engneering, University of Tokyo, Hongo, Bunkyo, Tokyo, Japan.

Carbon is one of the most widely used materials for first wall and divertor plate. However, carbon shows strong chemical reactions with oxygen and hydrogen, which can lead to an enhanced erosion by chemical sputtering. Therefore, it is important to know to which extent carbon containing molecules like CH_4 or CO play a role in fueling and impurity release during plasma discharges. A part of the generated impurity enters into the core plasma or redeposits on the divertor plate via many atomic and molecular processes in the divertor plasma. Hence it is vitally important to have thorough knowledge on impurity transport including atomic/molecular processes and rate constants of them. These studies can be effectively conducted by a steady-state plasma souce like MAP (Materials And Plasma). In the present paper, two kinds of hydrocarbons, CH_4, C_2H_2, were fed into the plasma. Luminescenses from the fragments of these species were measured and space distributions of them were investigated. These results were compared with a modeling study.

The MAP facility has been successful in generating linear steady-state plasma of hydrogen, argon and helium. The plasma density of $10^{11} - 10^{13} cm^{-3}$ and electron temperature of $5 - 15eV$ have been achieved. The neutral pressure of plasma working gas in the main chamber is in the order of 10^{-4} Torr. In experiments hydrocarbons (CH_4, C_2H_2) were verticaly introduced through a nozzle into a steady state hydrogen plasma and the emission in 380nm-660nm region from their excited or breakup species due to electronic collision etc. was recorded at various axial and radial points in the plasma. A specific interest of this work is to study transport of carbon containing impurities, breakup processes of molecules and radicals, and atom ionization processes.

Main results of the experiments were as follows:

(1) When CH_4 was introduced into the plasma, the band ($A^2\Delta - X^2\Pi$) of the CH-radical was identified near 430nm, and when C_2H_2 was introduced, not only CH-radical but also large C_2 band were identified, particularly the (0,0)-band of the ($A^3\Pi_g - X^3\Pi_u$)-transition at 516nm and the (1,2)-transition at 558nm of the Swan system.

(2) Luminescence intensity of CH-radical band decreased more rapidly than that of C_2 radical in the process of radial and axial transport in the plasma. This was attributable to the larger dissociation rate coefficient of CH than that of C_2.

(3) Axial and radial profiles of electric charged state of carbon atom (CI,CII,CIII,CIV) were obtained in both CH_4 and C_2H_2 injection. Regardless of axial or radial distribution and CH_4 or C_2H_2 injection, the state of CII was dominant. But the fraction of CI in C_2H_2 injection is a little larger than in CH_4.

Numerical model was constructed and compared with experimental results. This model includes radial and axial transports of impurities of molecules, radicals and various charged atoms. Electron impact dissociation and ionization were mainly considered.

Transport of Hydrocarbon in the Laboratory Plasma MAP (Materials And Plasma).

Satoru Tanaka, Seiji Matsuyama, and Michio Yamawaki

Faculty of Engineering, The University of Tokyo

2nd International Workshop on
Tritium Effects in Plasma Facing Components
May 19, 1994 Symposium Hall, Nagoya University

Contents

INTRODUCTION

(1) BACKGROUND

Impurities generation in carbon based materials due to chemical reaction
and erosion by physical and chemical sputtering.

Impurities behavior near first wall
Physical phenomena of edge plasma

- Impurities generation processes.
- Transport of impurities in the edge plasma.
- Atomic and molecular processes.
- Impurities redeposition processes to the first wall.

(2) SCOPE

Transport of carbon containing molecules in the divertor simulation experimental facility.

Molecular breakup and atom ionization processes

3. OBJECTIVES

Introduction of Hydrocarbons to the Steady-State plasma facility MAP (Materials And Plasma).

Measurement of impurities emission by the technique of spectroscopy.

Spectra Identification

Transport of Carbon-Containing Radicals

Transport of Carbon of Various Charged States (CI, CII, CIII, CIV)

↑

Modeling study considering collision processes

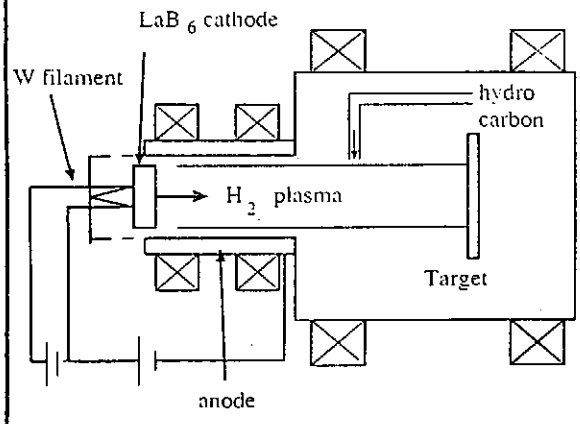

Schematic diagram of MAP

Electron Temperature : 5 - 15eV
Electron Density : up to 10^{19} $1/m^3$

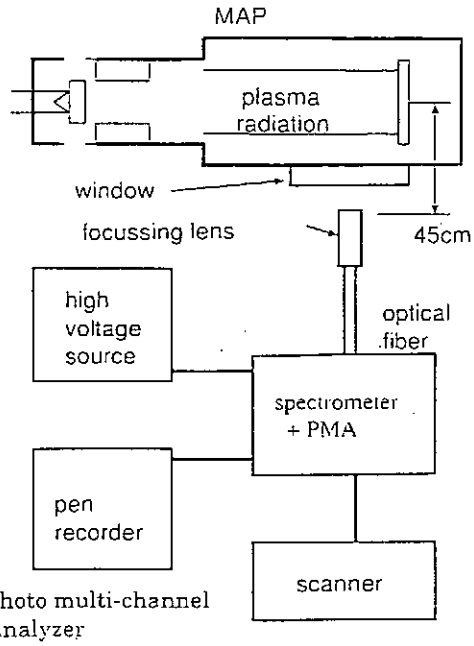

PMA: photo multi-channel analyzer
scanner: wave-length scanner

Emission Measurement System

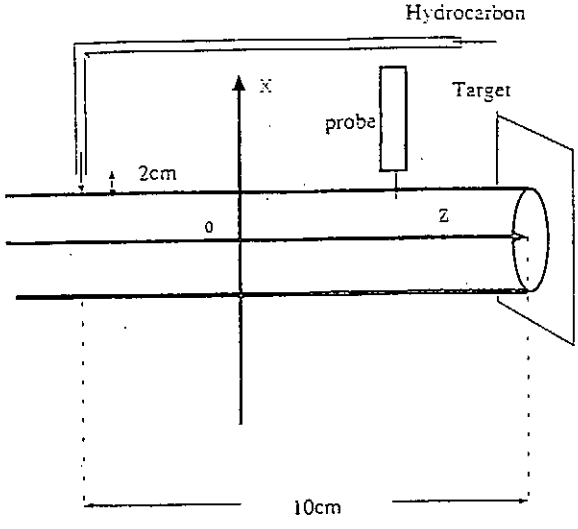

Working Gas : H_2

Hydrocarbon Charging System And Mesurement Geometry

Experimental Parameters

	Te (eV)	Ne ($x10^{18}$ $1/m^3$)	Pressure ($x10^{-4}$ Torr)	Hydrogen : Hydrocarbon
H_2	12	1.6	6	1 : 0
H_2+CH_4	10	1.8	7.5	4 : 1
H_2+C_2H_2	8.5	1.9	7.5	4 : 1

3.1 Spectra Identification

Spectra line from 380nm to 660nm.

INTERESTS

Spectrum Bands of Carbon Containing Radicals

Spectrum of Carbon Atom in Various Charged States (CI, CII, CIII, CIV)

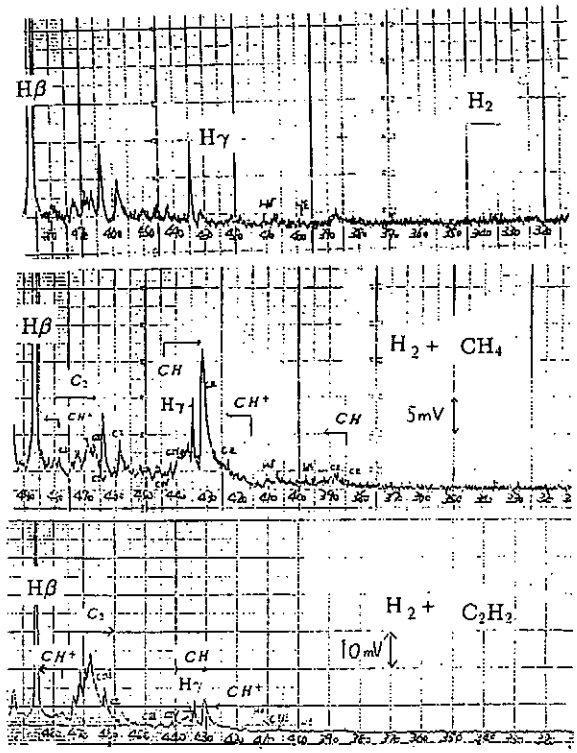

Spectral Line (300nm - 480nm)

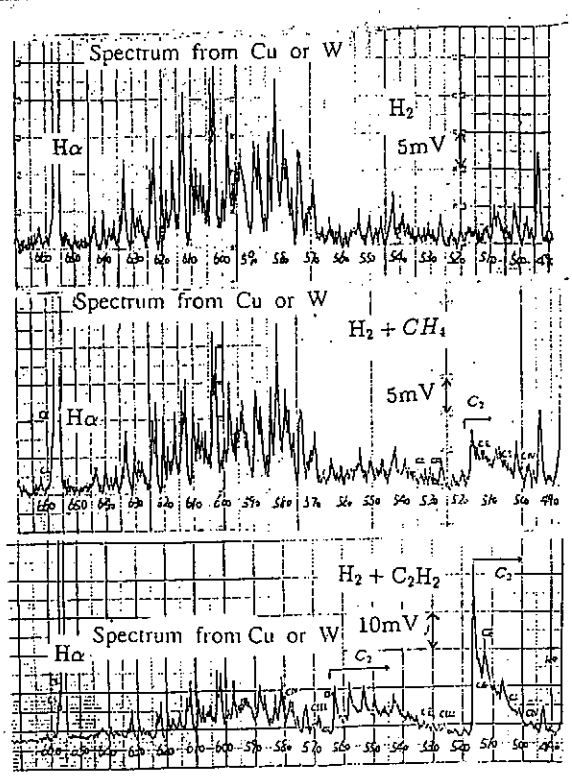

Spectral Line (480nm - 660nm)

3.2 Spatial Profiles of Carbon-Containing Radicals.

Spatial profiles of carbon-containing radicals (CH, C_2) were measured.

Intensity difference between CH_4 and C_2H_2 injection.

Comparison with modeling study.

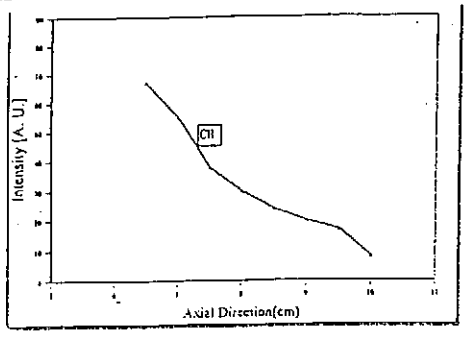

Axial profiles (experimental values) of CH-radical when CH_4 is introduced.

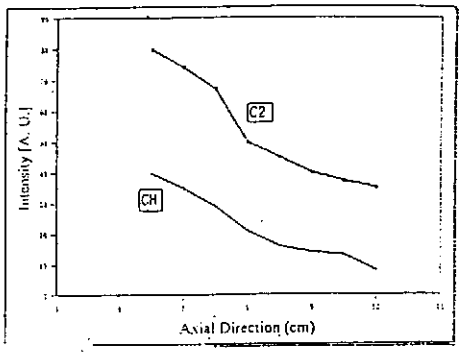

Axial profiles (experimental values) of C_2 and CH-radical when C_2H_2 is introduced.

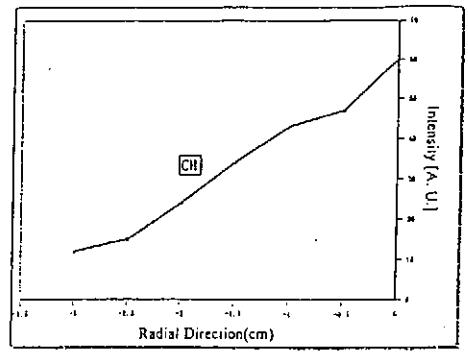

Radial profiles (experimental values) of CH-radical when CH_4 is introduced.

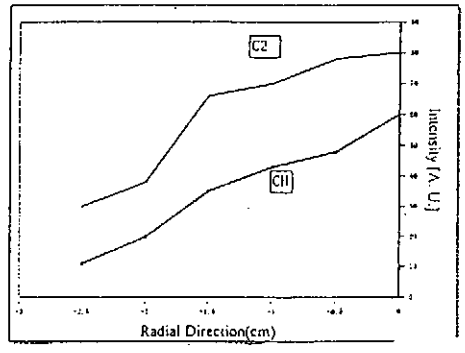

Radial profiles (experimental values) of C_2 and CH-radical when C_2H_2 is introduced.

Modeling

Mass conservative equation

$$\frac{\partial(vni)}{\partial x} + \frac{\partial(uni)}{\partial z} = S \qquad (1)$$

$CH + e^- \rightarrow C + H + e^-$ (a)

$C_2 + e^- \rightarrow 2C + e^-$ (b)

CH and C_2 are monotonously reduced by electron collision.

$$S = - < \sigma v > n_e n_i \qquad (2)$$

$< \sigma v >$: *rate coefficient of electron collision*

In the case of (a). $< \sigma v >_{CH \rightarrow C} = 2.0 \times 10^{-15}\ m^3/s$

In the case of (b). $< \sigma v >_{C2 \rightarrow C} = 1.0 \times 10^{-15}\ m^3/s$

Reference: H.Tawara et al.

Radial velocity: $v = - D \frac{\partial n_i}{\partial x} \cdot \frac{1}{n_i} \qquad (3)$

Anomalous diffusion coefficient D=1.0 m^2/s

Axial velocity: $u = \sqrt{\frac{2kTe}{m}} \qquad (4)$

Te = 10eV Constant

Ne $ne = 2.0 \times 10^{18} \times (1 - 0.8z)(1 - 0.1x^2)$ (5)

(from experiment z,x (cm))

Processes not considered

Particles reflection at target.

Particles neutralization at target

Charge exchange and recombination with neutral particles.

Acceleration by sheath potential.

CH and C_2 were assumed to be produced at the nozzle.

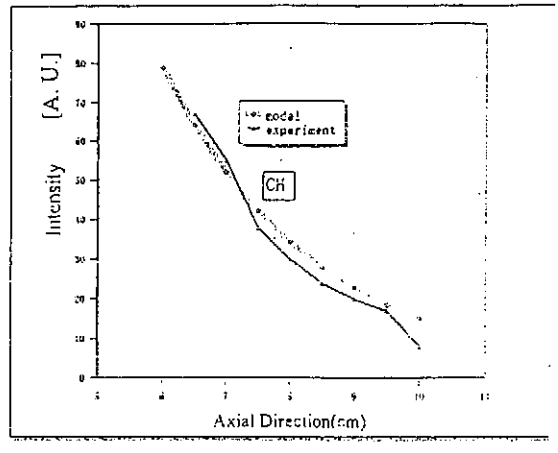

Radial profiles (modeling values) of CH-radical when CH_4 is introduced.

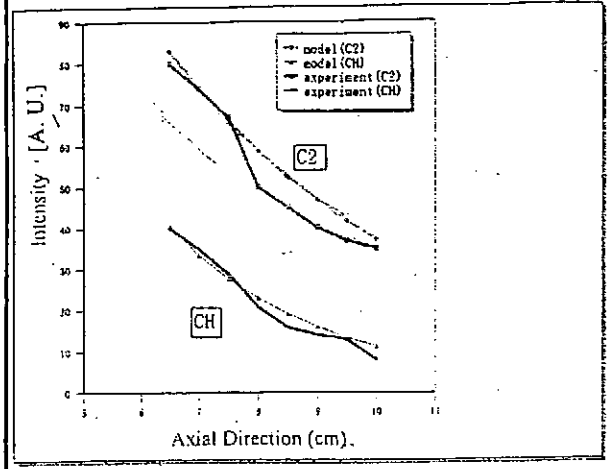

Axial profiles (modeling values) of C_2 and CH-radical when C_2H_2 is introduced.

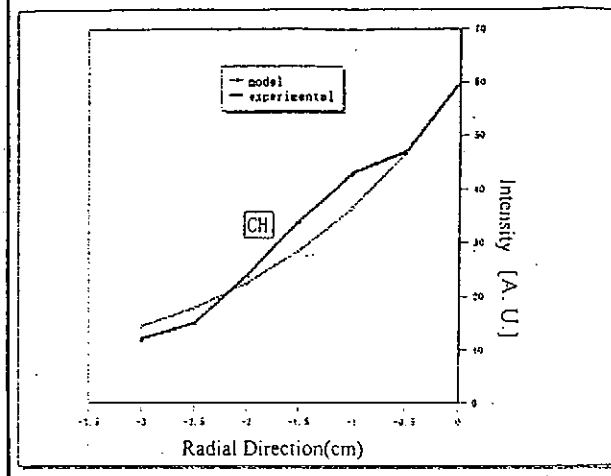

Axial profiles (modeling values) of CH-radical when CH_4 is introduced.

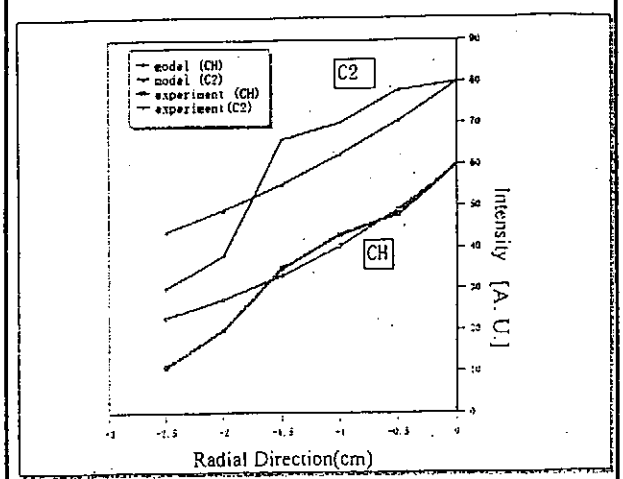

Radial profiles (modeling values) of C_2 and CH-radical when C_2H_2 is introduced.

3.3 Spatial Profiles of Carbon Atom in Various Charged State

Typical Spectrum

	Wave Length	Constant of Exciting Probability
CI	658.7nm	2.5
	505.3nm	1.3
	477.2nm	1.2
CII	658.2nm	1.3
	437.4nm	1.5
	426.7nm	2.0
CIII	432.5nm	1.6
	418.6nm	1.5
CIV	440.0nm	1.3
	418.2nm	1.9

Intensity in each charged state was obtained by normalizing each emission intensity by constant of exciting probabillity, and by taking an average in each charged state.

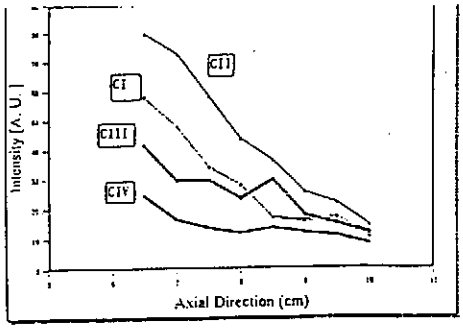

Axial profiles (experimental values) of carbon atom in each of charged state when CH_4 is introduced.

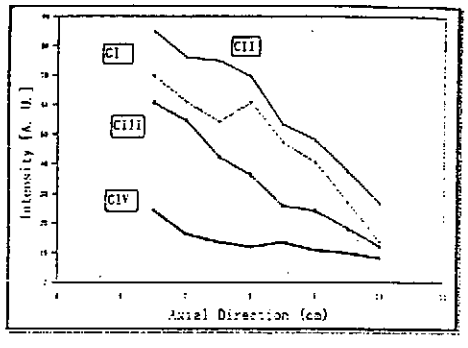

Axial profiles (experimental values) of carbon atom in each of charged state when C_2H_2 is introduced.

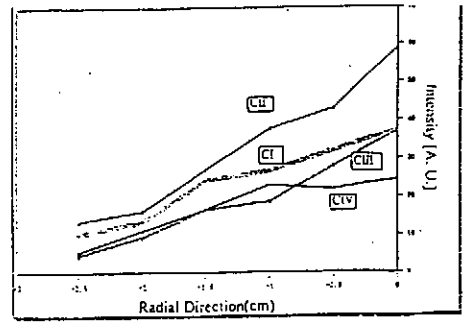

Radial profiles (experimental values) of carbon atom in each of charged state when CH_4 is introduced.

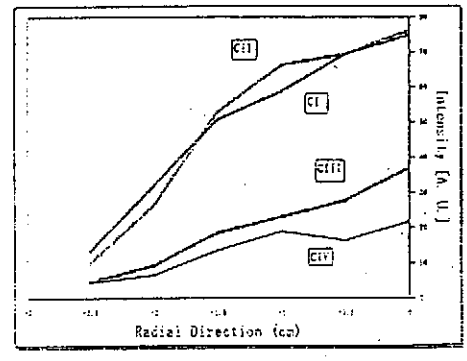

Radial profiles (experimental values) of carbon atom in each of charged state when C_2H_2 is introduced.

Modeling for distribution of charged state of carbon atom

Mass conservative equation

(Electron impact dissociation and ionization were considered.)

$$\frac{\partial(v n_i)}{\partial x} + \frac{\partial(u n_i)}{\partial z} = <\sigma v>_{i-1\to i} n_e n_{i-1} - <\sigma v>_{i\to i+1} n_e n_i$$

Source term Sink term

Applying this equation for particles of CI~CIV.

n_i is density of each carbon particles.

Rate coefficients for each electron collision reaction:

$CH + e^- \rightarrow C + H + e^-$; $<\sigma v> = 2.0 \times 10^{-15}\ m^3/s$

$C_2 + e^- \rightarrow 2C + e^-$; $<\sigma v> = 1.0 \times 10^{-15} m^3/s$

$C + e^- \rightarrow C^+ + 2e^-$; $<\sigma v> = 1.5 \times 10^{-15} m^3/s$

$C^+ + e^- \rightarrow C^{2+} + 2e^-$; $<\sigma v> = 1.0 \times 10^{-16} m^3/s$

$C^{2+} + e^- \rightarrow C^{3+} + 2e^-$; $<\sigma v> = 2.0 \times 10^{-17} m^3/s$

$C^{3+} + e^- \rightarrow C^{4+} + 2e^-$; $<\sigma v> = 2.0 \times 10^{-18} m^3/s$

Ionization by electron collision is assumed to occur stepwisely.

$$CH, C_2 \rightarrow C \rightarrow C^+ \rightarrow C^{2+} \rightarrow C^{3+}$$

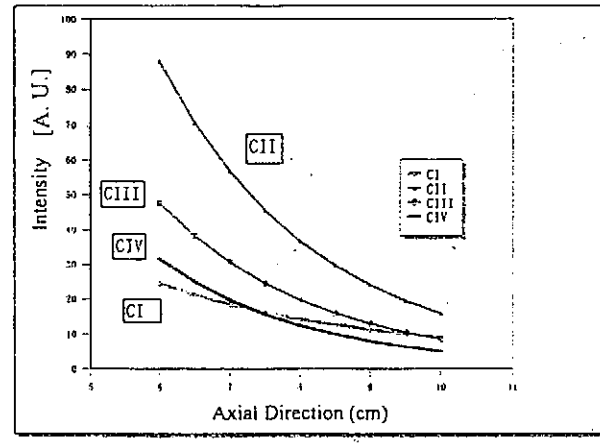

f

Axial profiles (modeling) of carbon atom in each of charged states when CH_4 is introduced.

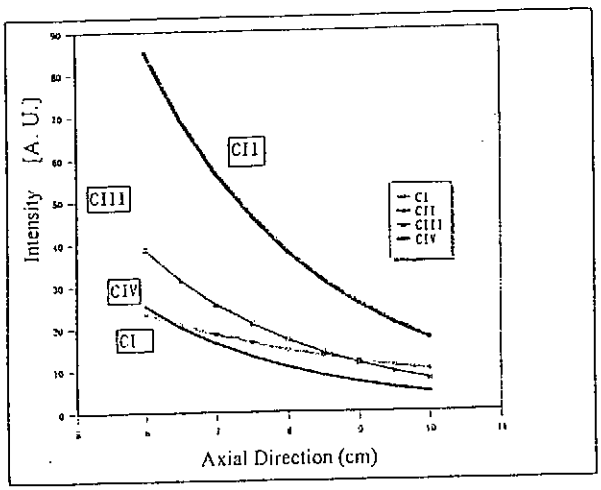

Axial profiles (modeled values) of carbon atom in each of charged state when C_2H_2 is introduced.

4. Summary

Hydrocarbons (CH_4, C_2H_2) were introduced into the laboratory plasma MAP (Materials And Plasma), and impurities transport and atomic and molecular porocesses were studied by measuring spatial distribution of emissions from radicals and various charged states of carbon atom.

(1) Identification of Spectra

(A) When CH_4 was introduced into the plasma.

The band of CH-radical was identified near 430nm. As carbon atoms, emissions from CI, CII, CIII, CIV were also identified.

(B) When C_2H_2 was introduced into the plasma.

Large C_2 band (Swan Band) was identified at 560nm, 515nm and 465nm and CH-band was also identified. But it was smaller comparing with that in CH_4 injection.
And as carbon atoms, Emissions from CI, CII, CIII CIV were identified.

(2) Spatial Profiles of Carbon-Containing Radicals

Luminescence intensity of CH-band decreased more rapidly than that of C_2 radical in the process of radial and axial transport in the plasma. This was attributable to the larger dissociation rate coefficient of CH than that of C_2.

(3) Spatial Profiles of Various Charged State of Carbon Atom.

Axial and radial profiles of various charged states of carbon atom (CI, CII, CIII, CIV) were obtained in both CH_4, C_2H_2 injection.
Regardless of axial and radial profiles and of the molecules injected, the fraction of CII was largest. And this was also verified by modeling considering electron collision processes.

(4)
From these experimental and modeling studies, it could be concluded that transport of hydrocarbon and carbon atom can be simulated if sufficient database are supplied.
Processes at the solid target and inclusion of more sophisiticated molecular processes are the next subjects to be studied and modeled.

Design of Carbon Sheet Pump for LHD and Demonstration of Hydrogen Pumping

A.Sagara , H.Suzuki, N.Ohyabu and O.Motojima

National Institute for Fusion Science,
Nagoya 464-01, Japan

The first design of Carbon Sheet Pump (CSP) for the Large Helical Device (LHD) is presented. The CSP is a new hydrogen pumping scheme with high efficiency, which has been proposed to achieve low overall recycling ratio below 0.7 and hence high divertor plasma temperature above 1keV, hopefully leading to a significant improvement in the core energy confinement.

The designed operation cycle of the CSP is as follows; (1) pumping of charge-exchanged(CX) fast H neutrals by trapping them in the sub-surface layers of the carbon at temperatures below 200°C, and, after main discharge operation with total duration time of about 100sec, (2) degassing of trapped hydrogen atoms by direct Joule heating of the carbon sheet at a temperature above 700°C, and then (3) cooling down to the operation temperature below 200°C.

According to our elastic recoil detection (ERD) experiments performed for 3keV D_2^+ implantation on carbon samples, the pumping duration time is expected to be at least 100 sec, which is estimated from the maximum trapped amount of about 5×10^{17}D atoms/cm^2 and an expected CX fast neutrals in the order of 10^{15}/cm^2.s. This pumping duration time is sufficient for the LHD confinement experiments. The CSP sheets are mounted on the vessel wall near the divertor plate at the small major radius side of the torus, where a high flux of CX neutrals is expected but the heat flux level is less than 0.05MW/m^2. In order to reduce the overall recycling ratio, a total CSP surface area of 60m^2 is required. The three dimensionally shaped CSP made of C/C composite can be degassed by direct Joule heating with a total electric power of about 3MW for 100sec which is enough to desorb most of trapped hydrogen atoms. The cooling time is estimated to be about 30min.

In order to demonstrate and confirm the design properties of CSP, hydrogen pumping capacity and degassing efficiency are successfully measured by using DC glow discharges in a plasma processing teststand.

Design of Carbon Sheet Pump for LHD and Demonstration of Hydrogen Pumping

A.Sagara , H.Suzuki, N.Ohyabu and O.Motojima
NIFS

1. Background
   - Control of hydrogen recycling to improve plasma confinement
   - Disruptive discharge cleaning of graphite limiter in TFTR
   - New idea of carbon sheet pumping (CSP) based on ERDA data
2. Concept of CSP
   - Principle
   - Pumping capacity
   - Regeneration
3. Designe for LHD
   - Location
   - Heating method
4. Demonstration

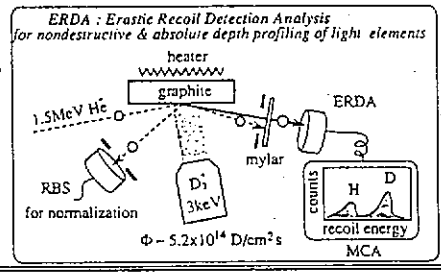

Principle

- trapping of implanted H isotopes in the projection range
- desorption of retained H isotopes by heating

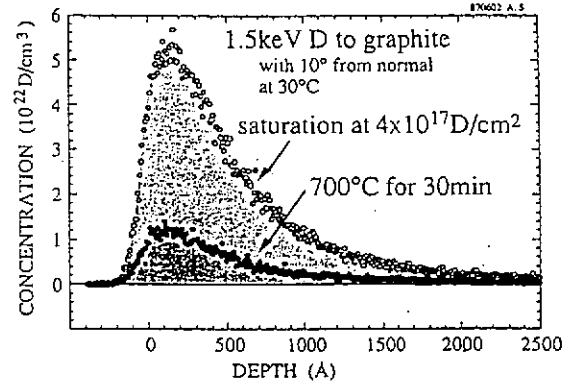

Pumping Capacity

1. Higher Hydrogen Energy
   - the saturation amount increases
   - the particle reflection decreases
2. Larger Pump Area

Capacity > 10^{21}D/m^2
↓
Lifetime > 100sec > 1 mi
for Φ_{cs}~ 10^{19}/m^{2}s
↓
Area 100m^2 required
for 20MW 160A NBI (H^0)
($1x10^{21}$ H^0/s)

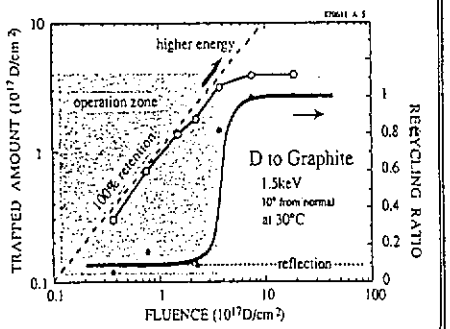

Regeneration (1)

- operation zone < 200°C
- regeneration zone > 800°C

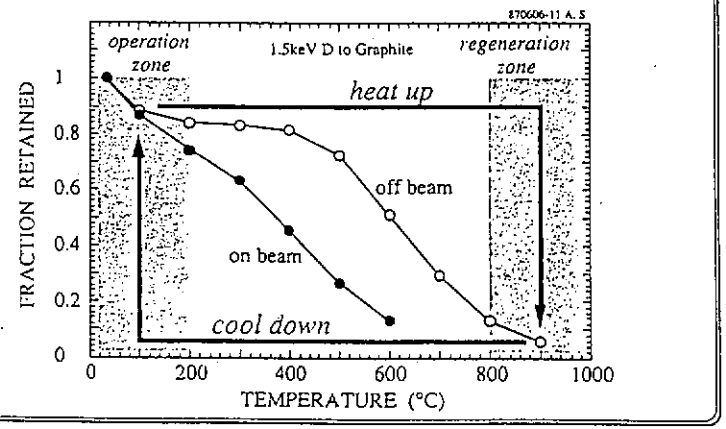

NIFS : 921128 A. Sagara

Regenetation (2)

- less than a few minutes at elevated temperature
- passive or active cooling between shots

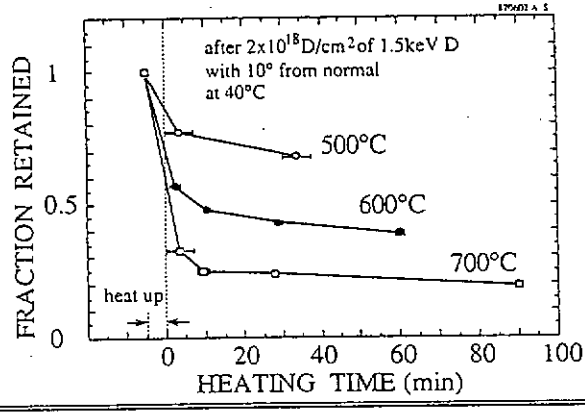

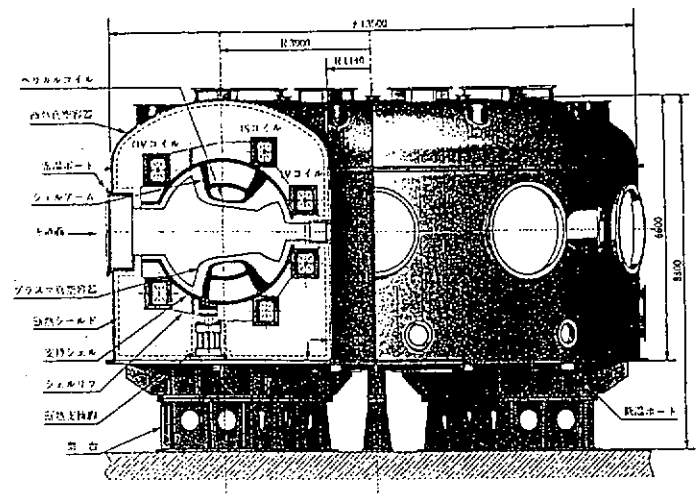

大型ヘリカル装置構造図

Preliminary Positioning of Carbon Sheet

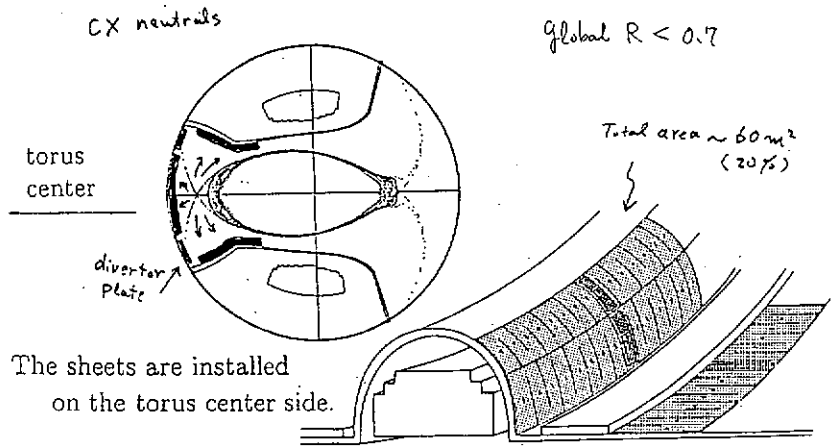

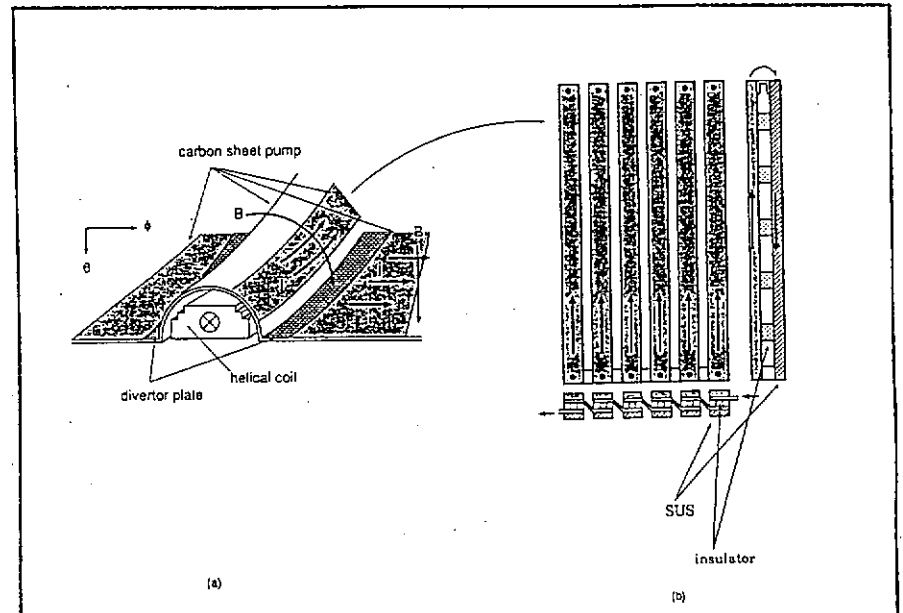

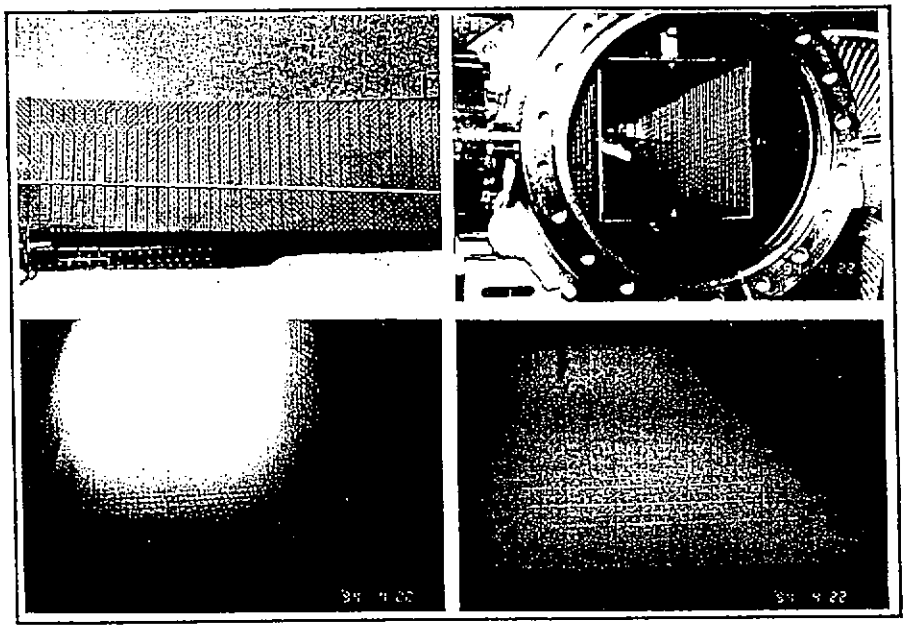

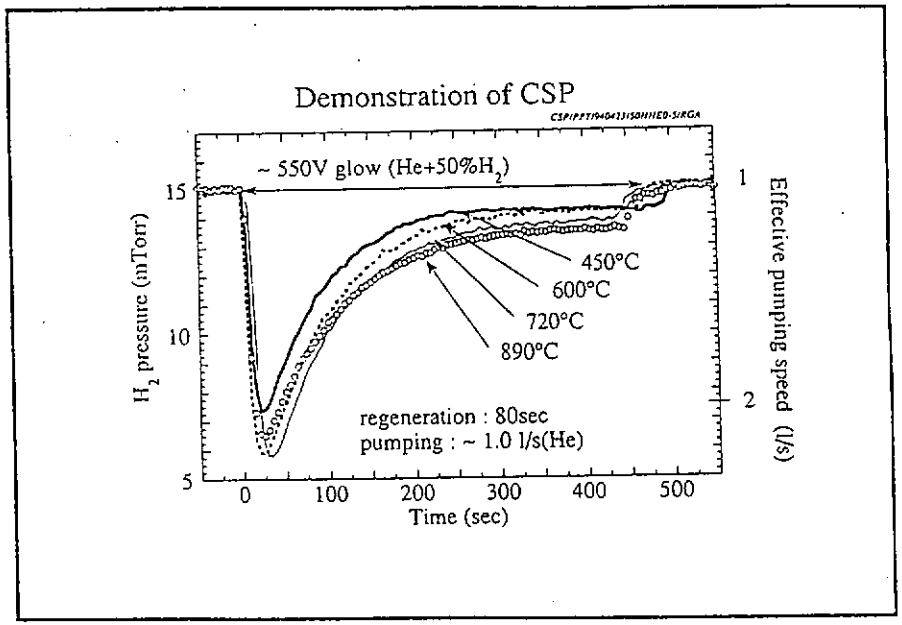

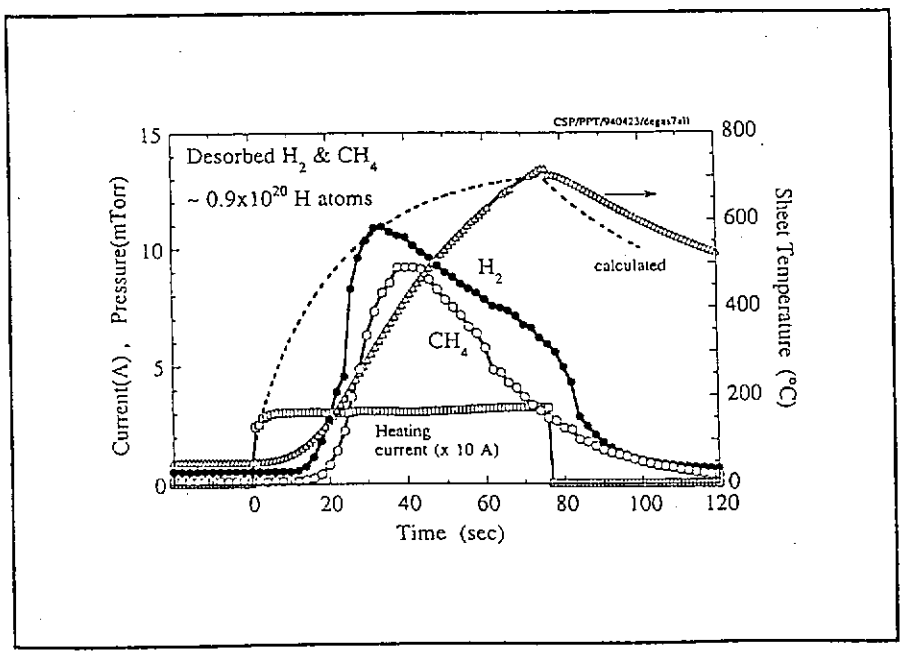

NIFS : 923128 A. Sagara

Merits of CSP

1. Low Z getter for hydrogen isotopes
2. Suitable for pumping CX fast neutrals with low heat flux
3. About 1min of pumping duration time
4. Regeneration between shots by direct heating of C/C sheets
5. Easy installation with low cost due to simple thin structures
6. No need to use large ports
7. Easy to replace
8. Material modification by adding B etc.

Session 2

APPLICATIONS OF SUPERPERMEABLE MEMBRANES IN FUSION: THE FLUX DENSITY PROBLEMS

A. I. Livshits [1], **M. E. Notkin** [1], **V. I. Pistunovich** [2], **M. Bacal** [3], and **A. O. Busnyuk** [1]

[1] *Bonch-Bruyevich University, 61 Moika, St. Petersburg 191065, Russia*
[2] *Kurchatov Institute, Kurchatov Sq., Moscow 123182, Russia*
[3] *École Polytechnique, 91128 Palaiseau, France*

It has been established that metal membranes may be almost as "transparent" to suprathermal hydrogen (*i.e.*, to energetic particles, or even to thermal hydrogen atoms) as an orifice in a wall: the ***superpermeability*** phenomenon.

Such membranes may be employed in the exhaust pumping ducts of a fusion machine (*e.g.*, of ITER) for an effective separation of **D/T** from **He**, its compression and return into the fuel cycle. For instance, a membrane of a reasonable surface area, if incorporated into the newest ***"gas target" divertor*** concept for ITER, might pump out $> 90\%$ of **D/T** with a very small tritium retention (1.5 g).

Installment of the membrane may also deliver an opportunity for arranging of a **D/T** recirculation contour in the divertor. Still the membranes should let through the fluxes of up to $10^{16} - 10^{17}$ cm^{-2} s^{-1} and operate at pressures of up to $3 \times 10^{-4} - 2 \times 10^{-3}$ mbar in this case, which exceeds by a factor of $10 - 100$ the values dealt with up to date.

The theory predicts that superpermeability with even much larger fluxes can be obtained on the ***V Group*** metals. Superpermeation with flux densities of up to 3×10^{16} cm^{-2} s^{-1} was reached up to date in direct membrane experiments on **Nb**. Model absorption experiments indicate at the possibility of superpermeation with a flux density of $> 4 \times 10^{17}$ cm^{-2} s^{-1} and a pressure of $> 5 \times 10^{-2}$ mbar. A further advancement to higher densities was only limited by the experimental equipment capabilities.

2nd International Workshop
on Tritium Effects in Plasma — Facing Components
May 19 – 20, 1994, Nagoya University, Nagoya, Japan

APPLICATIONS OF SUPERPERMEABLE MEMBRANES IN FUSION : *THE FLUX DENSITY PROBLEMS*

A. I. Livshits [a], M. E. Notkin [a], V. I. Pistunovich [b], M. Dacal [c] and A. O. Dusnyük [a]

[a] *Bonch-Bruyevich University, St. Petersburg, Russia*
[b] *Kurchatov Institute, Moscow, Russia*
[c] *École Polytechnique, Palaiseau, France*

SUPERPERMEABILITY: WHAT IS IT ?

Metal membranes may be *superpermeable* to hydrogen particles whose energy (kinetic, internal or chemical) exceeds ≈ 1 eV. The term superpermeability means that:

A. I. Livshits
Sov.Phys.Tech.Phys. 21 (1976) 187

> *permeability approaches its conceivable limit: the permeability of an opening of the same area.*

Superpermeability to *thermal atoms* and *fast ions* was experimentally observed on membranes of Fe, Ni, Pd, and Nb.

Superpermeable membranes are able to automatically *compress* the permeating hydrogen and to *purge* it of any impurity, *including He*.

The proposal has been put forward to install superpermeable membranes in the ITER pumping ducts in order to isolate the major part of D/T-mixture and thus to reduce the tritium load on the cryopumps serving to pump helium.

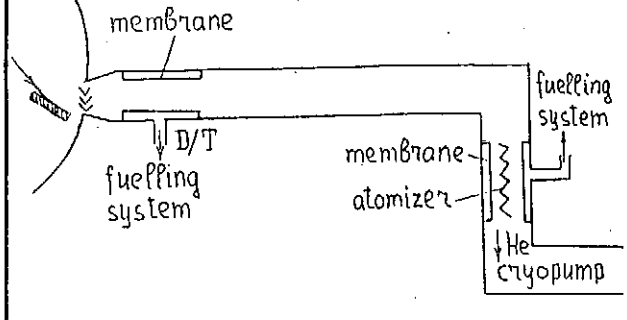

The *V Group metals* (V, Nb and Ta) are the most suitable materials for superpermeable membranes, while Nb and Ta may be also employed for atomizers.

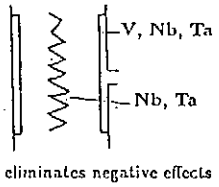

Making an atomizer of the same material eliminates negative effects from the evaporation of foreign materials onto the membrane.

There were *two key points* that required further examination:

1. What is the upper limit of flux density at superpermeation, and is this sufficient for fusion applications?

2. Will the membrane operate reliably enough, and particularly, in the presence of the expected gas impurities ?

THE IDEA OF SUPERPERMEABILITY

Potential diagram of an *"H – metal membrane"* system

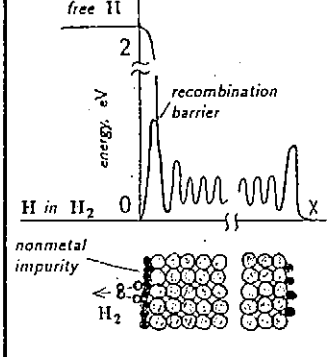

The superpermeable membrane is a "trap" for hydrogen. Suprathermal hydrogen particles pass freely into the metal, *in spite of* the barrier generated by a monatomic nonmetal film, but their back release through recombination into molecules is effectively suppresses by this very barrier.

Physical factors limiting the flux density

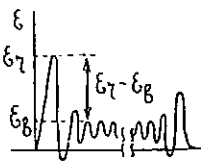

Disolved atoms overcome the recombination barrier only by associating in pairs: a second order process. → The trapping efficiency decreases with flux density rise. → Superpermeability may be destroyed. Corresponding flux density upper limit is determined by the surface barrier:

$j_{max} \sim \exp 2(\varepsilon_r - \varepsilon_B)/(RT)$

A.I. Livshits. Sov. Phys Tech. Phys. 21 (1976) 187.

It is this mechanism that usually limits the flux density. But it is not true for the V group metals where this barrier is inherently very high.

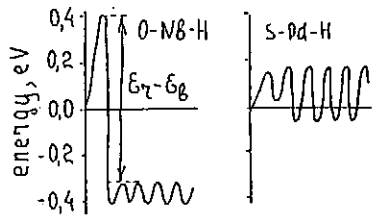

Physical factors limiting the flux density

An exact equation refering to this mechanism,

$j_{max} = \frac{1}{L^2}\frac{D^2}{K_r}$ — D diffusion coefficient; K_r recombination constant; L thickness

if applied to NB results in

$j_{max} \geq 10^{20}\,cm^{-2}s^{-1}$, at $L \approx 10^{-1}$ mm and $T \leq 900$ K,

when taking into account our experimental data for K_r

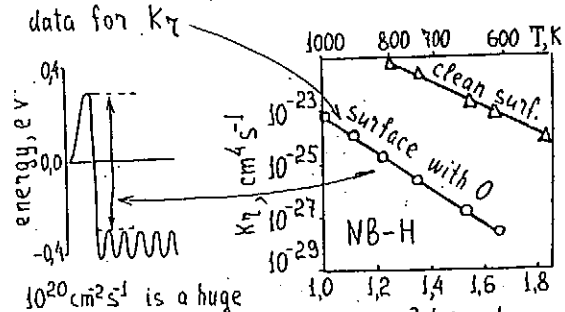

$10^{20}\,cm^{-2}s^{-1}$ is a huge flux density (~70 W/cm² are released even in the case of thermal atoms). Thus this mechanism put no actual limitations.

Physical factors limiting the flux density
Effect of induced re-emission

The barrier inhibits only thermal re-emission, and not the re-emission induced by energetic hydrogen. So superpermeation is only possible when the rate of induced re-emission is negligible.

In the case of thermal atoms, the induced re-emission is the Eley-Rideal recombination which goes due to the free atom chemical energy.

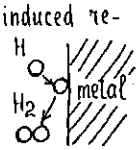

The Eley-Rideal recombination is negligible when the surface coverage with H atoms is much smaller than a monolayer. Correspondingly, it is the flux which leads to a monolayer coverage that will be a maximum one:

$j_{max} \approx 10^{15} \times 10^{13} \exp -\frac{2(\varepsilon_r - \varepsilon_{ad})}{RT}\,(cm^{-2}s^{-1})$

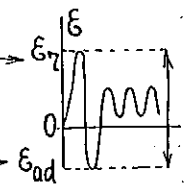

Flux density limitations due to the induced (Eley-Rideal) re-emission (continuation)

$j_{max} \approx 10^{15} \times 10^{13} \exp -\frac{2(\varepsilon_r - \varepsilon_{ad})}{RT}\,(cm^{-2}s^{-1})$

$T \geq 800$ K

$\varepsilon_r - \varepsilon_{ad} \leq 0{,}6$ eV

$\rightarrow j_{max} \geq 10^{20}\,cm^{-2}s^{-1}$ (no limitations)

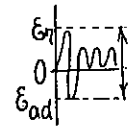

This condition is usually met, as indicated by our experimental studies of the potential reliefs of H-metal systems with controlled surface:

H-impurity-metal system	H-S-Pd	H-C-Pd	H-O(?)-NB	H-nt.sf-Fe
$(\varepsilon_r - \varepsilon_{ad})$ eV	$\leq 0{,}42$	$\leq 0{,}42$	$\leq 0{,}56$	$\leq 0{,}55$

That means that the monatomic nonmetal films responsible for the barrier dramatically reduce at the same time the depth of adsorption well. As a result, the induced re-emission would not practically limit the flux density, at least, in the case of thermal atoms.

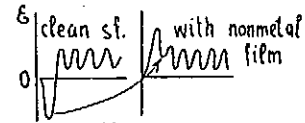

Physical factors limiting the flux density

Limitations due to the limitations on concentration.

Both the diffusion flux through the membrane

$j_{dif} \leq D c_{max}/L$ — V, NB and Ta: $D \approx 10^{-4}\,cm^2 s^{-1}$ at $T \geq 800K$

and the desorption flux through the outlet boundary

$j_{des}^{out} \leq K_r^{out} c_{max}^2$ — $K_r^{out} \geq 10^{-24}\,cm^4 s^{-1}$ at $T \geq 800K$ according to our membrane experiments with NB

are limited by a maximum permissible hydrogen concentration, C_{max}, in metal.

If we take the maximum tolerable concentration in NB (V, Ta) of 5at %, we come to coinciding estimats of maximum flux density from the both relations:

$$j_{max} \approx 10^{19}\,cm^{-2} s^{-1} \quad \text{at } L \approx 0{,}3\,mm,\ T \geq 800K$$

Apparently, this value should be considered as the theoretical flux density upper limit at least with thermal atomic hydrogen.

MN-1 DEVICE

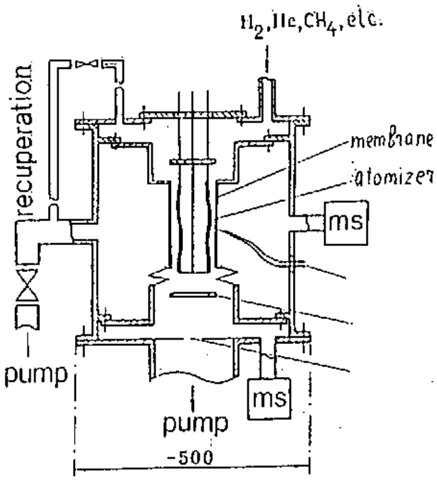

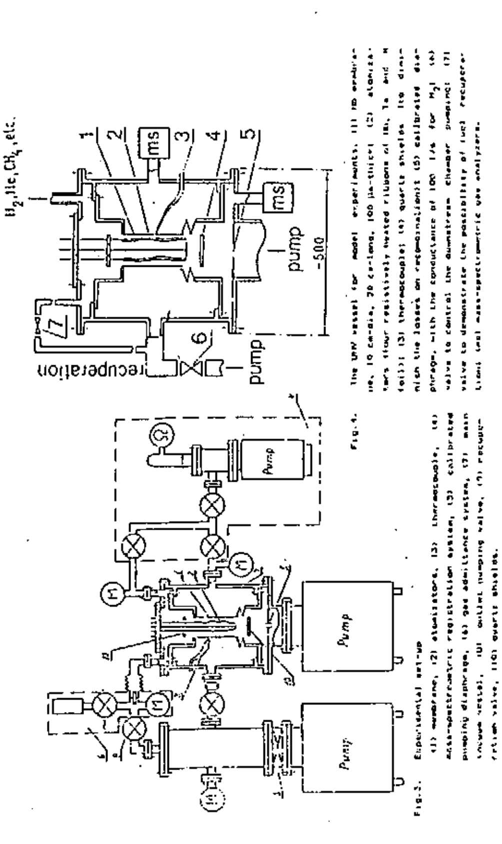

Experimental scheme

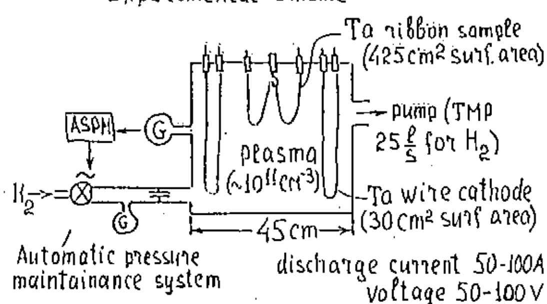

Two experimental modes:

1. The cathode is kept hot, but the discharge is switched off. In this case, the cathode serves as a hydrogen atomizer.
2. The discharge is switched on, the sample is at a floating potential. Different sorts of hydrogen particles can be absorbed along with atoms in this case.

Experimental procedure is based on the sharp dependence on temperature of the Ta ability to absorb hydrogen. Initially an H_2 pressure is established, then the atomizer or discharge is switched on while the sample temperature is high enough for the steady-state concentration of absorbed hydrogen to be negligible. After that, the sample temperature is quickly reduced to the operational one, and the sample starts to absorb the hot hydrogen. Thus, the absorption is started by a sample temperature decrease in the hot hydrogen.

High flux density problem: experiment

Superpermeation experiments with flux densities no higher than $5 \cdot 10^{14}\ cm^{-2}s^{-1}$ were only staged until very recently.

Our latest experiments:

Bonch-Bruevich University + Kurchatov Centre

Bonch-Bruevich Univ. + Ecole Polytechnique (France)

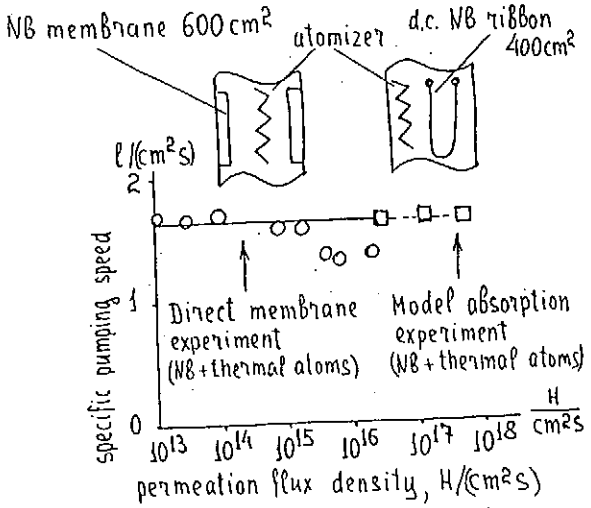

High flux density problem: experiment

The transient times and steady state concentrations in our membrane and absorption experiments behaved themselves in accordance with the model that we were using at our estimations for the maximum flux densities

$$\tau = \sqrt{\frac{L}{2 j K_r^{out}}} \sim \sqrt{\frac{L}{j}} \exp \frac{G_r^{out} - \Delta H}{RT}$$

$$C_\infty = \sqrt{j / K_r^{out}} \sim \exp \frac{G_r^{out} - \Delta H}{RT}$$

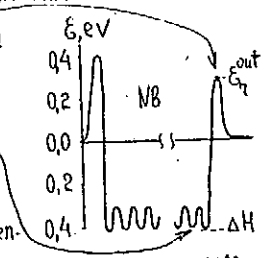

That pertains, in particular, to the temperature and flux dependences and such dependences are preserved up till the highest flux densities experimentally examined. That means that these experimental data indicate at the actual possibility of reaching the flux density given by above theoretical estimations. It was only experimental equipment limitations that stoppe our further advancement to the highest flux densities.

MEMBRANE SYSTEM IN THE UP-TO-DATE ITER CONCEPT

In order to take away a major part of tritium, the membrane should pump D/T much faster than the cryopump, while one must at the same time maintain high enough a pressure in the divertor.

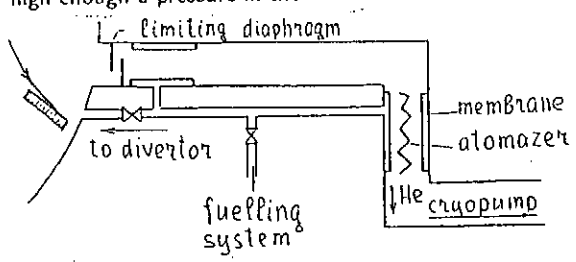

There are two ways to achive the latter:

(1) To cut the conductivity of the duct before the membrane down to a minimum value that would still guarantee the required pumping speed for He, or,

(2) To return a part of D/T back into divertor.

What shall we have with the first way, if we employ only the distant membrane with an atomizer?

MEMBRANE SYSTEM IN THE UP-TO-DATE *ITER* CONCEPT

Proceeding from:

Specific membrane pumping speed:
~ 16 m^3/s *per* 1 m^2

Total cryopump speed:
2 – 200 m^3/s (accepted in ITER at the moment)

If we occupy with the membranes:
1.6 m length in each of the 24 ducts

We get:

D/T separation efficiency:
90 – 99.9%

Total consumption of power:
0.05 – 5 MW

Total tritium inventory:
≤ 1.5 g

Attainable degree of compression:
$10^3 – 10^4$

Distribution of D/T concentrations and fluxes at the maximum fuelling rate and maximum cryopump speed

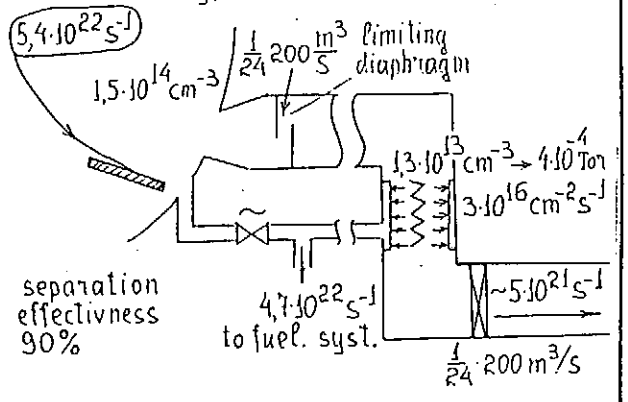

The gas pressure near the membrane is rather low ($\sim 4\cdot10^{-4}$ Torr) even at the maximum fuelling rate (due to a very high membrane pumping speed). The flux density will not exceed $3\cdot10^{16}cm^{-2}s^{-1}$, i.e., a value already examined in the direct superpermeation experiments.

CONCLUSIONS

(1) The *V Group* metals are the most suitable materials for superpermeable membranes operating with high flux densities.

(2) The theoretical upper limit for flux density at superpermeation is $\sim 10^{19}\ cm^{-2}\ s^{-1}$.

(3) A flux density of $3 \times 10^{16}\ cm^{-2}\ s^{-1}$ was obtained in direct superpermeation experiments.

(4) Superpermeable membranes of a reasonable size may secure separation of 90 – 99.9% of D/T within the up-to-date *ITER* concept with the permeation flux densities already reached.

VALIDITY OF NIOBIUM AS SUPERPERMEABLE MEMBRANE

V. Bandurko, M. Yamawaki, K. Yamaguchi
Nuclear Engineering Research Laboratory, University of Tokyo

In the last time several technical design have been proposed to particles pumping in the divertor chamber, which allows of the employment of superpermeable membranes. Hydrogen superpermeation through a pure iron membrane exposed to H-atoms have been investigated by Hackfort et. al.[1]. Livshits proposed to make the membrane and atomizer of the V Group metals [2]. Several experimental facts which are associated with the surface chemical composition were obtained by Livshits' group [2,3]: no "permeation spike" was observed under the H-ion bombardment; admitting of C_2H_2 at the inlet side leads to adramatic increase in permeability of the membrane due to the deposition of a carbon film at C_2H_2 pirolysis; there was no appreciable change in the hydrogen pumping speed during the CH_4 admission. A possible explanation of the observed facts was proposed by Livshits et.al., but they did not perform any surface analysis during permeation measurements. The attempt of ivestigation the correlation between the permeation rate and surface impurity composition was undertaken in present study.

The ion and gas driven deuterium permeation behavior in Nb was investigated (Figs. 1-4). It was shown that IDP and GDP are the recombination-recombination limited process. Recombination rate coefficient evaluated from the measured permeation rate coincide with the calculated result using the expression of Pick and Sonnenberg (Fig. 5). The Auger electron spectroscopy revealed that the specimen surface is covered by S, C and O. GDP rate through Nb depends on C and O surface cocentration. Increasing of C surface concentration suppress GDP rate (Fig. 6). In the presence O on the Nb surface no appreciable change in the C concentration was observed during CH_4 admission that can explain the deuterium permeation behavior at the presence of methane (Fig. 7).

Referances.

1. H. Hackfort et.al.- J.Nucl.Mater. 144(1987)10-16.
2. A.O. Busnyuk, A.I. Livshits, M.E. Notkin.- Proc. 2nd Japan-CIS Workshop IFPFM, St.-Petersburg (1994) 58-74.
3. A.I. Livshits et.al.- J.Nucl.Mater. 178(1991) 1.
4. M. Yamawaki et.al.- J.Nucl.Mater. 122&123(1984)1573.

VALIDITY OF NIOBIUM AS SUPERPERMEABLE MEMBRANE

V.Baranko, H.Yamawaki, K.Yamaguchi
Nuclear Engineering Research Laboratory, University of Tokyo

Experimental facts obtained by Livshits' group:

- no "permeation spike" was observed under the H-ion bombardment;

- admitting of C_2H_2 at the inlet side leads to suppression of recmission and to a dramatic increase in permeability of the membrane due to the deposition of a carbon film at C_2H_2 pirolysis;

- there was no appreciable change in the hydrogen pumping speed during the methane admission.

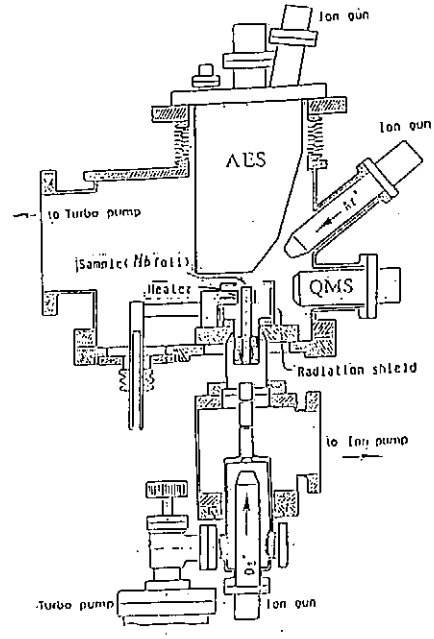

Fig. 1. A schematic drawing of the permeation system.

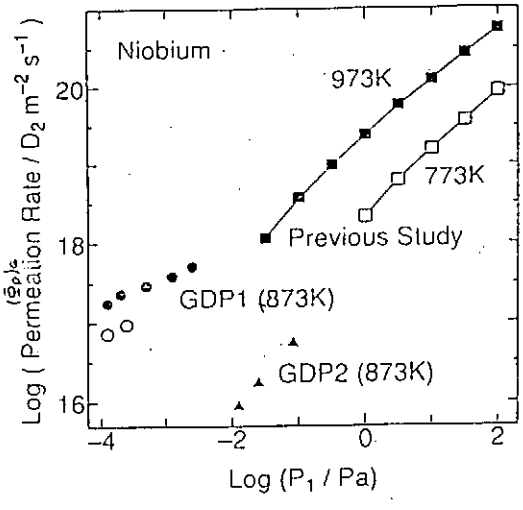

Fig.1: Dependence of gas driven permeation (GDP) rate, $(\Phi_P)_G$, on the D_2 pressure, P_1, in the upstream-side. GDP 1 and GDP 2 are obtained in the present study, which are compared with the result of previous study [4] denoted by the rectangles.

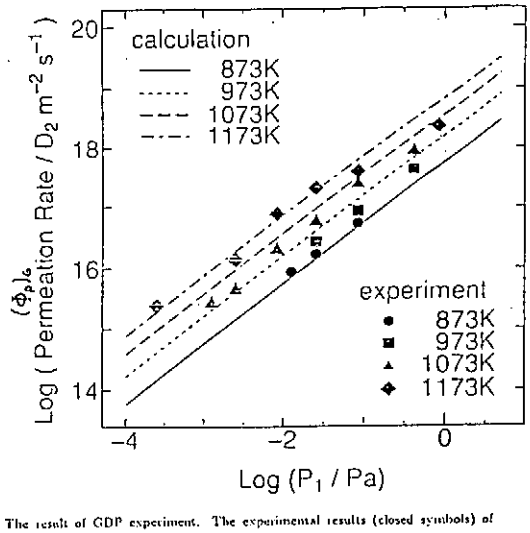

Fig.2: The result of GDP experiment. The experimental results (closed symbols) of $(\Phi_P)_G$ are plotted as a function of P_1 for four different temperatures. The lines are the calculated values of $(\Phi_P)_G$ using the theoretical formula.

$$(\Phi_P)_G = \frac{(k_R)_1(k_R)_2}{(k_R)_1 + (k_R)_2} K_S^2 P_1 \quad (1)$$

In the above equation, $(k_R)_1$ and $(k_R)_2$ are the recombination rate coefficients for upstream-side and downstream-side, respectively, $K_S = (K_S)_0 \exp(-E_S/RT)$ is the hydrogen solubility with E_S being the heat of solution.

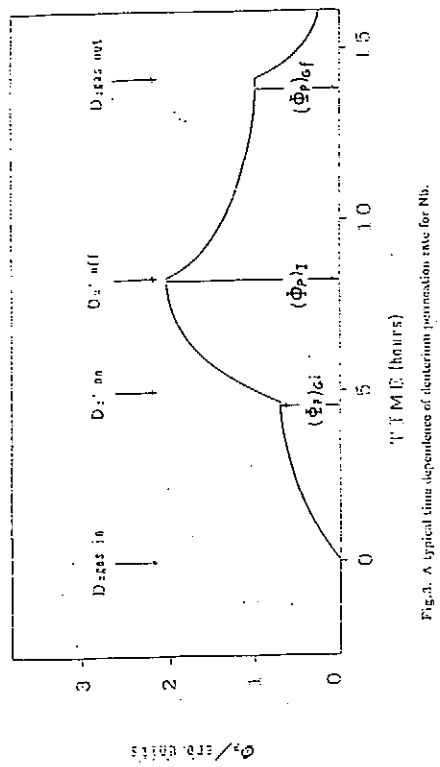

Fig.3. A typical time dependence of deuterium permeation rate for Nb.

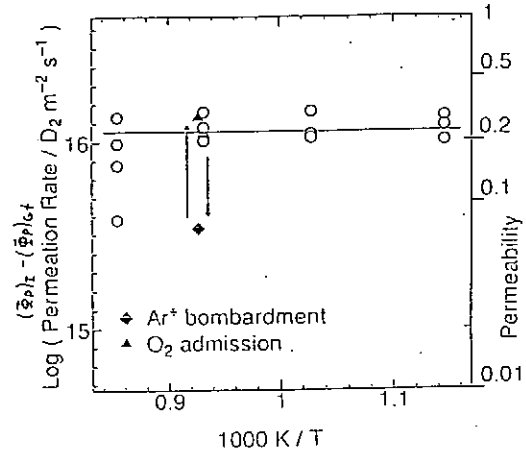

Fig.4: Temperature dependence of ion driven permeation (IDP) rate, $(\Phi_P)_I$, through niobium, where the ion flux (ϕ_P) and pressure (P_I) of deuterium were 9.4×10^{16} D_2 m^{-2} s^{-1} and 7.5×10^{-3} Pa, respectively.

$$(\Phi_P)_I - (\Phi_P)_{GI} = \frac{(k_R)_2}{(k_R)_1 + (k_R)_2}\frac{\phi_P}{2}, \qquad (\Phi_P)_{GI} = (\Phi_P)_G \qquad (2)$$

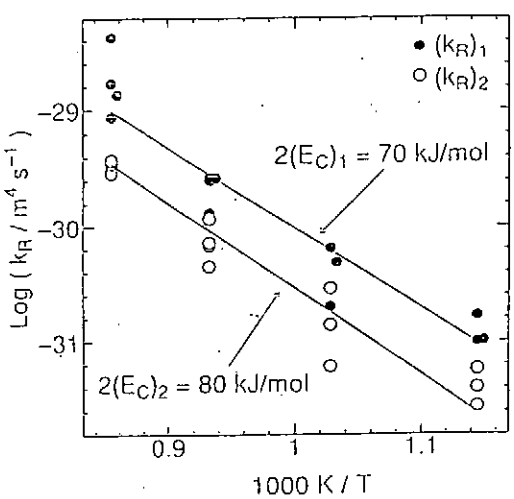

Fig.5: Recombination rate coefficient, k_R, of niobium for upstream-side ($(k_R)_1$; closed symbols) and downstream-side ($(k_R)_2$; open symbols).

$$k_R = (k_R)_0 \exp\frac{2(E_s - E_C)}{RT} \qquad (3)$$

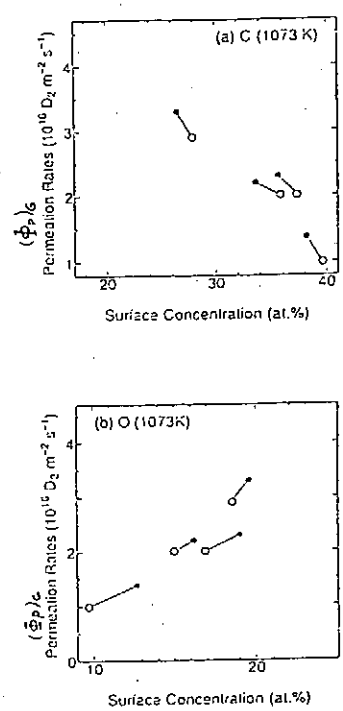

Fig.6: Correlation between deuterium permeation rate, $(\Phi_P)_G$, and surface impurity composition at 1073 K; (a) carbon (C) and (b) oxygen (O).

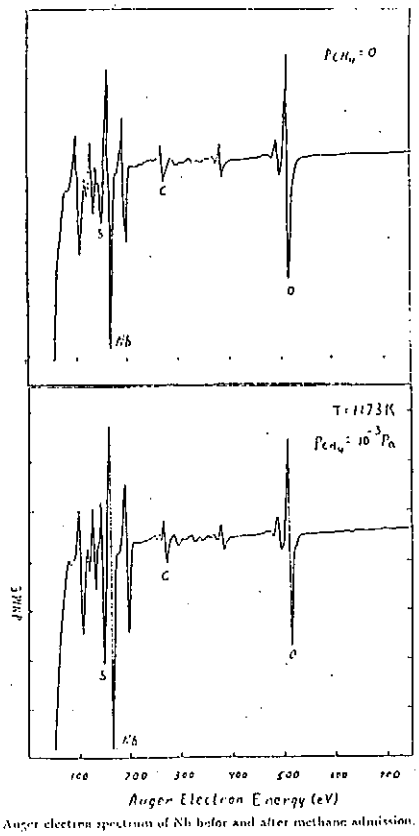

Fig.7. Auger electron spectrum of Nb befor and after methane admission.

Summary:

— The ion and gas driven deuterium permeation experiments for Nb with surface impurity control were performed. It was shown that IDP and GDP are the recombination - recombination limited process.

— Recombination rate coefficient evaluated from the experiments coincide with the calculated result using the expression of Pick and Sonnenberg.

— GDP rate through Nb depends on C and O surface concentration. Increasing of C surface concentration suppress GDP rate. O leads to increasing of GDP rate.

— In the presence O on the Nb surface no appreciable change in the C concentration was observed during methane admission that can explain the deuterium permeation behavior at the presence of methane.

Isotopic Effects on Hydrogen Trapping and Permeation in Plasma Facing Materials

E. Abramov and D. Eliezer

Ben-Gurion University of the Negev, P.O. Box 653, Beer-Sheva, ISRAEL

Abstract

The differences between tritium and hydrogen on deuterium regarding their diffusion and solubility in plasma facing materials are discussed. The main differences might arise from dissociation and recombination coefficients on the surface. Considerable contribution is also tritium decay to helium follow by clusters and bubbles formation.

Special examination should be conducted regarding the isotopic effects in beryllium, mainly due to the interaction of hydrogen isotopes with BeO.

Speculative curve for long-term tritium permeation through first-wall materials is suggested.

Isotopic Effects on Hydrogen Trapping and Permeation in Plasma Facing Materials

E. Abramov and D. Eliezer

Ben-Gurion University of the Negev
P.O. Box 653, Beer-Sheva, ISRAEL

The Differnces Between Tritium and Hydrogen / Deuterium

Diffusion DT / DH $\alpha \sqrt{MH} / \sqrt{MT} = 1/\sqrt{3}$

Solubility Dissociation rate might be higher

Surface behavior Recombination coefficient might be lower

Decay to Helium

Trapping characteristics ?

Trapping of Tritium due to the presence of Helium

- Increases effective tritium solubility
- Decreses effective tritium diffusivity

Trapping is affected by:

- host material
- helium content
  helium configuration
- thermal cycling
- existance of other traps for tritium

The nature of trapping

- Chemisorption - like trapping at the bubbles wall
- Interaction with the strains associated with:
  * Helium bubbles
  * Dislocation loops

Short - circuit diffusion path

- microcracks
- intrconnected bubbles
- elongated bubbles along grain boundaries
- surface blistering and exfoliation

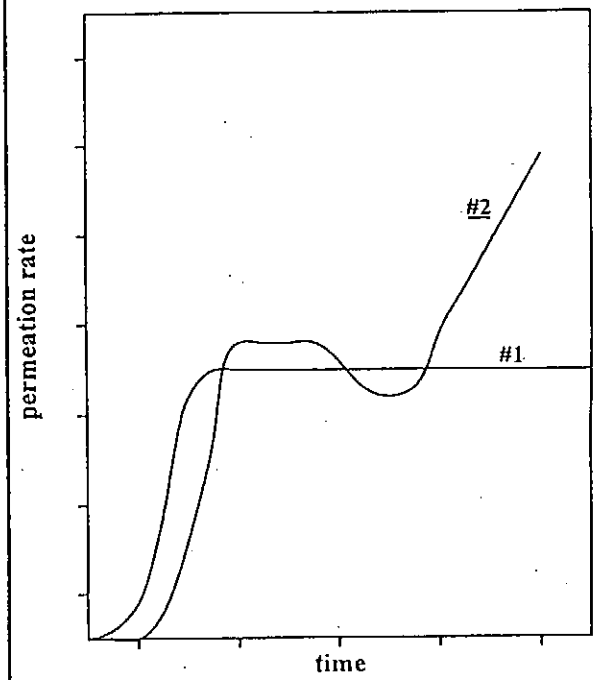

Speculative curves for hydrogen isotope permeation through F.W. materials.
#1 normal hydrogen permeation
#2 long term tritium permeation

Tritium in Beryllium

- Characteristic of BeH vs. BeT
- Intreraction with BeO
- Formation of Tritium bubbles

- Lack of data needed

Tritium Migration in Group-V Metals under Thermal and Electric Potential Gradient

M. Sugisaki and K. Hashizume
Kyushu University, Department of Nuclear Engineering
Faculty of Engineering, Fukuoka 812, Japan

It is important to examine whether isotope effect exists or not on diffusion process of hydrogen isotopes in plasma facing materials under fusion reactor conditions, because accurate estimation of diffusion flux of each hydrogen isotopes is essential to evaluate the hydrogen isotope recycling rate and tritium permeation rate. From such viewpoints, we have studied the diffusion behavior of hydrogen isotopes in group-V metals (V, Nb and Ta) under thermal and electric potential gradients.

In the present paper, our recent experimental results of those studies are given. The details of thermomigration and electromigration experiments are explained and the characteristic points of the experimental results are summarized. On the basis of these experimental data, the magnitude of contributions of thermomigration and electromigration are numerically evaluated by supposing the possible values of thermal and electric potential gradients and the followings are concluded:

(1) The contribution of thermomigration should not be neglected when the thermal gradient larger than 100 K/cm exists; in particular it is largest in the case of tritium. Then, the isotope dependence of Q* should be taken into consideration.

(2) The contribution of electromigration should not be neglected when the electric current larger than 1000 A/cm^2 exists continuously in the definite direction.

Tritium Migration in Group-V Metals
under Thermal and Electric Potential Gradient

GOALS

(1) to accumulate the experimental data of hydrogen isotopes concerning the diffusional behavior in metals and alloys under some potential gradients, in particular data for tritium.
(2) to understand the diffusional behavior of hydrogen isotopes, and in particular to understand the microscopic origin of isotope effect.

IMPACTS

(1) Diffusion data are important from aspects of hydrogen isotope recycling and tritium safety problems.
(2) Hydrogen isotopes are most appropriate to study isotope effect because of their largest relative mass difference.

Diffusion Equation under
Thermal and Electric Potential Gradients

$$J = -D\left(\frac{\partial C}{\partial x} + \frac{Q^* C}{RT^2}\frac{\partial T}{\partial x} + \frac{Z^* eC}{RT}\frac{\partial \phi}{\partial x}\right)$$

ordinary diffusion | thermo-migration | electro-migration

D : diffusion coefficient
Q* : heat of transport
Z* : effective valence

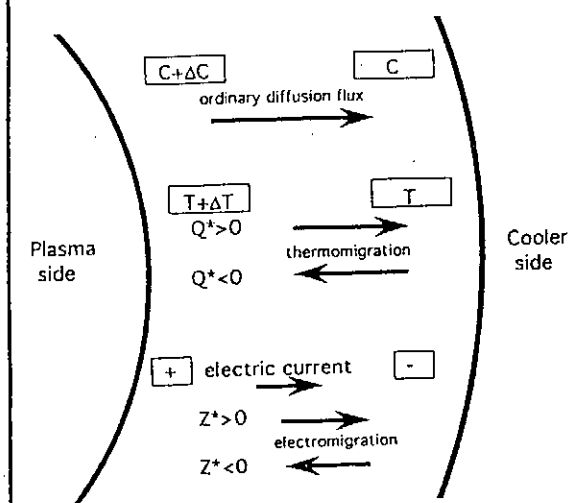

Thermomigration of Hydrogen in Metal
& Determination of Q*

Initial State

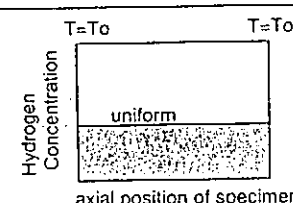

Thermal Gradient

Stationary State

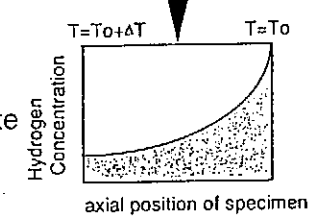

Hydrogen Flux J

$$J = -D\left(\frac{dC}{dx} + \frac{CQ^*}{RT^2}\frac{dT}{dx}\right)$$

In a Stationary State (J = 0)
Distribution C(x)

$$\ln C(x) = Q^* / (RT(x)) + \text{const.}$$

Electromigration of Hydrogen in Metals & Determination of Z*

Initial State

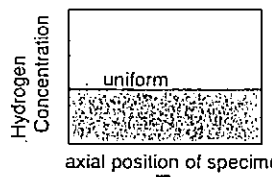

Electric Field E

Stationary State

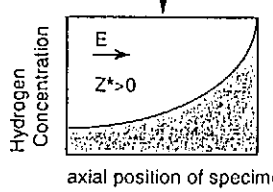

Hydrogen Flux J

$$J = -D\left(\frac{dC}{dx} - \frac{Z^*eC}{RT}E\right)$$

In a Stationary State (J = 0)
Distribution C(x)

$$\ln C(x) = Z^*eEx / (RT) + \text{const.}$$

Experimental condition:

Specimen size : 2 mm in diameter; 50 mm in length
Initial hydrogen concentration : 0.5 at%, α-phase
Temperature region : 320K-550K

(1) thermomigration:
thermal gradient : 10 K/cm

(2) electromigration:
electric bias : 5 mV/cm
electric current : 150 A/cm²

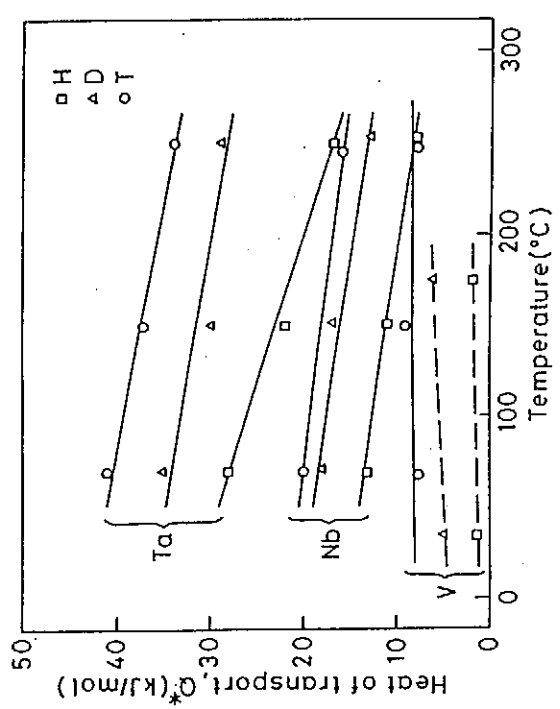

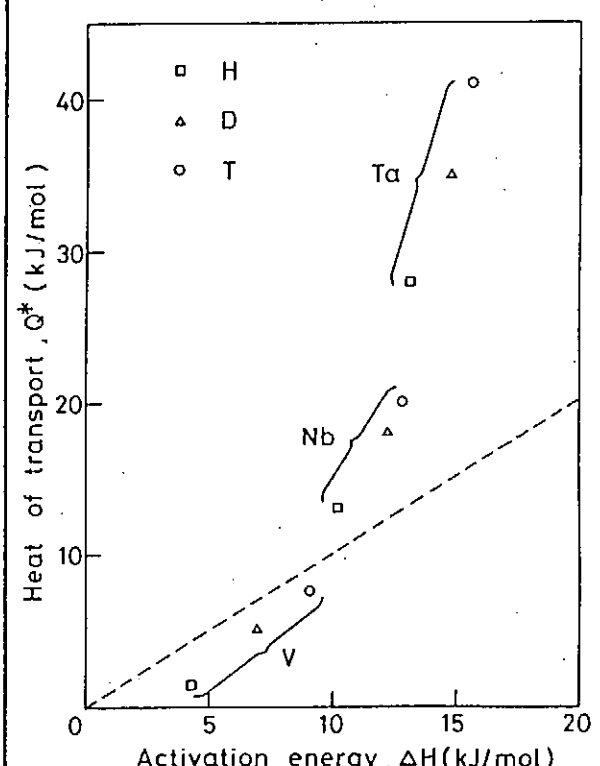

Characteristics of Q*

(1) Q* is positive; i.e. hydrogen isotopes are driven to colder side.

(2) Isotope dependence is appreciably large.

Q*(T) > Q*(D) > Q*(H)

Tritium data of Q* is important.

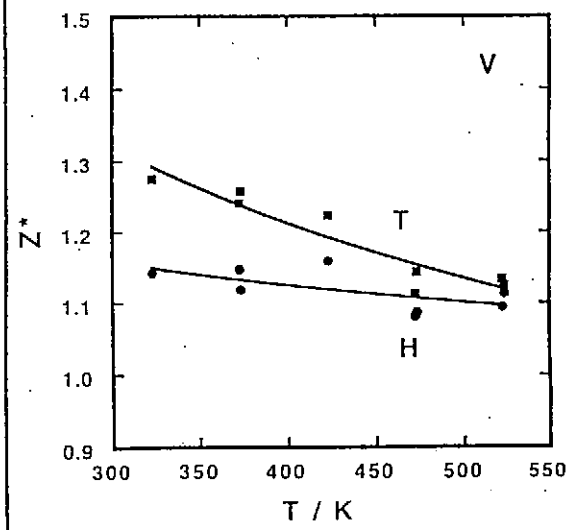

Temperature dependence of Z* of protium and tritium in V

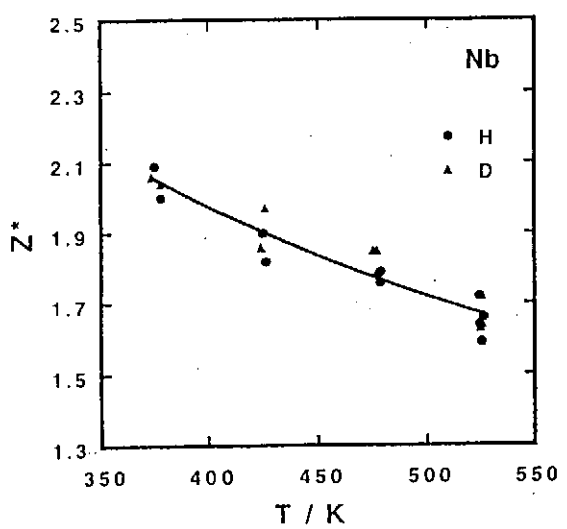

Temperature dependence of Z* of protium and deuterium in Nb

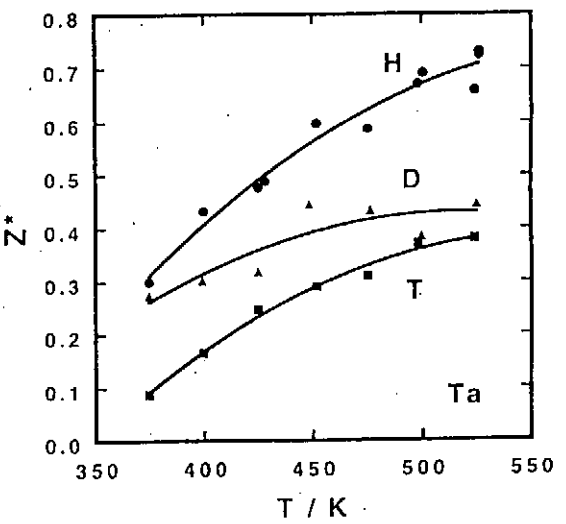

Temperature dependence of Z* of hydrogen isotopes in Ta

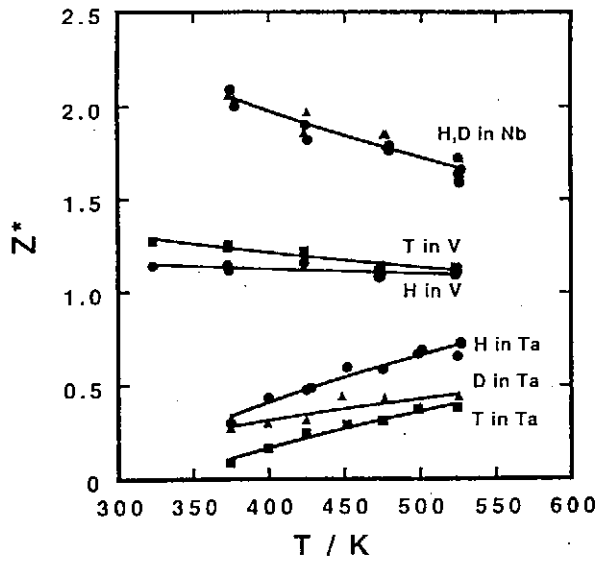

Temperature dependence of Z* of hydrogen isotopes in group-V metals

Characteristics of Z*

(1) Z* is positive and not necessarily +1. Hydrogen isotopes are driven in the direction against electric current.
(2) Z* is dependent upon temperature.
(3) Common trend of isotope dependence is not observed.

$$J = -D\left(\frac{\partial C}{\partial x} + \frac{Q^* C}{RT^2}\frac{\partial T}{\partial x} + \frac{Z^* eC}{RT}\frac{\partial \phi}{\partial x}\right)$$

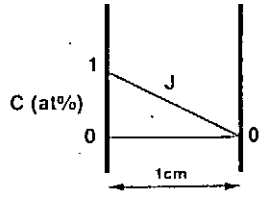

Q* : 30 kJ/mol
Z* : 1
T_{av} : 700 K
ρ (electric resistivity of material) : 50 μΩcm

$$J = J_C + J_T + J_E$$

$\left|\frac{\partial C}{\partial x}\right|$ = 1 at% /cm, $\left|\frac{\partial T}{\partial x}\right|$ = 10 K / cm, I = 100 A / cm²

$$|J_C| : |J_T| : |J_E| = 1 : 0.04 : 0.04$$

$\left|\frac{\partial C}{\partial x}\right|$ = 1 at% /cm, $\left|\frac{\partial T}{\partial x}\right|$ = 100 K/cm, I = 1000 A/cm²

$$|J_C| : |J_T| : |J_E| = 1 : 0.4 : 0.4$$

Conclusions

(1) The contributions of thermomigration should not be neglected when the thermal gradient larger than 100 K/cm exists. The isotope dependence of Q* should be taken into consideration.

(2) The contribution of electromigration should not be neglected when the electric current larger than 1000 A/cm² exists continuously in the definite direction.

2nd Int. Workshop on Tritium Effect in Plasma Facing Components
19-20 May 1994, Nagoya University Japan

INTERACTION OF ATOMIC HYDROGEN WITH METALS

Takashi Kiriyama and Tetsuo Tanabe
Department of Nuclear Engineering, Osaka University,
Yamada-oka, Suita Osaka 565, Japan
TEL +81-6-879-7884 FAX +81-6-875-5696

Although hydrogen reflection is well understood physical phenomena, those for low energy incidence especially below 100eV is still an open question both theoretically and experimentally.

Hydrogen physisorption and chemisorption at very low temperatures have been one of the most important subject in surface science. And particularly such metals like Ni, Pd and W have been extensively studied. Energetic hydrogen atoms or ions, owing to its high energy states compared to molecular hydrogen, can easily penetrate to the bulk over-through the surface. Such implanted hydrogen often desorbed more easily having hyper-thermal energy than chemisorbed one which makes the analysis of behavior of implanted hydrogen very difficult. On the other hand, determination of direct reflected hydrogen at the surface is not so difficult as the behavior of implanted hydrogen and also theoretical estimation using an elastic potential fits very well with experiments.

In case the initial kinetic energy of injected hydrogen becomes lower, one can not get the beam source easily to make experiment nor rely on an elastic potential often used in Monte-Carlo simulation such as TRIM. Thus the estimation of reflection coefficient becomes difficult too.

However if the initial energy state of hydrogen is near the potential barrier, it may be directly reflected. In this respect, endothermic hydrogen occluders like Pt and W do not allow hydrogen to penetrate to the bulk even if the barrier dose not exist.

In the present work, interaction of atomic hydrogen with metals is studied through the determination of hydrogen retention in metals after exposing to atomic hydrogen by means of thermal desorption, in terms of Z numbers and heat of solutions at temperatures above 400K where one can neglect physisorption and chemsirobed site always occupied.

At 410K initial retention coefficients(T) normalized to incident atoms are 0.1 to 0.5 and above 0.6 for endothermic and exothermic hydrogen occluding metals, respectively. On the other hand no clear relation between T and Z number is observed comparing with reflection coefficients for high energy ion injection. This indicates the importance of chemical effect in reflection of low energy hydrogen. With increasing the temperature T is markedly reduced in the endothermic occluders, while it stays rather constant in the exothermic ones. Since the kinetic energy of the atomic hydrogen presently used is around 0.3 eV, atomic hydrogen is very likely to directly reflected at those metals of which heat of solution are over this value. Unfortunately we could not distinguish the atomic hydrogen directly reflected at the surface from the reemitted molecules once absorbed and recombined at the surface. Further studies on an observation of directly reflected atoms and a measurement of their energy distributions are necessary.

2nd Int. Workshop on Tritium Effect in Plasma Facing Components
19-20 May 1994, Nagoya University Japan

INTERACTION OF ATOMIC HYDROGEN WITH METALS

Takashi Kiriyama and Tetsuo Tanabe, Osaka University

MOTIVATION
- Question to reflection of low energy hydrogen at higher temperatures
- No experimental data
- Adequacy of theoretical calculation

DIFFICULTY
- Low energy hydrogen source
- Distinction between reflected atoms and reemitted molecules

POINT
- Surface barrier
- Energy state or temperature of reflected atoms and reemitted molecules

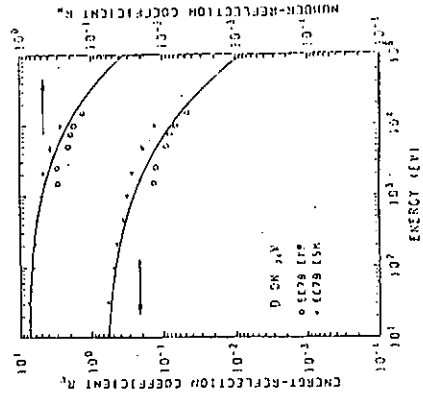

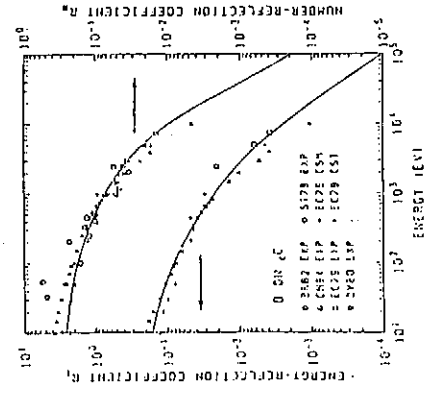

I. Chorkendorff et al. / Hydrogen implantation in Ni(111)

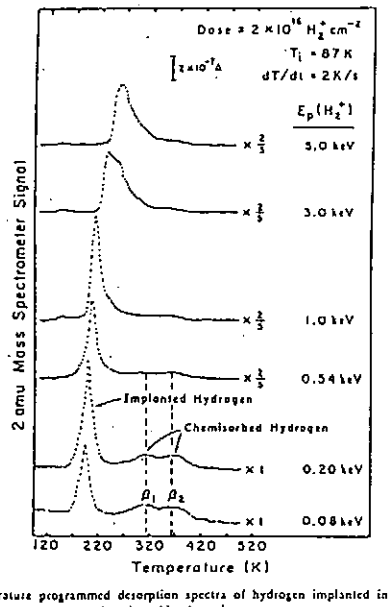

Fig. 1. Temperature programmed desorption spectra of hydrogen implanted in Ni(111) as a function of implantation energy.

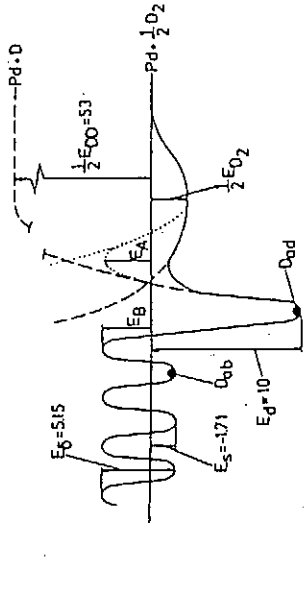

Fig. 2. Schematic potential energy diagram for the system D/Pd (energies in kcal/mole).

Figure 1 : Time sequences of deuterium reemission rate for the specimens exposed to oxygen gas at 1.3×10^{-5} Pa before measurements. Exposure is given in Langumiur unit (1×10^{-6} torr s)

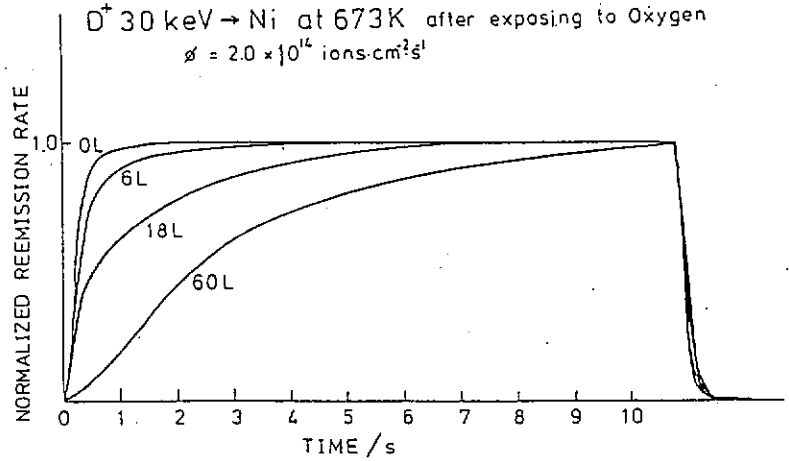

Fig. Sequence of TOF curves with sulphur coverage θ_S as parameter. P_{O_2} = 400 Torr; measuring time per curve between 10 and 60 min (all normalized to 60 min).

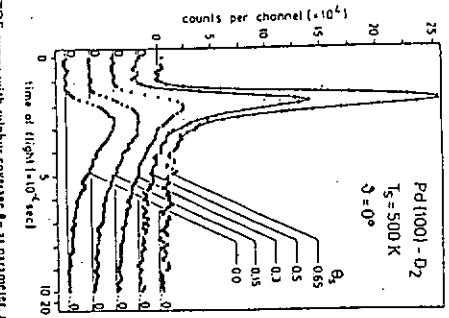

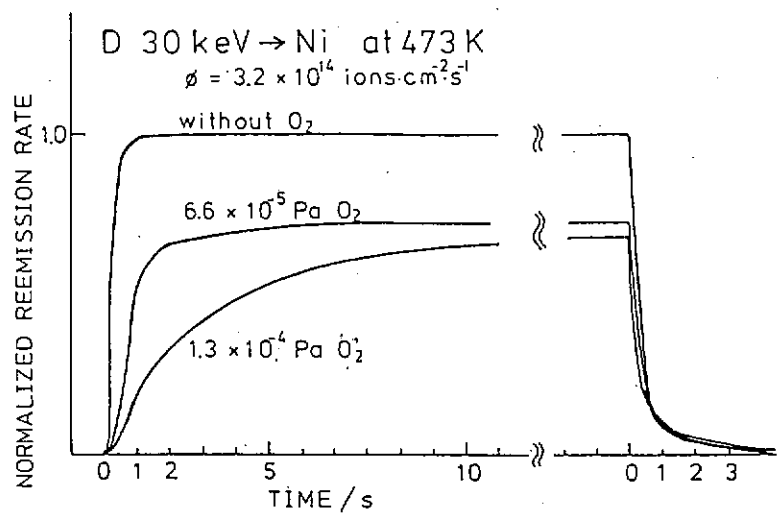

Figure 2 : Time sequences of deuterium reemission implanted into Ni under oxygen atmosphere.

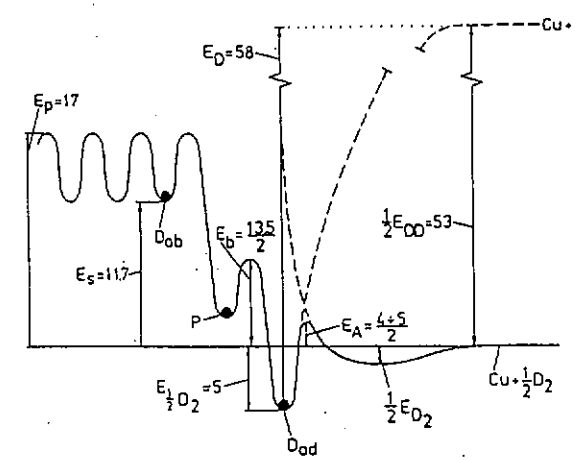

Fig. One-dimensional potential energy diagram for D_2/Cu and D/Cu. All energies are in kcal/mole per *D atom*.

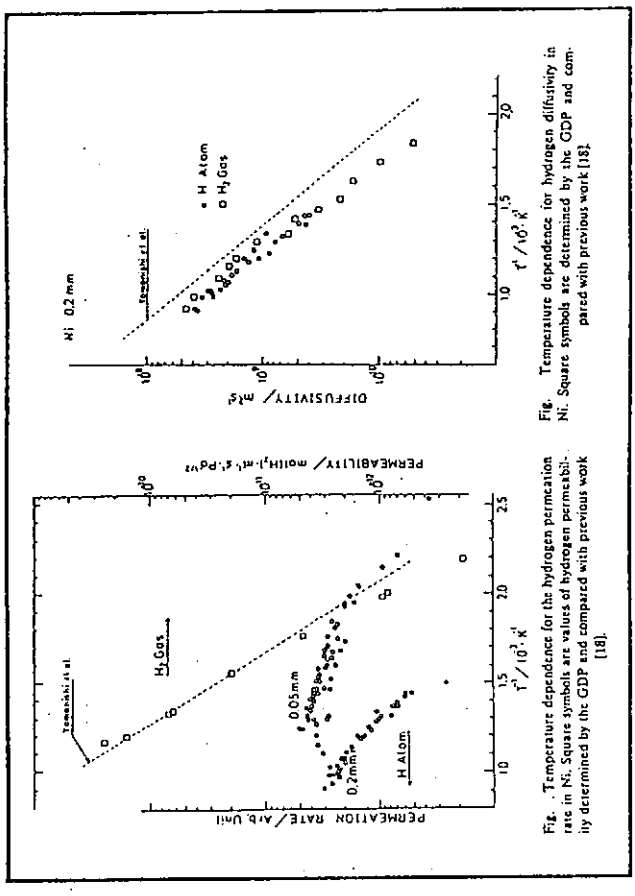

Fig. Temperature dependence for hydrogen diffusivity in Ni. Square symbols are determined by the GDP and compared with previous work [18].

Fig. Temperature dependence for the hydrogen permeation rate in Ni. Square symbols are values of hydrogen permeability determined by the GDP and compared with previous work [18].

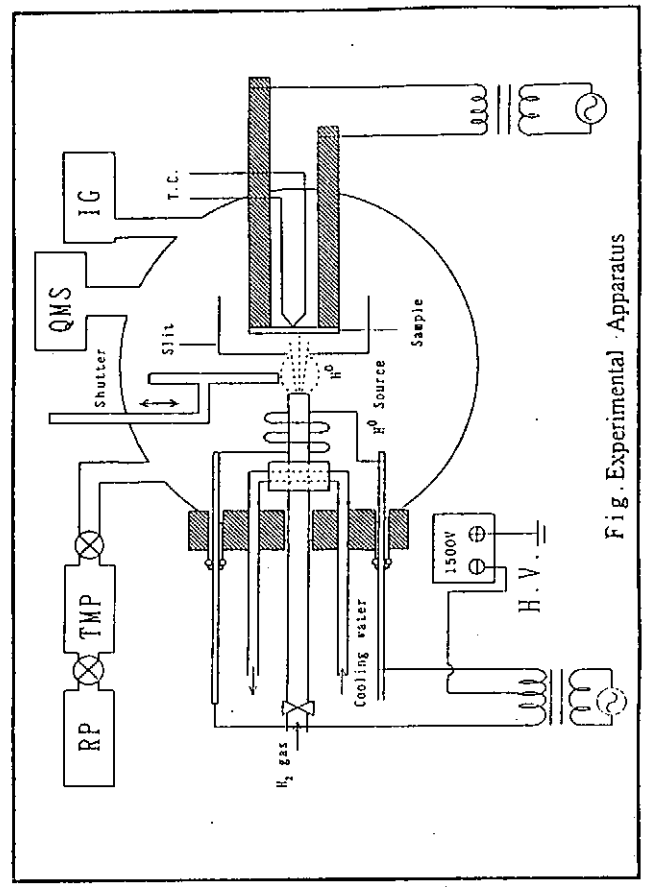

Fig. Experimental Apparatus

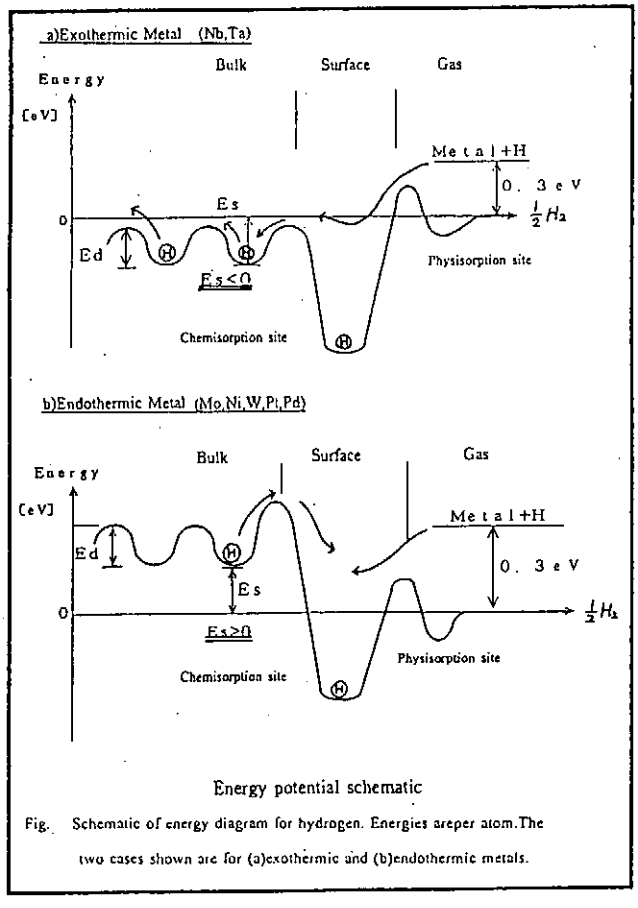

Energy potential schematic

Fig. Schematic of energy diagram for hydrogen. Energies areper atom.The two cases shown are for (a)exothermic and (b)endothermic metals.

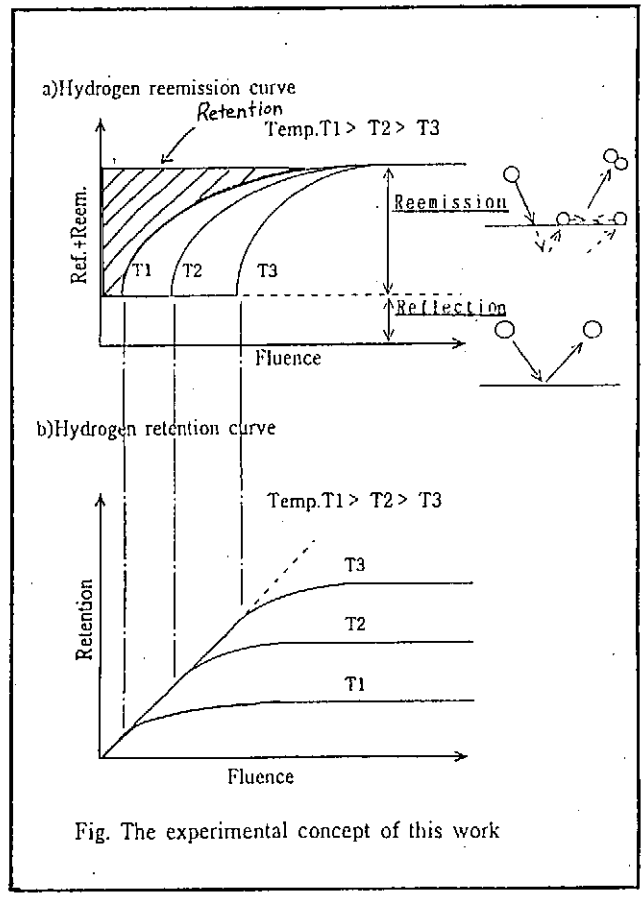

Fig. The experimental concept of this work

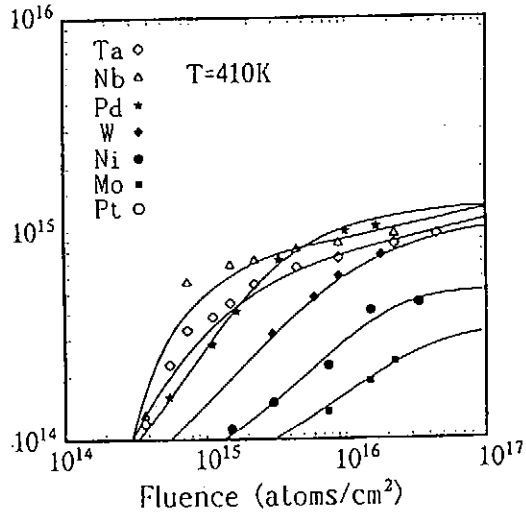

Fig. Fluence dependence of hydrogen retention for high Z metals at 410K.

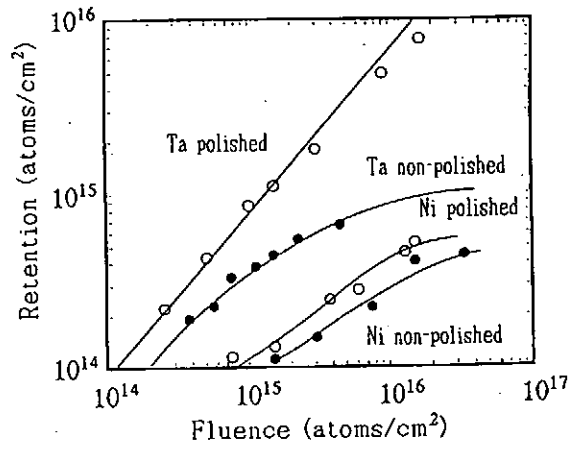

Fig. Fluence dependence of hydrogen retention for Ta,Ni with non-(○) and mechanical polished(●).

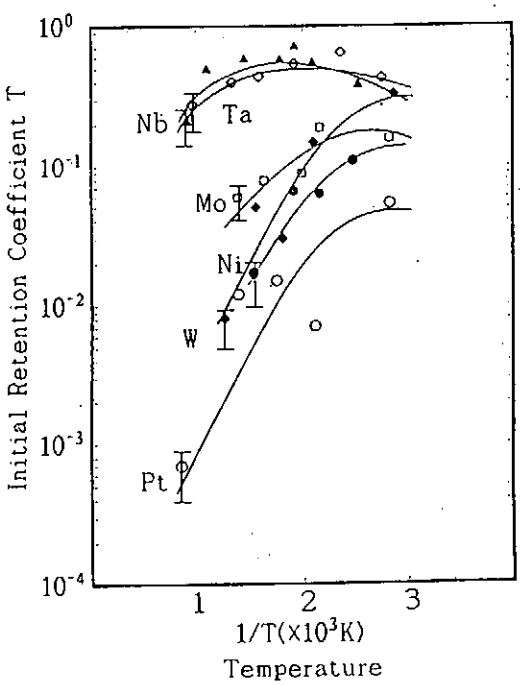

Fig. Temperature dependence of initial retention coefficient T at zero surface coverage with an error of ±30%. Solid lines in the figure are

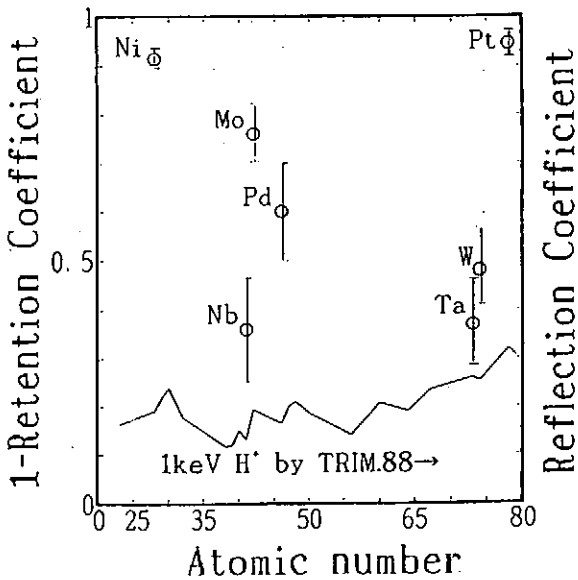

Fig. The measured value of release coefficient, including reflection and reemission, as a function of atomic number.The solid line inner figure is resulted from computer simulation of the reflection coefficient of 1keV H⁺ implantation using TRIM.88 code.

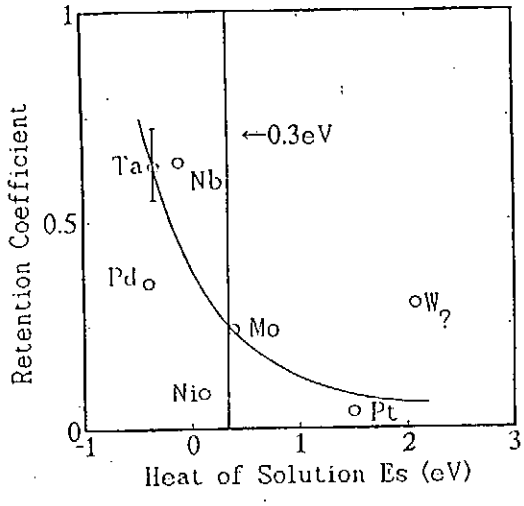

Fig. Retention coefficient as a function of heat of solution Es for each metals.The curve inner figureis only for a guide to the eye.

SUMMARY

Interaction of atomic hydrogen with metals is studied through the determination of hydrogen retention in metals after exposing to atomic hydrogen in terms of Z numbers and heat of solutions.

(1) At 410K initial retention coefficients normalized to incident atoms are 0.1 to 0.5 and above 0.6 for endothermic and exothermic hydrogen occluding metals, respectively. With increasing the temperature T is markedly reduced in the exothermic occluders, while it stays rather constant in the endothermic ones.

(2) Since the kinetic energy of the atomic hydrogen presently used is around 0.3 eV, atomic hydrogen is very likely to directly reflected at those metals of which heat of solution are over this value.

(3) No clear relation between the retention coefficient and Z number is observed different from reflection coefficients of high energy ions.

We could not distinguish the atomic hydrogen directly reflected at the surface from the reemitted molecules once absorbed and recombined at the surface. Further studies on observation of directly reflected atoms and measurements of their energy distributions are necessary.

TRITIUM PERMEATION

THROUGH BERYLLIUM AND VANADIUM.

M.V. Zhuk, V.I. Pistunovich.
Nuclear Fusion Institute,
RRC - Kurchatov Institute, Moscow, Russia.

1. Summary.

The problem of emergence and accumulation of tritium is one of the problems emerging in the option of the first wall material for a fusion reactor. A great attention is paid to the theoretical and experimental consideration of this problem. The following model is usually proposed: hydrogen atoms incident upon the wall from the plasma penetrate the wall their range R deep, being decelerated, and then diffuse within the bulk. Determination of boundary condition in the stationary case has been realized in a given paper, without consideration of a thermodynamic equilibrium state, that allows one to take into account of radiation-induced desorption. It has shown that the square flow dependence of concentration does not belong to the general case: linear dependence is realized in some cases. The results of model calculation of hydrogen isotopes permeation through berillium and vanadium are given in present paper. Permeability of Be is significantly lower compared with V. An additional experiments are necessary to obtain a reliable data for Be-H interaction.

TRITIUM PERMEATION THROUGH BERYLLIUM AND VANADIUM

M.V.Zhuk, V.I.Pistunovich

Nuclear Fusion Institute
RRC-Kurchatov Institute, Moscow
Russia.

2nd International Workshop
on Tritium Effects in Plasma
Facing Components

Nagoya, Japan
19-20 May, 1994.

1. Introduction.

The problem of emergence and accumulation of tritium is one of the problems emerging in the option of the first wall material for a fusion reactor. A great attention is paid to the theoretical and experimental consideration of this problem. The following model is usually proposed: hydrogen atoms incident upon the wall from the plasma penetrate the wall their range R deep, being decelerated, and then diffuse within the bulk. This process is represented by a diffusion equation with some boundary conditions determining the hydrogen desorption from the first wall surface.

Determination of boundary condition in the stationary case has been realized in a given paper, without consideration of a thermodynamic equilibrium state, that allows one to take into account of radiation-induced desorption. It has shown that the square flux dependence of concentration does not belong to the general case: linear dependence is realized in some cases.

The results of model calculation of hydrogen isotopes permeation through berillium and vanadium are given in present paper.

2. A Model of Kinetics of Surface Processes.

A model describes a hydrogen behaviour on the surface of first wall [1] was used for estimation of hydrogen permeability. This model based on the diagram of potential energy of hydrogen atom near the surface of metal (Fig. 1). Zero energy level corresponds to hydrogen atom energy in molecule H_2, C_0 - hydrogen concentration near the metal surface, θ - surface cover degree (relation of occupied

chemisorption centers number to the total number of this centers), K_S and K_B - coefficients of surface and bulk radiation-induced desorption, J_{IN} - incident flow of hydrogen atoms, $K_B \cdot J_{IN} \cdot C_0$ and $K_S \cdot J_{IN} \cdot \theta$ are the flow caused by the radiation-induced desorption from the bulk and the surface respectively, $\alpha \cdot \theta^2$ is the flow caused by associative desorption, $\gamma \cdot \theta$ is the flow of atoms escaping from the surface into the bulk and $\beta \cdot (1-\theta) \cdot C_0$ is the flow of atoms arriving at the surfce from the bulk. Constants from the expressions for flows defined by follows [1]:

$$\begin{aligned} &\alpha = 2 \cdot \nu \cdot n_s \cdot \exp(-2(E_{CS}+E_B)/kT); \\ &\beta = \nu \cdot b \cdot \exp(-E_{BS}/kT); \\ &\gamma = \nu \cdot n_s \cdot \exp(-E_{SB}/kT), \end{aligned} \qquad (1)$$

where E_{CS} - chemisorbtion energy, E_B - chemisorbtion barrier (E_B=0 on clean metal surface), E_S - energy of solution, E_D - activation energy of diffusion, E_{BS} - barrier of transition from bulk to surface, $E_{SB} \equiv E_{CS}+E_S+E_{BS}$, n_s - number of chemisorbtion centers per square unit, b - diffusion jump length, ν - jump frequency ($\approx 10^{13}$ s^{-1}). For metals $E_{CS} \approx 0{,}5$ eV and $E_{BS} \approx E_D$. From the requirements of steady-state we obtain the follow relationships between flows from Fig. 1:

$$\begin{aligned} &\alpha \cdot \theta^2 + \gamma \cdot \theta + K_S \cdot J_{IN} \cdot \theta = \beta \cdot (1-\theta) \cdot C_0; \\ &J_0 \equiv \left(D\frac{dC}{dx}\right)_{x=0} = K_S \cdot J_{IN} \cdot \theta + K_B \cdot J_{IN} \cdot C_0 + \alpha \cdot \theta^2 \end{aligned} \qquad (2),$$

where D - diffusion coefficient, C(x) - concentration profile. Adding the equations of diffusion problem trough the membrane with thickness d:

$$\begin{cases} D\,\dfrac{d^2C}{dx^2} + J_{IN} \cdot \delta(x-R) = 0; \\ D\left(\dfrac{dC}{dx}\right)_{x=0} = J_0; \\ C(x=d) = C_d, \end{cases} \qquad (3)$$

where $\delta(x)$ - Dirac delta-function, R - range of atoms in membrane and assuming for enough thick membrane C_d=0, we obtain a complete set of equaitions. Particulary, from (1) - (3) for θ we have

$$\theta^3 + P \cdot \theta^2 + S \cdot \theta + W = 0 \qquad (4),$$

where

$$\begin{aligned} P &\equiv 1 - K_S\frac{J_{IN}}{\alpha} + K_B\frac{J_{IN}}{\beta} + \frac{D}{\beta \cdot d}, \\ S &\equiv W + \frac{\gamma + K_S \cdot J_{IN}}{\alpha}\left(\frac{K_B \cdot J_{IN}}{\beta} + \frac{D}{\beta \cdot d}\right) + K_S\frac{J_{IN}}{\alpha}, \\ W &\equiv \frac{J_{IN} \cdot (d-R)}{\alpha \cdot d} \end{aligned} \qquad (5)$$

A general solution of (4) in Cardano form given in [1]. Taking into account that for temperature T = 500 - 700 K and $J_{IN} = 10^{15} - 10^{16}$ $cm^{-2}s^{-1}$ $\alpha \gg J_{IN}$ and expand the strictly solution into series, we obtain

$$\theta \approx \sqrt{\frac{J_{IN}}{\alpha}} \qquad (6).$$

From (6) follows that main contribution into desorption caused by surface recombination. Radiation-induced diffusion gives a less significant contribution.

As shown in [1], taking into account (6), it is possible to simplify (2) and (3):

1. For desorption flow J_0 at $\gamma/\alpha \gg 1$ ($E_{CS} > E_S + E_{BS}$) we have

$$J_0 \approx \kappa \cdot C_0^2, \quad \kappa \equiv \frac{\alpha \cdot \beta^2}{\gamma^2} \qquad (7).$$

2. At $\gamma/\alpha \ll 1$ ($E_{CS} < E_S + E_{BS}$):

$$J_0 \approx \beta \cdot C_0 \qquad (8).$$

In first case flow from surface to bulk ($\gamma \cdot \theta$ on Fig. 1) is enough to establish a quasi-equilibrium between θ and C_0. In second case magnitude γ is not enough to achieve

quasi-equilibrium, and atoms which jumps from bulk to surface will be desorbs rather than returns to the bulk.

The expressions for permeation flow J_d obtained from the solution of diffusion problem (3) with boundary conditions (7) and (8) respectively are

$$J_d = J_{IN}\cdot\left(1 - \frac{D^2}{4\cdot J_{IN}\cdot\kappa\cdot d^2}\cdot\left[\sqrt{1 + \frac{4\cdot J_{IN}\cdot\kappa\cdot d\cdot(d-R)}{D^2}} - 1\right]^2\right) \quad (9)$$

and

$$J_d = J_{IN}\,\frac{1 + \beta\cdot R/D}{1 + \beta\cdot d/D} \quad (10).$$

If $J_{IN}\cdot\kappa\cdot d^2/D^2 \gg 1$, from (9) we obtain:

$$J_d \approx J_{IN}\,\frac{R}{d} + \frac{D}{d}\sqrt{\frac{J_{IN}}{\alpha}} \quad (11).$$

The first term in (11) describes the contribution into J_d due to displacement of diffused atom source toward the rear side of membrane. Temperature dependence is determined by second term and it's proportionaly $\exp[-(E_D + E_S)/kT]$. Assuming $E_{BS} \approx E_D$ and taking into account that $\beta\cdot d/D \gg \beta\cdot R/D \gg 1$, from (10) obtain

$$J_d \approx J_{IN}\cdot R/d \quad (12).$$

3. Beryllium.

The literature data concerning hydrogen-beryllium interaction are very contradictory (Table 1). Such a wide scattered data may be caused by defect structure produced in process of berillium manufacturing. This structure is determined by the technology of manufacturing. Unfortunately, references on concrete technology is almost absent.

Sets of parameters used for calculations are represented in Table 2. Solutions (7), (9), (11) obtained for sets (1 - 4), solutions (8), (10), (12). - for sets (5, 6). The results of calculations of tritium permeation for sets (1 - 4) are represented on Fig. 2 in form of Arrenius plots.

4. Vanadium.

The literature data for vanadium-hydrogen interaction are represented in Table 3. These data are closed, except pre-exponential factor of diffusion coefficient. Table 4 contents sets of data used for calculations. Results are shown on Fig. 3. The formula (9) is used for all cases.

5. Discussion.

A wide scatter of results for tritium permeation through Be depicted on Fig. 2 is determined by the scatter of basic data (Table 1). The curves 1 and 2 are close to the straight lines, but due to different reasons. Set No. 2 corresponds to more diffusion coefficient, so the permeation flow is determined by second term in (11). Set No.1 corresponds to minimum diffusion coefficient, so the first term gives the main contribution and permeation flow is close to the constant value $J_{IN}\cdot R/d$. Sets No. 3 and 4 corresponds to maximum values of diffusion coefficient, and curves 3 and 4 close to curve 1 in low-temperature region because of a big value of activation energy of diffusion . A direct comparison of this results with experiment are difficult, because authors have no information about glow discharge-driven or ion-driven experiments with Be. But activation energy of permeation obtained for parameters set No. 1 ($E_D + E_S \approx 0{,}19$ eV, see (11) and Table 2) is the same as experimental one from [4] (Table 1).

A permeation flows for vanadium are significantly higher than for berillium in spite of the thickness of V membrane is 5 times higher than Be one. Temperature region above 400^0 C is considered, because at lowest temperatures V creates a stable hydrides [5]. A character of temperature dependence is determined by a great negative value of solution energy. The curves is almost parallel because the values $E_S + E_D$ for different sets of parameters are closed, and the distance between two groups of curves is determined by the differences in pre-exponential factors of diffusion coefficients. It's necessary to note that the values of permeation flows , obtained from (9), are overestimated, especially at low temperatures. It's caused by the fact that boundary condition at $x = d$ in (3) is not perfectly correct for metal with a great negative value of E_S, especially for thin membrane. In contrast to metals with $E_S > 0$, the concentration of hydrogen in exothermic metal near the rear side of membrane may be not negligible compared with C(0) and C(R), especially at low temperatures. This situation is qualitatively depicted on Fig.4. Fig. 5 shows an experimental data from [6] (permeability ≈ 18% at 773 - 823 K) and calculated results for the same conditions. The calculated flow is some higher than experimental one.

6 Conclusion.

1. The available experimental data of Be-H interaction are very contradictory. The differences in experimental results may be caused by the technology of Be manufacturing. It leads to a differences in calculated values of permeation flows. Permeability of Be is significantly lower compared with V. An additional experimental investigations are necessary to obtain a reliable data for Be-H interaction.

2. The experimental values for constants of V - H system are closed. The results of calculations show a high permeability of V compared with Be and with experimental data for austenitic and ferritic steels [7], and they are closed to experimental data [6].

References.

1. M.V. Zhuk, V.V. Pistunovich, I.V. Altovskl, Atomnaya energia (russian edition), 64 (1988), No. 3, pp. 209-212.
2. E. Abramov, M.P. Riehm, D.A. Thompson, Journ. of Nucl. Mat., 175 (1990), p. 90.
3. W.A. Swansinger, Journ. Vac. Science Technol., A4 (1986), p. 1216.
4. P.M.S. Jones, R. Gibson, Journ. of Nucl. Mat., 21, (1967), p. 353.
5. Hydrogen in Metals, edited by G. Alefeld and J. Volkl, Springer-Verlag, 1978.
6. Anderl, Longhurst, Struttman, Journ. of Nucl. Mat., 145 - 147 (1987), pp. 344 - 347.
7. Anderl, Longhurst, Struttman, Journ. of Nucl. Mat., 141 - 143 (1986), pp. 229 - 233.
8. O.L. Smith, B.A. Loomis, O.R. Diercks, Journ. of Nucl. Mat., 135 (1985), pp. 125 - 139.

Table 1. Literature data on beryllium-hydrogen interaction.

Diffusivity, $D=D_0 \cdot \exp(-E_D/kT)$

Isotope	D_0, cm^2/s	E_D, eV	T, K	Ref.
H	$3 \cdot 10^{-9}$	0	1133 - 1173	[2][1]
T	$3 \cdot 10^{-7}$	0,19	673 - 1173	[4]
T	$1,71 \cdot 10^{-5}$	0,19	573 - 873	[2][1]
T	$1,35 \cdot 10^{-6}$	0	> 873	[2][1]
D	$6,7 \cdot 10^{-5}$	0,3	620 - 775	[2][2]
D	$8 \cdot 10^{-5}$	0,37	620 - 775	[2][3]

Solubility, $S=S_0 \cdot \exp(-E_S/kT)$

Isotope	S_0, $cm^{-3}Pa^{1/2}$	E_S, eV	T, K	Ref.
T	$1,82 \cdot 10^{15}$	$-1,82 \cdot 10^{-5}$ ÷ $4,18 \cdot 10^{-5}$	673 - 1173	[4]
H	$1,35 \cdot 10^{15}$	$-1,9 \cdot 10^{-2}$	523 - 1173	[2][1]
T	$4,5 \cdot 10^{14}$	1,17	713 - 783	[2][1]
H	$7 \cdot 10^{21}$	1,0		[3]

Permeability, $J_d=(K_0/d) \cdot p^{1/2} \cdot \exp(-E_K/kT)$, where p - gas pressure before membrane.

Isotope	K_0, $mol/(m \cdot s \cdot Pa^{1/2})$	E_K, eV	T, K	Ref.
T	$5,8 \cdot 10^{-14}$	0,19	673 - 1173	[4]
H	$4,24 \cdot 10^{-7}$	0,9	773 - 873	[2][1]
H	$3,39 \cdot 10^{-11}$	0,28	773 - 923	[2][1]

1) - data of another authors, collected in [2];
2) - content of Be in sample - 99,8 at.%;
3) - content of Be in sample - 99,0 at.%.

Table 2. Sets of parameters, using in calculations for Be.

# of set	D_0, cm^2/s	E_D, eV	E_S, eV
1	$3 \cdot 10^{-7}$	0,19	$-1,82 \cdot 10^{-5}$
2	$1,71 \cdot 10^{-5}$	0,19	$-1,82 \cdot 10^{-5}$
3	$5,47 \cdot 10^{-5}$	0,3	$-1,82 \cdot 10^{-5}$
4	$6,53 \cdot 10^{-5}$	0,37	$-1,82 \cdot 10^{-5}$
5	$1,73 \cdot 10^{-5}$	0,19	1,17
6	$5,47 \cdot 10^{-5}$	0,3	1,17

All pre-exponential factors of diffusivity recalculate for tritium by the law of inverse square root of isotope mass.
Other parameters: $J_{IN} = 10^{15}$ $cm^{-2}s^{-1}$,
d = 1 mm,
R = 10^{-6} cm.

Table 3. Literature data on vanadium-hydrogen interaction.

Diffusivity, $D=D_0 \cdot \exp(-E_D/kT)$

Isotope	D_0, cm^2/s	E_D, eV	T, K	Ref.
D	$1,4 \cdot 10^{-4}$	0,11	723 - 823	[6]
D	$5,2 \cdot 10^{-4}$	0,08		[6][1]
D	$8,9 \cdot 10^{-4}$	0,13		[6][1]

Solubility, $S=S_0 \cdot \exp(-E_S/kT)$

Isotope	S_0, $Pa^{1/2}$	E_S, eV	T, K	Ref.
H	$2,5 \cdot 10^{-6}$	- 0,317		[6][1]
H		- 0,34		[8]

1) - data of another authors, collected in [6].

Table 4. Sets of parameters, using in calculations for Va.

# of set	D_0, cm^2/s	E_D, eV	E_S, eV
1	$1,14 \cdot 10^{-4}$	0,11	-0,34
2	$1,14 \cdot 10^{-4}$	0,11	-0.317
3	$4,25 \cdot 10^{-4}$	0,08	-0,34
4	$4,25 \cdot 10^{-4}$	0,08	-0,317
5	$7,27 \cdot 10^{-4}$	0,13	-0,34
6	$7,27 \cdot 10^{-4}$	0,13	-0,317

All pre-exponential factors of diffusivity recalculate for tritium by the law of inverse square root of isotope mass.
Other parameters: $J_{IN} = 10^{15}$ $cm^{-2}s^{-1}$
d = 5 mm,
R = 10^{-6} cm.

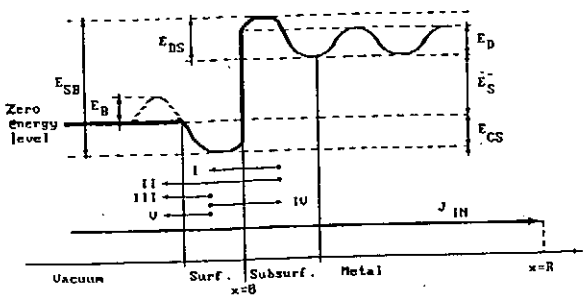

Fig. 1. A schematic diagram of potential energy of hydrogen atom near metal surface.

E_{CS} - chemisorbtion energy (=0,5 ev);

E_B - chemisopbtion barrier (=0 for clear surface);

E_S - solution energy;

E_D - activation energy of diffusion;

E_{BS} - barrier of bulk-to-surface jump (=E_D);

E_{SB} - barrier of surface-to-bulk jump.

Flowes:

I - bulk-to-surface ..... $\beta\cdot(1-\theta)\cdot C_0$;

II - radiation-induced desorption from bulk .... $K_B\cdot J_{IN}\cdot C_0$;

III - radiation-induced desorption from surface .. $K_S\cdot J_{IN}\cdot\theta$;

IV - surface-to bulk ..... $\gamma\cdot\theta$;

V - assotiative desorption ..... $\alpha\cdot\theta^2$.

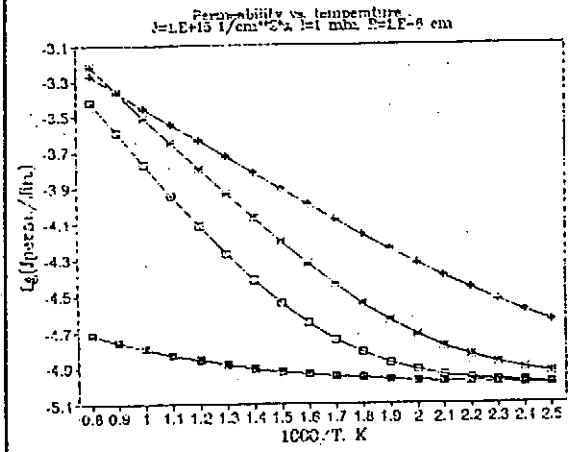

Fig.2 Permeability of Be membrane vs. temperature - results of calculations.

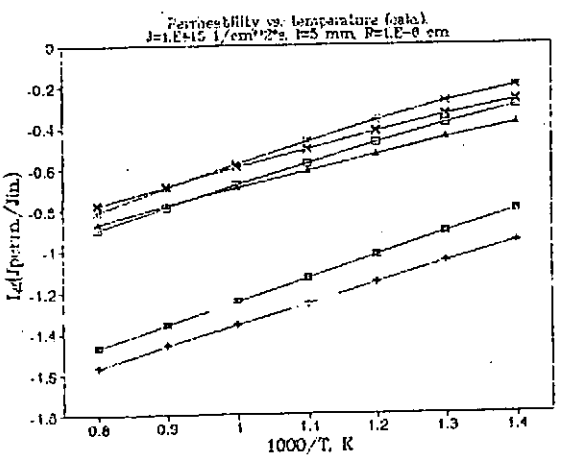

Fig.3 Permeability of V membrane vs. temperature - results of calculations.

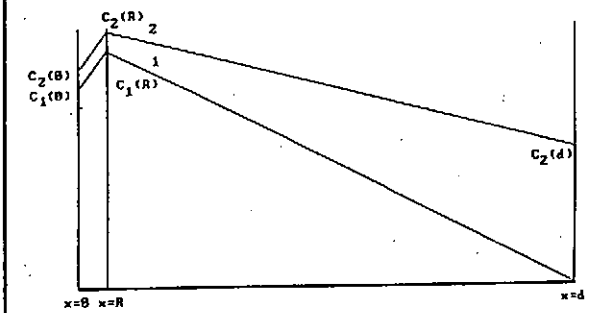

Fig. 4. A qualitatively illustration of influence of boundary condition on the rear side of membrane on the permeation flow.

Curve 1 corresponds C(x=d)=0.

Curve 2 corresponds to more realistic situation for exothermic metal.

$$J_{d1}=D\cdot\frac{C_1(x=R)-C_1(x=d)}{d-R}=D\cdot\frac{C_1(R)}{d-R};$$

$$J_{d2}=D\cdot\frac{C_2(x=R)-C_2(x=d)}{d-R}$$

Because for enough thick membrane $C_1(R)=C_2(R)$, $J_{d1} > J_{d2}$.

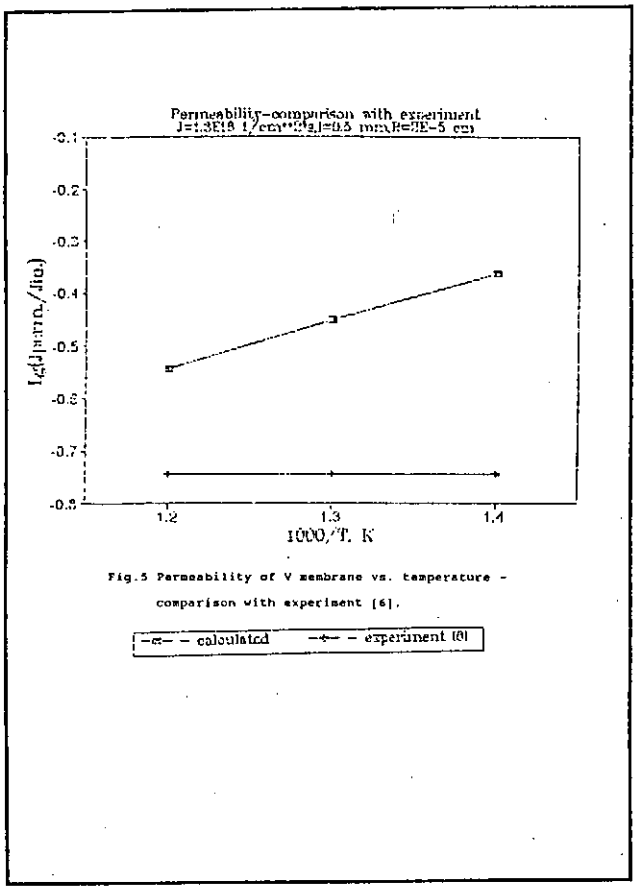

Fig.5 Permeability of V membrane vs. temperature - comparison with experiment [6].

SURFACE EFFECTS ON MARTENSITIC STAINLESS STEELS

A. Perujo, S. Alberici[1] and E. Serra

European Commission, Joint Research Centre, Ispra Site. Safety Technology Institute,

Ispra (VA), 21020 Italy.

[1]Dipartimento di Energetica. Politecnico di Torino, Corso Duca degli Abruzi 24, 10129 Torino, Italy

The martensitic steel DIN 1.4914 (**MA**rtensitic for **NET**, MANET) is a Nb bearing steel that has better swelling resistance, lower sensitivity to helium embrittlement, and more suitable thermophysical properties when compared with austenitic stainless steel AISI 316L. A further development of this steel has lead to MANET II. It is a candidate material for the first wall and structure for the demonstration power reactor DEMO.

Low or/and reduced activation steels are of great interest for fusion reactor applications as structural and first wall materials (FW). Their reduced activation will lower the radioactive waste produced during reactor operations and simplify its handling, storage and final disposal. The development of low activation martensitic (LAMS) and ferritic steels have been pursued by substituting Molybdenum and Niobium (the primary producer of long lived activity) by tungsten and vanadium, and by using lower carbon and nitrogen content (table 1)

Table 1. Chemical analysis of the steels considered in wt%.

Steel	Fe	C	Si	Mn	Cr	V	W	N	Ta	Change factor
LA7TaLN	Balance	0.18	0.04	0.70	11.1	0.24	2.95	0.005	0.10	2
LA12TaLC	Balance	0.09	0.03	1.01	8.9	0.39	0.76	0.019	0.09	100
LA12TaLN	Balance	0.17	0.02	0.74	9.1	0.25	0.77	0.004	0.10	10
MANET	Balance	0.13	0.37	0.82	10.6	0.22	_	0.02	_	100

MANET contains in wt%: Ni=0.87, Mo=0.77 and Nb = 0.16.

The study the interaction of hydrogen with MANET and LAMS has been done by gas evolution and gas permeation methods. It was found that the diffusivity of these materials suffered a strong reduction when they were heat treated at 900 K in presence of hydrogen, while the solubility remains invariable.

Further study of the absorption and recombination coefficients yielded the following values:

$$\sigma k_1 = 3.42 \cdot 10^{-6} \exp(-54867/RT) \ (\text{mol m}^{-2}\ \text{Pa}^{-1}\ \text{s}^{-1})$$

$$\sigma k_2 = 2.895 \cdot 10^{-6} \exp(-6133/RT) \ (\text{mol}^{-1}\ \text{m}^{4}\ \text{s}^{-1})$$

where σ is the surface roughness, R=8.314 J mol^{-1} K^{-1} and T is the temperature in Kelvin.

However these surface coefficient values together with the independence of the diffusivity with varying pressure (ie, remain in the diffusion limited regime) in the studied range cannot justify the strong reduction observed. Studies of the surface composition of the material by ESCA (XPS) showed a strong increase of chromium and manganese oxide when compared with the untreated material (around 120 Å). Cr and Mn at the temperatures of this study (600 - 900 K) have sufficient diffusivity in the bulk of the material to come to the surface and oxidise, increasing the thickness of the preexisting oxide layer.

The magnitude of the diffusivity reduction has been observed to depend on the amount of Mn present in the alloy. That is, for those alloys where the amount of Mn is relatively large and the amount of Cr is small (ex. LA12TaLC) the effect is more pronounced. This effect can be explained by a competition effect between the natural oxide present at the surface (chromium oxide) and the new produced oxide during the heat treatment due to the Mn migration to the surface of the sample. This is confirmed by the maximum change observed presented in the last row of table 1.

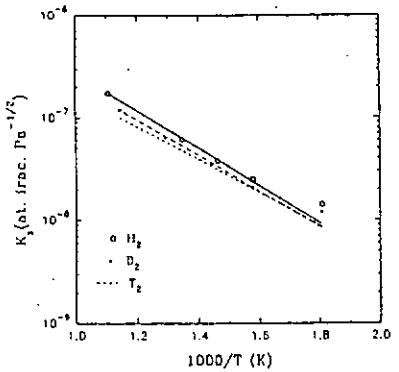

Fig.1 Sievert' constant of hydrogen isotopes in MANET

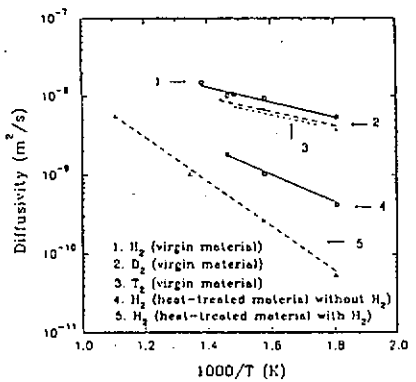

Fig.2 Diffusivities of hydrogen isotopes in MANET

SURFACE EFFECTS ON MARTENSITIC STAINLESS STEELS

A. PERUJO, S. ALBERICI and E. SERRA

Fusion Materials Studies Sector

Commission of the European Communities
Joint Research Centre - Ispra
Safety Technology Institute

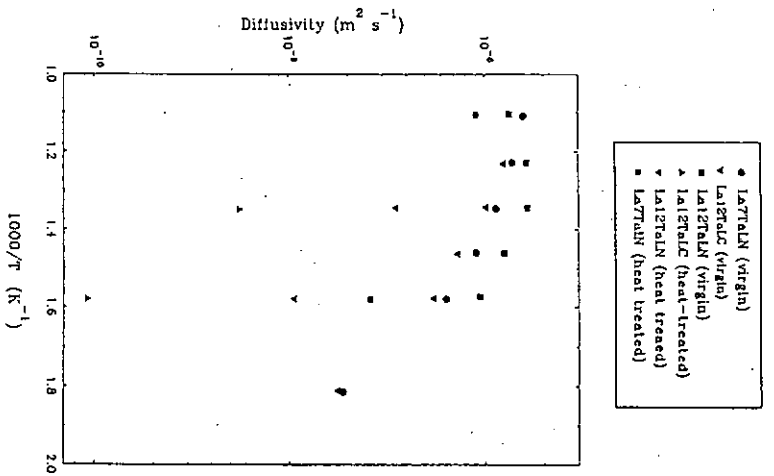

Chemical analysis of the steels considered in wt%

Steel	Fe	C	Si	Mn	Cr	V	W	N	Ta
LA7TaLN	Balance	0.16	0.04	0.70	11.1	0.24	2.95	0.035	0.10
LA12TaLC	Balance	0.09	0.03	1.01	6.9	0.29	0.76	0.019	0.09
LA12TaLN	Balance	0.17	0.02	0.74	5.1	0.25	0.77	0.004	0.10
MANET	Balance	0.13	0.37	0.62	10.6	0.22	-	0.02	-

MANET contains in wt%: Ni=0.67, Mo=0.77, Nb = 0.16

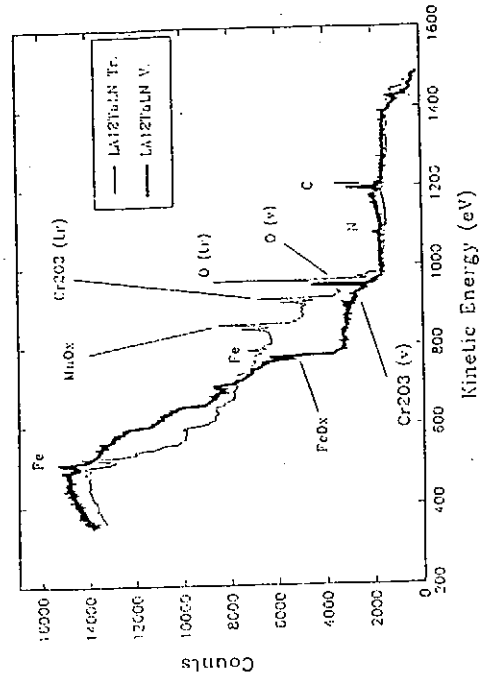

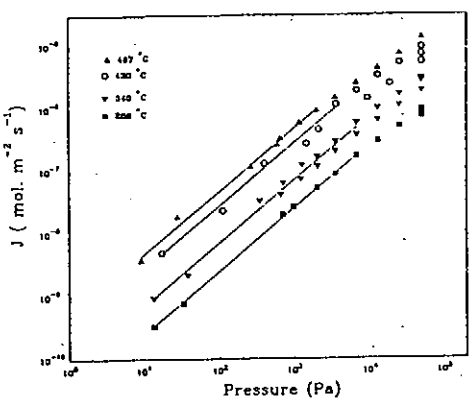

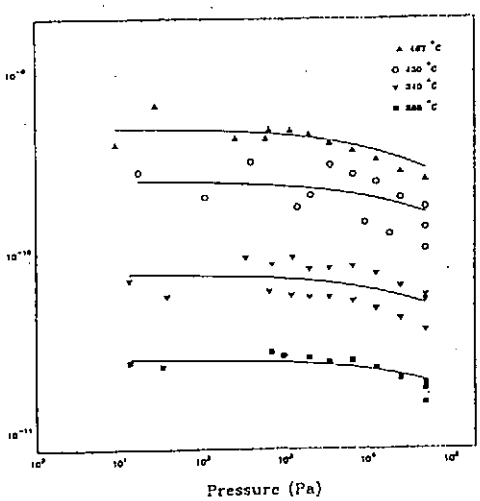

$$S = c_{\text{solution}} = K_s\, p^{1/2} \qquad (1)$$

$$J = \frac{DK_s}{d}\left(p_u^{1/2} - p_l^{1/2}\right) \qquad (2)$$

$$J = \frac{\Phi}{d}\, p_h^{1/2} \qquad (3)$$

$$J = \alpha k_1\, p \qquad (4)$$

$$J_r = 2\,\alpha k_1\, p \qquad (5)$$

$$J_r = 2\,\alpha k_2\, c^2 \qquad (6)$$

$$c^2_{\text{equilibrium}} = \frac{k_1}{k_2}\, p \qquad (7)$$

$$k_1 = k_2\, K_s^2 \qquad (8)$$

$$J_1(d) = J_2(d) = J_3(d) = 2\,(\alpha k_1)\,p(d) = 2\,(\alpha k_2)\,C^2(d) \tag{9}$$

$$J_1(0) = J_2(0) = J_3(0) = 2\,(\alpha k_2)'\,C^2(0) = 2\,(\alpha k_3)'\,p(0) \tag{10}$$

$$J_1(0) = J_2(0) = 2\,(\alpha k_3)'\,C^2(0) \tag{11}$$

In steady state:

$$J = J_1(d) = J_2(0) \tag{12}$$

and for the Fick's law, the diffusion flux within the metal is:

$$J = -D\frac{\partial C}{\partial x} = D\frac{C(d) - C(0)}{d} \tag{13}$$

Now we introduce the dimensionless number:

$$W = \frac{2\,\alpha k_2\,d}{D}\,p^{1/2}(d) \tag{14}$$

and a reduced concentration C:

$$C(0) = \frac{c(0)}{c_{saturation}} \tag{15}$$

W^2 is the reduced penetration flux density.
If $J_\infty = 2\,(\alpha k_2)\,p\,(d)\,d$ follows from eqs. (11) and (1) that:

$$\frac{J}{J_\infty} = C^2(0) \tag{16}$$

Substitution of eq. (13) into eq. (16), using the definition of W (eq. (14)) and eq. (1), provides that:

$$C^2(0)\,W = (C(d) - C(0)) \tag{17}$$

Substitution of eqs. (11) and (9) back in eq. (12), using Sievert' law and eq. (8), provides that:

$$C^2(d) = 1 - C^2(0) \tag{18}$$

Eq. (17) and (18) may be combined to give:

$$W^2\,C^4(0) + 2\,W\,C^2(0) + 2\,C^2(0) - 1 \tag{19}$$

This is the general equation for the steady state permeation across a symmetrical membrane.
When W<<1 eq. (19) becomes $2C^2(0)=1$. Combining with eq. (16) gives $J=(\alpha k_1)\,p\,(d)$ (=eq. (4)): the permeation flux is directly proportional to the pressure.
When W>>1 eq. (19) gives $C^2(0)=1/W$. Using the definition of W and C we can obtain, as expected, eq. (3): the permeation flux is directly proportional to the pressure square root.
A convenient way to determine the adsorption coefficient (αk_1) is to plot the ratio J / J_∞ (or J / p) as function of W^2 (or p). The fit of the measurements onto the theoretical curve allows to extrapolate accurately (αk_1).
Since there is not an analytical expression for J/J_∞ function of W^2, (it is not possible to eliminate C(0) from eqs. (16) and (19) in an analytical way), we have determined an analytical expression for J/J_∞ function of W^2 by a non linear least square fitting of the couple of points (J/J_∞, W^2). The expression:

$$\frac{J}{J_\infty} = \exp\left\{\frac{1 + a\exp\left[-\frac{b\,(-\ln(W^2 + c))}{1 + d\exp\left[-e\,(-\ln(W^2 + c))\right]}\right] + g}\right\} \tag{20}$$

where a=1.0015972, b=0.60190894, c=1.8832142, d=1.0201605, e=0.4155761, f=1.9707415, g=-1.69508, fits the theoretical curve with %ERR (W^2) = 100 abs [$((J/J_\infty)_{th} - (J/J_\infty)_{fit}) / (J/J_\infty)_{th}$] for $10^{-5}<W^2<10^{4}$) less than 1%.

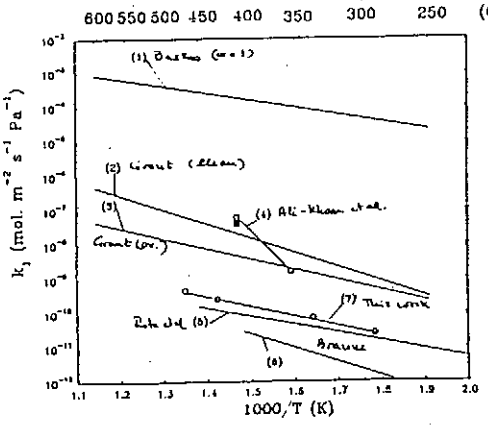

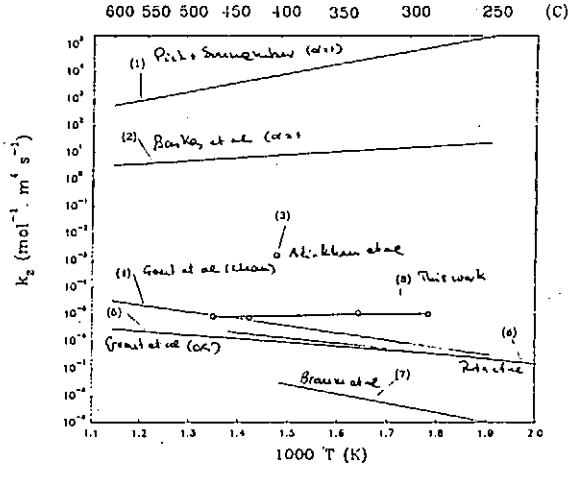

References

[1] NET §4-038ΓΓ, KfK report, compiled by K. Ehrlich (1986).
[2] K.J. Dietz, F. Waelbroeck, P. Wienhold, Jül-1448 (1977).
[3] M.I. Baskes, SAND 83-8231 (1983).
[4] F. Waelbroeck et al., Jül-1825 (1983).
[5] W. Möller, IPP 9/44 (1983).
[6] G. Gervasini and F. Reiter, J. Nucl. Mater. 155-157 (1988) 754.
[7] K.S. Forcey, D.K. Ross, J.C.B. Simpson and D.S. Evans, J. Nucl. Mater 160 (1988) 117.
[8] F. Reiter, S. Alberici, J. Campositvan, E. Serra, K.S. Forcey and A. Perujo, Z. Phys. Chem., 181 (1993) 151-157.
[9] I. Ali-Khan, K.J. Dietz, F. Waelbroeck, P. Wienhold, J. Nucl. Mater. 76 & 77 (1978) 337-343.
[10] M.I. Baskes, J. Nucl. Mater. 92 (1980) 318-324.
[11] D.M. Grant, D.L. Cummings and D.A. Blackburn, J. Nucl. Mater. 152 (1988) 139-145.
[12] E. Rota, F. Waelbroeck, P. Wienhold and J. Winter, J. Nucl. Mater. 111-112 (1982) 733-739.
[13] M. Braun, B. Emmoth, F. Waelbroeck, P. Wienhold, J. Nucl. Mater. 93-94 (1980) 861-865.
[14] M.A. Pick and K. Sonnenberg, J. Nucl. Mater. 131 (1985) 208-220.
[15] F. Reiter, S. Tominetti and Perujo, Fusion Eng. Des. 15 (1992) 223.

Measurements of D Concentration Profile in Metal Films During D Implantation

S . Yamaguchi, S. Nagata, K. Takahiro and S. Yamamoto*

Institute for Materials Research, Tohoku University, Sendai 980, Japan

Re-emission, retention and permeation behaviors of deuterium in Al, Ni, Cu and 304 SS membranes have been studied for 5 keV D_2^+ implantation at temperatures between RT and 493 K. The D atoms trapped in the membranes as well as the permeating D atoms were detected simultaneously by means of the elastic recoil detection(ERD) analysis technique of transmission geometry. The amounts of the trapped and permeated D atoms were measured as a function of fluence at various temperatures. From these experiments, we estimated the fractions of trapped, permeated and re-emitted D fluxes at the steady state, where the re-emission fraction was evaluated by subtraction of the trapping and permeating fluxes from the incident flux. The observed transport behaviors were analyzed to determine the recombination coefficients in these metals.

---

*Present adress: Takasaki Radiation Chemistry Research Establishment, Japan Atomic Energy Research Institute, Takasaki 370-12, Japan.

Measurements of D Concentration Profile in Metal Films During D Implantation

S. Yamaguchi, S. Nagata, K. Takahiro and S. Yamamoto

Institute for Materials Research, Tohoku University, Sendai, Japan

By the use of ERD analysis technique of transmission geometry, the hydrogen concentration profile in the whole thickness of a membrane can be measured. We show that this method is very useful to investigate hydrogen transport during hydrogen implantation.

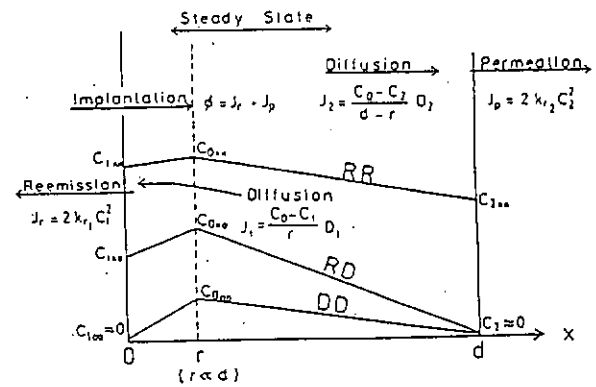

Simplified models for ion permeation at steady state. ϕ, incident flux; r, range; c, H concentration; k, recombination coefficient; D, diffusion coefficient.

Experimental

Analyzing beam : 2.8 - 3.2 MeV $^4He^+$, 5×10^{13} He/cm^2 s

Implant beam : 5.0 kev D_2^+, 10 uA/cm^2

Specimens : Al(2.4 um), Ni(1.4 um), Cu(1.1 um), 304 ss(1.9 um)

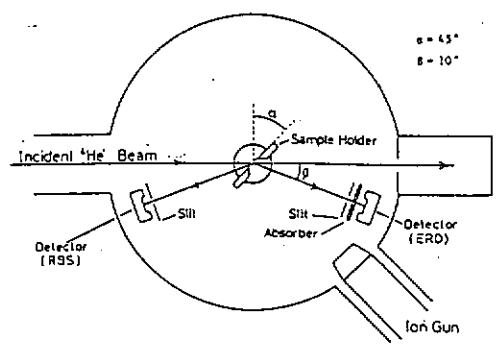

Schematic illustration of the experimental set up.

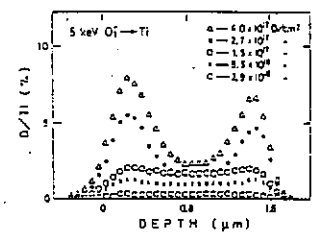

Sequence of D profiles in a Ti film of 1.6 μm thickness

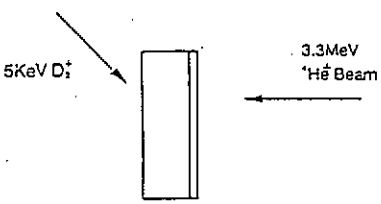

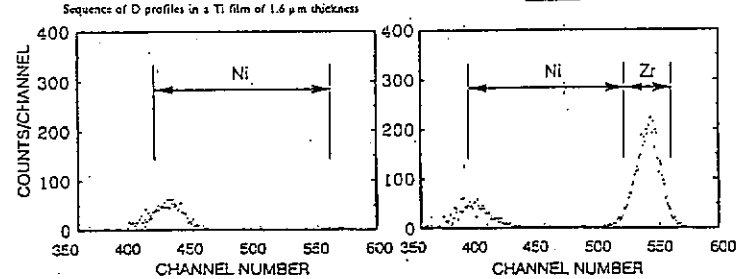

D profiles in Ni and Ni + Zr films during 5 keV D_2^+ implantation at room temperature. Implantation fluence is 1×10^{17} D/cm^2.

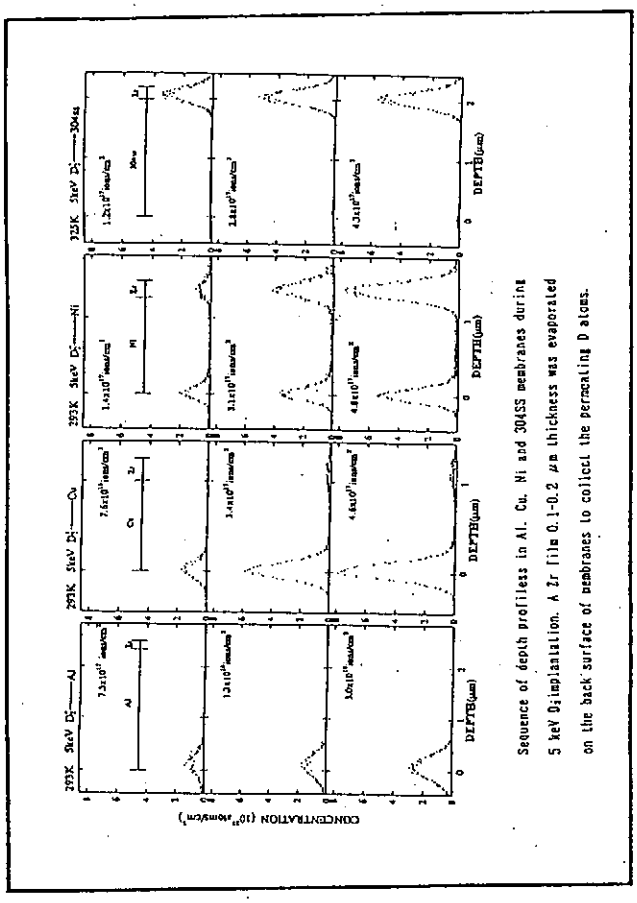

Sequence of depth profiles in Al, Cu, Ni and 304SS membranes during 5 keV D implantation. A Zr film 0.1-0.2 μm thickness was evaporated on the back surface of membranes to collect the permeating D atoms.

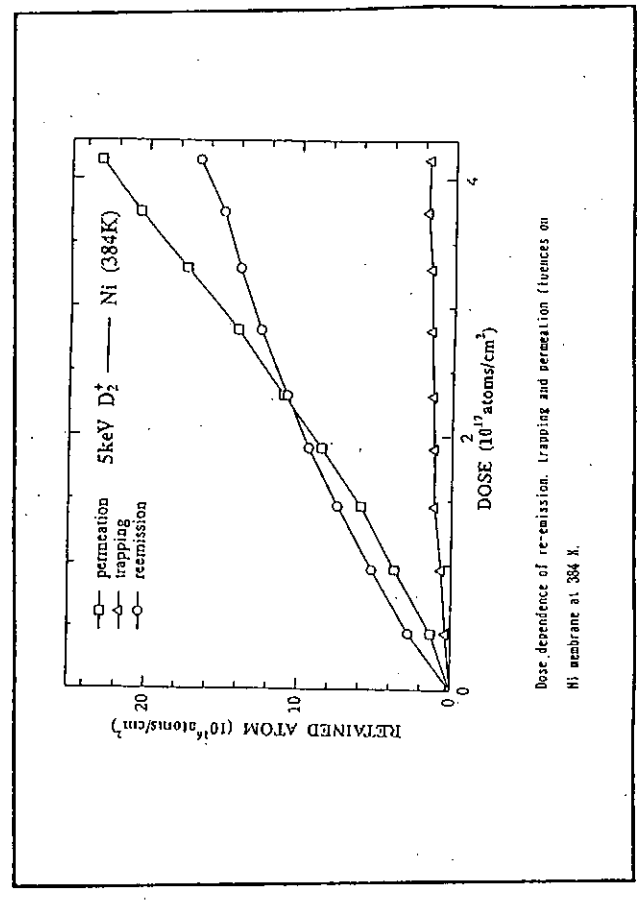

Dose dependence of re-emission, trapping and permeation fluences on Ni membrane at 384 K.

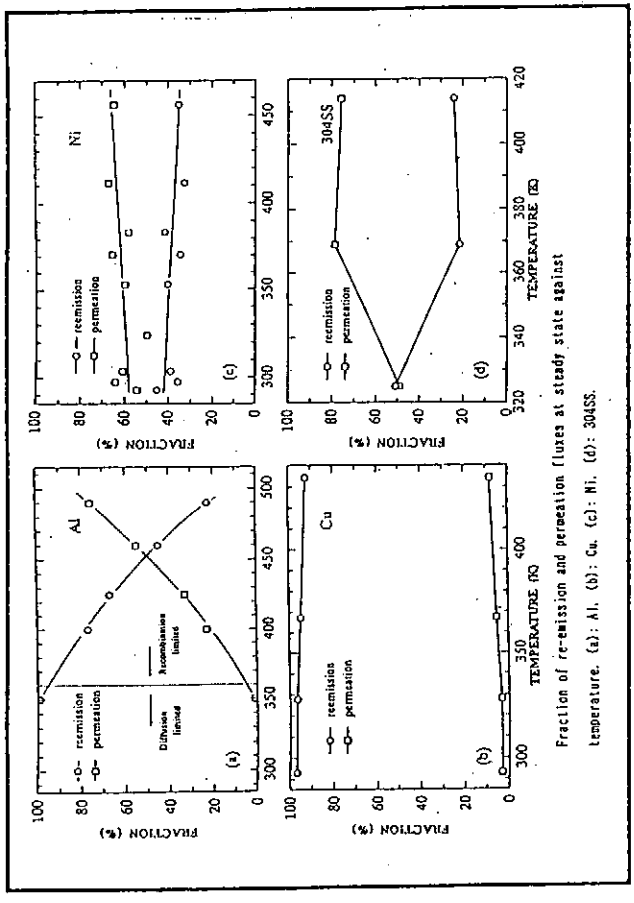

Fraction of re-emission and permeation fluxes at steady state against temperature. (a): Al, (b): Cu, (c): Ni, (d): 304SS.

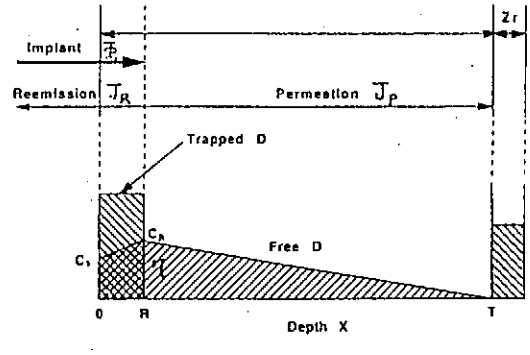

$$\Phi = J_R + J_P + \eta$$

$$J_P = D\frac{C_R}{(T-R)}, \quad J_R = D\frac{C_R - C_1}{R}$$

$$J_P/J_R = \frac{R}{(T-R)}, \quad K_r = \frac{J_R \cdot D^2}{J_P^2 (T-R)^2} \quad (C_R \gg C_1)$$

A key diagram for D depositin profile.

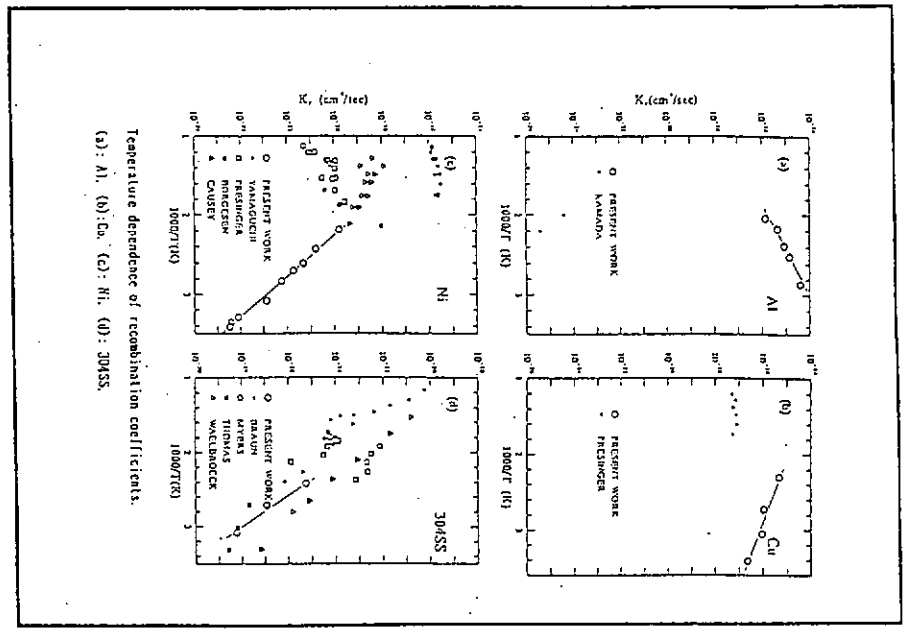

Temperature dependence of recombination coefficients.
(a): Al, (b):Cu, (c): Ni, (d): 304SS.

§ Summary

The ERD method of transmission geometry by 3.2 MeV He ions was applied to investigate re-emission, trapping and permeation behavior of implanted deuterium during simultaneous 5 keV D_2^+ implantation on Al, Cu, Ni and 304SS membranes at various temperatures. The D transport behaviors were different considerably on the kind of metals implanted. The release at the injection surface of Ni, Cu and 304SS samples above RT was limited by the surface recombination. On the other hand, the transition between the different transport was appeared on Al membrane; the release at Al surface was limited by diffusion below 360 K and surface recombination limited the D transport at higher temperatures. At high temperatures correspond to the recombination limited regime, the recombination coefficients for these metals were obtained.

Deuterium Capture and Release during Low Energy Ion Implantation in Beryllium

V.A.Kurnaev,D.P.Levchuk,A.A.Pisarev,V.M.Sotnikov,O.V.Zabeida

Be is one of the most interesting PFC for fusion devices. So data on fuel particle interaction with Be in reactor relevant conditions are needed.

This report presents some preliminary experimental and computer simulation results which seem to be of interest for T - Be interaction. Experiments has been performed on ion mass-separator with deep differential pumping which can be used for measurement of particle reflection R_N and retention coefficients in a broad range of ion energies (10 - 2500 eV) and angles of incidence $0° < \theta < 75°$.

Measurements with two different ways for 0.5keV D ions incident on Be surface at $\theta = 30°$ showed that R_N have exceed calculated one. For computer simulations TRIM like code is used. Possible reason of deviation is connected with BeO layer.

Thermodesorption measurements agree with known data and show 1eV and 1.8eV TDS spectra maxima. For high fluences TDS become more complicated.

Computer simulations showed that there is a great difference between R_N values for normal and sliding incidence. Very strong isotop effect is seen at normal incidence on Be :$R_N(H) \cong 1.5R_N(D) \cong 2.5R_N(T)$. Binding energy, modeled with attractive potential E_S, influences R_N at low energies noticeably. Energy corresponding to the maximum value of R_N increases with θ and M_1.

Computer simulations of regular relief showed weak dependence of retention coefficient on relief consisting from triangle ridges with slope angle inclination 30°-60° for proton 20 -1000eV energy, bombarding Be at $\theta_0 = 0$.

Plasma Physics Department — МИФИ

Deuterium Capture and Release
during Low-energy Ion Implantation
in Beryllium

V.A.Kurnaev, D.P.Levchuk, A.A.Pisarev
V.M.Sotnikov, O.V.Zabeida

- Introduction
- Experimental set up and methods
- TDS spectra and D retention
- Particle reflection coefficient Rn
- Results of computer simulations
- Summary

Department of Plasma Physics
Moscow Engineering Physics Institute
Kashirskoe str. 31,, 115409, Moscow,, USSR
tel: 324-30-24, fax: 324-21-11, PLASMA @ ETP, MEPI, MSK, SU

1. Introduction.
2. Experimental set up and methods description
3. Particle reflection coefficient R_N measurements
4. Computer simulation data on R_N for low energy region when eff-tive attractive potential can affect R_N
5. Computer simulation of roughness simulations influence on R_N
6. D retention and release
7. Summary.

- Be is one of the most interesting PEC Materials for fusion devices.
- So data on fuel particle interaction with Be in reactor relevant conditions are needed.

  -hydrogen isotopes retention for different fluences and Be temperature

  -particle reflection data

  -surface topography influence on reflection and retention

  for broad range of primary energies, angles of incidence, surface conditions.

- We have recently started Be program. So this report presents some preliminary experimental and and computer simulations results which seem to be of interest for T → Be interaction problem.

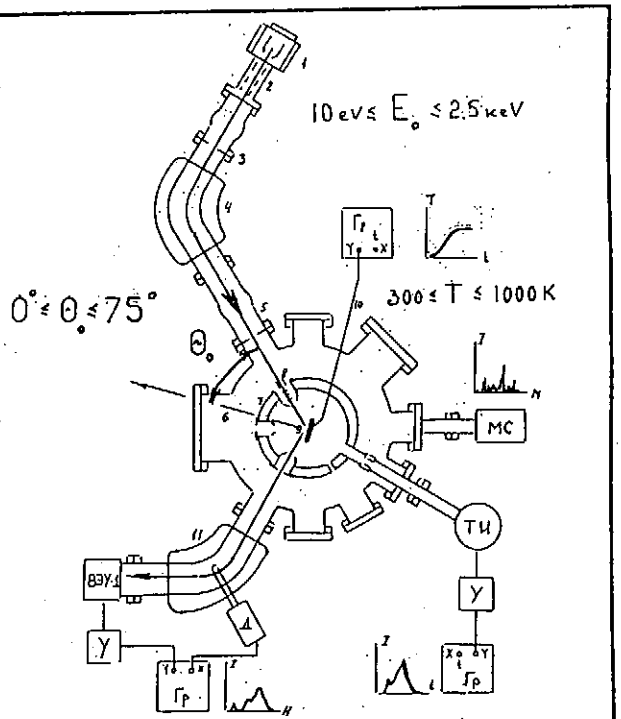

Рис. 12. Схема установки: 1- ионный источник; 2- электростатическая линза; 3- диафрагма; 4- электромагнитный масс-сепаратор; 5- диафрагма; 6- камера взаимодействия; 7- вольфрамовый экран; 8- система откачки и термопара; 9- мишень; 10- термопара; 11- электромагнитный масс-спектрометр; Гр- генератор-построитель; Д- датчик Холла; МС- монопольный масс-спектрометр; ТИ- камера течеискателя; У- усилитель.

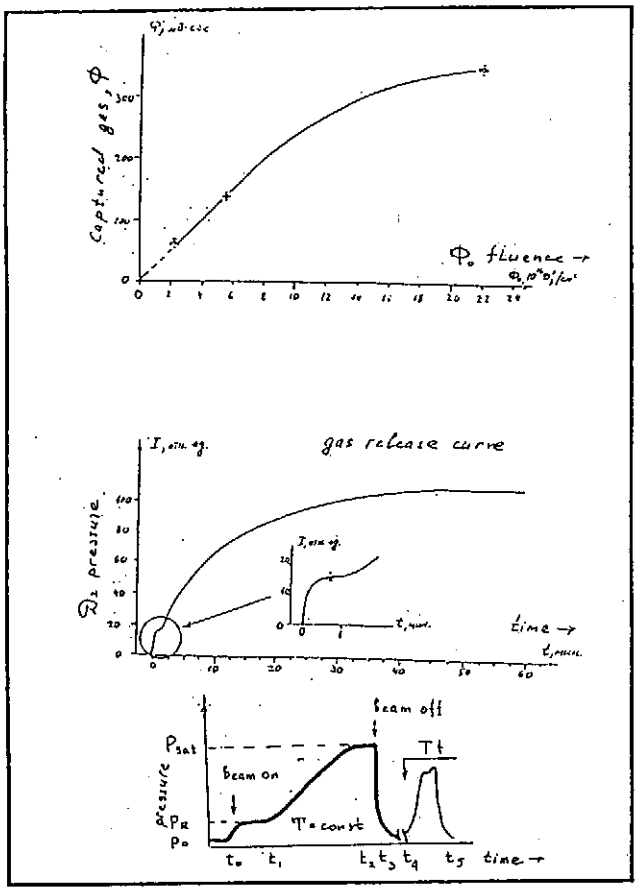

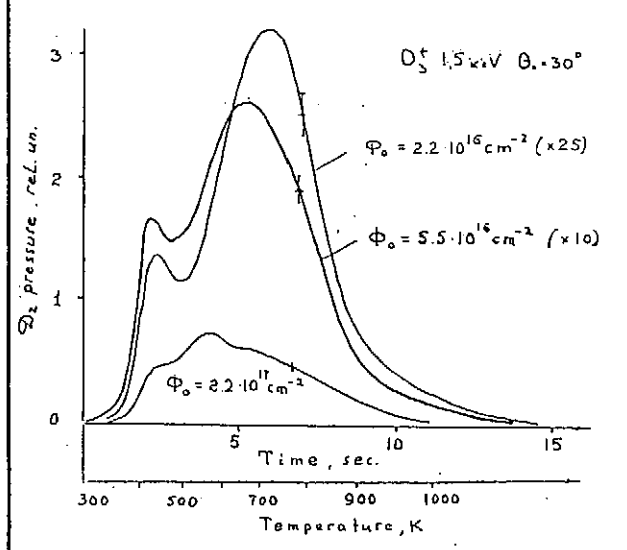

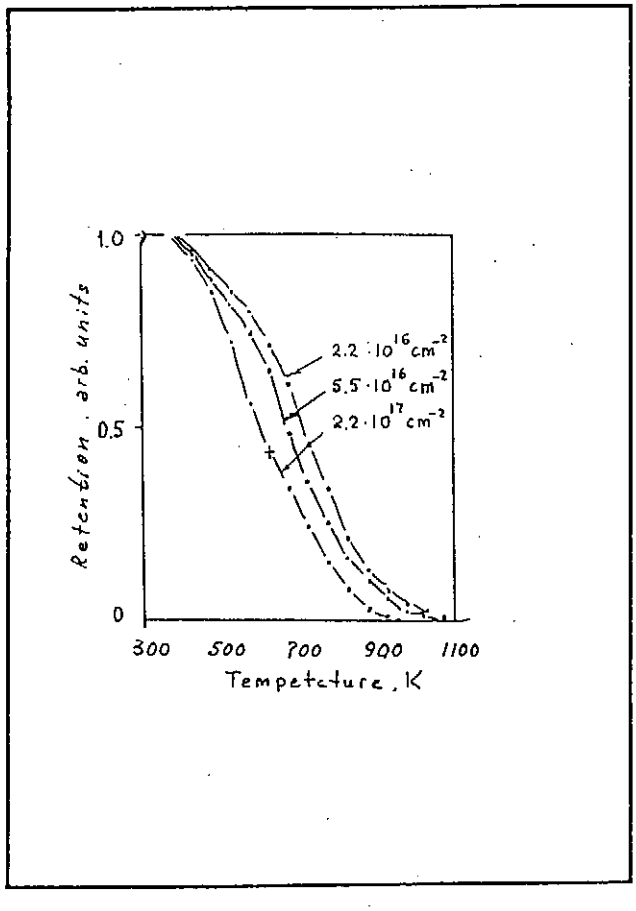

Experimental results on R_N for energy, when R_N is low and doesn't influence retention data

$$D_3^+ \; 1.5keV \rightarrow Be \qquad \theta_0 = 30°$$

1. $R_N = \frac{P_R - P_0}{P_{sat} - P_0} \Rightarrow R_N = \underline{0.14} \pm 0.01$
2. $R_N = \lim(1 - \frac{d\phi}{d\phi_0}) \Rightarrow R_N = \underline{0.145} \pm 0.015$

computer simulations using binary collisions Monte-Carlo code similar to TRIM.SP

	$\Rightarrow R_N$
Be	→ 0.125
BeO	→ 0.186
BeO (10Å) + Be	- 0.134
BeO (50Å) + Be	- 0.151

So difference is due to BeO contamination and (or) surfase roughness

Attempt to control BeO layer has not been succesful, so we started the reconstruction of control system and used computer simulation to estimate R_N values (or retention values) for low energy hydrogen isotopes interaction with Be

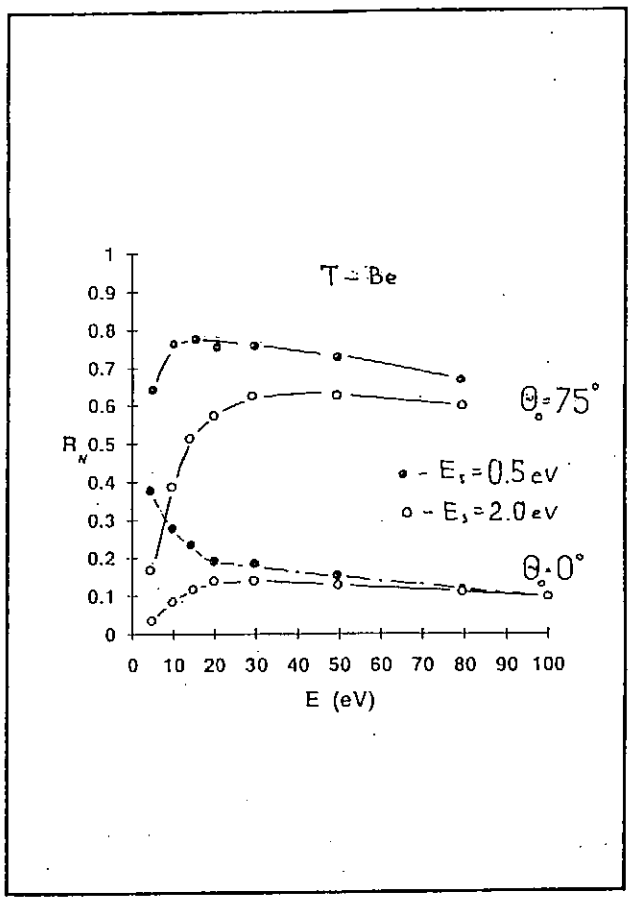
T → Be
R_N
E (eV)
Θ_0=75°
Θ_0=0°
• - E_s=0.5 eV
o - E_s=2.0 eV

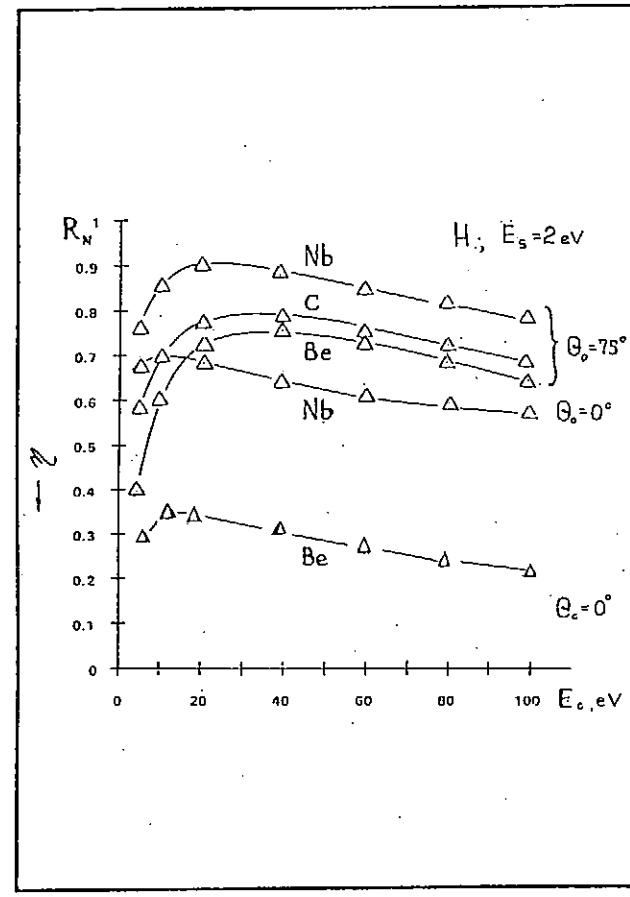
R_N^1
H, E_s=2 eV
Nb
C
Be
Nb
Be
Θ_0=75°
Θ_0=0°
Θ_0=0°
E_0, eV

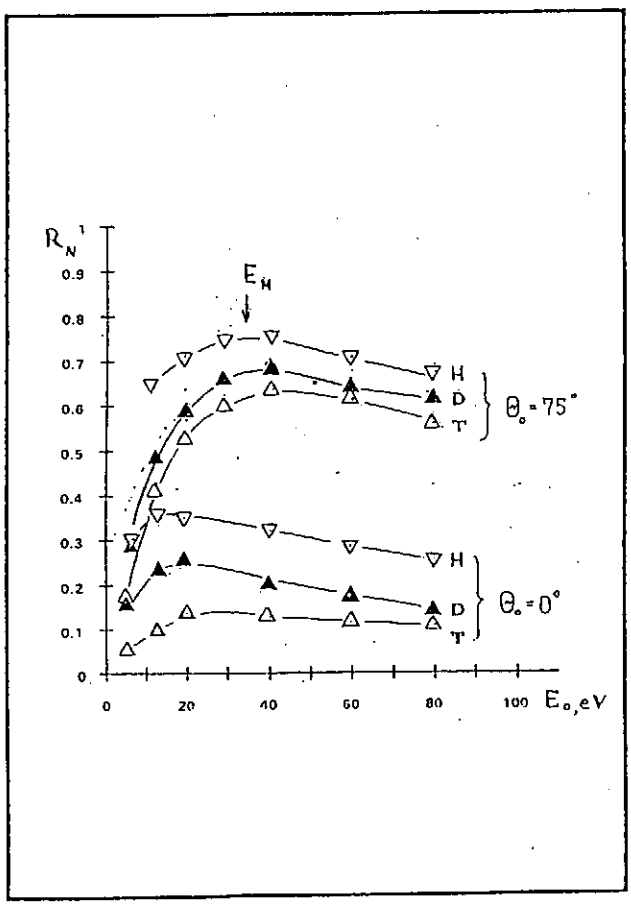
R_N^1
E_H
H
D
T
Θ_0=75°
H
D
T
Θ_0=0°
E_0, eV

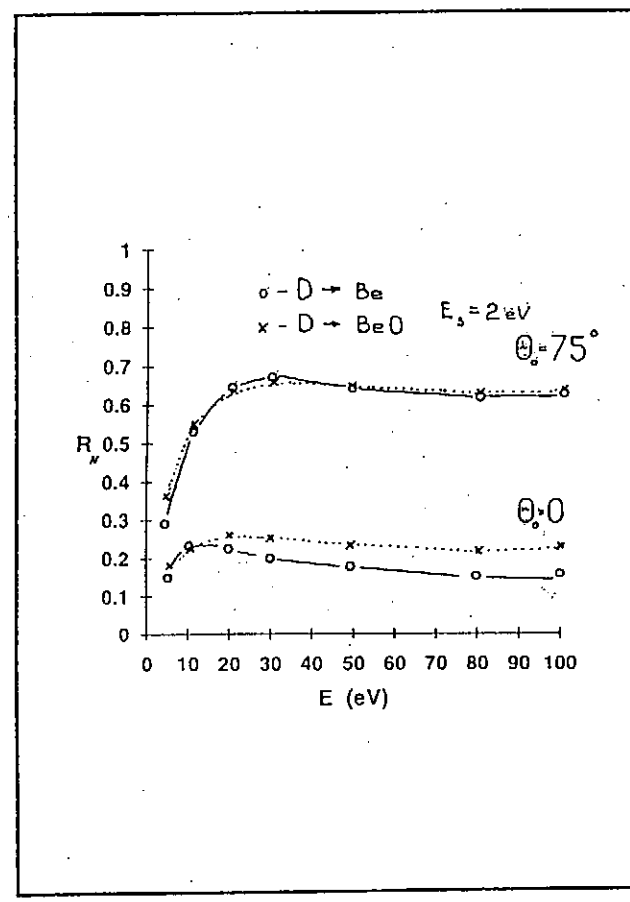
o - D → Be
x - D → BeO
E_s=2 eV
Θ_0=75°
Θ_0=0
R_N
E (eV)

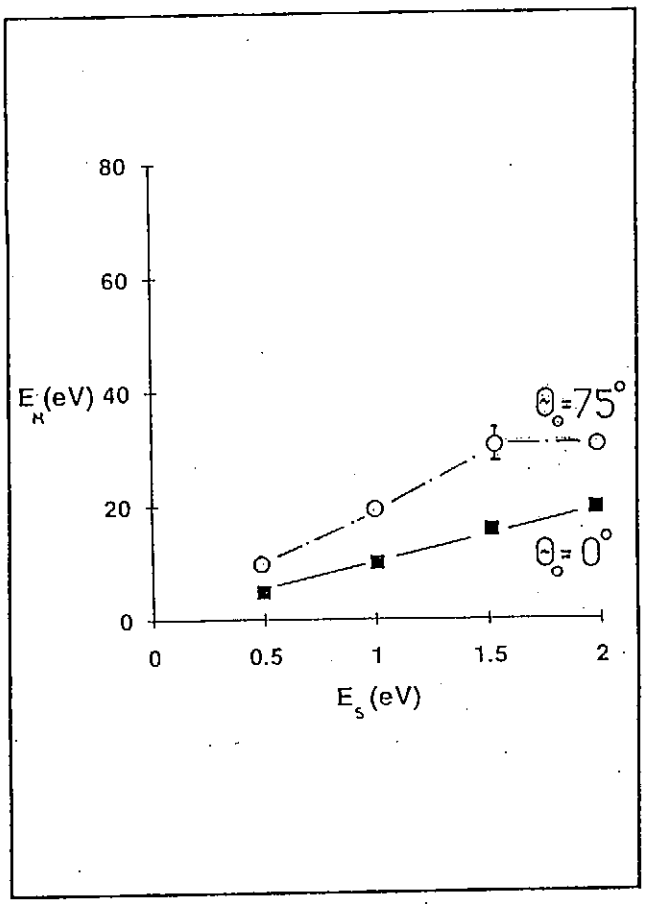

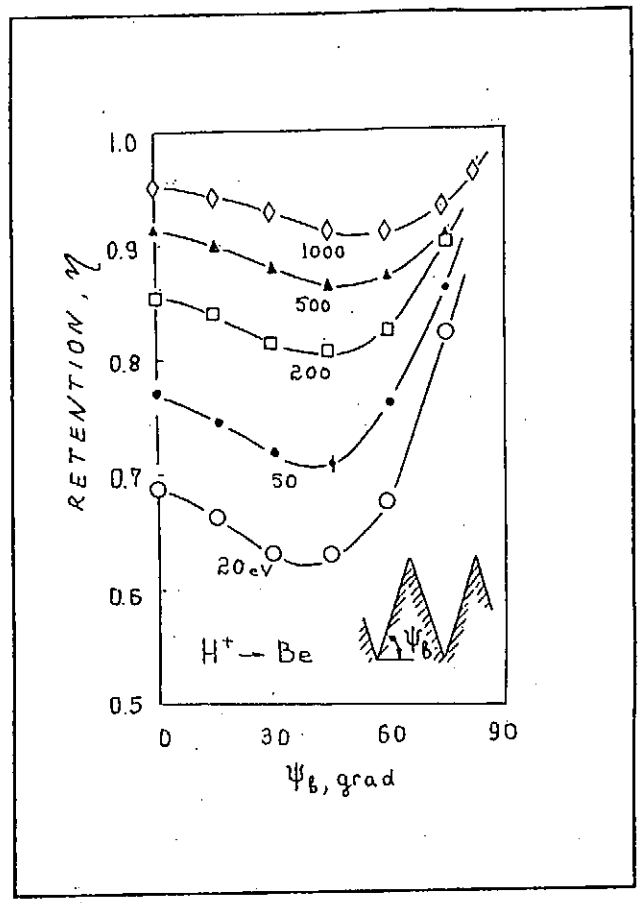

SUMMARY

Preliminary experiments showed:

R greater then calculated one -possible reason a thin BeO layer,

TDS measurements agree with known data on Be [BeD_2 destruction, gas release from point defects],

TDS spectra for high fluences reveals complicated structure.

Computer simulations shows:

There is a great difference between R values for normal and sliding incidence [R > 0.7 can be reached for H 40 eV Θ_0=75],

Very strong isotop effect is seen at normal incidence on Be:

R (H) = 1.5R (D) = 2.5R (T),

Attractive potential E_s influence R noticaebly, E_H corresponding to maximum value of R increases with Θ_0 and M_1

Computer simulatins of regular relief on the surface shows its weak influence on retention parameter for normal incidence.

2nd Int. Workshop on Tritium Effect in Plasma Facing Components
19-20 May 1994, Nagoya University Japan

HYDROGEN DIFFUSION AND PERMEATION IN BERYLLIUM

Kaname Kizu and Tetsuo Tanabe

Department of Nuclear Engineering, Faculty of Engineering,
Osaka University, Yamada-oka, Suita, Osaka 565 Japan
TEL +81-6-879-7884, FAX +81-6-875-5696

Hydrogen behavior in Be has extensively studied for the application of Be as a plasma facing material and in the blanket. There remains, however, some discrepancy in the interpretation of hydrogen migration mechanism in Be. And even the release mechanism under thermal desorption of tritium in neutron irradiated Be is not clarified yet. Wide data scattering for diffusion, trapping and permeation are most likely the reason. The influence of surface oxygen on Be is considered to be also large.

We have made a hydrogen permeation study with gaseous hydrogen drive permeation technique(GDP) and determined the diffusion coefficient(D) and permeation coefficient(Φ) independently, which made an estimation of the solubility possible according the relation $\Phi = D\,S$.

Hydrogen permeation rate is found to be proportional to the square root of hydrogen pressure ($P^{1/2}$) without any anomaly in its temperature dependence, which indicates that the diffusion is a rate controlled process. Consequently we can determine the diffusion coefficient from the permeation transient.

Preliminary values of D and Φ thus determined are

$D = 1.3 \times 10^{-8} \exp(-49(kJ/mol)/RT)$ $\quad m^2 s^{-1}$

and

$\Phi = 1.4 \times 10^{-6} \exp(-74(kJ/mol)/RT)$ $\quad mol\ m^{-1} s^{-1} Pa^{-1/2}$.

S is calculated from the relation $\Phi = D\,S$ as

$S = 1.1 \times 10^{2} \exp(-25(kJ/mol)/RT)$ $\quad mol\ m^{-3} Pa^{-1/2}$

These values, however, are still influenced by surface oxide which is very stable and hard to be removed.

HYDROGEN PERMEATION AND DIFFUSION IN BERYLLIUM

Kaname Kizu and Tetuo Tanabe

Beryllium → Blanket (n,2n)

→ Plasma Facing Material

Low Z material
Low tritium inventory

*: Permeation method
#: Desorption method

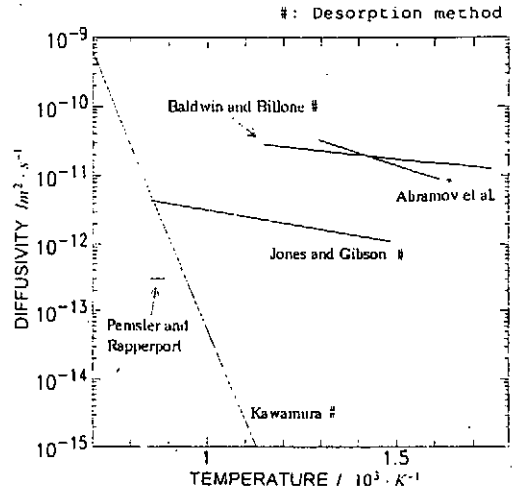

True diffusion?

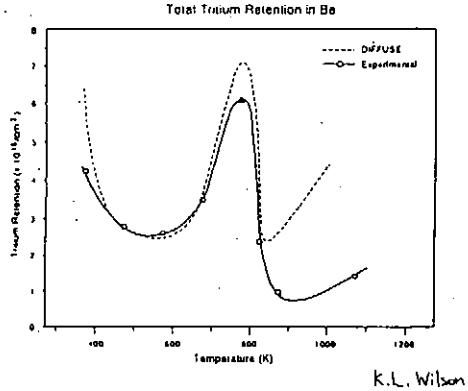

K.L. Wilson

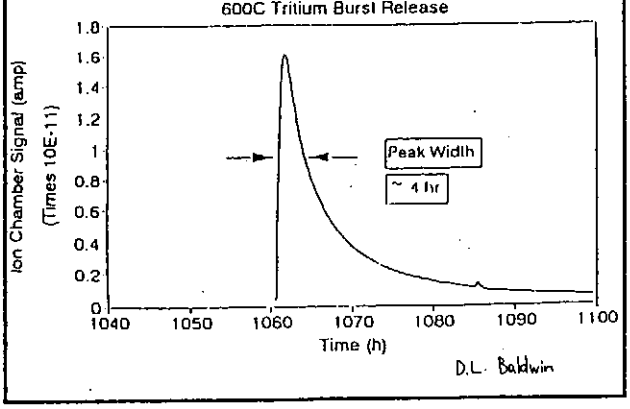

D.L. Baldwin

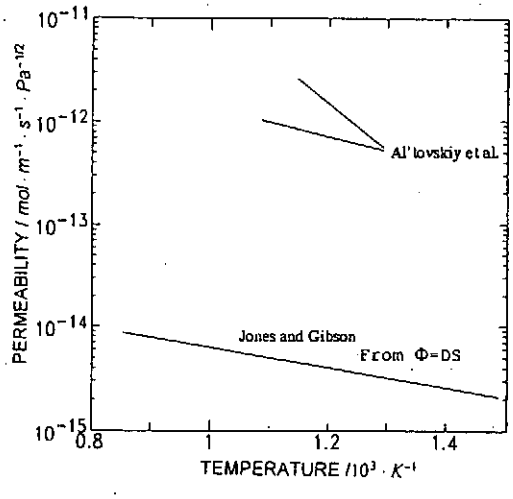

Which is corect?

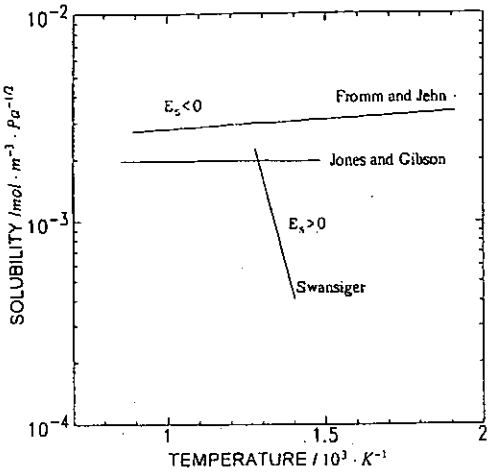

Consistent values but E_S?

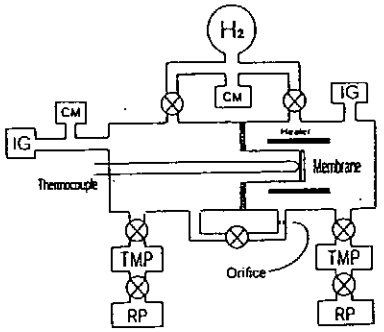

Experimental apparatus

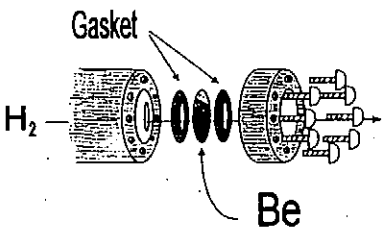

Sample holder

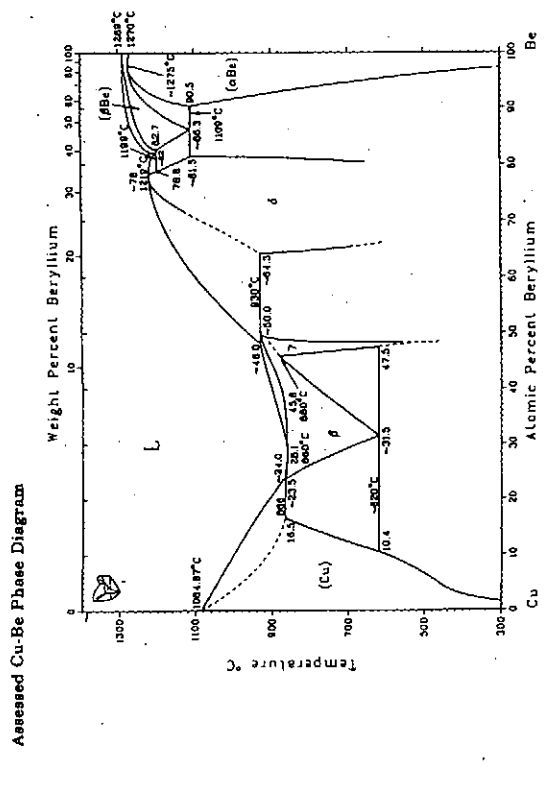

Assessed Cu-Be Phase Diagram

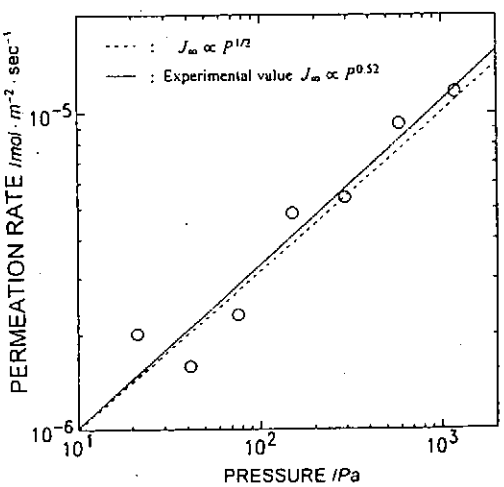

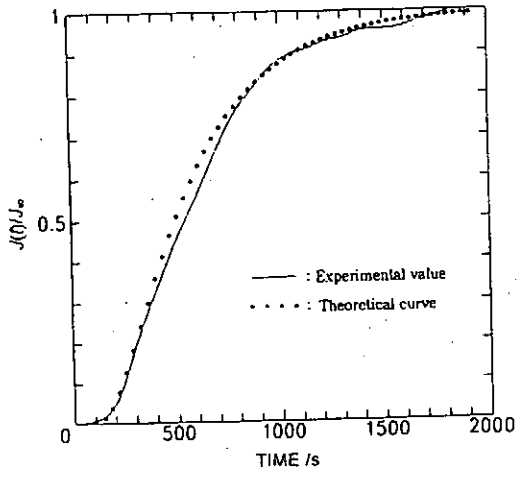
J(t)/J∞
1
0.5
0
500
1000
1500
2000
TIME /s
: Experimental value
: Theoretical curve

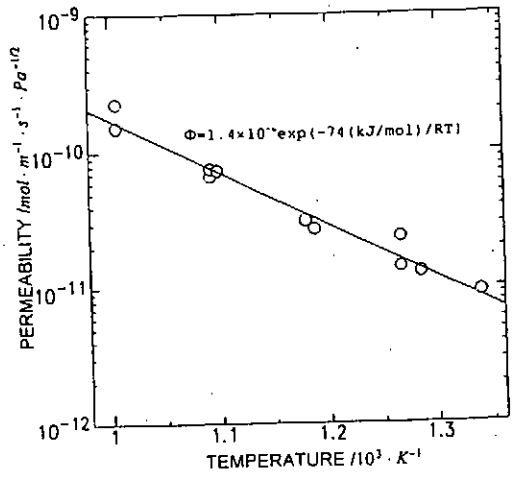
PERMEABILITY /mol · m⁻¹ · s⁻¹ · Pa⁻¹/²
10⁻⁹
10⁻¹⁰
10⁻¹¹
10⁻¹²
Φ=1.4×10⁻⁶exp(-74(kJ/mol)/RT)
1
1.1
1.2
1.3
TEMPERATURE /10³ · K⁻¹

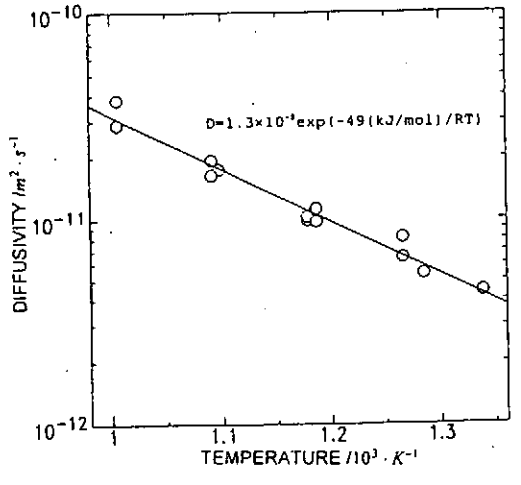
DIFFUSIVITY /m² · s⁻¹
10⁻¹⁰
10⁻¹¹
10⁻¹²
D=1.3×10⁻⁶exp(-49(kJ/mol)/RT)
1
1.1
1.2
1.3
TEMPERATURE /10³ · K⁻¹

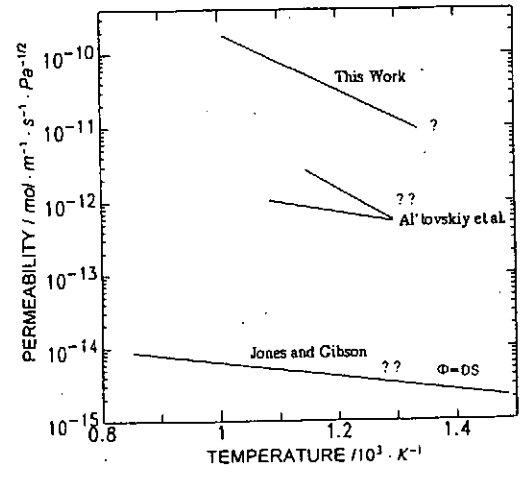
PERMEABILITY / mol · m⁻¹ · s⁻¹ · Pa⁻¹/²
10⁻¹⁰
10⁻¹¹
10⁻¹²
10⁻¹³
10⁻¹⁴
10⁻¹⁵
This Work
?
??
Al'tovskiy et al.
Jones and Gibson
??
Φ=DS
0.8
1
1.2
1.4
TEMPERATURE /10³ · K⁻¹

Summary

The diffusion coefficient and permeation coefficient are determined by means of gas-driven permeation technique independently.

$$D=1.3\times10^{-8}\exp(-49(kJ/mol)/RT)$$
$$\Phi=1.4\times10^{-6}\exp(-74(kJ/mol)/RT)$$

And, solubility coefficient is calculated from the relation $\Phi=DS$

$$S=1.1\times10^{2}\exp(-25(kJ/mol)/RT)$$

However, present values of Φ are about two orders of magnitude higher than the literature data. The reason is not clear at present. The difference may be due to material itself (production method, impurity etc.) and surface oxygen are possible reason.

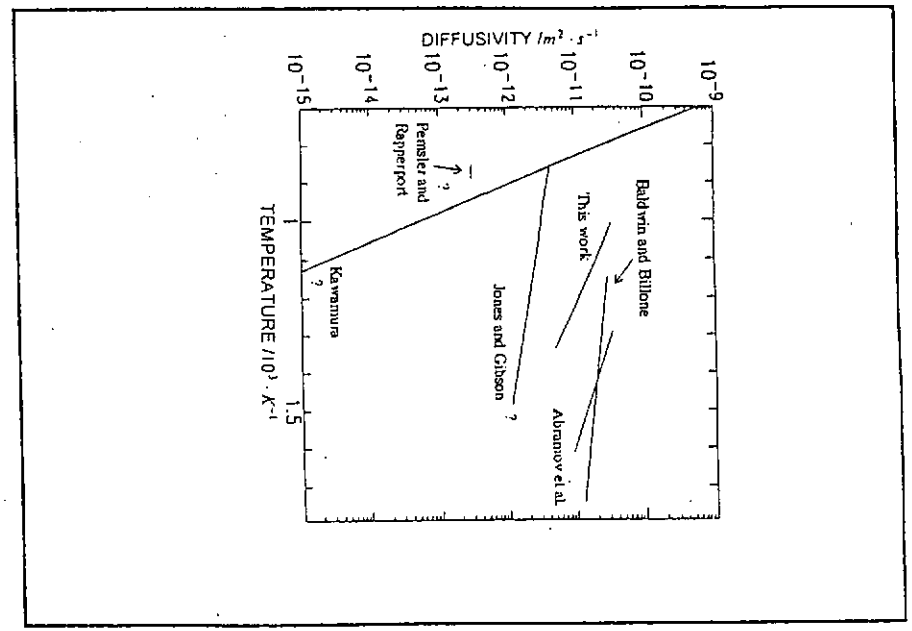

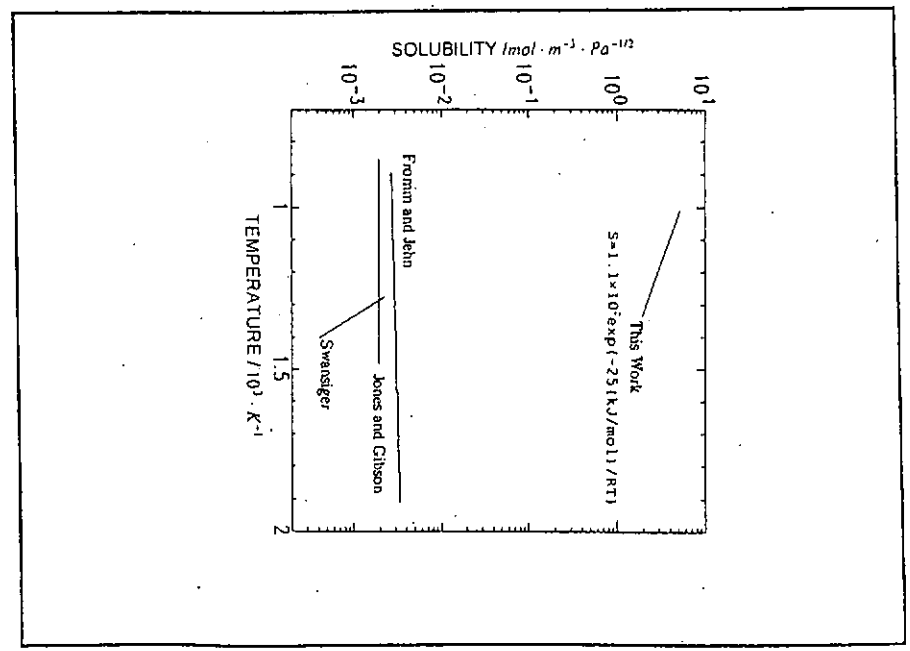

2nd International Workshop on Tritium Effects in Plasma Facing Components
May 19-20, 1994, Nagoya University

Secondary ion emission from beryllium surfaces

Kan ASHIDA[1], Hiroshi KAWAMURA[2], and Kuniaki WATANABE[1]

An effort has been made to reduce the radiation loss of burning plasma by heavy impurity ions in controlled thermonuclear fusion devices. One solution is to use low-Z materials such as graphite and/or carbon composite as the first wall. The recent successful operations of the Joint European Torus (JET) showed that Be is a leading candidate for plasma-facing material. Extensive investigation has been carried out to understand the interactions, such as fuel retention, erosion by sputtering, and so on, between Be and energetic particles. Little is known, however, about the chemical forms or species emitted from the Be surface owing to physical and/or chemical sputtering as well as trapped states of hydrogen isotopes.

In the present study, we investigated the chemical forms or species of Be emitted by sputtering with ions of argon and/or a mixture of argon and deuterium by means of secondary ion mass spectrometry (SIMS) along with surface characterization using x-ray photoelectron spectroscopy (XPS). The results indicate that the secondary ion species emitted from the Be surface could be classified into three groups when Ar and/or (Ar + D_2) probes were used: namely, (i) Be and Be-cluster, (ii) oxide and hydroxide, and (iii) hydride an/or deuteride. They appear to be strongly related each other.

1. Hydrogen Isotope Research Center, Toyama University
2. JAERI, Oarai establishment

2nd International Workshop on Tritium Effects in Plasma Facing Components
May 18-20, 1994, Nagoya University

Secondary Ion Emission from Beryllium Surfaces

Kan ASHIDA[1], Hiroshi KAWAMURA[2], and Kuniaki WATANABE[1]

[1]Hydrogen Isotope Research Center, Toyama University

[2]JAERI, Oarai Research Establishment

Presentation Items:

- Sample Fabrication & Impurities
  1. Fabrication Process & Impurities
- Surface Characterization of Beryllium (XPS)
  1. Conditioning by Vacuum Heating
  2. Conditioning by Ar^+ Sputtering
- Secondary Ion Emission from Beryllium (SIMS)
  1. Ar^+ as Primary Ions
  2. $(Ar+D_2)$ as Mixed Primary Ions
  3. Classification of Secondary Ions

Sample Preparation & Impurity

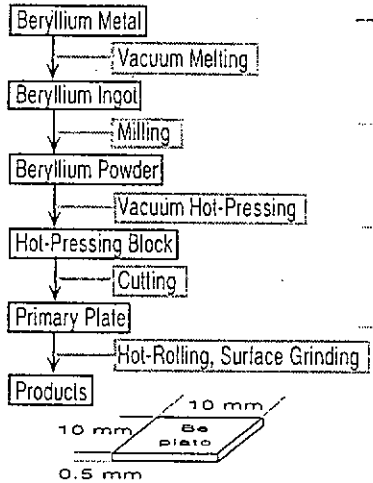

Element	Content(at%)
Be	99.86
Al	0.011
B	0.00008
Cd	0.00002
Ca	0.00070
C	0.073
Cr	0.0023
Co	0.00012
Cu	0.00031
Fe	0.0099
Pb	0.00010
Li	0.00039
Mn	0.0017
Mg	0.0035
Mo	0.00018
Ni	0.0034
Si	0.0076
Ag	0.00003
Cl	0.00077
N	0.0249

Conditioning by Vacuum Heating (XPS)

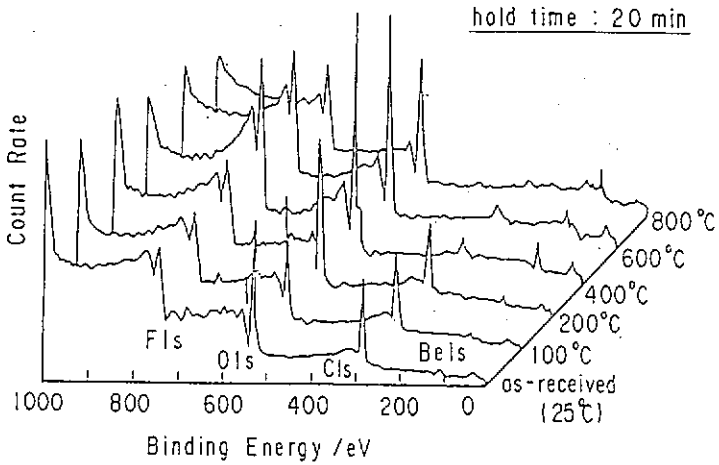

Conditioning by Ar^+ sputtering (XPS)

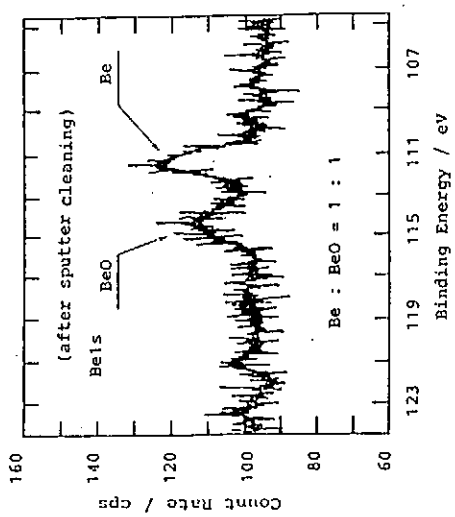

Ar^+ as Primary Ions (SIMS)

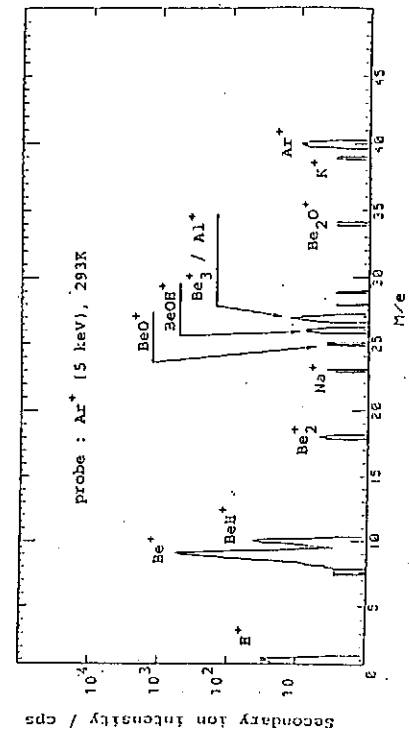

High Resolution SIMS...26.90≦M/e≦27.10 amu

(O^+ as Primary Ions)

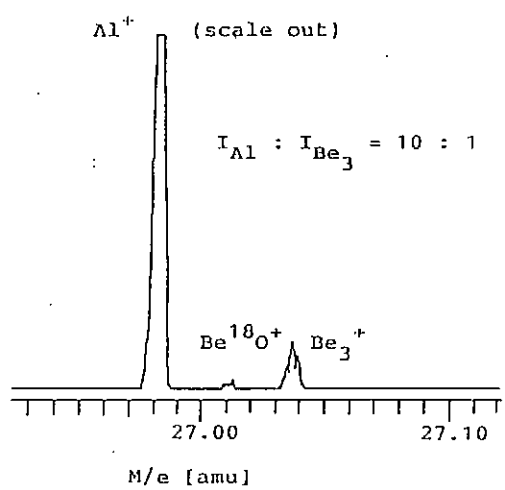

Temperature Dependence

(Ar^+ as Primary Ions)

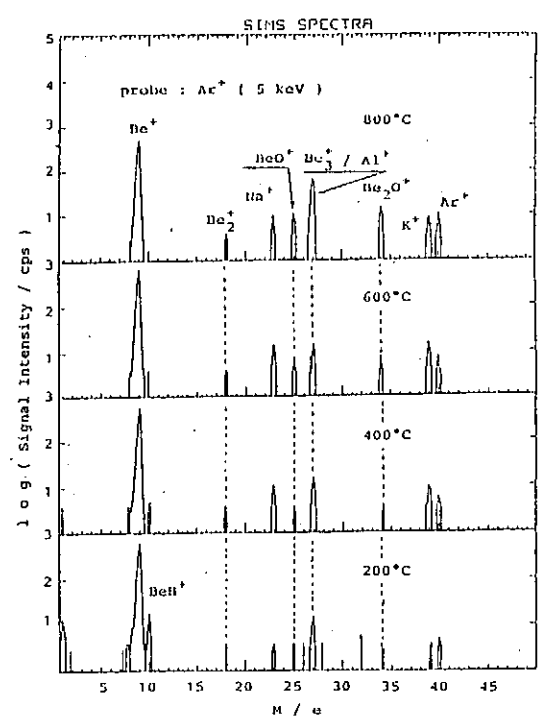

Classification of Observed Secondary Ions

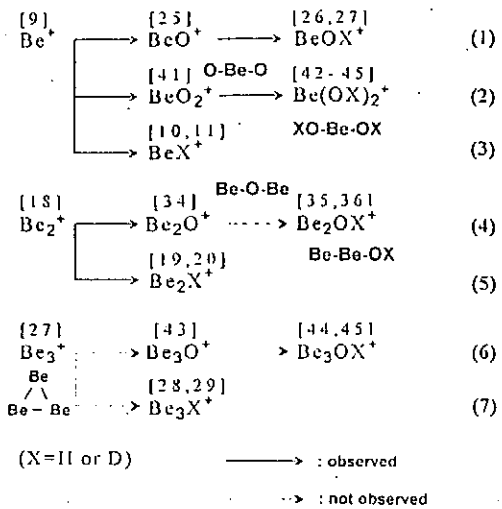

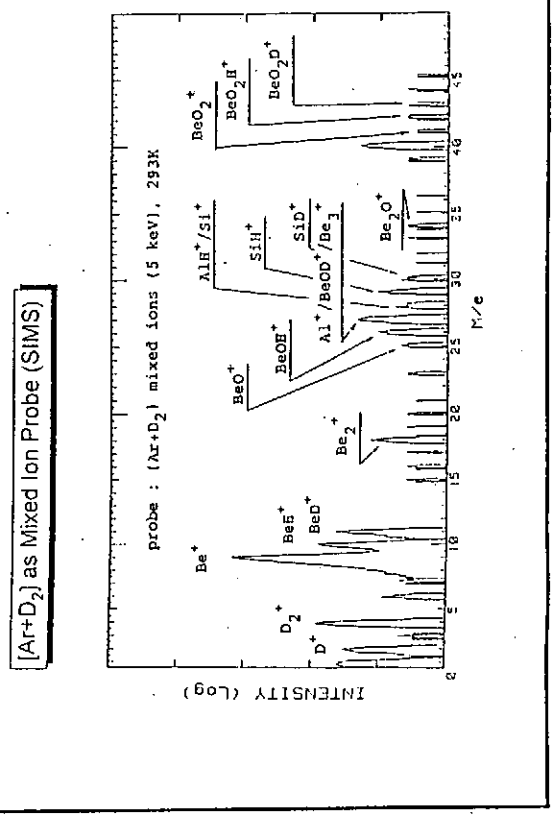

Temperature Dependence ([Ar+D_2] as Mixed Ion Probe)

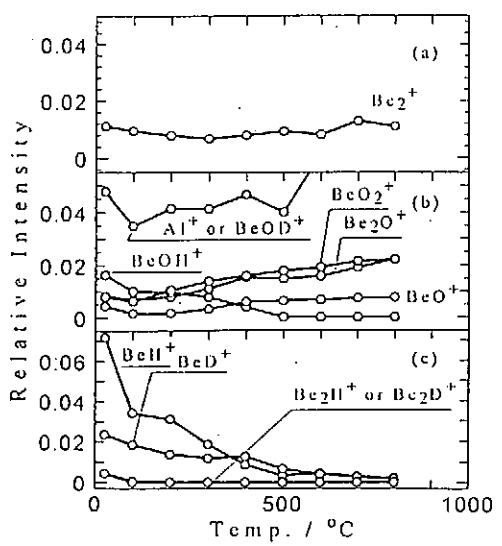

Summary

Varieties of cluster ions such as Be_n^+, Be_mX^+, $Be_mO_k^+$ and $BeO_mX_m^+$ (X=H, D, n=1-3, k, m=1,2) were observed when Ar and/or an (Ar + D_2) mixture was used as source of probe ions. These secondary ion species emitted from the Be surface could be classified into three groups:

(i) Be and Be-cluster,

(ii) oxide and hydroxide, and

(iii) hydride and/or deuteride.

They appear to be strongly related each other and atomic configrations of them could be proposed based on the observations:

(1) ions containing one X are formed for Be_m^+ (m=1,2) and BeO^+, on the other hand, they are not for Be_lO^+ (l=2),

(2) two X's are captured by BeO_2^+ and X-O-Be-O-X configuration is proposed for $BeO_2X_2^+$, and

(3) Be-O-Be configuration is proposed for Be_2O^+.

Session 3

A Critical Review of the Data Available for Tritium in Beryllium

A. A. Pisarev
Moscow Engineering Physics Institute

The data on both solubility and diffusivity of T in Be available from literature differ many orders of magnitude. These data are strongly influenced by oxide layer on the surface, internal network of oxide, lattice damage, and impurities.

The solubility data obtained by Swansiger [1] and usually used as the most reliable data seems to give wrong both absolute values and temperature dependence. These data do not follow the universal temperature dependence as reviewed by Fromm & Jehn [2] for all other metals. The peculiar temperature dependence obtained by Swansiger have not been observed for other metals and can not be explained quantitatively using the expression proposed for solubility. These experiments based on measurements of T activity in acid after disolution of the sample in acid did not take into account T that can be found not in acid but in gas over acid as observed by Causey [3].

Other measurements, performed by Jones & Gibson [4], Pemsler & Rapperport [5] Fromm & Jehn [2], Macaulay- Newcombe *et al* [6] have their own uncertainties.

Solubility in BeO can be 30~100 times higher than that in Be according to Macaulay- Newcombe [6].

From qualitative speculations one may expect that solubility of T in Be has the temperature dependence close to that in Fe.

Diffusion data obtained by Jones & Gibson [4] are usually used as " the most reliable data " . They are measured using thermodesorption after Be saturation. These data are influenced by oxide layer and hydrogen- defect interaction and therefore can not be considered as the most reliable data. Besides these data can be influenced by diffusion and desorption of various T containing species.

Diffusion through oxide is many orders of magnitude less than diffusion through Be metal as shown by Fowler *et al* [2]. Therefore, the effective diffusion coefficient can be several orders of magnitude less than that through Be metal as shown by Abramov [7].

Abramov *et al* [7] give the diffusion data that can be considered as the most reliable. The experiment was performed with denterium using permeation technique and taking into account influence of oxide layer. Nevertheless these data perhaps are influenced by both heavy water and HD desorption that have not been taken into account.

Tritium can diffuse through oxide perhaps in the form of heavy water molecules as suggested by Macanlay- Newcombe [6], and water give rise pressure increase during desorption as shown by Fowler *et al* [2].

Heterogeneous molecules HD or HT are often observed for example in ion implantation experiments.

References

1. W. A. Swansiger, J. Vac. Sci and Technol. 1986, 4(3), 1216
2. J. D. Fowler *et al* . J. Amer. Ceramic Soc. 1977, 60(3-4), 155
3. R. A. Causey et al. J. Nucl. Mater, 1990, 176/177, 654
4. P. M. S. Jones and R. Gibson, J. Nucl. Mater. 1967, 21, 353
5. J. P. Pemsler and E. J. Rapperport. Trans. Met. Soc. AIME,1964, 230, 90
6. R. G. Macaulay- Newcombe et al. J. Nuel. Mater. 1992, 191/192, 263
7. E. Abramov et al J. Nucl. Mater. 1990, 175, 90

A Critical Review of Data Available For Tritium in Beryllium

A.A.Pisarev
Moscow Engineering Physics Institute
Moscow 115409 Russian Federation
Fax: 095 324-70-24
e-mail: root@plasm.mephi.msk.su

This work was financially supported by
Contract 94-2-021-139
from the Ministry of Atomic Energy, RF
Grant MJG000
From the International Science Foundation

Calculation of tritium content in defects with various E^B in Be in equilibrium with T_2 in gas phase at 1 atm and E_S=1 eV given by W.A.Swansiger

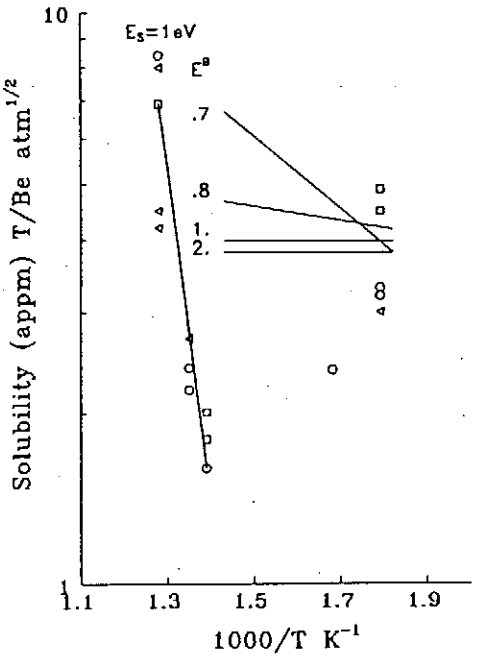

Tritium solubility at 1 atm in various metals reviewed by E.Fromm & H.Jehn and the experimental points for Be obtained by W.A.Swansiger.

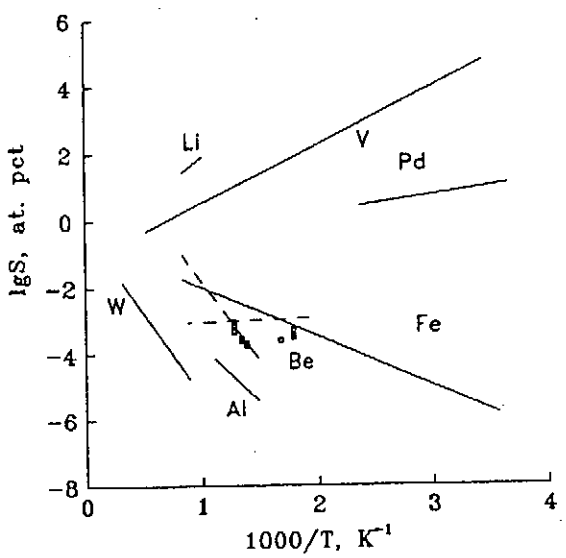

Tritium retained in Be exposed to a DT plasma and measured as HTO in acid solution used to dissolve Be samples and as HT in a sweep gas sent over acid.

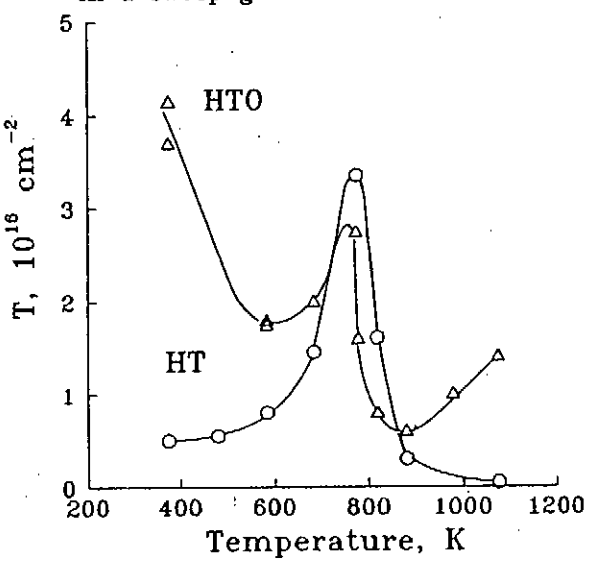

Comparison of temperature dependence of equilibrium solubility of T in Be measured by Swansiger et al with temperature dependences of T content measured as HTO and HT in Be exposed to DT plasma . Both measurements are performed by Be dissolution in acid.

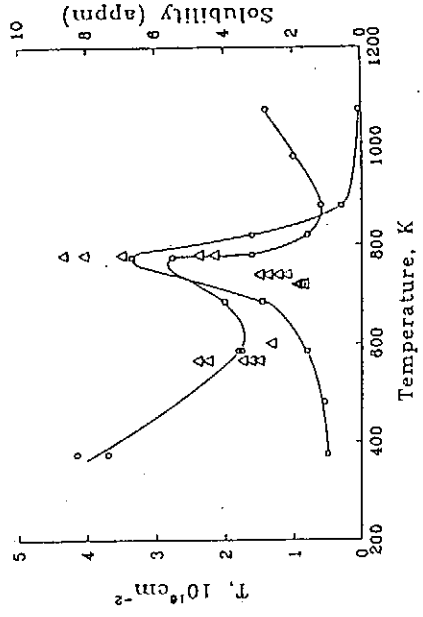

Diffusivities of tritium in Be
1,2 – Bilone et al
3 – Jones & Gibson
4 – Pemsler & Rapperport
5 – Abramov et al
6,7 – D_{eff} from Abramov et al

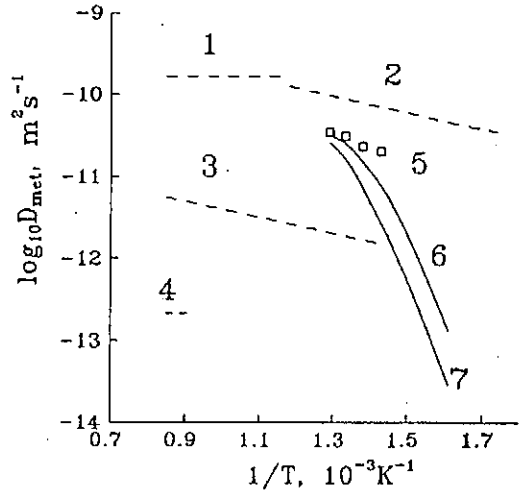

Diffusivities of tritium in BeO measured by Fowler et al in different samples and diffusivities in BeO calculated from experiment performed by Abramov et al with two samples of different thickness

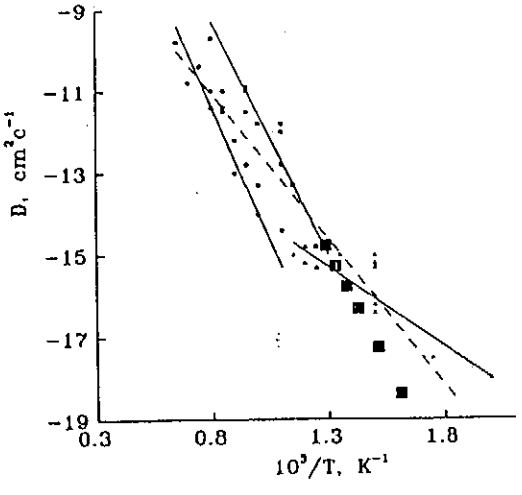

Hydrogen Isotope Exchange in Boronization

M. Yamage, T. Saito, H. Toyoda, M. Saidoh*, N. Ogiwara* and H. Sugai

Department of Electrical Engineering, Nagoya University, Nagoya 464-01, Japan
* Japan Atomic Energy Research Institute, Naka-machi, Ibaraki-ken 311-01, Japan

Extensive basic studies on the control of hydrogen concentration and the isotope exchange in boronization are reported. The H content of boron layer depends on species of boron-source gas (B_2H_6, $B_{10}H_{14}$) and dilution gas (He, H_2) and it is considerably reduced by heating up the vessel wall from 50 to 300°C. Furthermore, a low-pressure ECH discharge turned out to give the remarkably low H content in spite of room temperature, in comparison with a conventional DC glow discharge.

Two methods of deuterated boronization, i.e., isotope exchange from H to D, are proposed to solve a dilution problem caused by H desorption from boronized walls. One is the H-D exchange in a continuous deposition mode where deuterium is used as a dilution gas. The other is the H-D exchange in a digital deposition mode where thin layer deposition and subsequent deuterium glow conditioning are repeated. The deuteration ratio D/(D+H) attains to 80-95 % in both methods. The hydrogen desorption in the deuterium glow discharge is almost proportional to the residual hydrogen concentration in the deuterated boron film, irrespective to the deposition conditions.

Hydrogen Isotope Exchange in Boronization

M. Yamage, T. Saito, H. Toyoda, M. Saidoh*, N. Ogiwara* and H. Sugai

Nagoya University
*Japan Atomic Energy Research Institute

Background

1) Boronization by decaborane ($B_{10}H_{14}$)
less hazardous than diborane (B_2H_6)

2) Dilution of deuterium by hydrogen
D_2 shots after boronization
→ H_2 desorption from boron film
(e.g., H^+/D^+ ~1 during a shot just after boronization in JT-60U)
need to prepare deuterated boron film

Deuterated boronization

$B_{10}D_{14}$ → Very expensive, not available from companies

Purpose

$B_{10}H_{14}$, D_2 → Deuterated boronization

To find optimum conditions

1) Deuteration ratio D/(D+H) ↗
2) Total concentration (D+H) ↘

Experimental apparatus

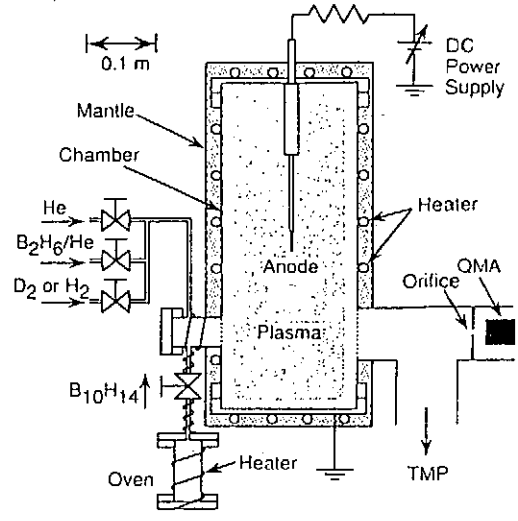

Typical Experimental conditions

Material Gas	$B_{10}H_{14}$	
Pressure	0.023~0.068	(Pa)
Dilution gas	D_2 / He	
Pressure	0.80	(Pa)
Discharge Voltage	380~630	(V)
Discharge Current	0.07	(A)
Wall Temperature	250	(°C)
Deposition Time	0.5~1.3	(h)
Film Thickness	100~180	(nm)

Factors determining the hydrogen content

(Before deuteration)

1) Wall temperature
2) Boron-source gas (B_2H_6, $B_{10}H_{14}$)
3) Plasma (DC glow plasma, ECH plasma)

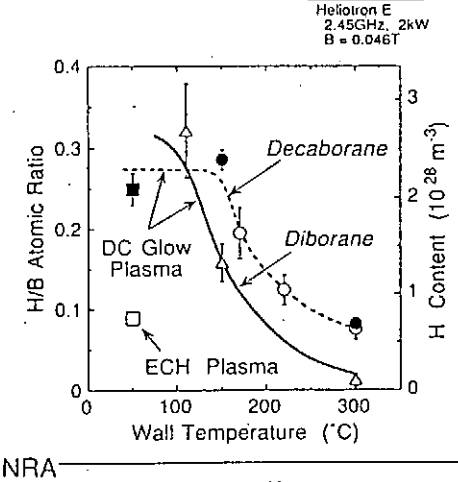

NRA

^{15}N ion beam → H → γ - ray

$^{15}N + H = {}^{12}C + {}^{4}He + \gamma$ - ray (4.43MeV)

Count number ∝ H/B atomic ratio

Film properties of deuterated boronization

measured by ERD

He 0.8 Pa
$B_{10}H_{14}$ 0.068 Pa
V_d ~400V
I_d = 0.07A
T_w = 250°C
Film thickness ~180nm

1) Deuteration ratio (~80%)

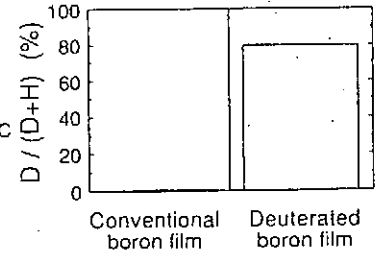

D_2 0.8 Pa
$B_{10}H_{14}$ 0.068 Pa
V_d ~550V
I_d = 0.07A
T_w = 250°C
Film thickness ~130nm

2) Total Concentration

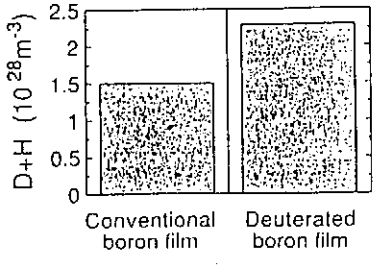

Gas ratio $B_{10}H_{14}/D_2$ vs Deuteration ratio, Total concentration

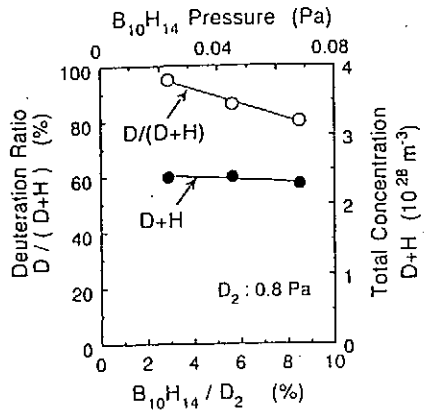

Decrease in decaborane partial pressure

High deuteration ratio — Constant total concentration

$B_{10}H_{14}$ / D_2 = 3 % → D / (D+H) = 95 %

Effect of He addition

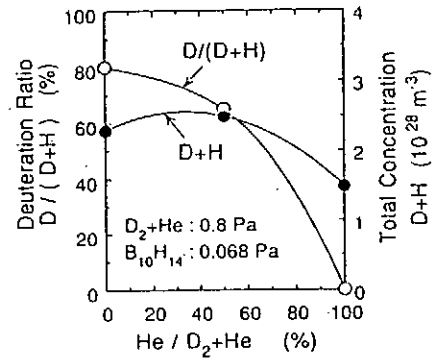

Increase in helium pressure

↓

1) No reduction in the total concentration

2) Appreciable decrease in deuteration ratio

Digital deposition mode

Repeats deposition / conditioning cycle

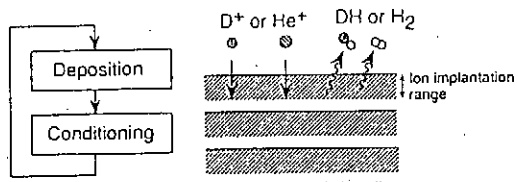

a) $B_{10}H_{14}/D_2$ Deposition + D_2 glow conditioning

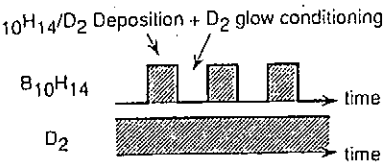

b) $B_{10}H_{14}$/He Deposition + D_2 glow conditioning

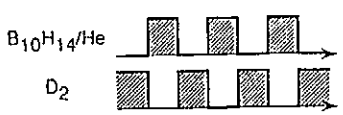

c) $B_{10}H_{14}/D_2$/He Deposition + He glow conditioning

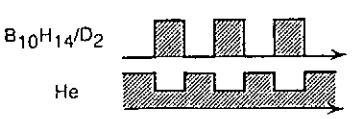

Monolayer thickness vs Deuteration ratio, Total concentration

a) $B_{10}H_{14}/D_2$ deposition + D_2 glow conditioning

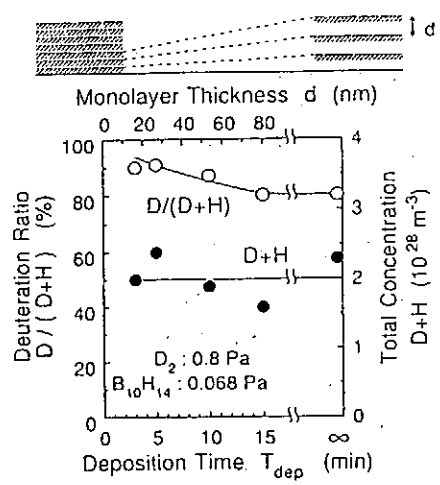

Thin layer deposition → Improves deuteration ratio
(comparable to implantation range)

TRIM code simulation → Implantation range : 15-30nm

Summary of digital deposition mode

	Digital deposition			Conventional boron films
	Mode (a)	Mode (b)	Mode (c)	
Deposition gas	$B_{10}H_{14}/D_2$	$B_{10}H_{14}$/He	$B_{10}H_{14}/D_2$/He	$B_{10}H_{14}$/He
Conditioning gas	D_2	D_2	He	

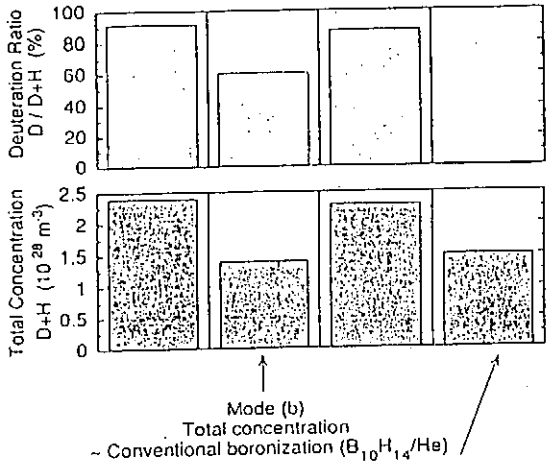

Mode (b)
Total concentration
~ Conventional boronization ($B_{10}H_{14}$/He)

H content vs H desorption

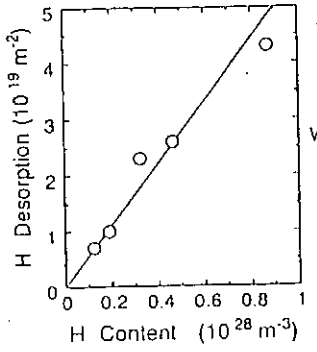

D_2 discharge
Pressure 8.0 Pa
V_d – 500 V
I_d = 0.3 A
Wall Temp. = 250 °C

H desorption ∝ H content

$\frac{\text{H desorption}}{\text{H content}}$ = Implantation range – 5nm

TRIM code simulation → Implantation range : 10-20 nm

Conclusion

I. Factors determining the hydrogen content

1) Wall temperature
2) Boron-source and dilution gas
3) Plasma (DC glow , ECH)

II. H-D exchange in continuous deposition mode

$B_{10}H_{14}/D_2$ boronization

Deuteration ratio D/(D+H) > 80%

Total concentration (D+H) > Conventional boronization ($B_{10}H_{14}$/He)

III. H-D exchange in digital deposition mode

Deuteration ratio D/(D+H) > 90%

Total concentration (D+H) ~ Conventional boronization ($B_{10}H_{14}$/He)

EFFECT OF a-B/C:H FILMS POROSITY ON DIFFUSION AND EROSION UNDER DEUTERIUM PLASMA IRRADIATION

V.M.Sharapov, A.I.Kanaev, S.Yu.Rybakov and L.E.Gavrilov

Institute for Physical Chemistry, Russian Academy of Sciences
Leninsky prospect, 31, Moscow 117915, Russia

EFFECT OF a-B/C:H FILMS POROSITY ON DIFFUSION AND EROSION UNDER DEUTERIUM PLASMA IRRADIATION

V.M.Sharapov, A.I.Kanaev, S.Yu.Rybakov and L.E.Gavrilov

Institute for Physical Chemistry, Russian Academy of Sciences
Leninsky prospect, 31, Moscow 117915, Russia

Scheme of experimental set-up

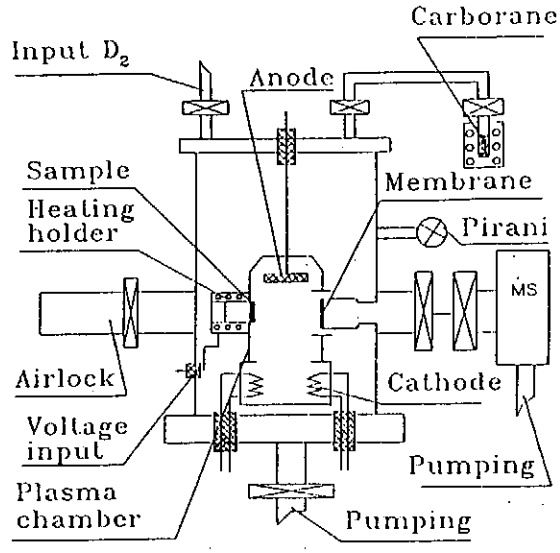

The initial part of kinetic curve of deuterium permeation through nickel at T=330°C

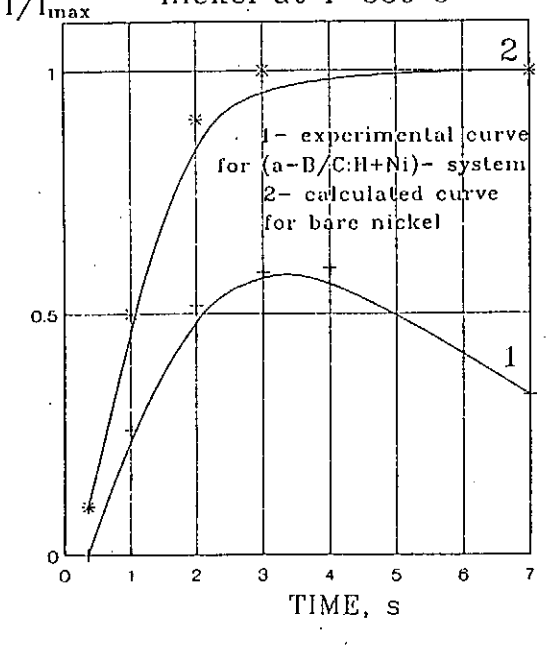

Kinetic curve of non-stationary stage of deuterium permeation through the (a-B/C:H+Ni)- system

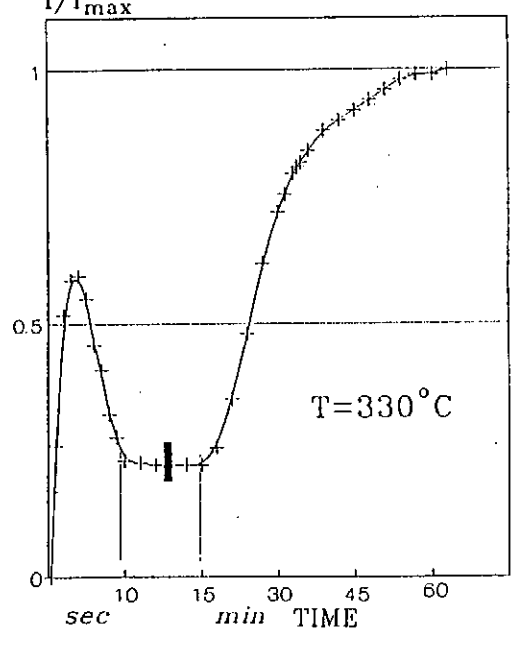

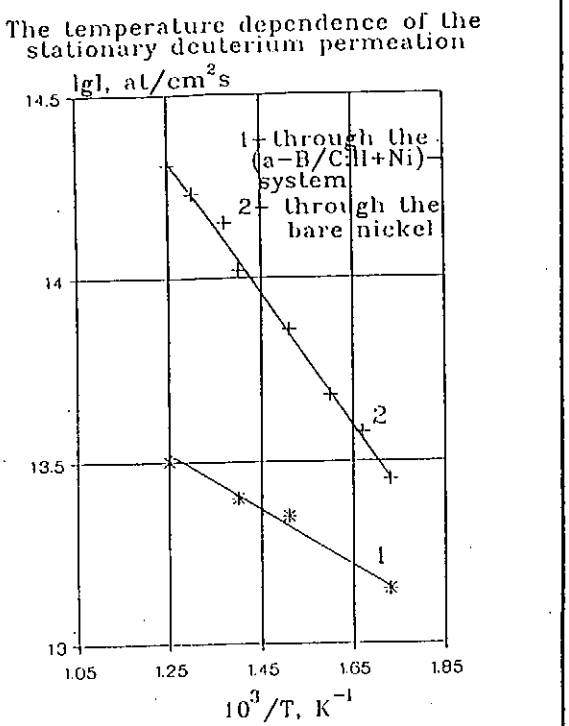

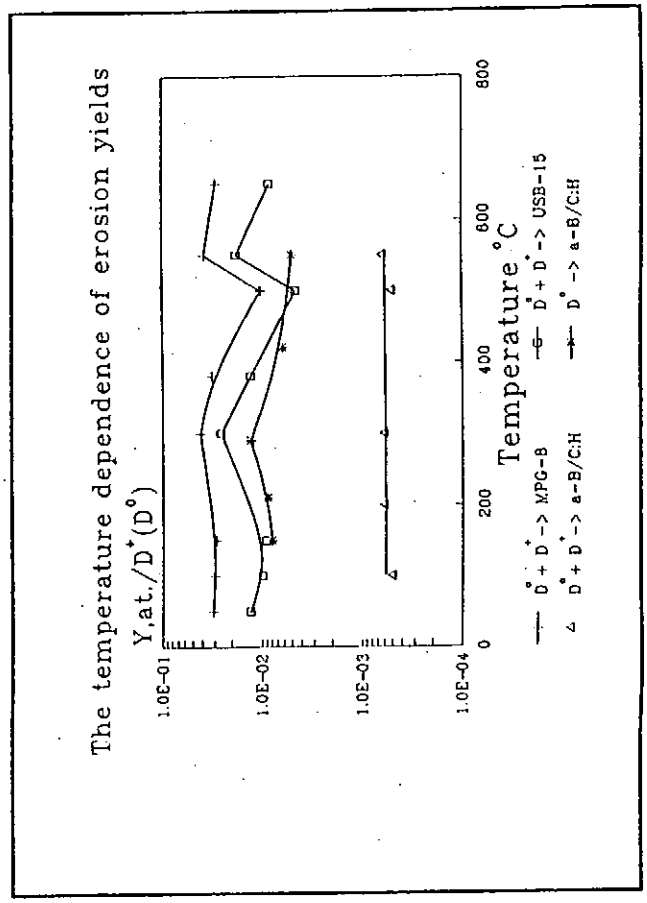

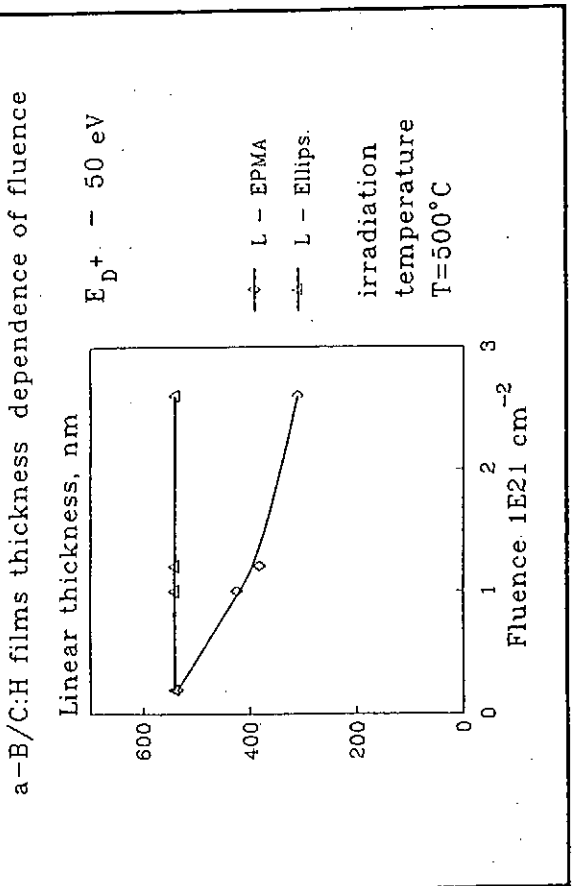

SUMMARY

The boronized carbon a-B/C:H films were produced by PCVD-method using non-toxic and non-explosive solid powder of carborane $C_2B_{10}H_{12}$ as a precursor. Due to high pressure of saturated vapour (~ 100 torr at 150°C) carborane can be used for boronization of large chambers. This technique was applied for boronization of Russian tokamaks T-11M, T- 3M, TUMAN-3 and T-10. The specific feature of the film which were obtained with using carborane is a wide range of variation of B/C ratio from 1 to 3.6 depending on the deposition conditions.

The influence of porosity of these films on the diffusion and erosion under deuterium plasma irradiation is being considered.

The set-up with ion-plasma source on the base of d.c glow discharge with heated cathode was used for the experiments.

In the permeation experiments with nickel the plasma-chemical deposition of films was being initiated simultaneously with the deuterium permeation start.

The analysis of non-steady stage of permeation leads to conclusions that the kinetic curve reflects the peculiarities of film growth. Film coverage of nickel surface is not continuous. Film grows by island mechanism and has porous structure.

The deuterium penetrates through a-B/C:H films by two channels - along the open pores and through the film bulk. This determines non- typical diffusion kinetics and the decreasing of the steady-state permeation comparing with bare nickel by a factor of 5-7 at temperatures lower than 530°C.

The erosion experiments were fulfilled in the similar device. The erosion yields were determined on the base of mass thickness loss measured by EPMA. It was shown that erosion of film under the deuterium plasma and in contact with thermal deuterium atoms has a chemical nature and film erodes through the developing of porosity. The erosion under thermal deuterium atoms exposure is higher than that under plasma irradiation. The reason is assumed to be the smoothing down the surface relief during the ion bombardment which decreases partly the access to inner pores.

Thus, for the chemically active gases the porosity increases the erosion yields in result of increasing of real surface for chemical interaction.

REFLECTION OF LOW ENERGY HYDROGEN FROM CARBON AT OBLIQUE INCIDENCE

M.Mayer, W.Eckstein, B.M.U.Scherzer
Max-Planck-Institut für Plasma Physik, D-85748 Garching, Germany
EURATOM-Association

The particle reflection coefficient is determined experimentally and by computer simulation for the bombardment of two different kinds of carbon with deuterium at normal and oblique incidence in the energy range from 1 keV down to 33 eV. Well polished HOPG graphite and EK98 served as targets, the former as an example with a relatively flat surface, the latter with a rough surface topography. The experimental technique is based on the measurement of the trapped amount by the nuclear reaction analysis using the reaction $d(^3He,p)\alpha$; protons are detected with a surface barrier detector. It is found that the usual assumption of complete trapping at low fluences is not fulfilled at low energies ($\leq$ 100 eV). This is demonstrated by measuring the decrease of the implanted deuterium with further bombardment of protons at the same energy. This loss of implanted atoms can be described by an exponential function which can be used to determine the correct trapping coefficient and from this the correct particle reflection coefficient.

The experimentally determined particle reflection coefficients for HOPG agree reasonably well with data calculated with the Monte Carlo program TRIM.SP (version TRVMC); only at the lowest energy of 33 eV the experimental values are somewhat higher at intermediate angles of incidence than the calculated ones. The rough surfaces of EK98 are investigated with a scanning tunneling microscope. It is found that these surfaces can be described by a fractal surface of dimension 2.05. For these surfaces agreement of the experimental values with those calculated with the program VFTRIM (based on TRIM.SP, assuming a fractal surface) is found.

REFLECTION OF LOW ENERGY HYDROGEN FROM CARBON
AT OBLIQUE INCIDENCE

M.Mayer, W.Eckstein, B.M.U.Scherzer
Max-Planck-Institut für Plasma Physik, D-85748 Garching, Germany
EURATOM-Association

Problem
Reflection from flat and rough surfaces

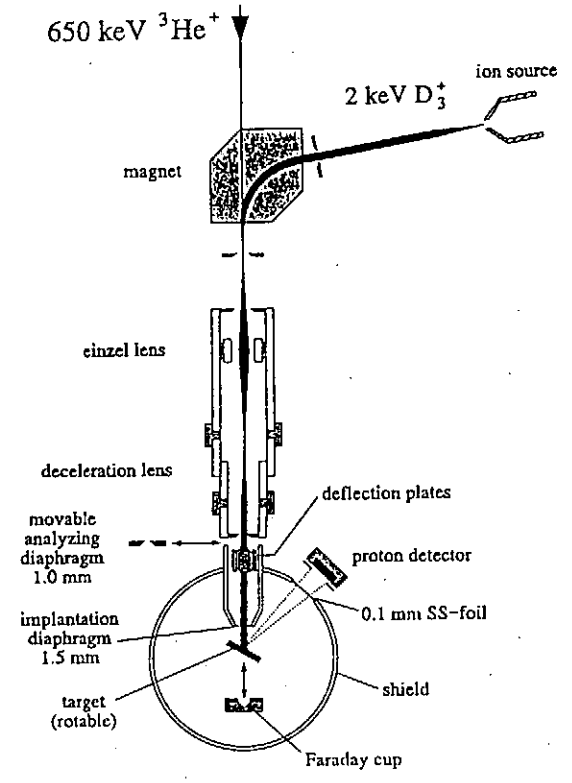

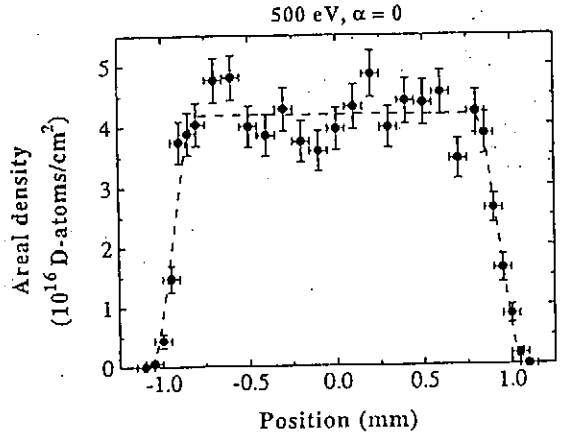

Basic principle of the experiment

Measurement of the trapped amount T of D in Carbon by the nuclear reaction

$^3He(d,p)^4He$

Particle reflection coefficient

$R_N = 1 - T$

assumption: no losses of particles

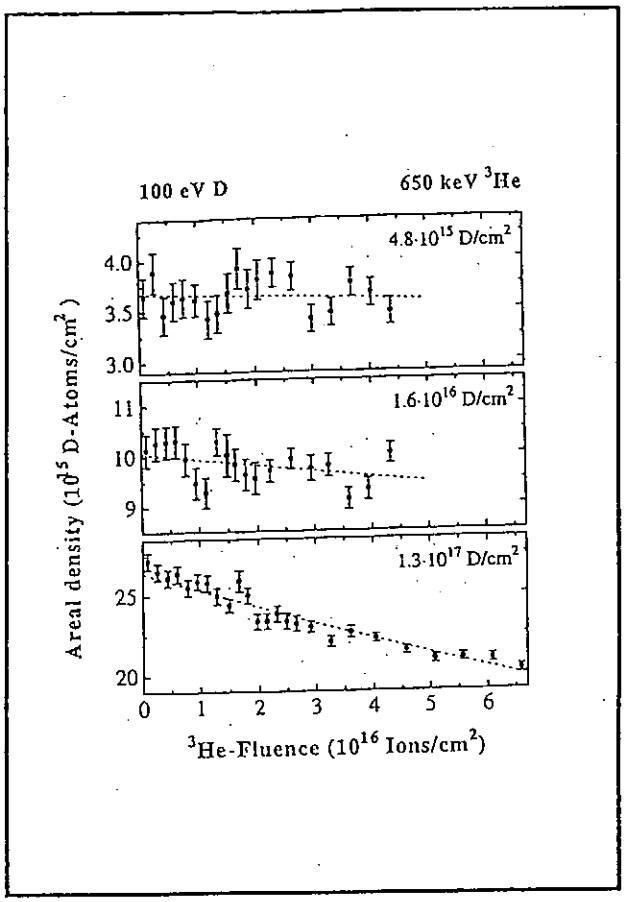
100 eV D
650 keV ^{3}He
4.8·10^{15} D/cm^2
1.6·10^{16} D/cm^2
1.3·10^{17} D/cm^2
Areal density (10^{15} D-Atoms/cm^2)
^{3}He-Fluence (10^{16} Ions/cm^2)

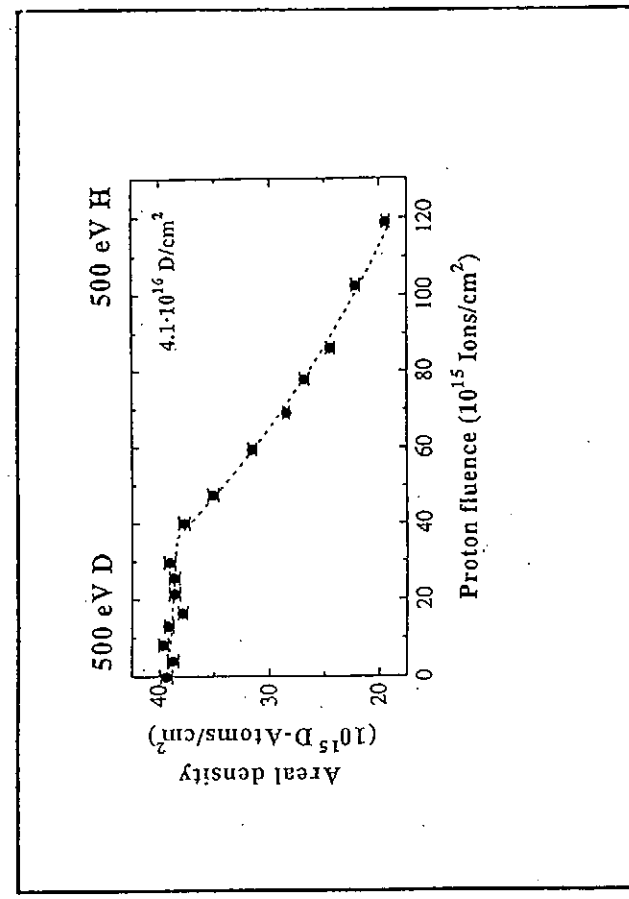
500 eV H
500 eV D
4.1·10^{16} D/cm^2
Areal density (10^{15} D-Atoms/cm^2)
Proton fluence (10^{15} Ions/cm^2)

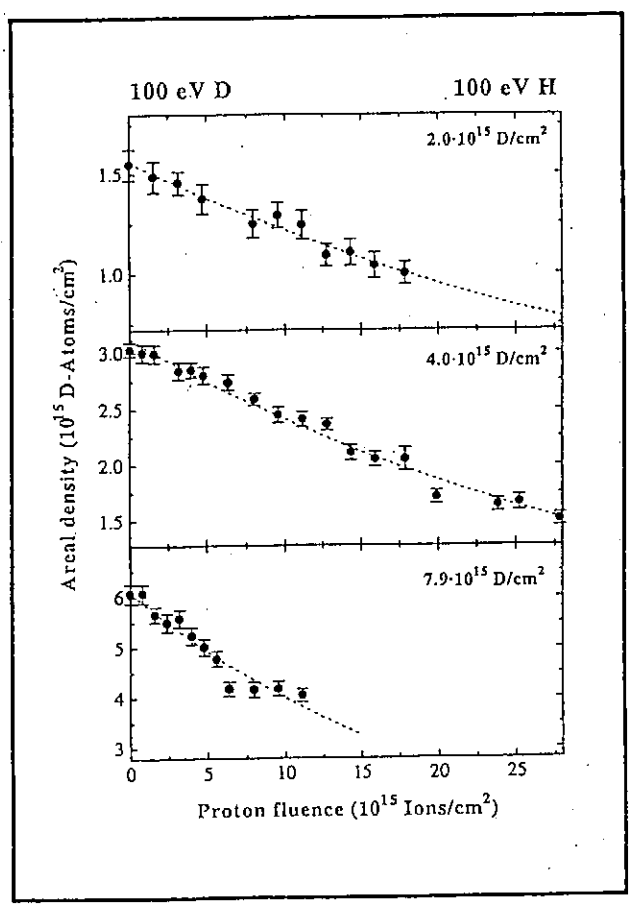
100 eV D
100 eV H
2.0·10^{15} D/cm^2
4.0·10^{15} D/cm^2
7.9·10^{15} D/cm^2
Areal density (10^{15} D-Atoms/cm^2)
Proton fluence (10^{15} Ions/cm^2)

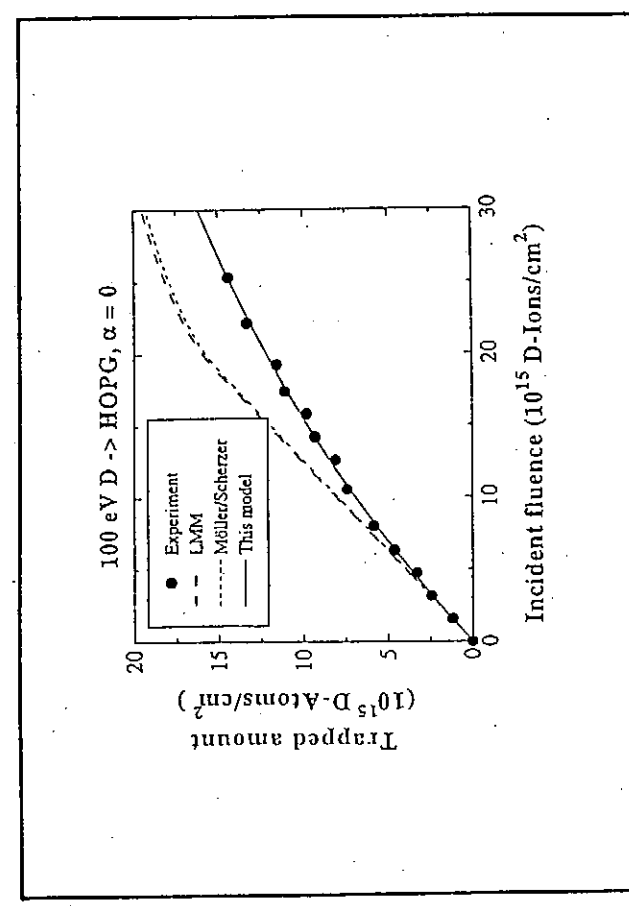
100 eV D -> HOPG, α = 0
Experiment
LMM
Möller/Scherzer
This model
Trapped amount (10^{15} D-Atoms/cm^2)
Incident fluence (10^{15} D-Ions/cm^2)

Modelling

TRVMC
Monte Carlo Program , BCA , amorphous target

VFTRIM
fractal surface , based on TRVMC

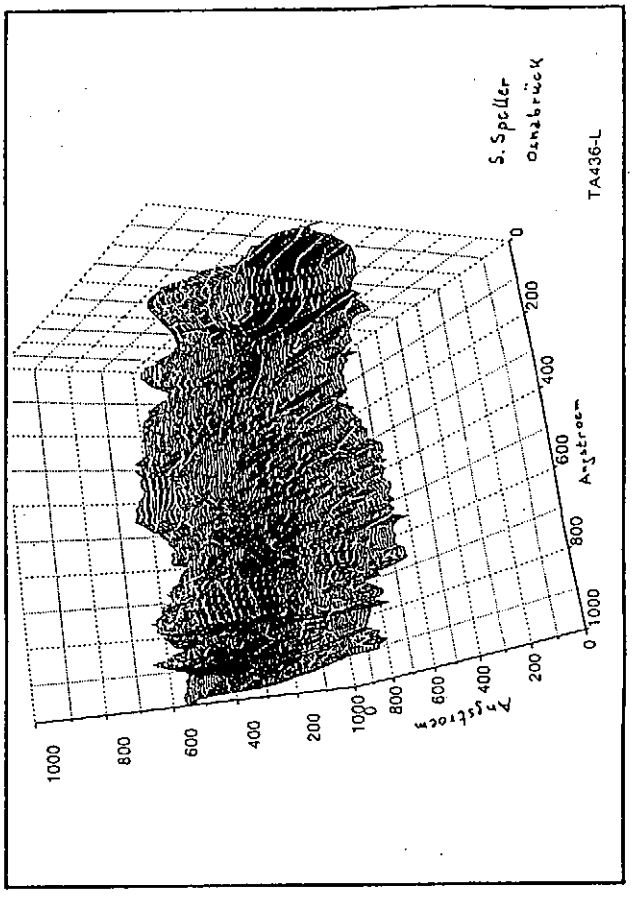

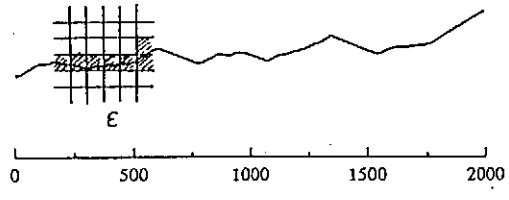

Number of squares : $N(\varepsilon) \sim \varepsilon^{-d}$

d: fractal dimension

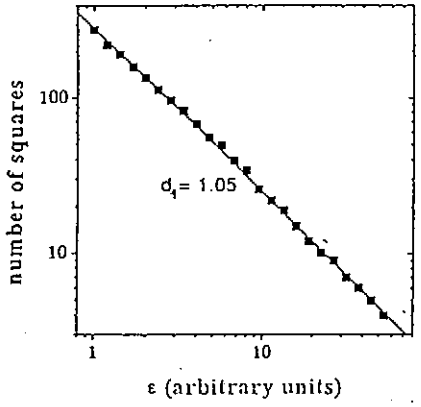

dimension of surface: $d_\perp = 1 + d$.

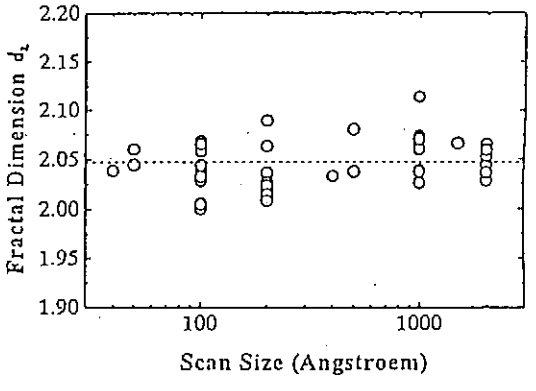

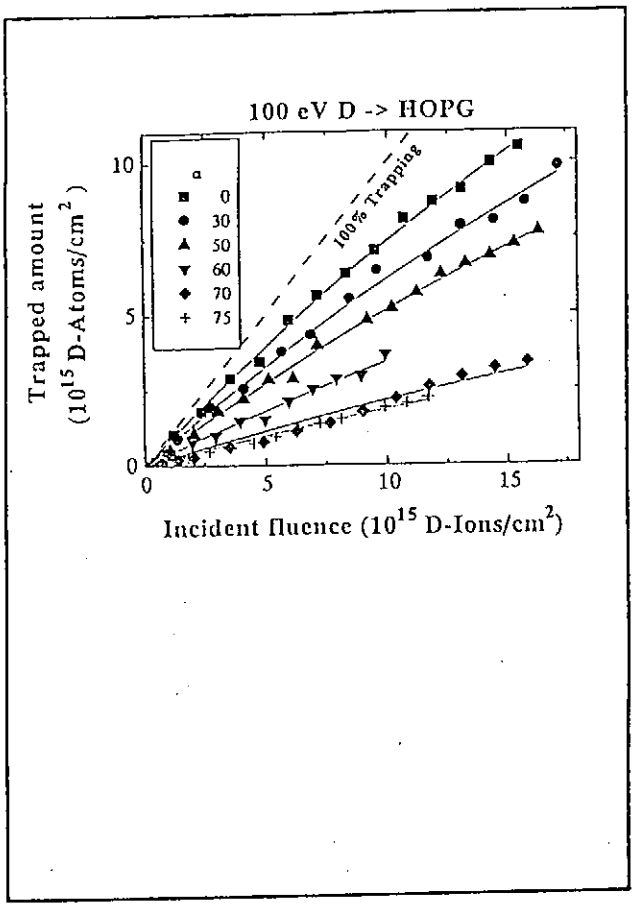
100 eV D -> HOPG
Trapped amount
(10^{15} D-Atoms/cm^2)
Incident fluence (10^{15} D-Ions/cm^2)
α
0
30
50
60
70
75
100% Trapping
0
5
10
15

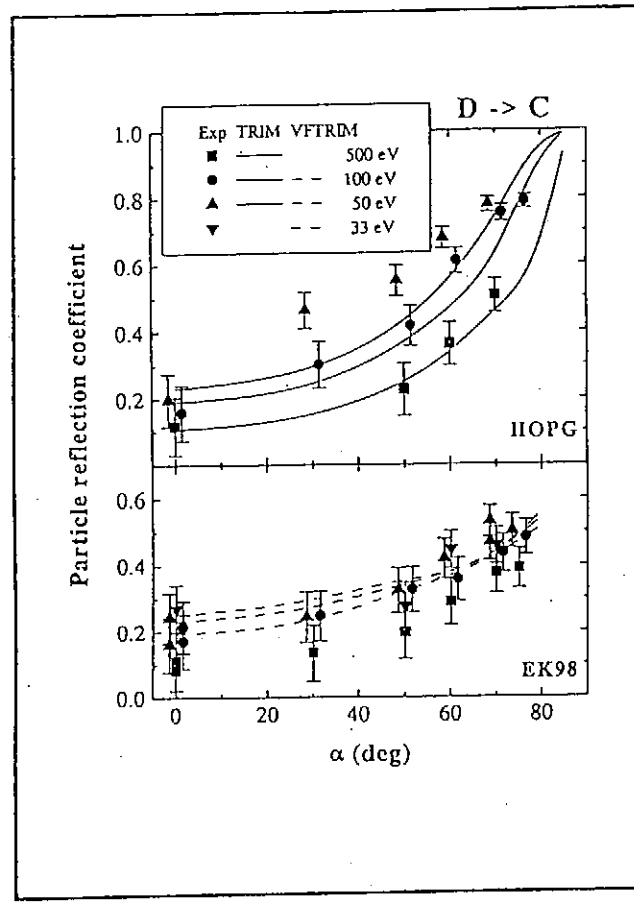
D -> C
Exp TRIM VFTRIM
500 eV
100 eV
50 eV
33 eV
Particle reflection coefficient
HOPG
EK98
α (deg)
0.0
0.2
0.4
0.6
0.8
1.0
0
20
40
60
80

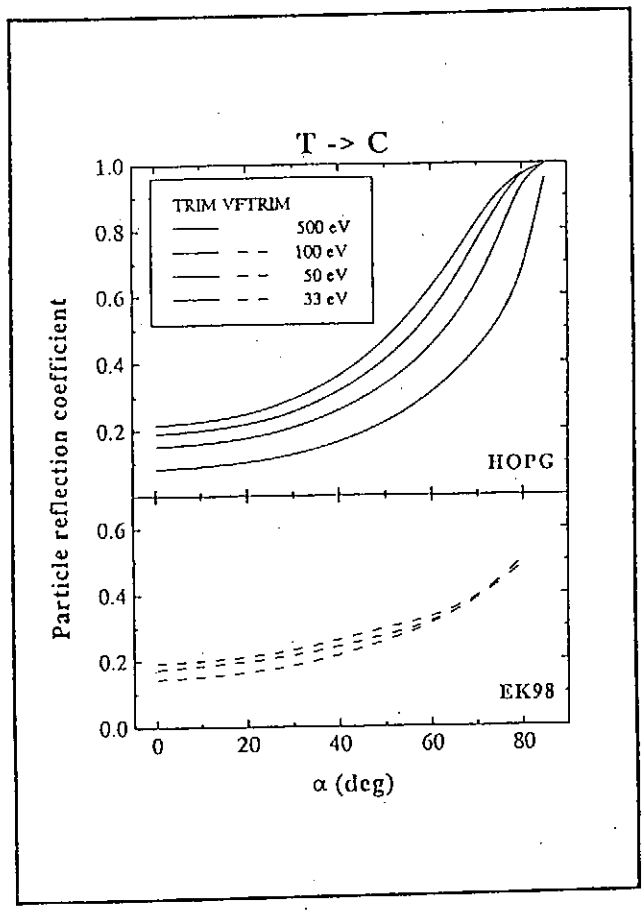
T -> C
TRIM VFTRIM
500 eV
100 eV
50 eV
33 eV
Particle reflection coefficient
HOPG
EK98
α (deg)
0.0
0.2
0.4
0.6
0.8
1.0
0
20
40
60
80

Atomic Reemission of Hydrogen from Pure and Boronized Carbon and Code Calculations for the Consequences in Tokamaks

E. Vietzke*, P. Franzen+, D. Reiter*, V. Philipps*, A. A. Haasz#, J.W. Davis#

*Institut für Plasmaphysik, Forschungszentrum KFA Jülich, Euratom Association, Jülich,FRG;
+Max Planck Institut für Plasmaphysik, Euratom Association, Garching, FRG;
#University of Toronto, Institute for Aerospace Studies, North York, Ontario, Canada

The understanding of retention and release processes of hydrogen and its isotopes in carbon materials is essential to plasma density control and tritium inventory considerations in future fusion devices. Experimental results published by Erents in 1976 for D reemission during D+ implantation in graphite (measured in the residual gas), as a function of temperature, showed a decrease in the steady-state reemission with increasing temperature above 1000 K. The observed D "loss" was interpretated by the authors by inward diffusion of D into graphite. The consequences of such a process would be a strong pumping effect and consequently a high H inventory, which is not acceptable for wall materials in a D-T burning reactor. The explanation of the observed decrease in H reemission is the reemission of H atoms from graphite. The reemitted H atoms recombine only partly at the chamber walls, the rest being pumped by the walls.

Thus, the release of implanted hydrogen from pure and boronized graphites was investigated for reemission and thermal desorption experiments using a line-of-side quadrupole mass spektrometer. At both experiments, also the release of hydrogen atoms was observed. At low temperatures the release of hydrogen occurs in form of molecules only. Above temperatures of about 900 K to 1100 K an increasing fraction of the implanted hydrogen is released in form of atoms. For the pure graphite the reemission of hydrogen atoms starts about 900 K, whereas the onset of the atomic reemission is shifted to higher temperature for the boronized C. At the TDS experiments the release of hydrogen molecules peaks around 1000~K, the release of atomic hydrogen peaks around 1200~K, being above this temperature higher than the release of molecular hydrogen. At both experiments, reemission and thermal desorption, the relative amount of released hydrogen atoms is the same at a given temperature. Thus, the atomic release of hydrogen from graphite is a thermal effect.

In order to asses the implications of these results on edge physics, EIRENE code calculations have been performed for ohmic discharges in TEXTOR. No large differences in the penetration depth of the neutral hydrogen was found.i.e., the radial distribution of D is very similar in molecular and atomic reemission. First calculations for the behavior in a divertor have been consistenly taken into account the mutual influence of neutral and plasma transport. They indicate a significant shift of energy fluxes to the targets (30%) due to reemission of thermal H atoms instead of molecules.

Atomic Reemission of H from Pure and Boronized Carbon and Code Calculations for the Consequences in Tokamaks

E. Vietzke*, P. Franzen+, D. Reiter*, V. Phillipps*, A. A. Haasz#, J.W. Davis#

*Institut für Plasmaphysik, Forschungszentrum KFA Jülich, Euratom Association, Jülich, FRG;
+Max Planck Institut für Plasmaphysik, Euratom Association, Garching, FRG;
#University of Toronto, Institute for Aerospace Studies, North York, Ontario, Canada

- Processes at the H-implantation und -reemission
- Reemission results in the residual gas
- Reemission results from direct observation
- Reemission model
- Consequences atomic H-reemission in Tokamaks (Eirene-Code)

- H^+-implantation und reemission in graphite:

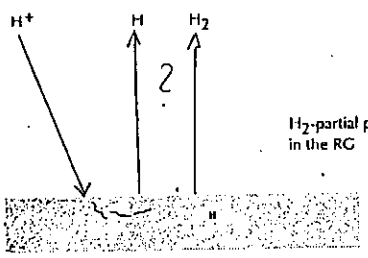

H_2-partial pressure change in the RG

Temp. dependence of D_2 re-emission in the residual gas:

S.K. Erents et al., J. Nucl. Mater. 63 (1976)399

- Transient phase at low fluences:

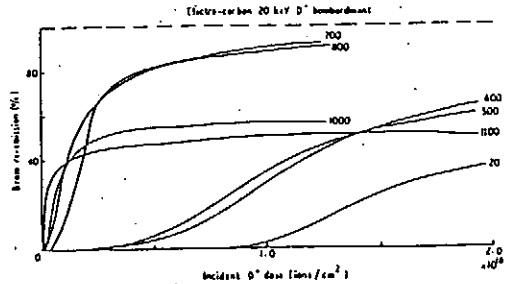

- D_2 Re-emission at steady state:

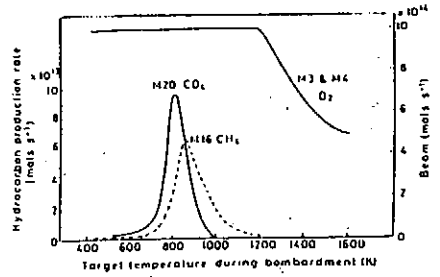

- Loss at high T:
  - Diffusion into the bulk ?
    - high pump effect in tokamaks (density control!)
    - high T/D inventory (Tritium)
  - Atomic re-emission? not observeable in RG due to wall pumping

Recent results of D_2 re-emission in the residual gas

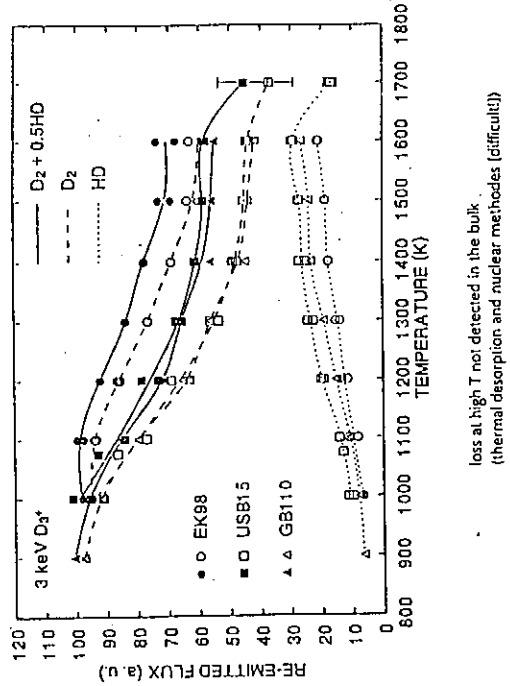

- loss at high T not detected in the bulk (thermal desorption and nuclear methodes [difficult!])
- hints for atomic re-emission at high T

Direct detection of H, H_2 by a line-of-sight mass spectrometer

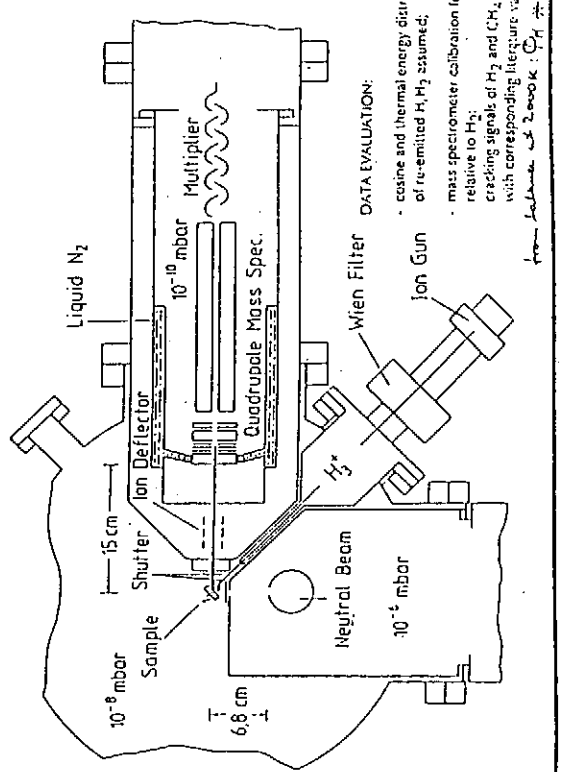

H_2,H reemission of 3 keV H_3^+ --> Graphite (EK98)
--> USB15 (15% B in C)

lines: model calc. with $\tau_0 K_\tau F$ = 3.1·10⁻⁴ and $2E_\tau - E_T$ = .96 eV for EK98
= 4.3·10⁻⁴ = 2 eV for USB15.

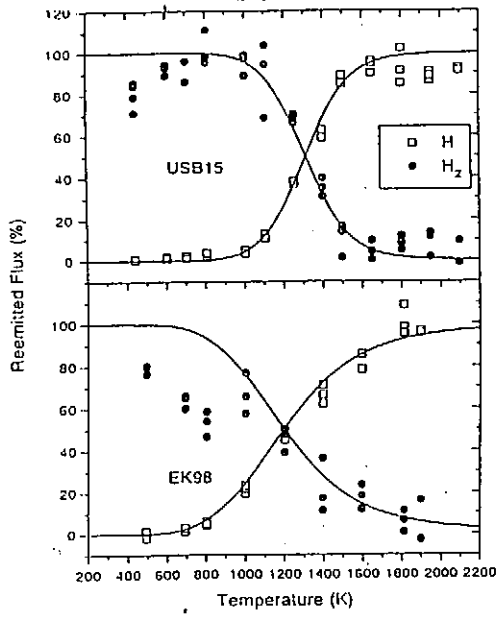

- at high T: H reemission only
- $T_{50\%}^{USB15} > T_{50\%}^{EK98}$ and steeper for USB15
- Reemission as H_2 at 500 K only 80%. why?

"Fig. 5": Reemission model:

Release of atoms without recombination due to a temperature dependent residence time in competition to the recombination to H_2.

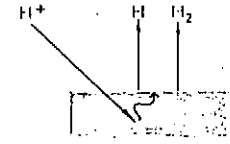

n [H/cm²] Surface concentration
τ residence time of H atom
K Recombination rate to H_2
F [H/cm².s] Ion flux density

Balance of surface density:

$$dn/dt = F - n^2K - n/\tau$$

In the steady state:

$$n = \frac{\sqrt{1 + 4\tau^2 K F} - 1}{2K\tau}$$

With $K = K_\tau \exp(-E_\tau/kT)$ and $\tau = \tau_0 \exp(E_\tau/kT)$ the temperature of x% H emission is given by

$$T_{x\%} = 5040 \cdot \frac{2E_\tau - E_\tau}{\log a \cdot \log(\tau_0^2 K_\tau F)} \qquad x = 50\%: a = 2 \qquad x = 90\%: a = 10/01$$

From experimental result in Fig.4:

$(\tau_0^2 K_\tau F) = 3 \cdot 10^{-4}$ and $(2E_\tau - E_\tau) = 0.92$ eV.

H_2,H reemission of 3 keV H_3^+ --> Graphite (EK98)
with two diff. flux densities

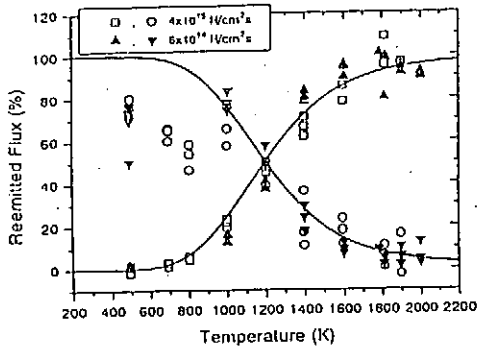

- The model fails with respect to the flux density

H ~ defects ~ flux density?

H_2,H reemission of 3 and 7 keV H_3^+ --> USB15

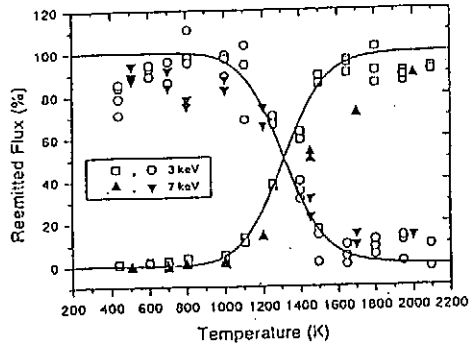

H_2,H desorption after 3 keV H_3^+ → Graphite (EK98)
→ USB15 (15% B in C)

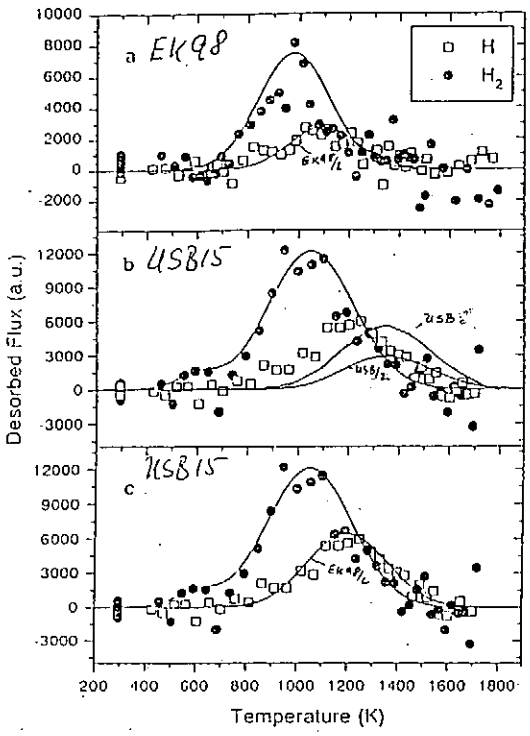

Boron depth profile of USB15 sample after thermal desorption experiment; obtained with the nuclear reaction $^{11}B(p,\alpha)^{8}B$

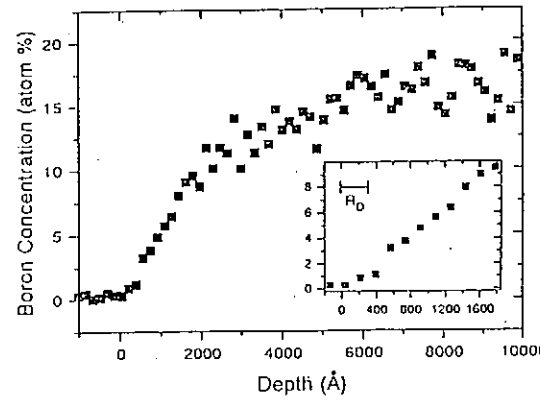

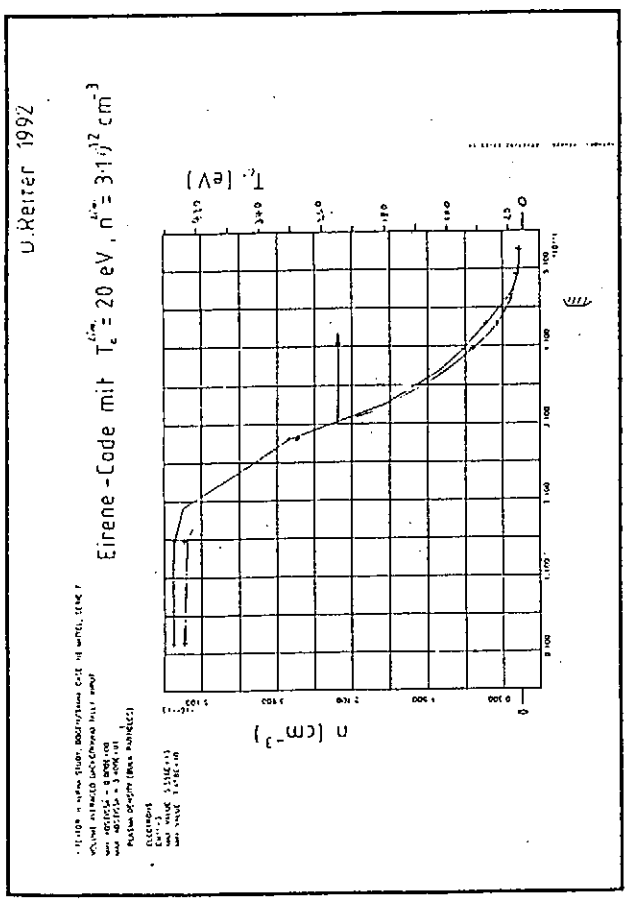

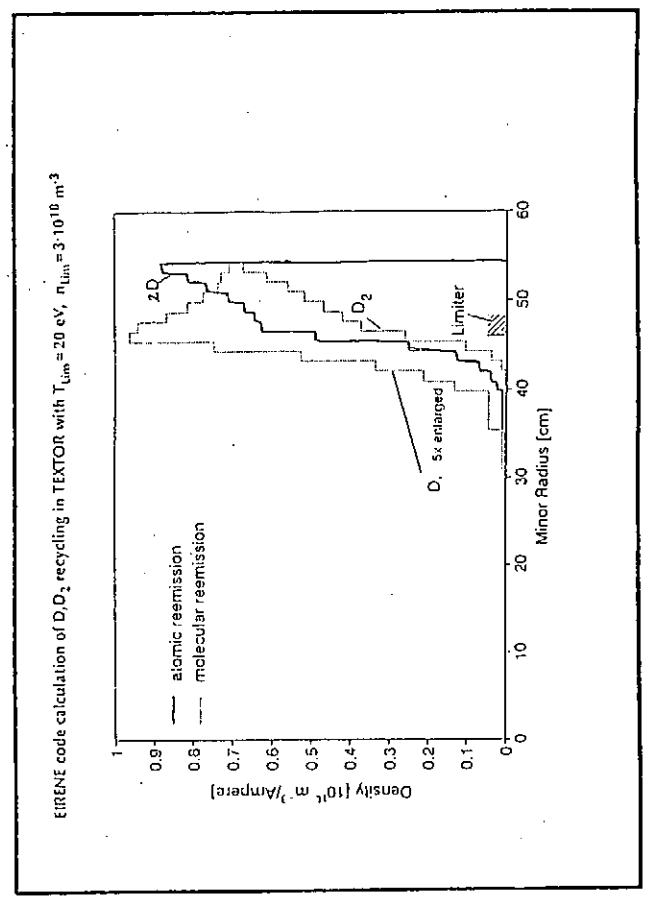

Divertor: high recycling conditions in Asdex-UG configuration

EIRENE code calculation:
Incoming H^+: standard reflection model-Train
Recycled H_2: case1: H_2 case2: $H_{/500k}$

Results:
- Differences in the effects of first SOL plasma contact very small.
- However, after many ionizations: neutrals – plasma contacts – ... rather different energy balance due to nonlinear response of plasma on neutral particles:

	H_2 reemission	H reemission
ion energy into SOL (pessimist):	300 kW	300 kW
ion energy dissipated via neutrals in SOL (Charge exchange, ionization...):	14 kV / 6.5 } 20.5 kV	1840 / 34 } 68 kW (3x)
energy flux onto divertor plates: target 1 / target 2	54 kW / 96 } 150 kW	34 kW / 66 } 100 kW (-1/3)
	170 kW	162 kW

Conclusions from divertor calc.:

- thermal H atoms are more effective to dissipate energy from plasma ions than thermal molecules (they have less kinetic energy than Franck-Condon atoms produced from H_2: penetration depth + Cox + 4.5 eV recombination energy).
- energy shift to electron channel due to less effective electron cooling by H_2 dissociation rather small. From balance: $\Delta E \approx 8$ kW

Summary:

- Implanted hydrogen in Graphite and boron-doped carbon is reemitted
  - below 1000 K in form of molecules only,
  - above 1000 K as H and H_2.
    H fraction increasing with T, reaching at 2000 K nearly 100 %.
- The thermal desorption of implanted hydrogen occurs in both forms, H_2 peaks around 1000 K, H peaks around 1200 K. The relative ratio of H/H_2 of released hydrogen is the same as in the reemission. Thus,

→ the atomic release of hydrogen from carbon is a thermal effect.

- Consequences:
  - No additional inward diffusion is observed at high temperatures.
    No additional tritium inventory problem.
  - EIRENE code calculation:
    - no noticeable implications on the edge plasma physis for limiter machines are expected.
    - Divertor machines: first calculation indicate a significant shift of the energy fluxes to the target due to a more effective energy dissipation from plasma ions by H atoms than by thermal molecules.

DEUTERIUM INTERACTION WITH CARBON COMPOSITES DOPED WITH Si, SiC and TiC

M. Rubel[1], B. Emmoth[1], L. Grobusch[2], and C.H. Wu[3]

[1]Physics Department - Frescati, Royal Institute of Technology, Association EURATOM - NFR, Frescativägen 24, S-104 05 Stockholm, Sweden

[2]Institute of Plasma Physics, Forschungszentrum Jülich, Association EURATOM - KFA, D-52425 Jülich, Germany

[3]The NET Team, Max-Planck-Institut für Plasmaphysik, D-85748 Garching, Germany

Silicon or titanium containing carbon-based composites are considered as candidate materials for plasma facing components in controlled fusion devices. Comparative studies of deuterium interaction with carbon based substrates were performed for: pure graphites and carbon fibres, graphite - silicon mixtures (5 - 50 wt % Si), graphites doped with SiC or TiC, carbon fibres doped with SiC (2.5 - 40 %). The materials were exposed to the deuterium plasma both in fusion devices and laboratory simulators of plasma-surface interactions. Target temperature during the irradiation was from 50 to 700 °C.

Retention, thermal or ion induced release of deuterium and surface damage caused by the irradiation were investigated. Characterization of the non-exposed and deuterium irradiated surfaces was performed by means of Rutherford backscattering spectroscopy, nuclear reaction analysis, energy dispersive X-ray spectroscopy, X-ray photoelectron spectroscopy, laser profilometry and electron microscopy. The most interesting results were connected with migration of the deposited deuterium into the bulk (even a few millimeters beneath the surface) of the composites. The rate of migration was found to be related to the structure of materials and, to some extent, to the content of dopants. Thermally stimulated desorption resulted in release of approx. 20, 70 and 96 % of the deposited deuterium at 300, 550 and 800 °C, respectively. Bombardment of the D-irradiated composites with high energy He ions (MeV range) stimulated release of 20 - 60 % deuterium atoms, dependently on the Si content in the material.

OUTLINE

1. INTRODUCTION
2. MATERIALS & EXPOSURES & METHODS
3. RESULTS
   - STRUCTURE OF SILICON CONTAINING MATERIALS
   - RETENTION OF DEUTERIUM
   - IN-DEPTH DISTRIBUTION OF DEUTERIUM
   - ION INDUCED RELEASE OF DEUTERIUM
4. SUMMARY [EVALUATION OF COMPOSITES]

INTRODUCTION

1. SILICON IN FUSION DEVICES
   - SILICONIZATION (WALL CONDITIONING)
   - Si - CONTAINING COMPOSITES AS CANDIDATES FOR PFC
2. PROPERTIES OF SILICON AS A PFM
   - MEDIUM Z (14) ELEMENT
   - INTERATOMIC COMPOUNDS WITH BORON AND CARBON
   - HIGH AFFINITY FOR OXYGEN (GETTERING)
   - LOW EROSION RATE BY HYDROGEN ISOTOPES
   - QUICKLY DECAYING RADIOATIVITY AFTER N - IRRADIATION

STABLE ISOTOPES: ^{28}Si 92.23 %, ^{29}Si 4.67 %, ^{30}Si 3.10 %

RADIOACTIVE ISOTOPES: ^{25}Si, ^{26}Si, ^{27}Si ($\lambda_{1/2}$ = 0.1 - 3 s), ^{31}Si ($\lambda_{1/2}$ = 2.62 h), ^{32}Si ($\lambda_{1/2}$ = 650 y)

COMPOSITES

CARBON FIBRES: TWO -, THREE -, UNIDIRECTIONAL

CARBON FIBRES doped with SiC

CARBON FIBRES covered with CVD layer of SiC

GRAPHITE covered with CVD layer of SiC

GRAPHITE doped with Si: 5, 10, 15, 20, 30, 50 wt. % Si

GRAPHITE doped with SiC

SILICON CARBIDES: α, β, doped with AlN, TiB_2, C

SiC in plasma spayed layers of Al on Cu, SS or C substrate

GRAPHITE doped with Ti

GRAPHITE - REFERENCE MATERIAL

EXPOSURES TO DEUTERIUM PLASMA

RF GLOW DISCHARGE:	T = 60 °C, D = 10^{17} - 10^{18} cm^{-2}
HOLLOW CATHODE:	T = 60 °C, D = 10^{20} - 10^{21} cm^{-2}
MAGNETRON:	T = 700 °C, D = 10^{20} - 10^{21} cm^{-2}
TEXTOR TOKAMAK:	1 - 30 EXPOSURES (3 - 100 s) TO THE SCRAPE-OFF-LAYER PLASMA

ANALYTICAL METHODS

NUCLEAR REACTION ANALYSIS

RUTHERFORD BACKSCATTERING SPECTROSCOPY

ENERGY DISPERSIVE X-RAY SPECTROSCOPY

X-RAY PHOTOELECTRON SPECTROSCOPY

LASER PROFILOMETRY

SCANNING ELECTRON MICROSCOPY

ATOMIC FORCE MICROSCOPY

SCANNING TUNNELING MICROSCOPY

QUADRUPOL MASS SPECTROMETRY

RBS SPECTRA OF CFC + 2.5 % SiC

A. "As delivered" outer surface

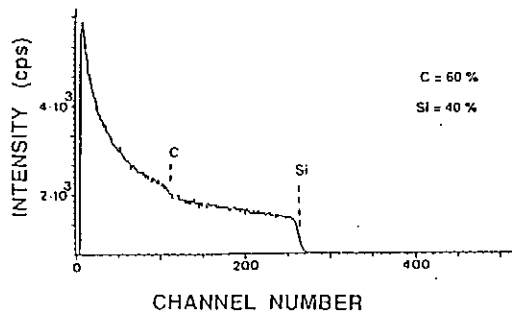

B. After machining

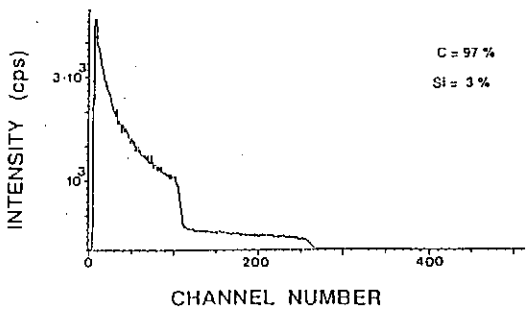

SECONDARY AND BACKSCATTERED IMAGES OF CFC + 2.5 %

"AS DELIVERED" AFTER MACHINING

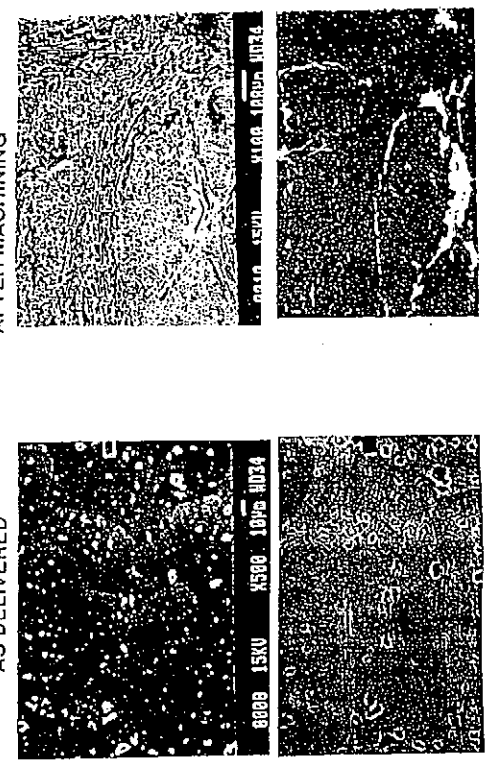

RBS SPECTRA OF CFC + 8 % SiC

A. "As delivered" outer surface

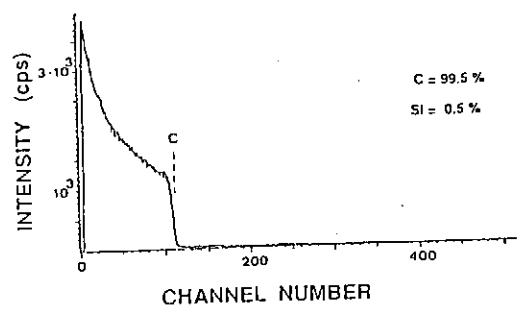

B. After machining

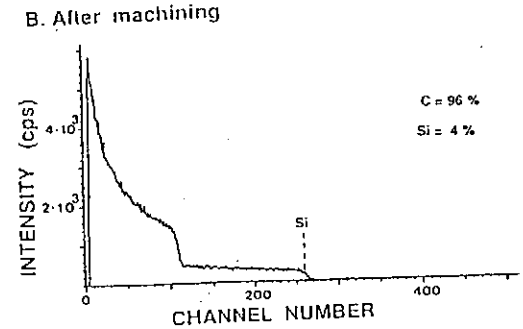

SECONDARY AND BACKSCATTERED IMAGES OF CFC + 8 % SIC

"AS DELIVERED" AFTER MACHINING

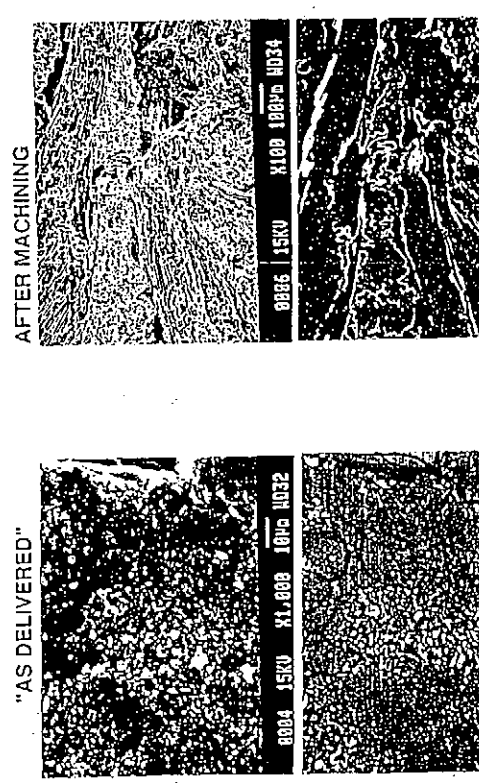

AREAL CONCENTRATION OF DEUTERIUM ON SURFACES OF CARBON-BASED COMPOSITES EXPOSED TO THE DEUTERIUM PLASMA

(GLOW DISCHARGE IN DEUTERIUM: 1 x 10^{18} cm^{-2})

AND SURFACE ROUGHNESS OF COMPOSITES

SAMPLE	C_D x 10^{16} cm^{-2}	R_a (μm)	R_z (μm)
SEP	9.3	6.5	44.4
CFC + 2.5 % SiC	10.2	10.2	67.0
CFC + 8 % SiC	8.5	7.1	53.5
CFC + 40 % SiC	11.0	10.4	69.1

R_a = average roughness for the whole area under investigation (10 mm^2)

R_z = average of 5 highest amplitudes: top to valley

AREAL CONCENTRATION OF DEUTERIUM ON SURFACES OF CARBON-BASED COMPOSITES EXPOSED TO THE DEUTERIUM PLASMA

(GLOW DISCHARGE IN DEUTERIUM: 1.5 x 10^{18} cm^{-2})

AND SURFACE ROUGHNESS OF COMPOSITES

SAMPLE	C_D x 10^{16} cm^{-2}	R_a (μm)	R_z (μm)
Isotropic graphite	14.5	2.6	21.6
C + 5 % SiC	9.4	1.6	13.4
C + 10 % SiC	12.6	1.5	13.1
C + 5 % TiC	8.8	1.4	13.0
C + 10 % TiC	8.8	1.5	13.1

R_a = average roughness for the whole area under investigation (10 mm^2)

R_z = average of 5 highest amplitudes: top to valley

IN-DEPTH PENETRATION OF DEUTERIUM

BULK CONCENTRATION OF DEUTERIUM IN COMPOSITES EXPOSED TO 1 X 10^{21} cm^{-1} D^+ IONS (MEASURED APPROX. 1.5 mm BENEATH THE SURFACE)

MATERIAL	BULK CONCENTRATION (ppm)			
	TIME AFTER EXPOSURE (days)			
	7	90	270	450
CFC	31	60	240	
C-Si 15%	21	100		1000
C-Si 20%	12	72		600

SUMMARY

1. NON-UNIFORM DISTRIBUTION OF DOPANTS
2. NON-UNIFORM GRAIN SIZE OF DOPANTS
3. COMPOSITION OF THE OUTER LAYER ("AS DELIVERED") OF COMPOSITES DIFFERS DISTINCTLY FROM THE BULK COMPOSITION
4. IMPURITIES IN THE SURFACE LAYER AND IN THE BULK
5. HIGH SURFACE ROUGHNESS
6. MIGRATION OF THE DEPOSITED DEUTERIUM INTO THE BULK OF THE COMPOSITES
7. THERMAL RELEASE OF DEUTERIUM FROM SILICON DOPED COMPOSITES SIMILAR AS FOR GRAPHITE

Session 4

Satellite Workshop of 11th PSI Conference on
Tritium Effects in Fusion Reactor Plasma Facing
Material, May 19-20, 1994, Nagoya

Hydrogen Retention of B_4C Overlaid Graphite

T. Hino[1], Y. Yamauchi[1], Y. Hirohata[1], T. Yamashina[1],
T. Ando[2] and M. Akiba[2]

[1] Department of Nuclear Engeneering, Hokkaido University, Kita-13, Nishi-8, Kita-ku, Sapporo, 060 Japan
[2] Japan Atomic Energy Research Institute, Naka Institute, Naka-machi, 311-01 Japan

Boron contained graphite has several advantages as plasma facing material, e.g. low chemical sputtering yield and gettering action for oxygen impurities. The properties of hydrogen retention, however, are not sufficiently clarified yet. In addition, the reduction of the hydrogen retention by such helium ion bombardment has not been systematically examined yet.

In the present study, the hydrogen retention of B4C converted graphite was investigated by using ECR hydrogen ion irradiation apparatus. The retention amount was measured by a technique of thermal desorption spectroscopy after the irradiation. Compared with the graphite, the chemical sputtering yield was observed to be 1/20 times smaller. The H2 desorption peaks appeared both at 400°C and 700°C. The former peak is due to the formation of B4C layer, and the latter the same as graphite. The H2 desorption data showed that the retention was (20-30)% reduced in the temperature range from 300 to 800°C, compared with the graphite. The activation energies of H2 and CH4 desorptions were also obtained, and these were compared with those of graphite.

In addition, the reduction of the retention by the irradiation of helium ions was tried, and the fluence of helium ions required for the retention to be considerably reduced was estimated.

Satellite Workshop of 11th PSI Conference on
Tritium Effects in Fusion Reactor Plasma Facing
Material, May 19-20, 1994, Nagoya

Hydrogen Retention of B_4C Overlaid Graphite

T. Hino[1], Y. Yamauchi[1], Y. Hirohata[1], T. Yamashina[1],
T. Ando[2] and M. Akiba[2]

[1] Department of Nuclear Engeneering, Hokkaido University, Kita-13, Nishi-8, Kita-ku, Sapporo, 060 Japan
[2] Japan Atomic Energy Research Institute, Naka Institute, Naka-machi, 311-01 Japan

INTRODUCTION

B_4C Overlaid Graphite
- Used as Divertor Tiles in JT-60U for Oxygen Gettering

Conversion Method
- Graphite Surface - Boronized
- B_4C Layer = 200 μm
- Atomic Ratio B/C = 2

Hydrogen Retention Properties
- Not Examined in Detail

Our Studies for B_4C Overlaid Graphite

(1)Hydrogen Ion Irradiation(10^{19} H/cm^2, 4.5 keV H^+_3)
Hydrogen Retentions of B_4C Overlaid Graphite and Substrate Graphite(PD-330S)

(2)Thermal Desorption Spectroscopy (TDS)
Desorptions of H_2 and CH_4
Activation Energies

Temperature Dependence of Hydrogen Retention

(3)Irradiation During Heating
Hydrogen Retention vs Irradiation Temperature

(4)Helium Ion Impact Desorption(4.5 keV He^+)
Required Fluence for Reduction of Hydrogen Retention

ECR Ion Irradiation Apparatus

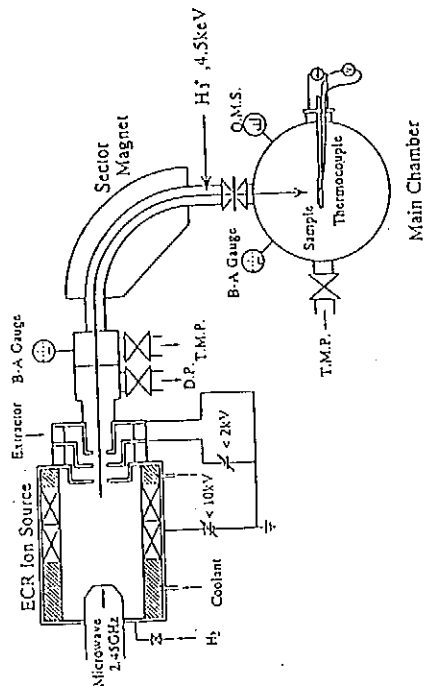

Desorption After Hydrogen Ion Irradiation

B_4C Converted Graphite

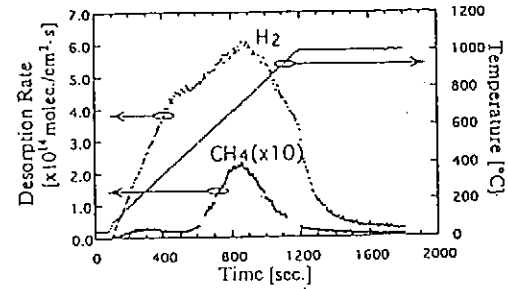

Graphite

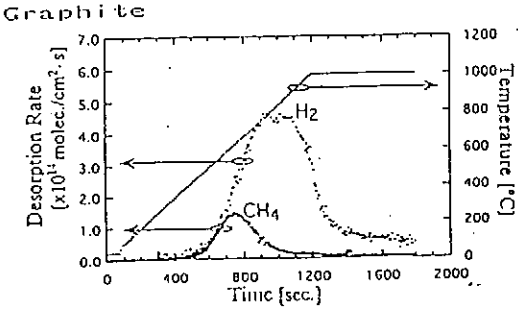

Activation Energies for H_2 and CH_4

Gas \ Sample		B_4C/PD-330S	PD-330S
H_2	Higher Temp.	1.7±0.3	2.6±0.7
	Lower Temp.	1.2±0.4	
CH_4	Higher Temp.	1.5±0.1	2.1±0.4
	Lower Temp.	1.0±0.1	

Ratio of Retained Hydrogen Both for B_4C and Graphite

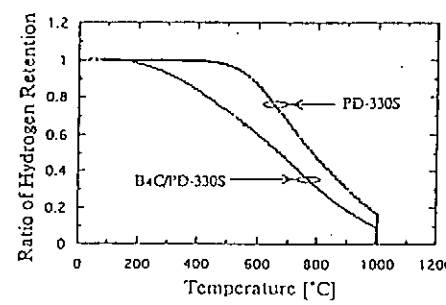

Ratio of Hydrogen Retention
(when H ion was implanted during heating)

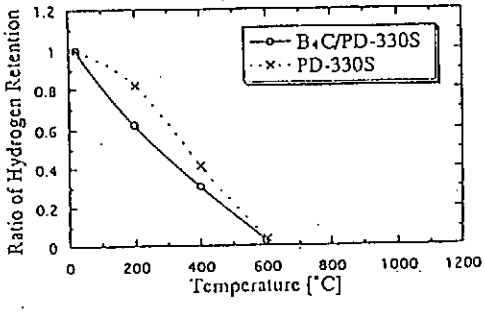

Change of Desorption Spectra After He Ion Irradiation

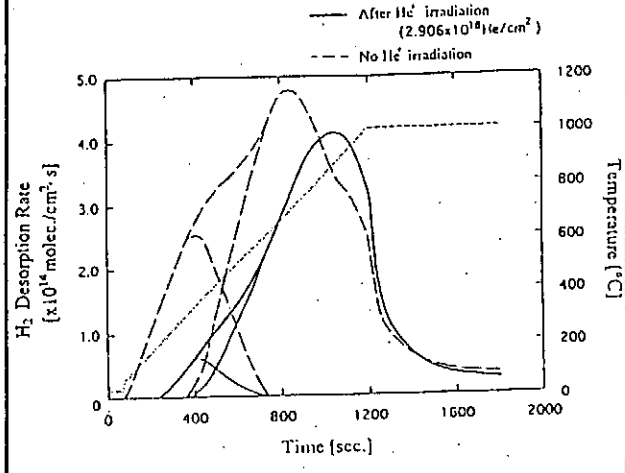

Reduction of Hydrogen Retention Due to He Ion Irradiation
(H Retention versus He Ion Fluence)

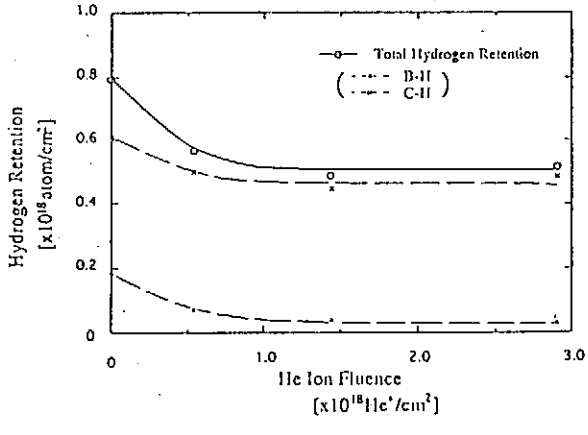

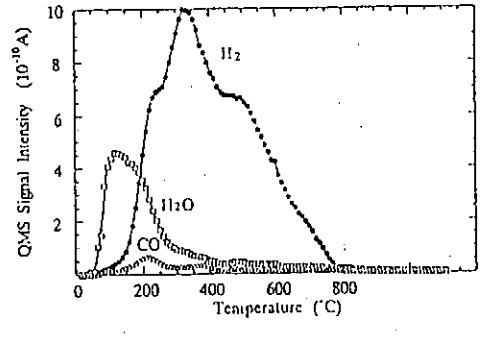

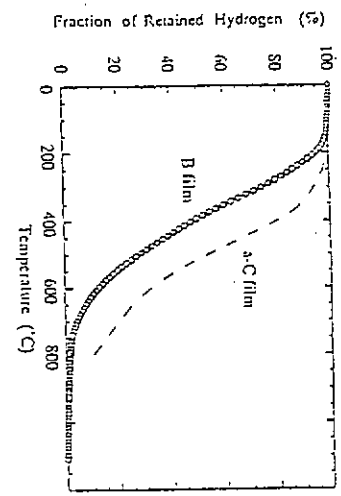

SUMMARY

(1)Retention Amount: 1.5 Times Larger Than Graphite
(2)Hydrogen be Trapped Mainly in Forms of B-H and C-H Bondings
(3)Desorption from B-H Bonding: 350 C
Desorption from C-H Bonding: 700 C
(4)CH_4 Desorption: 1/5 Times Reduced
(5)Activation Energies: Smaller Than Those of Graphite
(6)Helium Ion Impact Desorption:
Very Much Effective for Detrapping of B-H Bonding
(7)Conditionings for Removal of H Trapped by B: 300 C Baking or He Discharge Cleaning with Low Current Density

HYDROGEN TRANSPORT/RETENTION/REEMISSION IN / FROM GRAPHITE

A. A. Haasz, S. Chiu, J. W. Davis, P. Franzen
University of Toronto

Reemission of hydrogen and methane from graphite during H^+/D^+ irradiation and postirradiation TDS has been investigated for graphite temperatures in the range 300 K - 1900 K. During simultaneous steady-state irradiation by H^+ and D^+ the reemitted hydrogen is in the form of $H_2/D_2/HD$ and methane molecules. Based on the mixed HD and CH_xD_y results, we conclude that hydrogen diffuses in the form of atoms in the implantation zone, and that methane formation occurs at the end of ion range. Methane diffusing through the implantation zone may be fragmented by incident ions. Postirradiation TDS results show that both H recombination and methane formation depend on the range separation of H^+ and D^+. Reemission, during D^+ irradiation at T > 1000 K, consists of both D_2 molecules and D° atoms, with the atom fraction increasing with increasing temperature; essentially all of the reemitted hydrogen is in the form of atoms at 2000 K. During postirradiation TDS, the released deuterium is in the form of D_2, D° and C_xD_x; the D° atom fraction is ~15% of the total D released for incident ion fluences above the saturation fluence.

H-retention of graphite for high H^+ fluences was also investigated. The amount of retained hydrogen in polycrystalline graphite was found to increase with fluence, well above the saturation levels observed in the implantation zone. The extent of the increase appears to depend on the structure of graphite. We proposed the hypothesis that "mobile H" from the implantation zone, during H^+ irradiation, diffuses "deeper" into the material and becomes trapped on "internal surfaces."

2nd International Workshop on T- Effects in PFC, Nagoya, Japan, May 19-20, 1994

HYDROGEN TRANSPORT / RETENTION / REEMISSION IN / FROM GRAPHITE

A. A. Haasz
University of Toronto

Coinvestigators

S. Chiu
J. W. Davis
P. Franzen (from IPP, Garching)

1. REEMISSION AT T < 1000 K

   ※ Reemission of hydrogen and methane molecules from graphite

   - during irradiation by H^+ and D^+
   - during postirradiation TDS

2. REEMISSION AT T > 1000 K

   ※ Atomic hydrogen reemission

   - during irradiation by D^+
   - during postirradiation TDS

3. H-RETENTION IN GRAPHITE FOR HIGH H^+ FLUENCES

1. REEMISSION AT T < 1000 K

※ Reemission of hydrogen and methane molecules

Objectives

- To study the mechanisms for:
  - H-transport and recombination in graphite
  - the effect of graphite structure on H-transport
  - the methane formation and release process

Apparatus

- Dual beam ion accelerator (H^+, D^+, He^+, etc.)
  - independently controlled fluxes and energies
- QMS for RGA

Specimens

- "As deposited" pyrolytic graphite (HPG99, Union Carbide)
  - 2.2 g/cm³; 30° mosaic spread
- Pseudo monocrystal carbon (Carbone Lorraine)
  - 2.26 g/cm³; 0.4-3.4° mosaic spread; 10-80 μm crystallites
- Isotropic fine grain graphite (EK98, Ringsdorff)
  - 1.84 g/cm³; 10-100 nm crystallites

Experiment

- H^+ and D^+ implanted into graphite, either individually or simultaneously (using dual ion beam accelerator)
- Observe reemission of H_2, HD, D_2 and CH_xD_y during irradiation
- Thermal desorption of H_2, HD, D_2 and CH_xD_y from previously implanted graphite

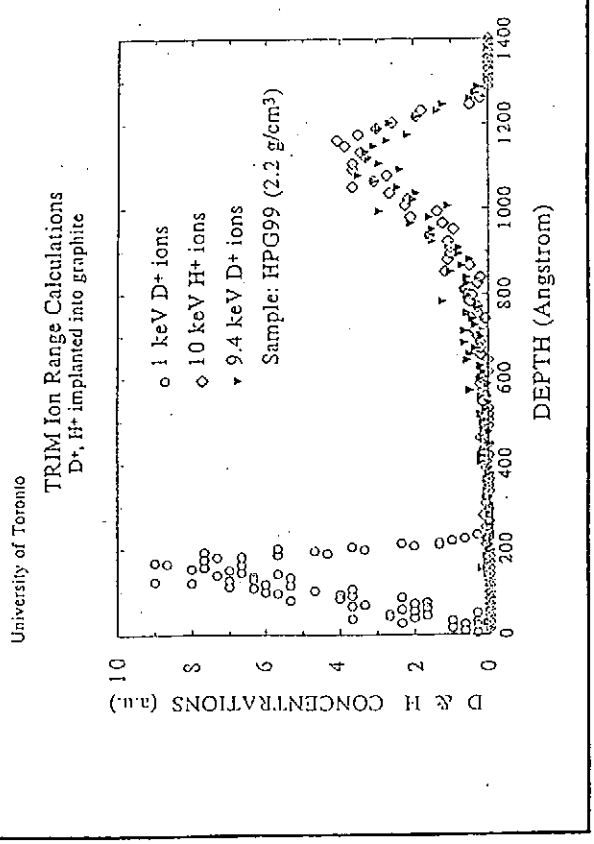

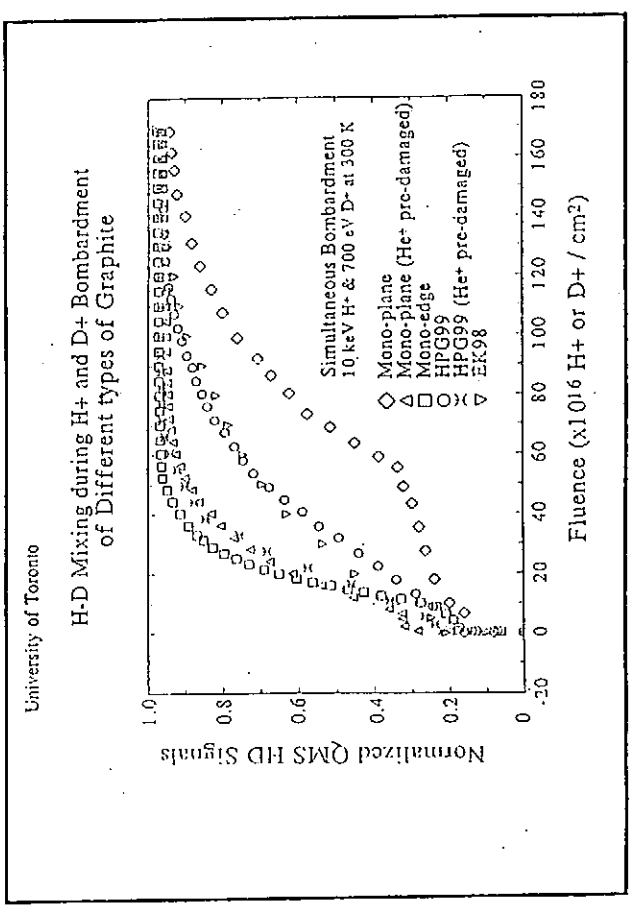

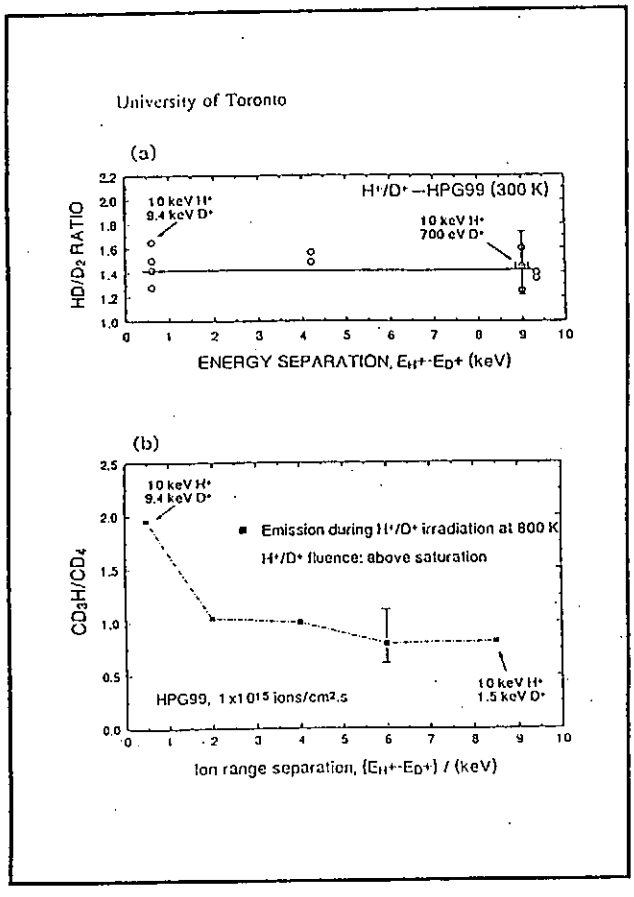
University of Toronto
(a)
H+/D+ —HPG99 (300 K)
10 keV H+
9.4 keV D+
10 keV H+
700 eV D+
HD/D2 RATIO
ENERGY SEPARATION, EH+-ED+ (keV)
(b)
10 keV H+
9.4 keV D+
Emission during H+/D+ irradiation at 800 K
H+/D+ fluence: above saturation
HPG99, 1x10^15 ions/cm2.s
10 keV H+
1.5 keV D+
CD3H/CD4
Ion range separation, (EH+-ED+) / (keV)

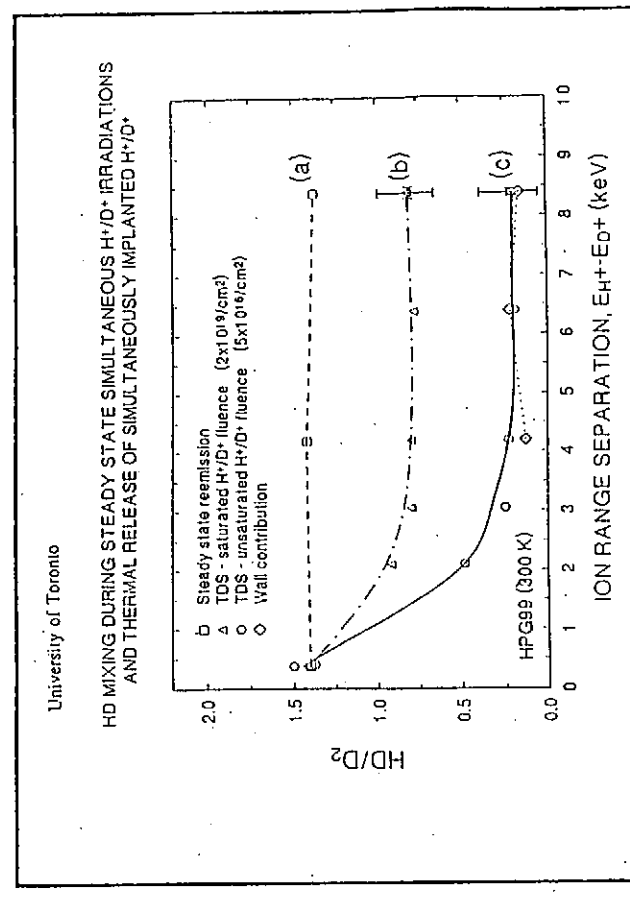
University of Toronto
HD MIXING DURING STEADY STATE SIMULTANEOUS H+/D+ IRRADIATIONS
AND THERMAL RELEASE OF SIMULTANEOUSLY IMPLANTED H+/D+
Steady state reemission
TDS - saturated H+/D+ fluence (2x10^19/cm2)
TDS - unsaturated H+/D+ fluence (5x10^16/cm2)
Wall contribution
(a)
(b)
(c)
HPG99 (300 K)
HD/D2
ION RANGE SEPARATION, EH+-ED+ (keV)

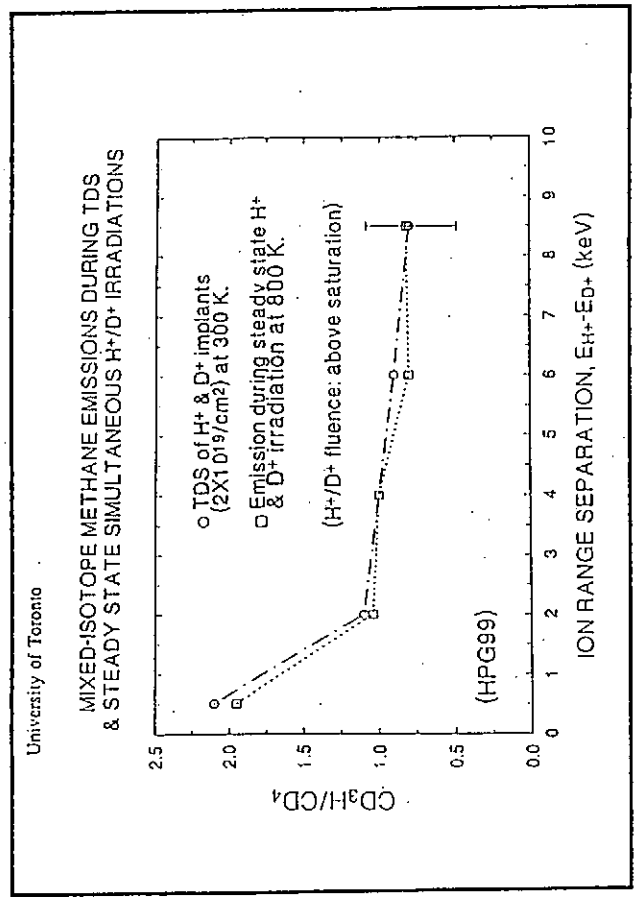
University of Toronto
MIXED-ISOTOPE METHANE EMISSIONS DURING TDS
& STEADY STATE SIMULTANEOUS H+/D+ IRRADIATIONS
TDS of H+ & D+ implants
(2X10^19/cm2) at 300 K.
Emission during steady state H+
& D+ irradiation at 800 K.
(H+/D+ fluence: above saturation)
(HPG99)
CD3H/CD4
ION RANGE SEPARATION, EH+-ED+ (keV)

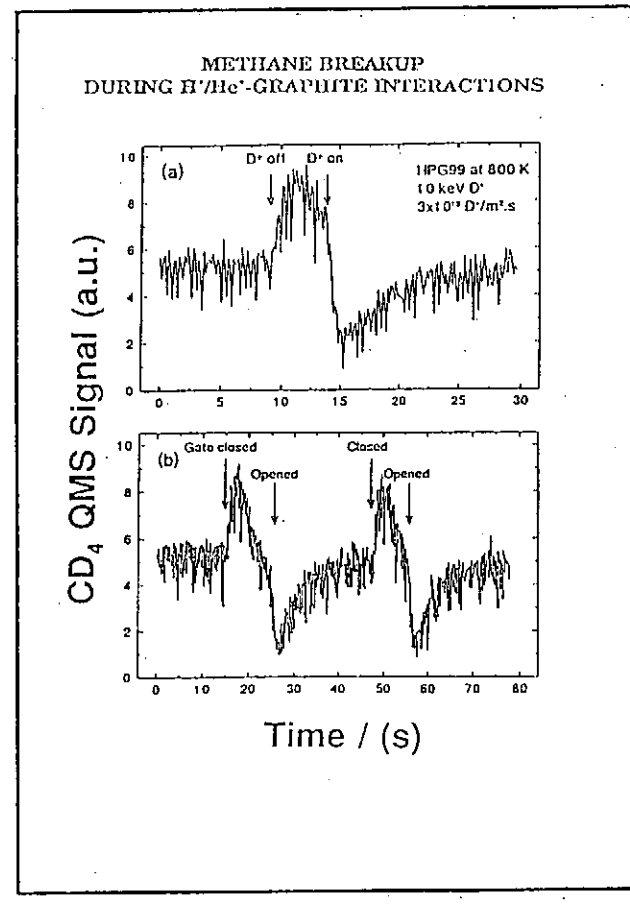
METHANE BREAKUP
DURING H+/He+-GRAPHITE INTERACTIONS
(a)
D+ off
D+ on
HPG99 at 800 K
10 keV D+
3x10^19 D+/m2.s
(b)
Gate closed
Opened
Closed
Opened
CD4 QMS Signal (a.u.)
Time / (s)

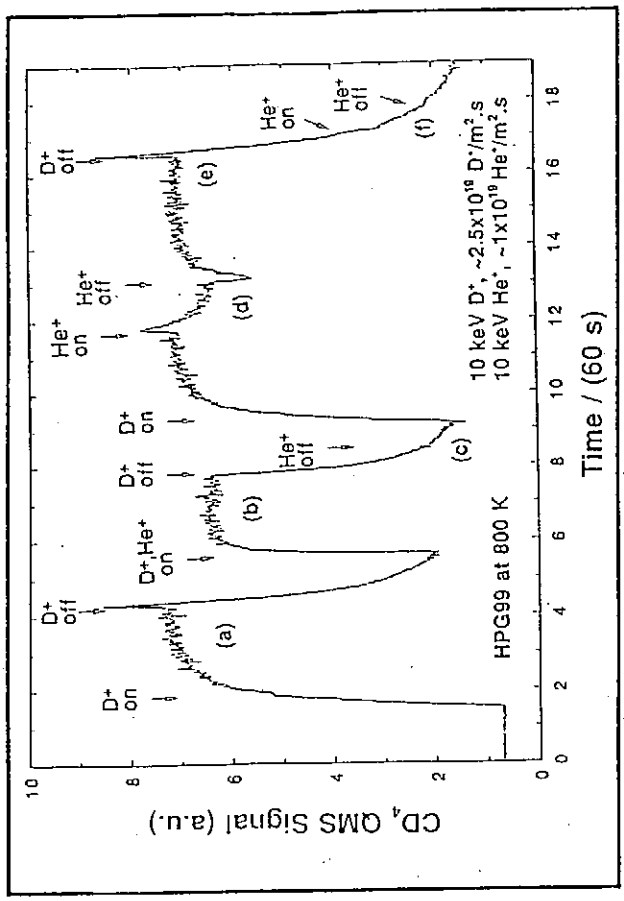

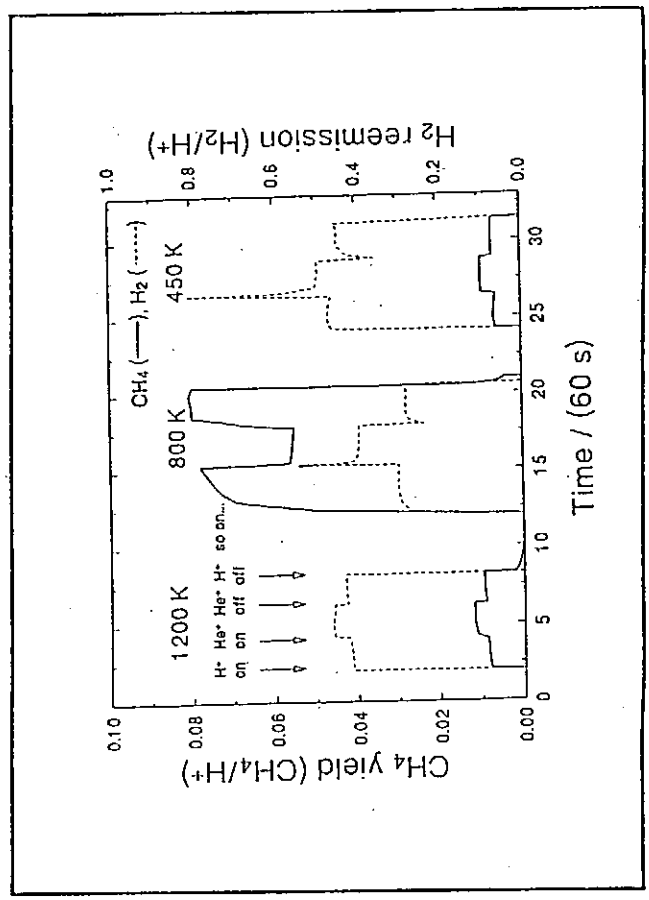

2. REEMISSION AT T > 1000 K

※ Atomic hydrogen reemission

Objective

- To investigate the mix of molecular and atomic hydrogen
  - during irradiation by D+ (as a function of temperature)
  - during postirradiation TDS

Apparatus

- accelerator
- line-of-sight QMS detection

Specimen

- pyrolytic graphite

Experiments

(a) Steady-State Irradiation
- irradiation of graphite with D+
- line-of-sight QMS detection of reemitted species
  - D_2, D° and CD_4

(b) Postirradiation TDS
- D+ implantation of graphite
- subsequent heating to 1900 K and line-of-sight QMS detection of D_2, D° and CD_4

2nd International Workshop on T-Effects in PFC, Nagoya, Japan, May 19-20, 1994

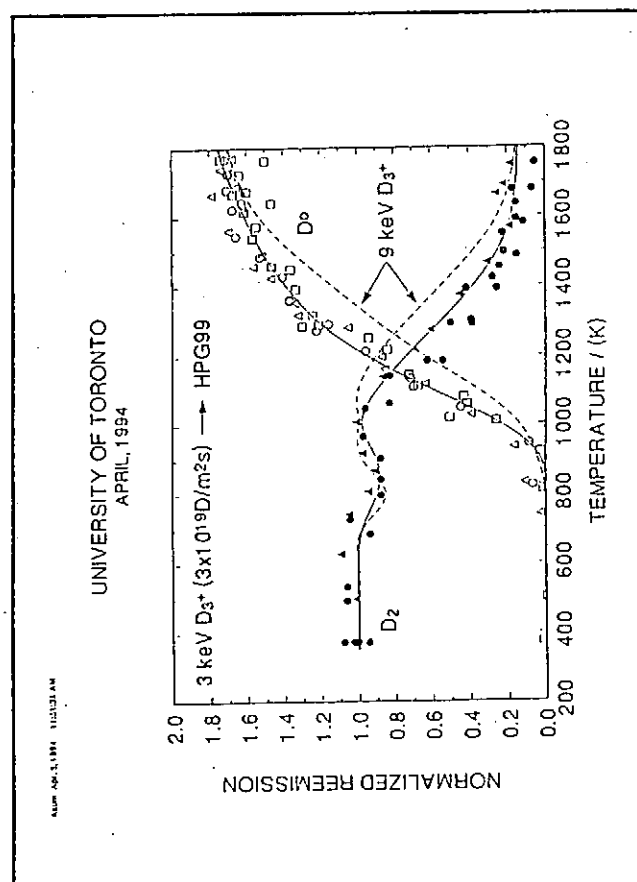

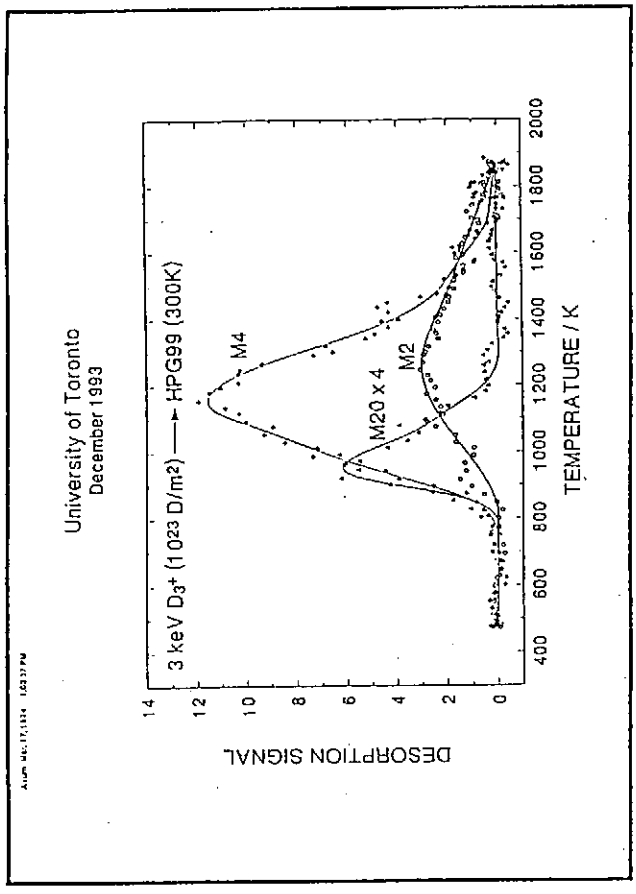

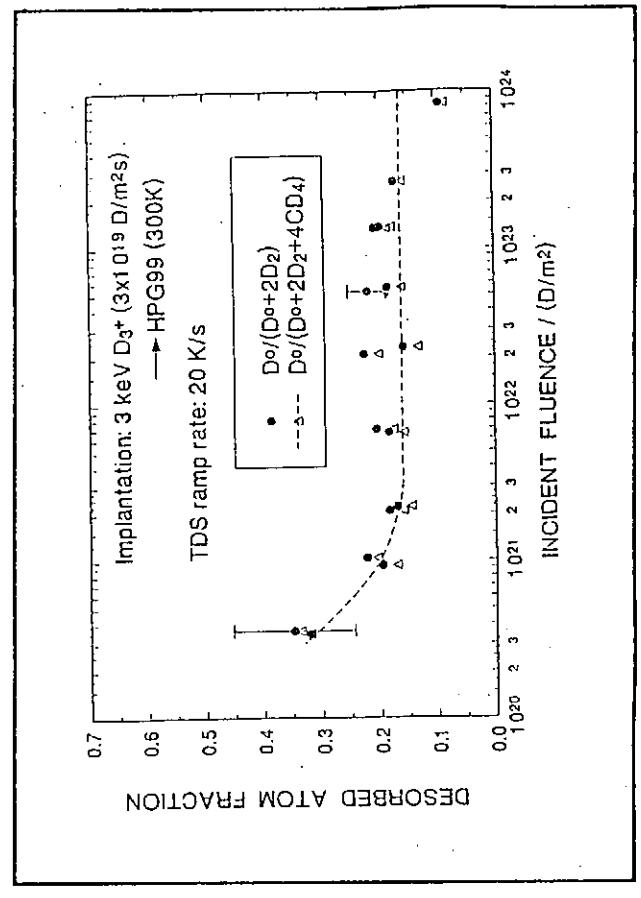

3. H-RETENTION IN GRAPHITE FOR HIGH H⁺ FLUENCES

Objectives

- To study H retention in graphite as a function of H⁺ fluence
- To investigate the effect of graphite structure on H retention

Apparatus

- Dual-beam ion accelerator
- QMS for RGA

Specimens

- Pseudo monocrystal graphite
- Pyrolytic graphite
- Isotropic fine grain graphite

Experiments

- Graphite specimens were implanted with D⁺ to fluences in the range 10^{17} - 10^{21} D⁺/cm²
- Retained D was measured using Thermal Desorption Spectrometry (TDS); up to 1900K at ~15 K/s

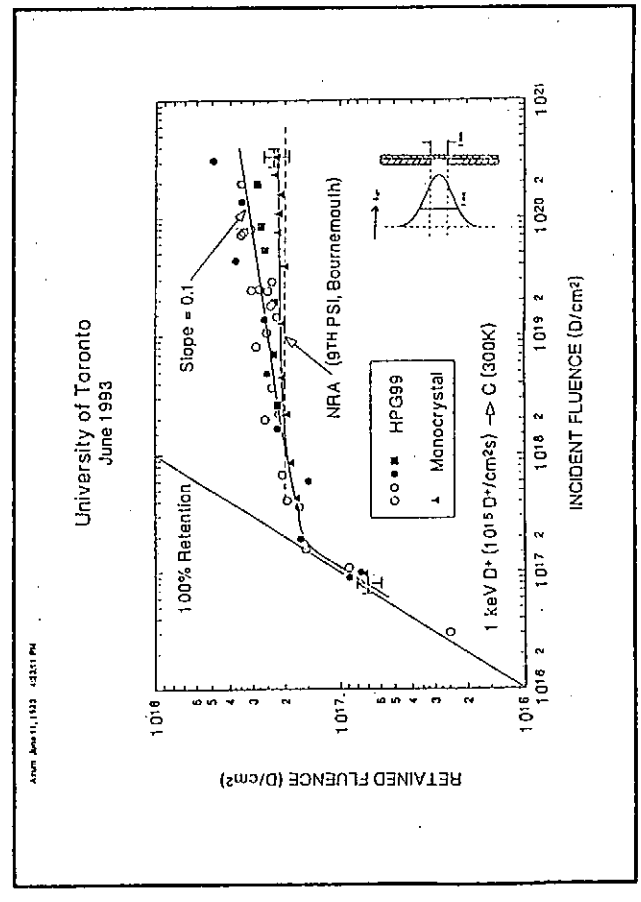

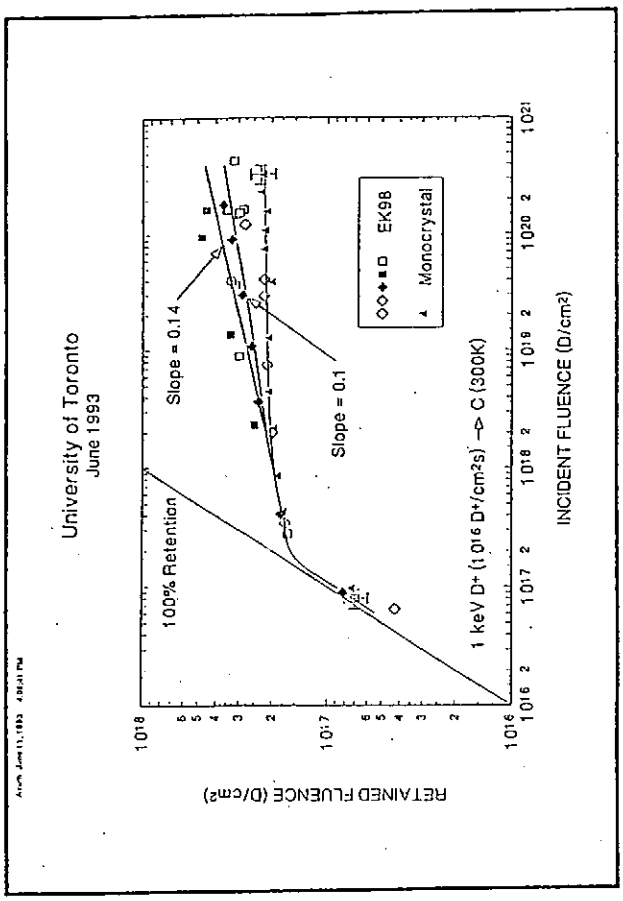

SUMMARY

1. REEMISSION AT T < 1000 K

(a) Steady-State Irradiation by H^+ and D^+

- Transient behaviour of HD reemission depends on graphite structure.
  - — structural dependence disappears at high fluences
- During steady-state irradiation by H^+ and D^+, the formation of HD molecules is independent of the ion range separation.
  - — complete mixing of mobile H/D occurs
  - — H recombination occurs throughout the implantation zone, possibly on internal surfaces
- implication: hydrogen diffuses in the form of atoms in the implantation zone
- Methane formation during irradiation occurs at end of ion range (consistent with previous findings by Vietzke et al/Jülich and Roth et al/IPP Garching).
- Methane diffusing through the implantation zone may be fragmented by incident ions.
  - — "apparent threshold" for incident beam energy, fluence, flux and ion mass.

(b) Thermal Desorption

- Post-implantation TDS results show that both H-recombination and methane formation depend on the range separation of H^+ and D^+.

SUMMARY (continued)

2. REEMISSION AT T > 1000 K

(a) Steady-State Irradiation by D^+

- Below 1000K, implanted D from graphite is reemitted in the form of D_2 molecules (and C_xD_y at ~800K).
- Above 1000K, both D_2 molecules and D° atoms are reemitted; the atom fraction increases with increasing temperature; essentially all atoms at 2000K.

(b) Thermal Desorption

- During TDS, the released deuterium is in the form of D_2, D° and C_xD_y
  - — the D° atom fraction is ~15% of total D released for fluences above the saturation fluence.

SUMMARY (concluded)

3. H-RETENTION IN GRAPHITE FOR HIGH H^+ FLUENCE

- The amount of retained hydrogen in polycrystalline graphite increases with increasing fluence, well above the saturation levels observed in the implantation zone.
- The extent of the increase appears to depend on the structure of graphite.
- Proposed Hypothesis: mobile H from the implantation zone, during H^+ impact, diffuses "deeper" into the material and becomes trapped on "internal surfaces."

Thermal re-emission of hydrogen isotopes from graphite in the high temperature regime above 1000 K

B. Tsuchiya and K. Morita

Department of Crystalline Materials Science, School of Engineering, Nagoya University, Furo-cho, Chikusa-ku, Nagoya 464-01, Japan

Trapping and re-emission of hydrogen isotopes by plasma facing materials control predominately fuel retention and recycling in magnetically confined fusion devices. In order to establish the ignition condition in D-T burning experiments, evaluation and prediction of the fuel recycling during main discharge shots are of essential importance. However, the re-emission process at high temperatures above 1000 K has been not sufficiently understood yet.

In this paper, change in the depth profile of hydrogen isotopes implanted into graphite by annealing in the high temperature regime above 1000 K has been measured by means of an elastic recoil detection (ERD) technique. Implantation of hydrogen isotopes into the specimen was done with 5 keV H_2^+ or D_2^+ ion beams up to saturation at room temperature. The specimen was isothermally annealed at temperatures from 850 °C to 1000 °C. As the annealing time increases, the concentration of retained hydrogen decreases over the whole depth, while the relative retained number of hydrogen decreases gradually with decreasing the depth toward the surface. The results indicate that the thermal desorption of atomic hydrogen takes place at the surface.

The change in the depth profile of hydrogen isotopes retained in graphite by the annealing was analyzed using the mass-balance equations, in which diffusion, thermal detrapping, retrapping and atomic emission of hydrogen isotopes at the surface were taken into account. The experimental data were found to be excellently well reproduced by the analytical solution of mass-balance equations. The activation energies of the effective diffusion constant and the thermal desorption rate constant were determined to be 3.1 eV and 3.8 eV, respectively. It is concluded that such high activation energies of thermal detrapping and atomic ejection at the surface are ascribed to the strong binding of hydrogen atoms at the lattice defects in the bulk and at the surface.

Thermal Re-emission of Hydrogen Isotopes from Graphite in the High Temperature Regime above 1000 K

B. Tsuchiya and K. Morita

Department of Crystalline Materials Science, School of Engineering, Nagoya University

Introduction

Carbon materials

- Excellent thermal properties
- High hydrogen retention

Purpose of studies

- To evaluate and predict the transient recycling fluxes of D and T from the plasma facing components and the D/T ratio.
- To clarify the re-emission process of hydrogen isotopes from graphite and construct the model.

Hydrogen re-emission

At temperatures below 900 K

- Local molecular recombination between activated hydrogen atoms in the bulk.

$$\frac{dn(t)}{dt} = \Sigma_d n_T(t) - \Sigma_T(C_0 - n_T(t))n(t) - \alpha K_{HC} n_T(t)n(t) - Kn_T(t)n(t) - 2K_r n(t)^2$$

$$\frac{dn_T(t)}{dt} = -\Sigma_d n_T(t) + \Sigma_T(C_0 - n_T(t))n(t) - \alpha K_{HC}\beta n_T(t)n(t) - Kn_T(t)n(t)$$

Y. Muto and K. Morita (1992)

At temperatures above 1000 K

- Thermal desorption of atomic hydrogen at the surface.

P. Franzen, E. Vietzke, A. A. Haasz, J. W. Davis and V. Philipps (1992)

Purpose of This Study

In order to establish the modeling of the hydrogen recycling at temperatures above 1000 K, the depth dependence of the hydrogen re-emission by isothermal annealing of graphite was measured by means of the ERD technique.

- To confirm the thermal desorption of atomic hydrogen at the surface
- To determine the activation energies of the thermal desorption rate constant and the effective diffusion constant

Mass Balance Equations: a model for re-emission of hydrogen in the high temperature

for activated hydrogen

$$\frac{\partial n(x,t)}{\partial t} = D\frac{\partial^2 n(x,t)}{\partial x^2} + \Sigma_d n_T(x,t) - \Sigma_T(C_0 - n_T(x,t))n(x,t)$$

for trapped hydrogen

$$\frac{\partial n_T(x,t)}{\partial t} = -\Sigma_d n_T(x,t) + \Sigma_T(C_0 - n_T(x,t))n(x,t)$$

$C_0 \gg n_T(x,t)$

C_0 : trap sites density

initial condition

$$n_T(x,0) = n^0$$

boundary condition

$$\left| D\frac{\partial n(x,t)}{\partial x} \right|_{x=0} = -\alpha n(0,t)$$

Analytical Solution: theoretical depth profile

$$\frac{n_T(x,t)}{n^0} = \mathrm{erf}(y) + \exp(2yz)\exp(z^2)\,\mathrm{erfc}(y+z)$$

$$y = \frac{x}{2\sqrt{D't}} \qquad z = \frac{\alpha t}{\sqrt{D't}} \qquad D' = \frac{\Sigma_d}{\Sigma_T C_0} D$$

D' : effective diffusion constant

α : thermal desorption rate constant

Σ_d : thermal detrapping rate constant

Σ_T : trapping rate constant $\quad \Sigma_T = 4\pi r_T D\xi$

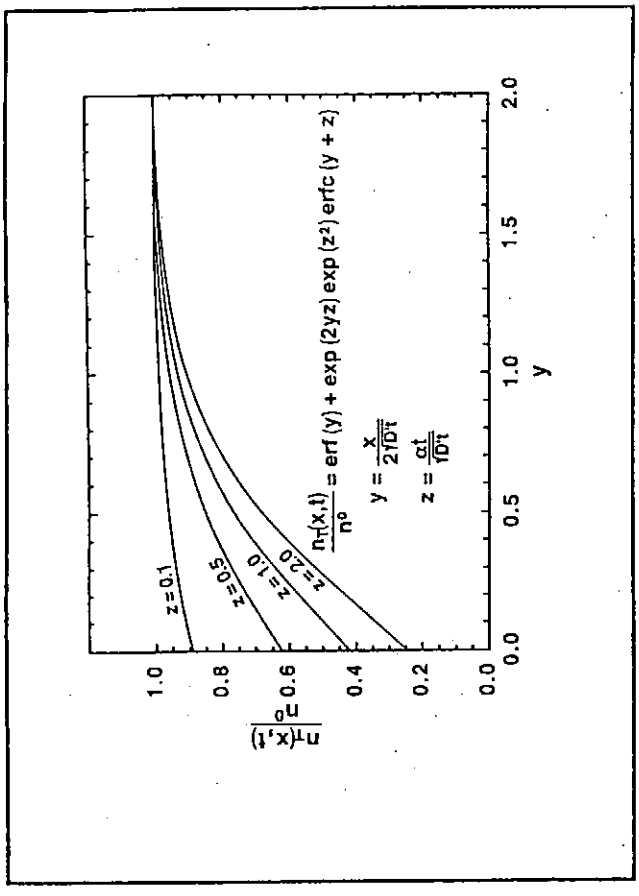

Experiments

Specimen Used:

isotropic graphite (IG110U)
10x15x1 mm³ in size
the specimen was preheated at 1000°C for 20 min

Hydrogen Implantation:

5 keV H_2^+ or D_2^+ ions
up to saturation at room temperature

Isothermal Annealing:

temperature range from 850°C to 1000°C

Method Used:

the elastic recoil detection (ERD) technique

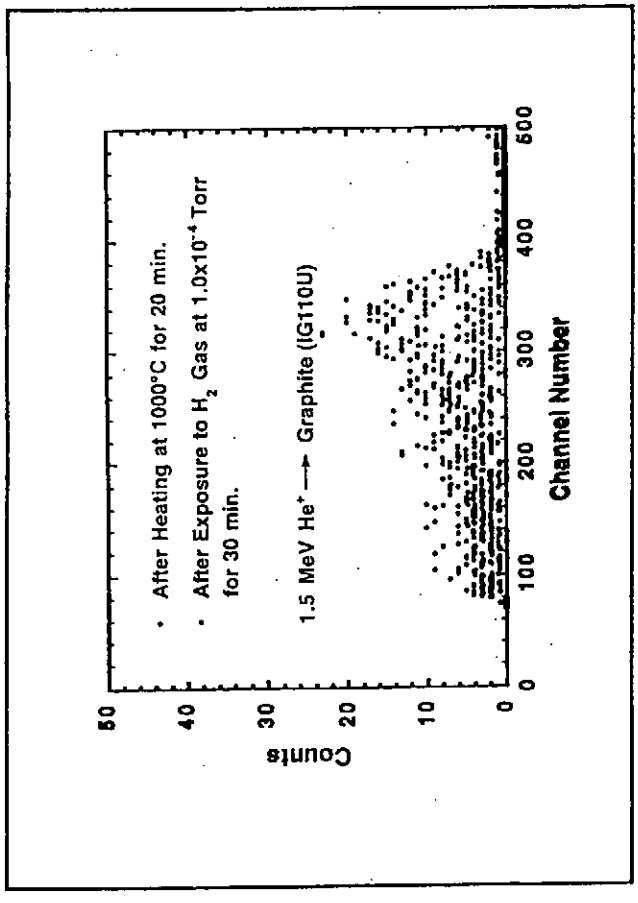

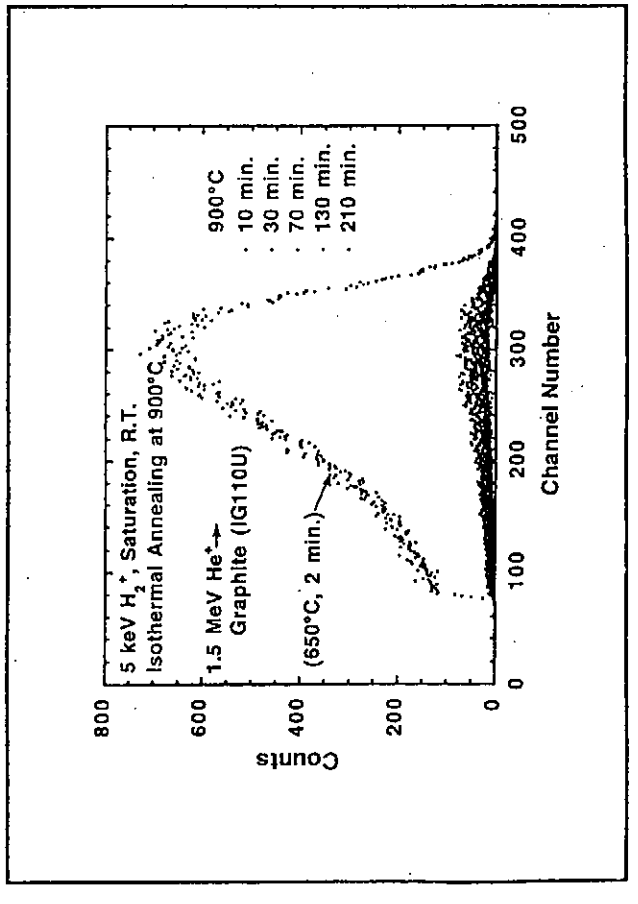

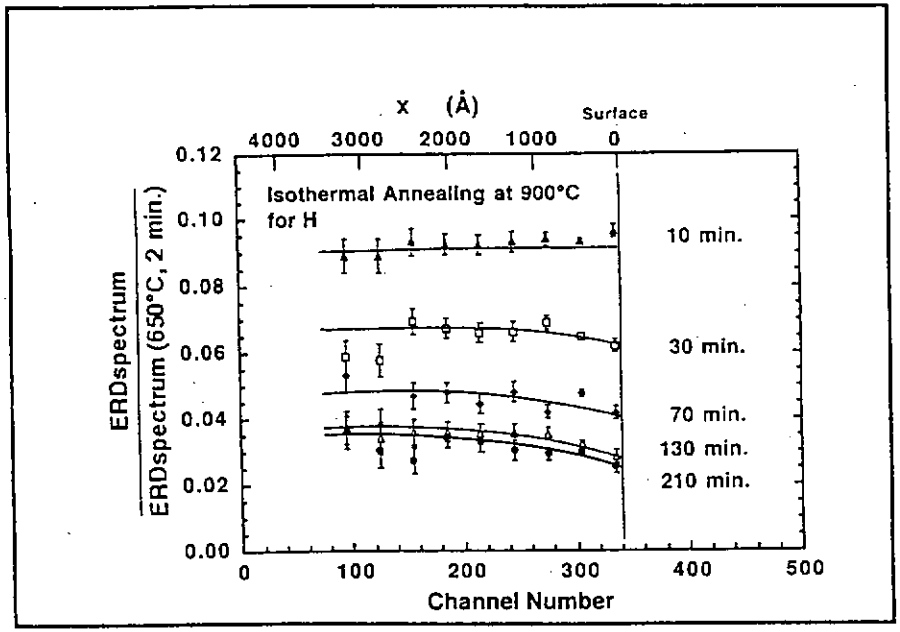
x (Å)
Surface
4000 3000 2000 1000 0
Isothermal Annealing at 900°C
for H
10 min.
30 min.
70 min.
130 min.
210 min.
ERDspectrum
ERDspectrum (650°C, 2 min.)
Channel Number

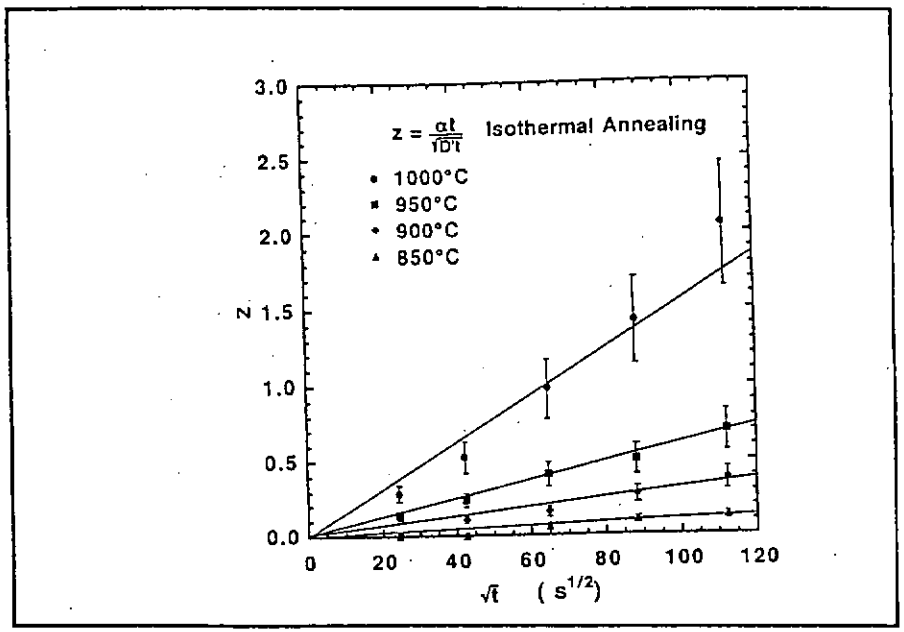
z = αt / √D't
Isothermal Annealing
1000°C
950°C
900°C
850°C
z
√t (s^1/2)

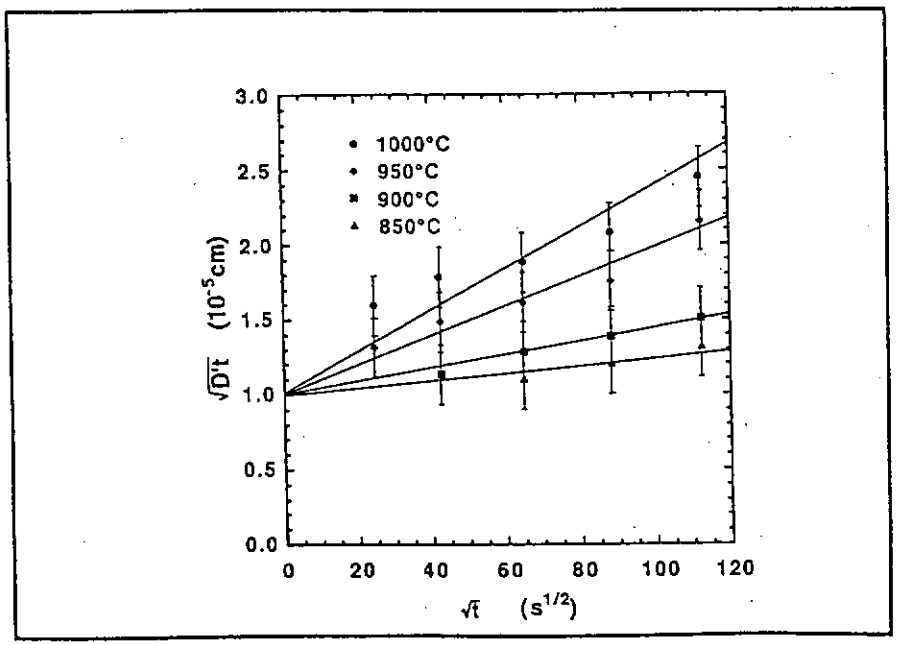
1000°C
950°C
900°C
850°C
√D't (10^-5 cm)
√t (s^1/2)

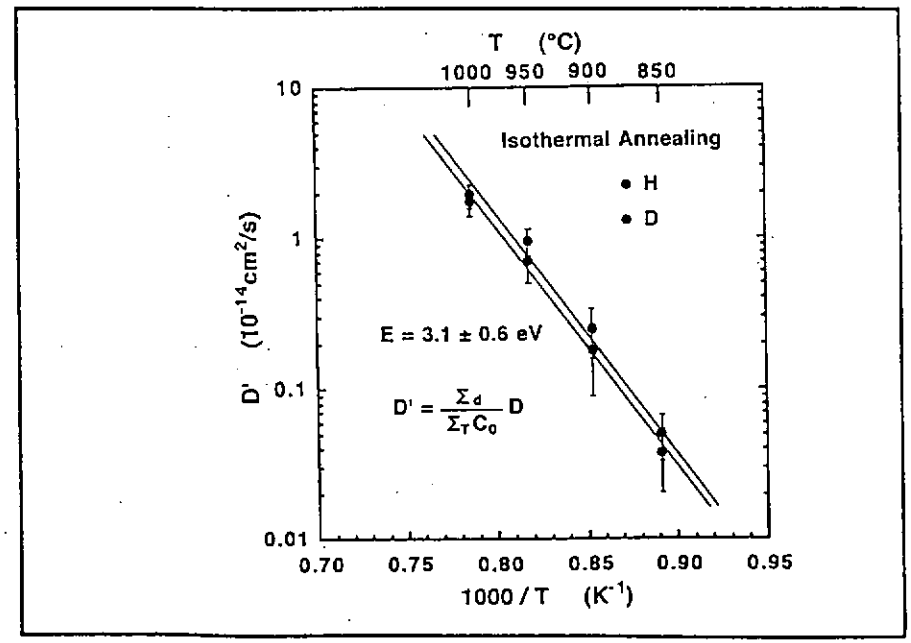
T (°C)
1000 950 900 850
Isothermal Annealing
H
D
E = 3.1 ± 0.6 eV
D' = Σd / ΣT C0 D
D' (10^-14 cm^2/s)
1000 / T (K^-1)

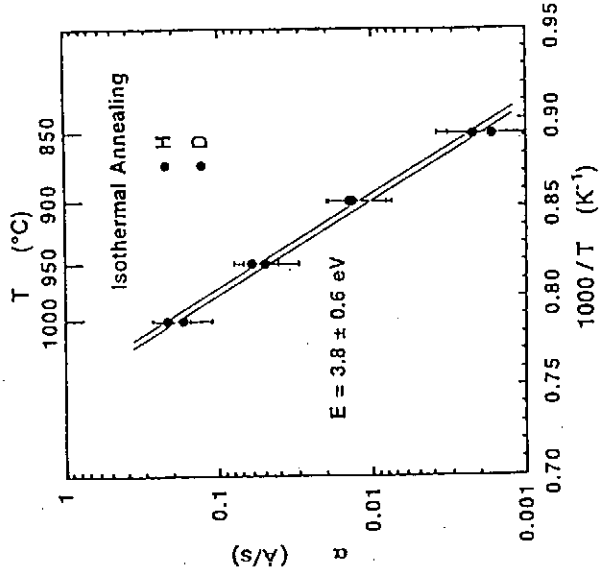

Discussion

Based on the diffusion-limited reaction model

Trapping rate constant

$$\Sigma_T = 4\pi r_T D \xi$$

r_T : the effective trapping radius

ξ : the trapping probability (~1)

The effective diffusion constant

$$D' = \frac{\Sigma_d}{\Sigma_T C_0} D = \frac{\Sigma_d}{4\pi r_T C_0}$$

The activation energy of D' reflects the activation energy of thermal detrapping rate constant Σ_d.

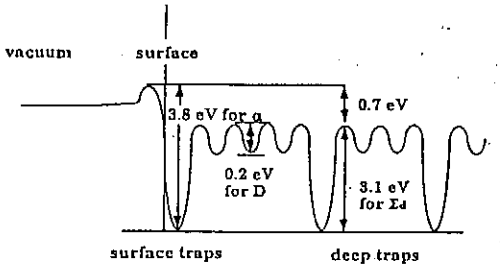

Summary

In order to establish the modeling of the hydrogen recycling at temperatures above 1000 K, the depth dependence of the hydrogen re-emission by isothermal annealing of graphite was measured by means of the ERD technique.

It is found that as the annealing time increases the concentration of retained hydrogen decreases over the whole depth, while the relative retained one decreases gradually with decreasing the depth toward the surface.

It is shown that the activation energy of the effective diffusion constant is 3.1±0.6 eV and reflects the activation energy of thermal detrapping. It is also shown that the activation energy of thermal desorption of the hydrogen atom is 3.8±0.6 eV. It is concluded that such high activation energies of thermal detrapping and desorption reflect the strong binding of hydrogen atoms at the lattice defects in the bulk and at the surface, which is responsible for the isolated chemical bond between carbon and hydrogen atoms.

2nd Int. Workshop on Tritium Effect in Plasma Facing Components
19-20 May 1994, Nagoya University Japan

INTERACTION OF HYDROGEN WITH DEFECT IN GRAPHITE

Naoki KANGAI and Tetsuo TANABE
Department of Nuclear Engineering, Osaka University,
Yamada-oka, Suita Osaka 565, Japan
TEL +81-6-879-7884 FAX +81-6-875-5696

Keisuke NIWASE
Hyogo University of Teacher Education, Yashiro-cho, Hyogo 673-14, Japan

Hisao ATSUMI
Department of Nuclear Reactor Engineering, Kinki University
Kowakae, Higashi-Osaka 577, Japan

Owing to recent extensive studies of hydrogen interaction with graphite, we could attribute hydrogen retention in graphite to the defect trapping. Nevertheless chemical states of trapped hydrogen or hydrogen trapping sites are not fully understood yet. In addition sophisticated behavior of implanted hydrogen such as various hydrocarbon formation, atomic hydrogen remission and radiation enhanced sublimation at higher temperatures confuses us and makes difficult to interpret such complex behaviors of hydrogen in graphite without any contradictions especially at high temperatures.

In order to get more clear information on behavior or chemical state of hydrogen in graphite and on a role of hydrogen both for damaging and annealing processes, we have performed in-situ AES analysis under hydrogen or inert gas (He or Ar) ion bombardment of graphite as well as annealing and compared the present results with already existing knowledge on radiation damage of graphite given by various analysis technique such as a laser Raman spectroscopy, a transmission electron microscopy, an X-ray diffraction analysis, a thermal desorption spectroscopy and so on. The results are summarized as following.

Damaging process introduced by either H, He or Ar ion bombardment is found to be quite similar with each other depending only on the lattice displacement effect, and both electronic excitation effect and chemical effect of implanted hydrogen are hardly seen in AES spectra as well as laser Raman spectra. Considering the large enhancement of hydrogen retention in neutron irradiated graphites it is very likely that hydrogen is trapped damage sites prior produced. Suppose damaging sites are related to sp^3 single bond, it is difficult to distinguish the C-H bond and C-C single bond even by the AES analysis. Accumulation of hydrogen molecules in closed pore or lenticular openings in-between the basal planes introduced by ion bombardment, is also the possible explanation. However, a certain difference does appear in the annealing behavior between the hydrogen implanted graphite and He implanted ones. These makes us to conclude that hydrogen is trapped with a chemical bond to carbon atoms even at higher temperatures.

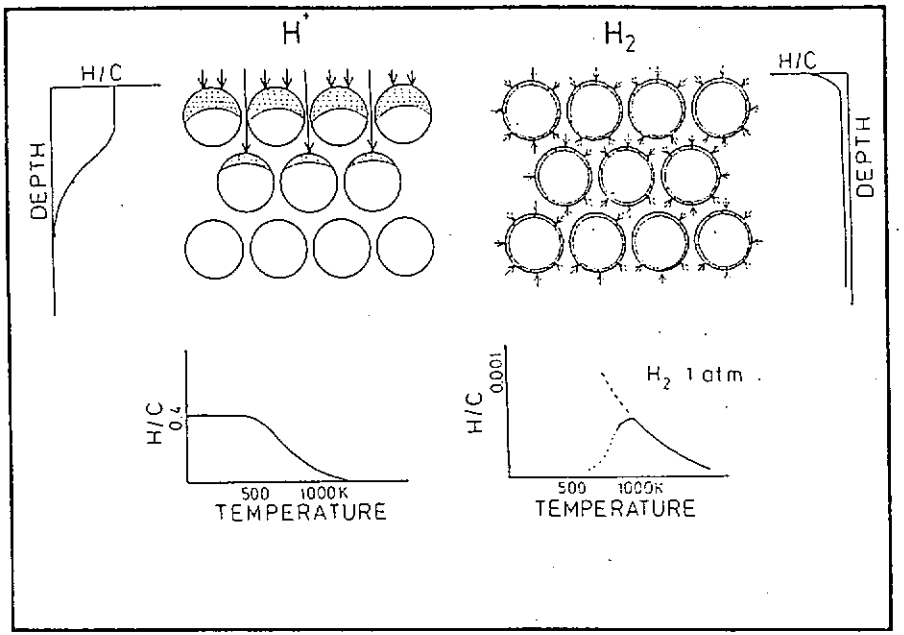

2nd Int. Workshop on Tritium Effect in Plasma facing Components
19-20 May 1994, Nagoya University Japan

INTERACTION OF HYDROGEN WITH DEFECT IN GRAPHITE

Naoki KANGAI and Tetsuo TANABE, Osaka University

Keisuke NIWASE, Hyogo University of Teacher Education

Hisao ATSUMI, Kinki University

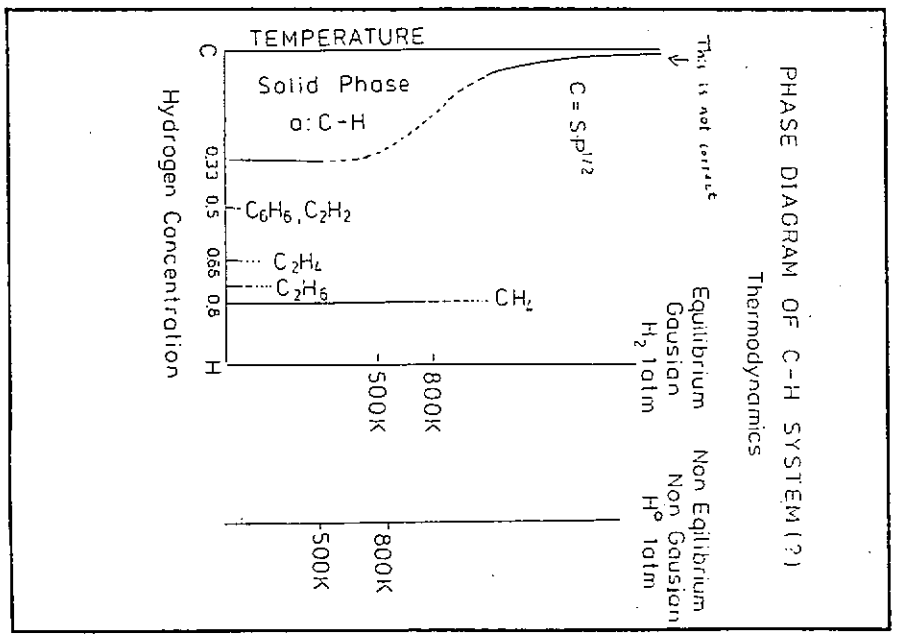

CONTENTS

1. Hydrogen Retention at high temperatures
   $P^{1/2}$ dependence like hydrogen solution in metals
2. Effect of Neutron Irradiation
   Large enhancement of hydrogen retention
3. Consideration of trapping site
   C-H bond, Bubbles, Lenticular openings
4. Present knowledge on damage in graphite
   Laser Raman, TEM, X-ray etc.
5. In-situ AES analysis of damaging and annealing
   (Presented by N. Kangai)

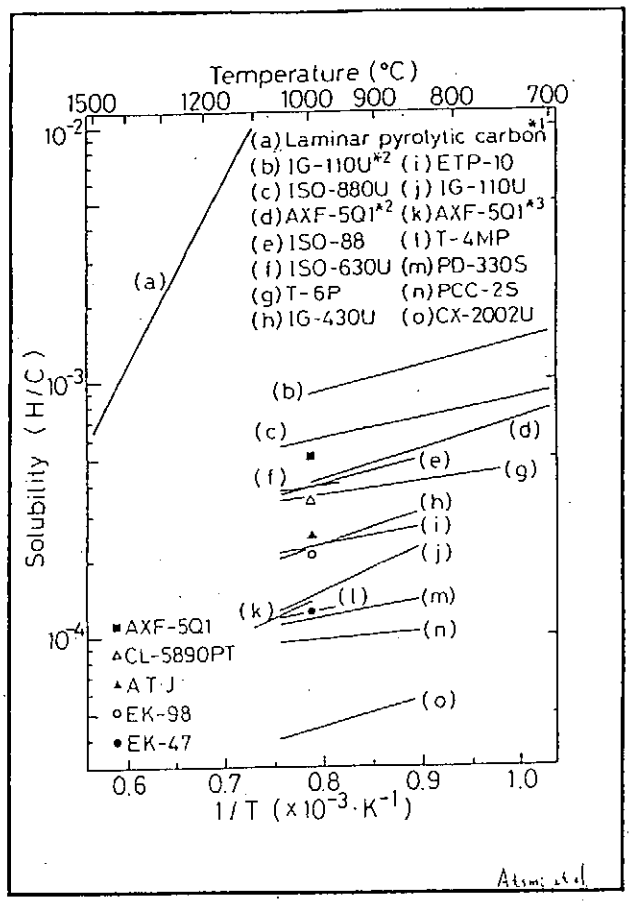

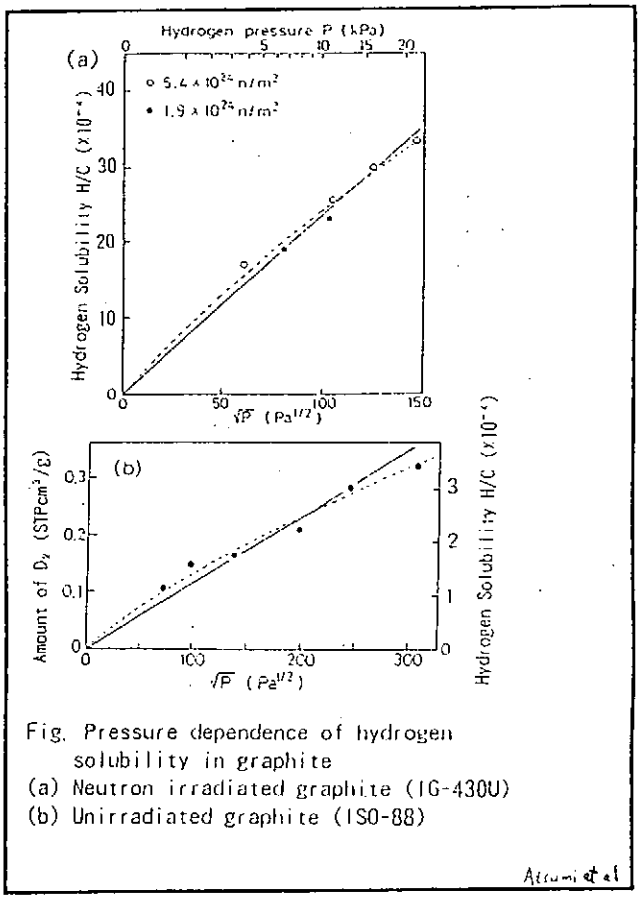

Fig. Pressure dependence of hydrogen solubility in graphite
(a) Neutron irradiated graphite (IG-430U)
(b) Unirradiated graphite (ISO-88)

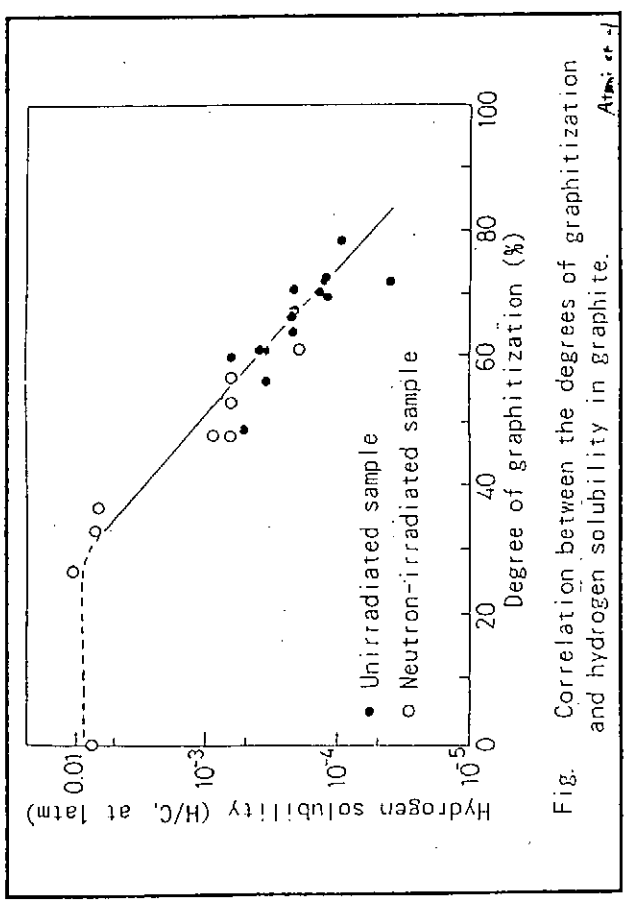

Fig. Correlation between the degrees of graphitization and hydrogen solubility in graphite.

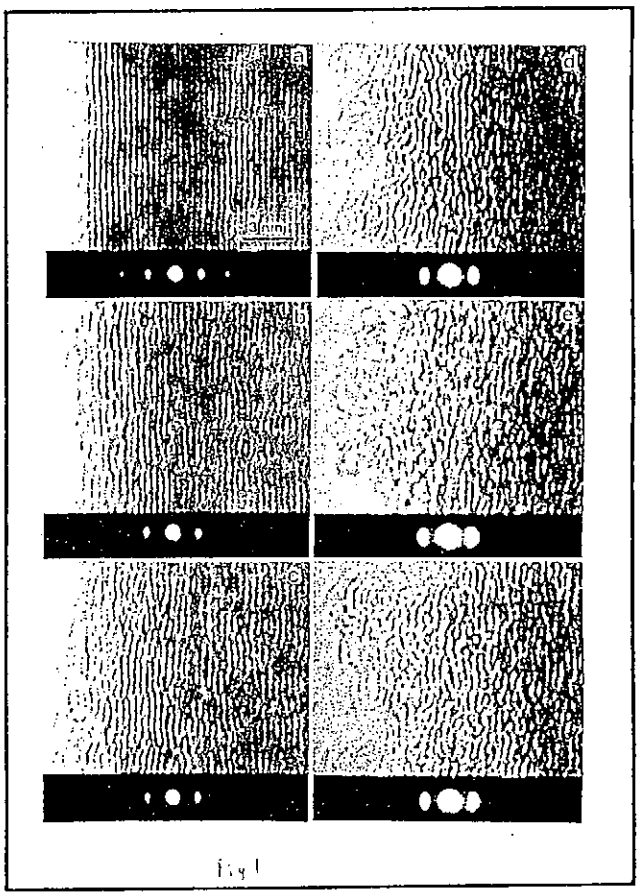

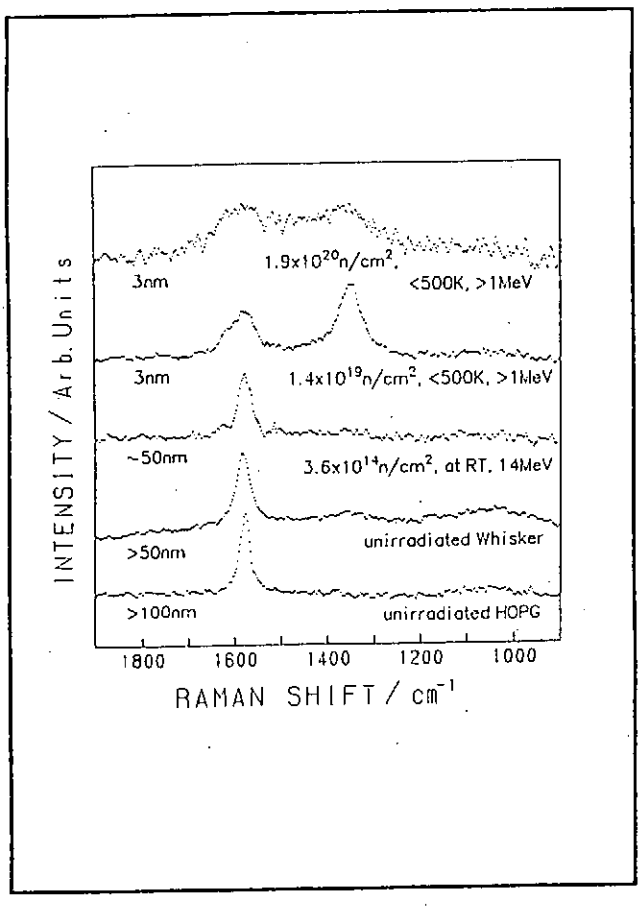
INTENSITY / Arb. Units
3nm
1.9x10²⁰n/cm², <500K, >1MeV
3nm
1.4x10¹⁹n/cm², <500K, >1MeV
~50nm
3.6x10¹⁴n/cm², at RT, 14MeV
>50nm
unirradiated Whisker
>100nm
unirradiated HOPG
1800
1600
1400
1200
1000
RAMAN SHIFT / cm⁻¹

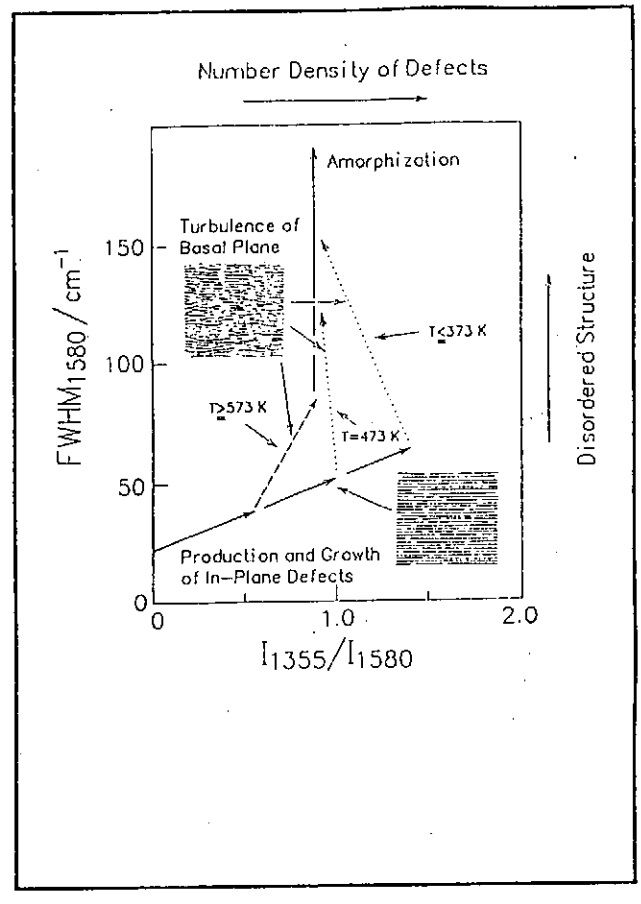
Number Density of Defects
Amorphization
Turbulence of Basal Plane
T≤373 K
T≥573 K
T=473 K
Production and Growth of In-Plane Defects
Disordered Structure
FWHM1580 / cm⁻¹
150
100
50
0
0
1.0
2.0
I1355/I1580

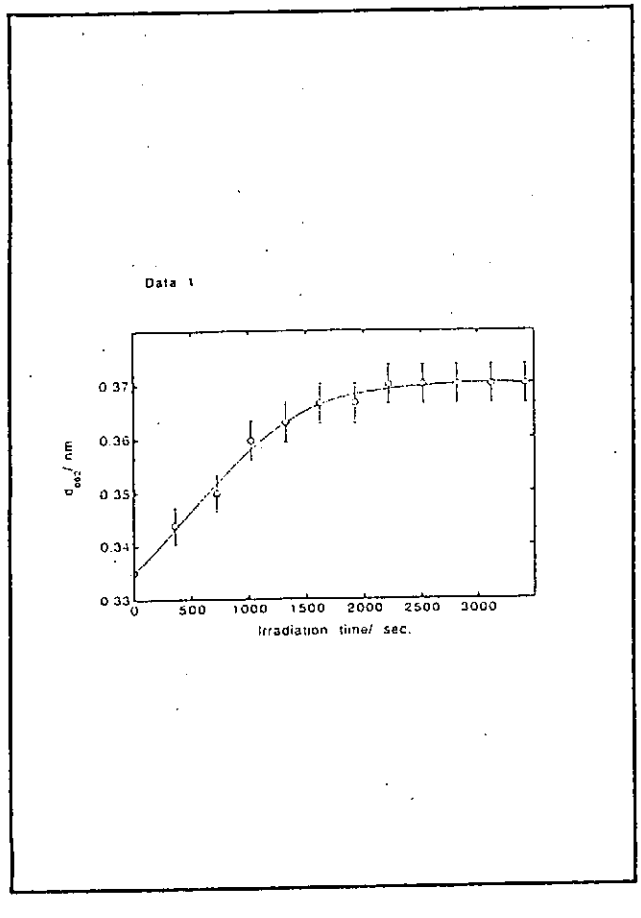
Data 1
d002 / nm
0.37
0.36
0.35
0.34
0.33
0
500
1000
1500
2000
2500
3000
Irradiation time/ sec.

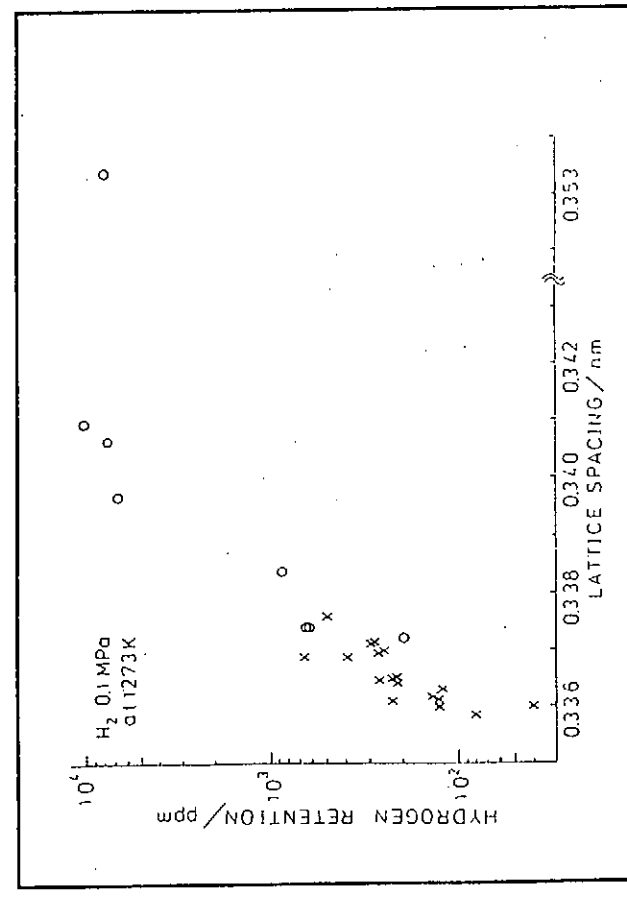
H2 0.1MPa
at 1273K
HYDROGEN RETENTION / ppm
LATTICE SPACING / nm
0.353
0.342
0.340
0.338
0.336

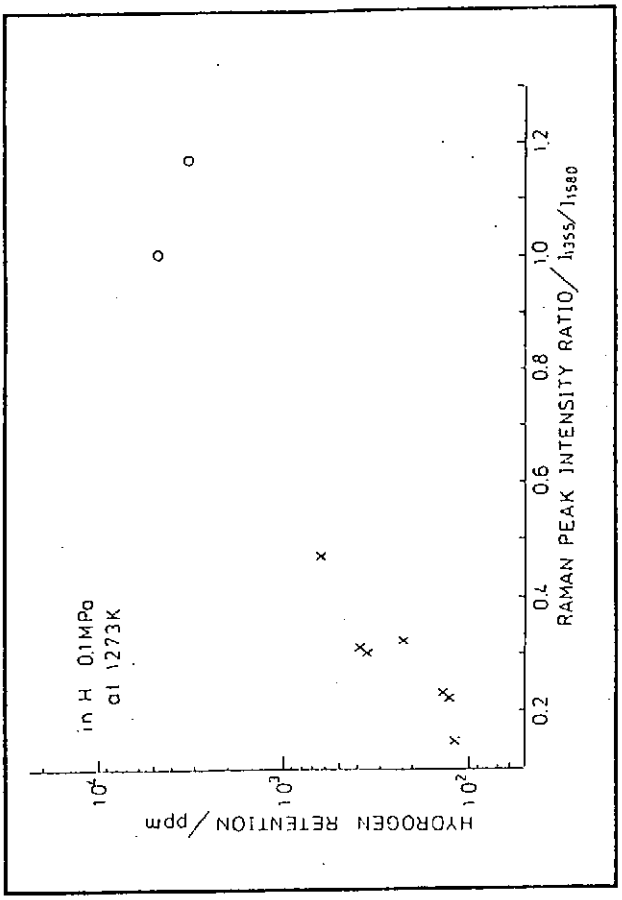

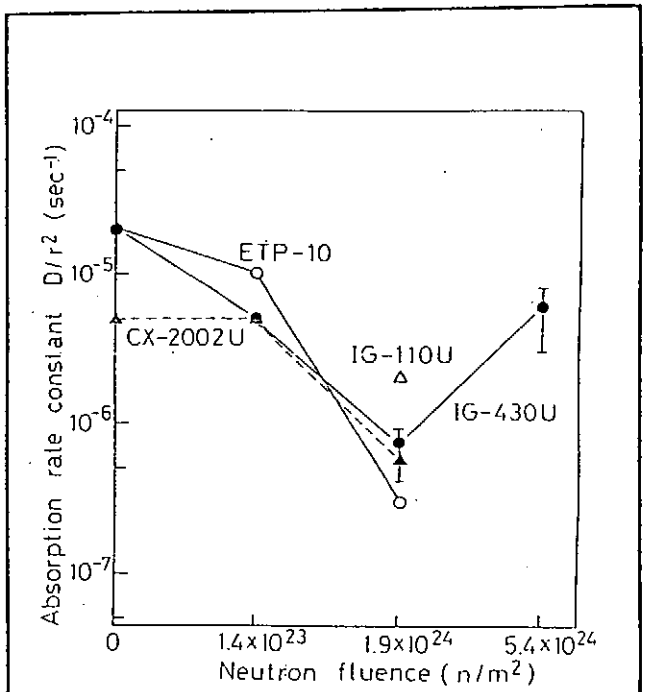

Fig. 5. Rate constants of hydrogen absorption for graphite samples irradiated with neutrons at various fluences.

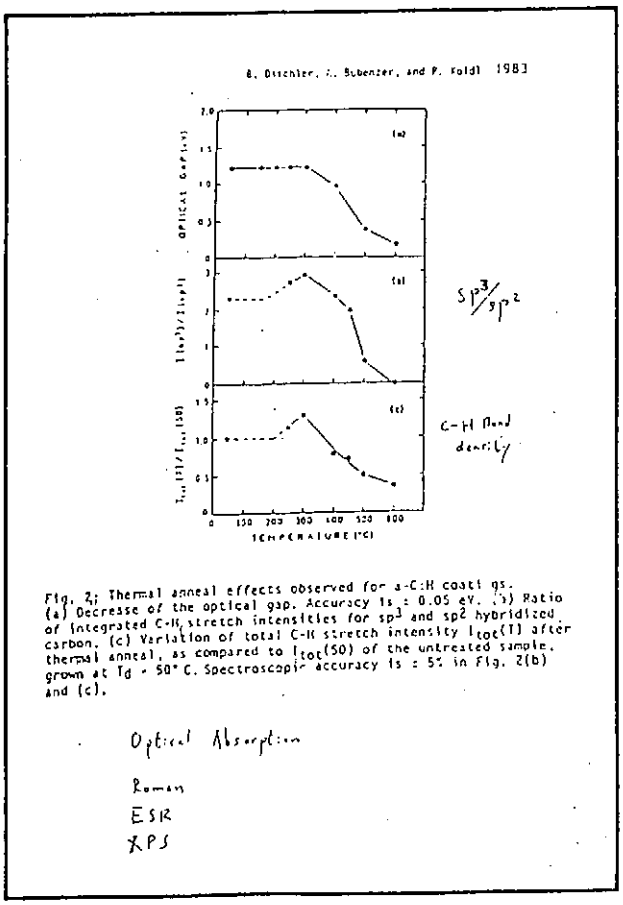

Fig. 2: Thermal anneal effects observed for a-C:H coatings. (a) Decrease of the optical gap. Accuracy is ± 0.05 eV. (b) Ratio of integrated C-H stretch intensities for sp^3 and sp^2 hybridized carbon. (c) Variation of total C-H stretch intensity $I_{tot}(T)$ after thermal anneal, as compared to $I_{tot}(50)$ of the untreated sample, grown at T_d = 50° C. Spectroscopic accuracy is ± 5% in Fig. 2(b) and (c).

Optical Absorption
Raman
ESR
XPS

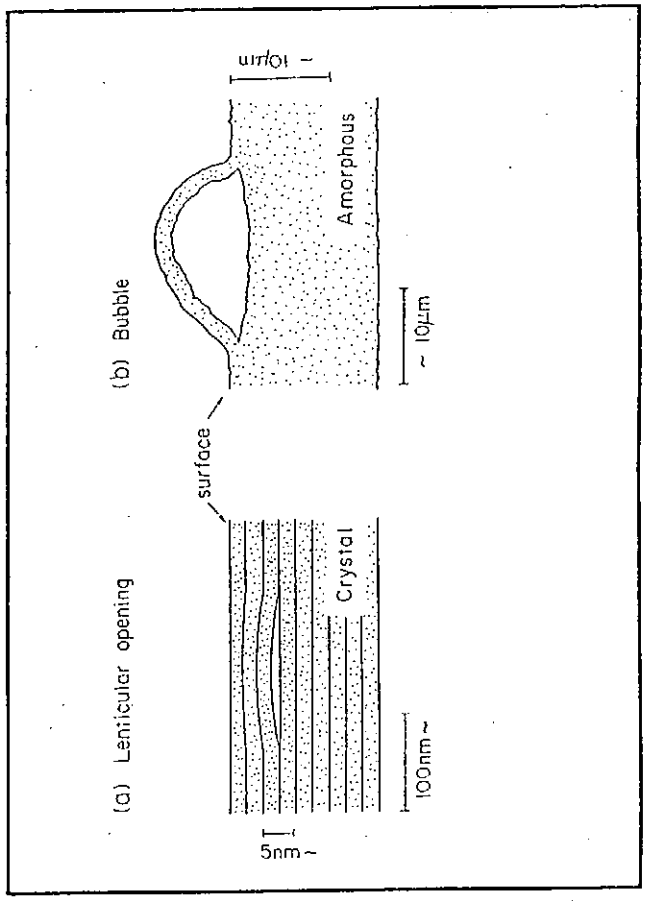

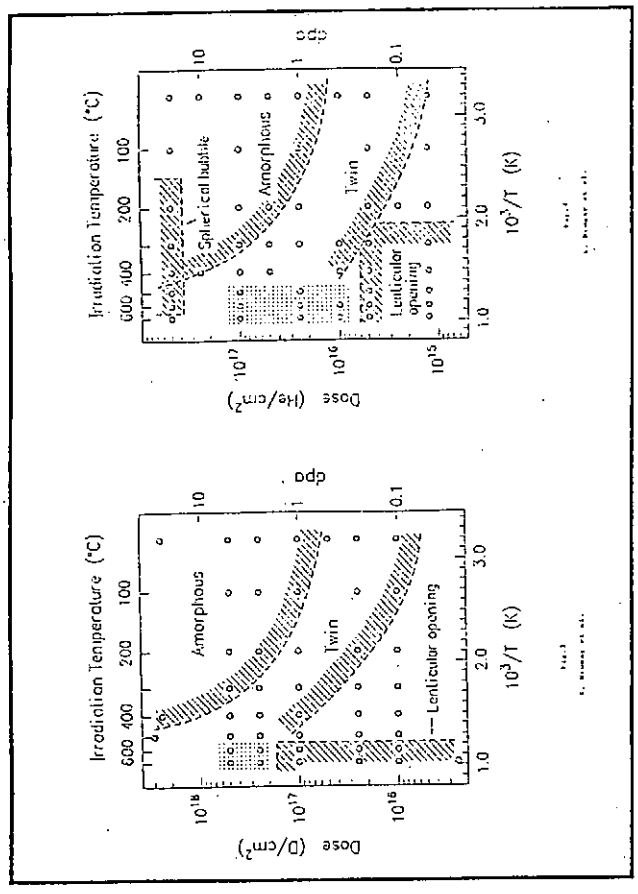

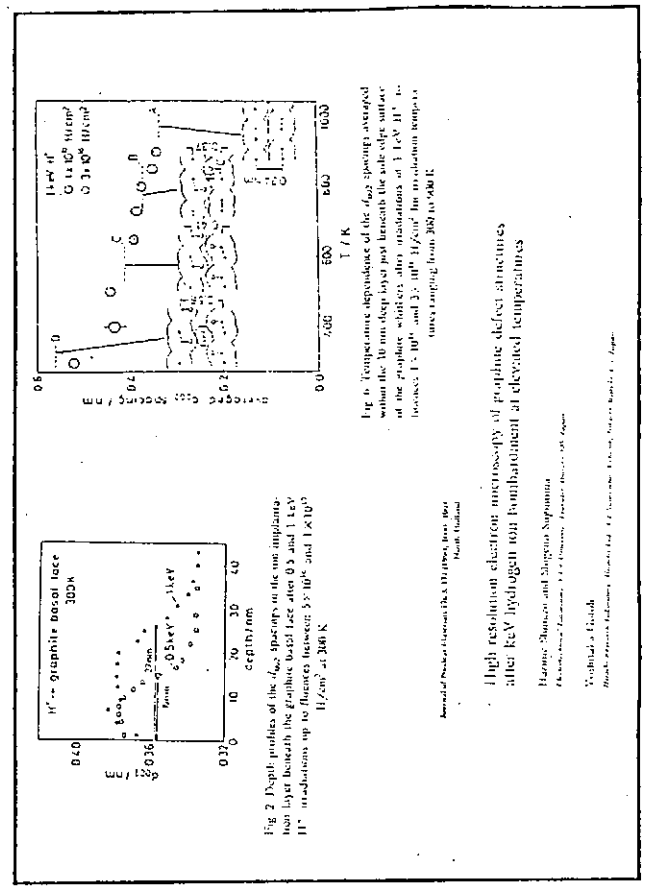

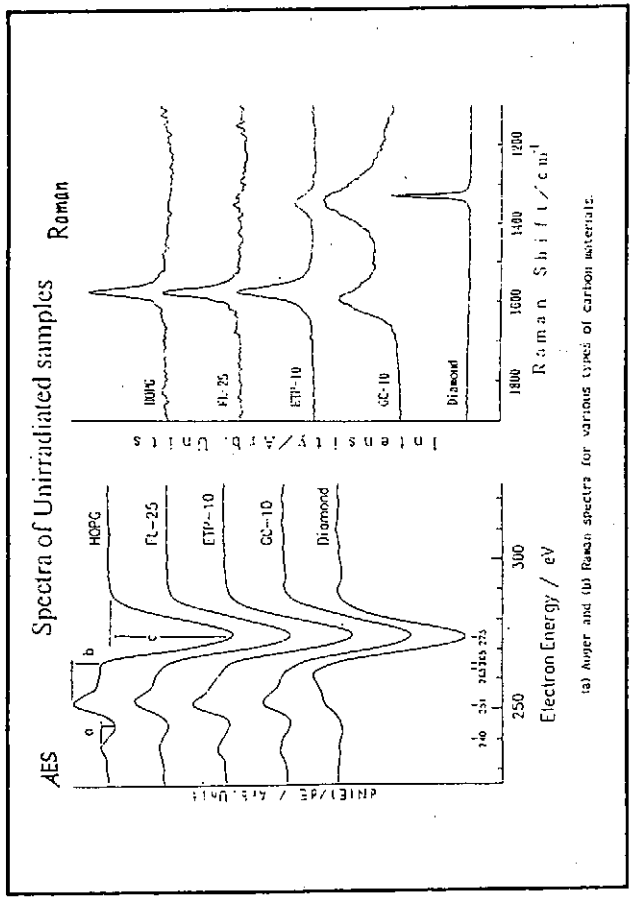

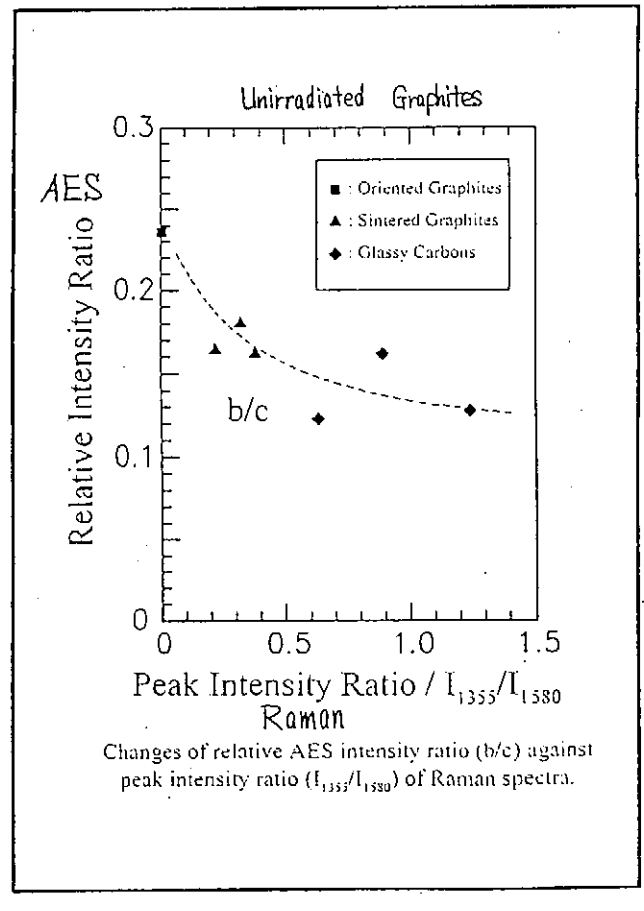

Changes of relative AES intensity ratio (b/c) against peak intensity ratio (I_{1355}/I_{1580}) of Raman spectra.

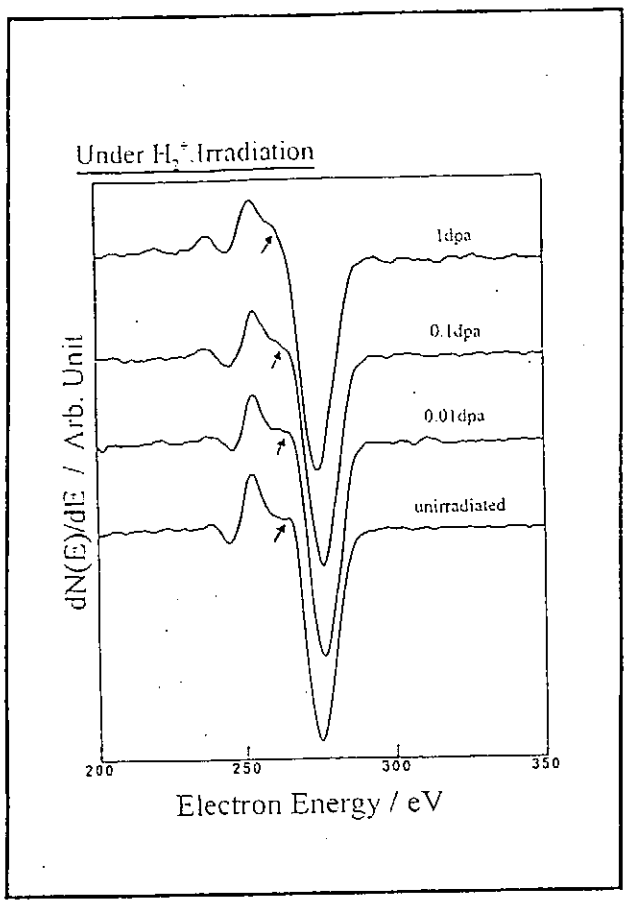
Under H_2^+ Irradiation
1dpa
0.1dpa
0.01dpa
unirradiated
dN(E)/dE / Arb. Unit
200
250
300
350
Electron Energy / eV

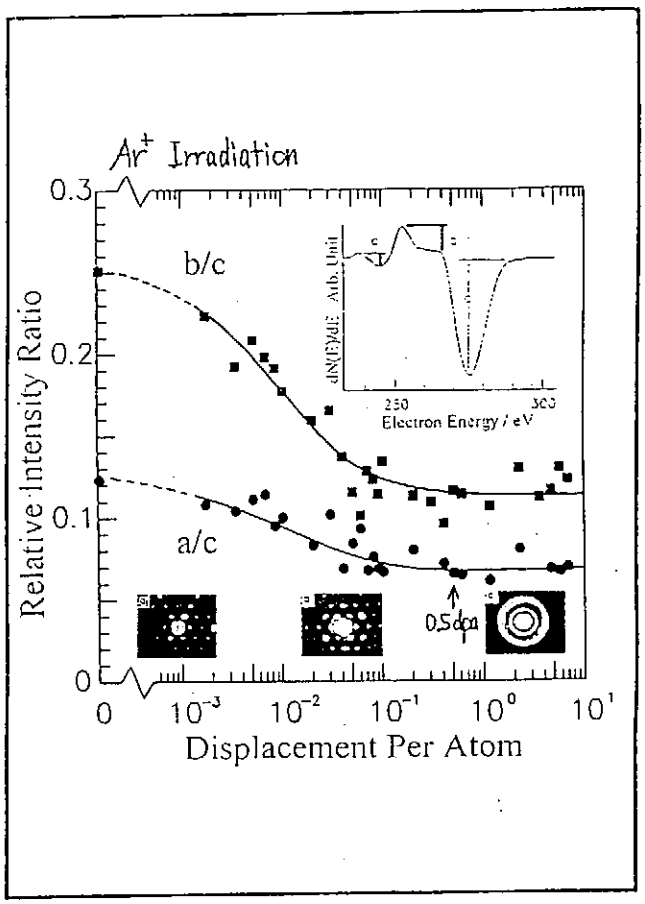
Ar^+ Irradiation
b/c
a/c
0.5dpa
Relative Intensity Ratio
0.3
0.2
0.1
0
10^{-3}
10^{-2}
10^{-1}
10^{0}
10^{1}
Displacement Per Atom
dN(E)/dE Arb. Unit
250
300
Electron Energy / eV

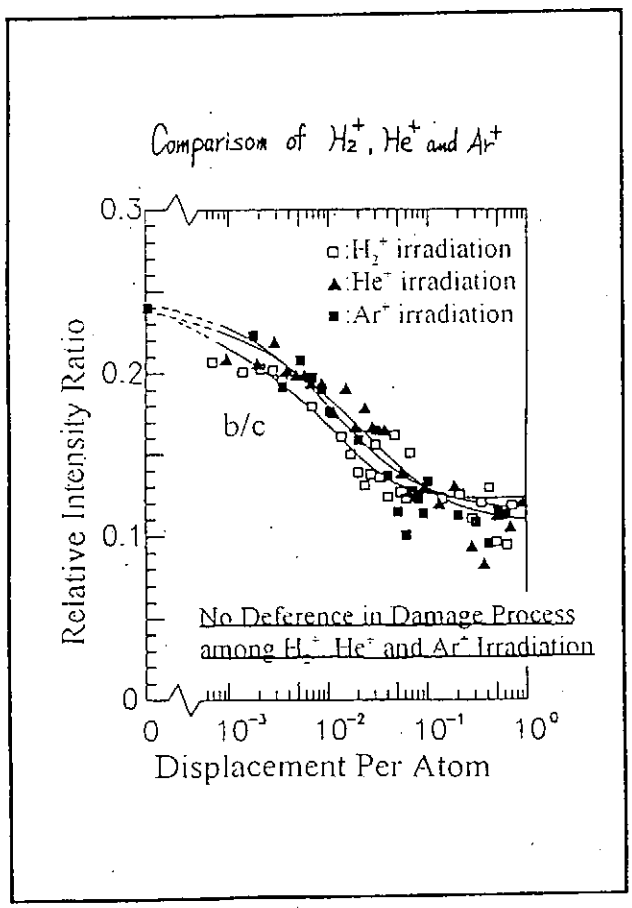
Comparison of H_2^+, He^+ and Ar^+
□:H_2^+ irradiation
▲:He^+ irradiation
■:Ar^+ irradiation
b/c
No Deference in Damage Process
among H_2^+, He^+ and Ar^+ Irradiation
Relative Intensity Ratio
0.3
0.2
0.1
0
10^{-3}
10^{-2}
10^{-1}
10^{0}
Displacement Per Atom

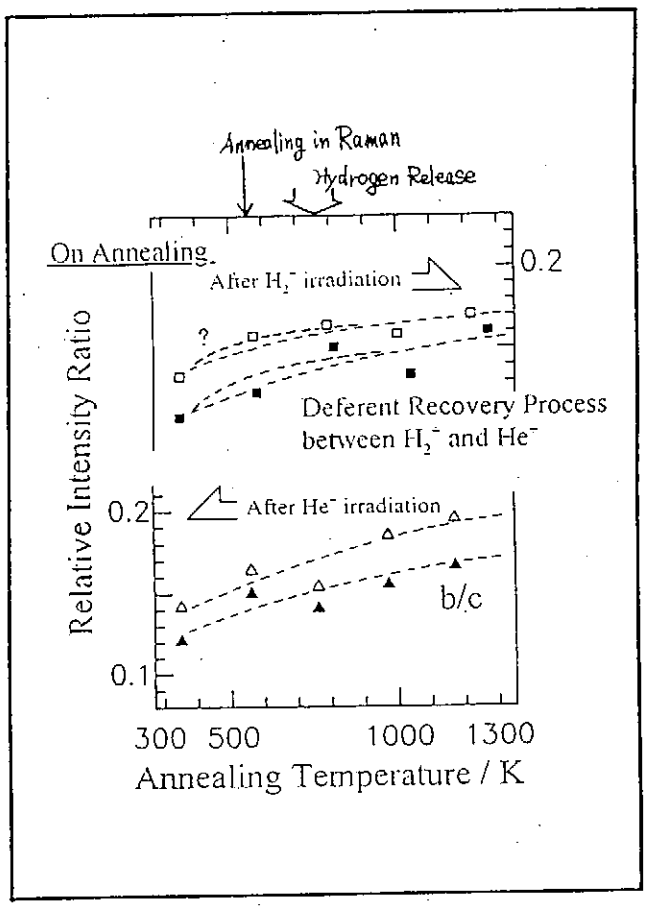
Annealing in Raman
Hydrogen Release
On Annealing
After H_2^+ irradiation
0.2
?
Deferent Recovery Process
between H_2^+ and He^+
After He^+ irradiation
0.2
b/c
0.1
Relative Intensity Ratio
300
500
1000
1300
Annealing Temperature / K

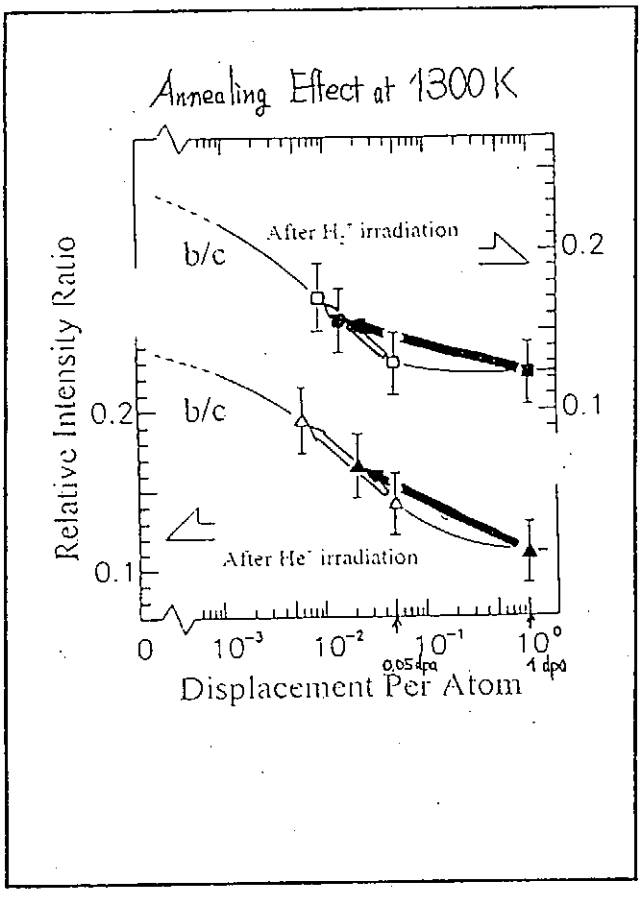

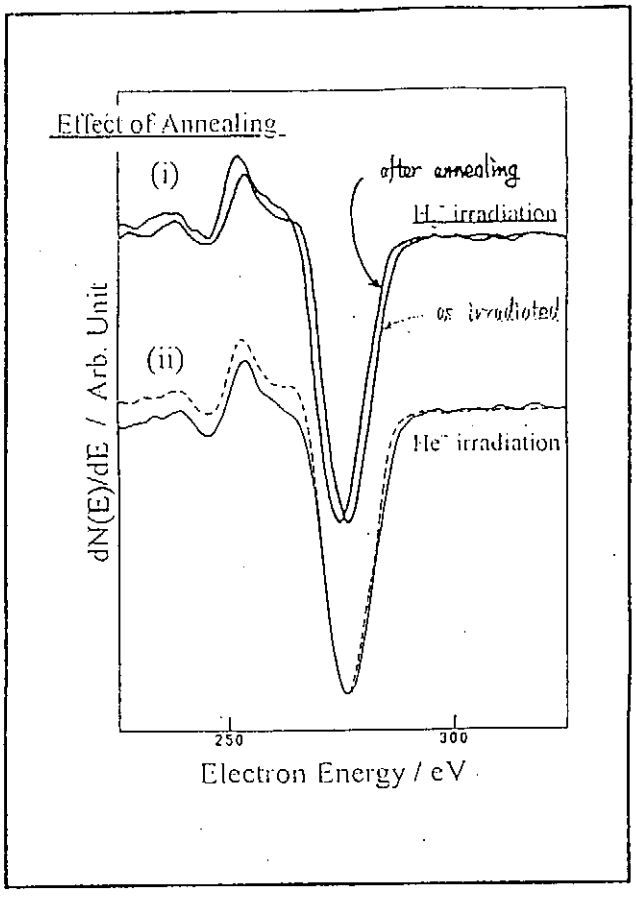

Summary

1. • No difference is seen in damaging process introduced by either H, He or Ar ion bombardment.
   • Only depending on the lattice displacement.
   • Chemical effect of implanted hydrogen are hardly seen.
2. • Hydrogen is trapped at damage sites prior produced.
3. • It is difficult to distinguish the C-H bond and C-C single bond even by the AES analysis.
4. • Accumulation of hydrogen molecules in closed pore or lenticular openings may be the possible explanation, but...
5. • Some difference does appear in the annealing between hydrogen implanted graphite and helium implanted one.

These makes us to conclude that hydrogen is trapped with a chemical bond to carbon atoms even at higher temperatures.

Study for Estimation of Tritium Inventory in Plasma Facing Materials

Shigeru O'hira, Kusuo Ashibe, Yumi Yaita and Kenji Okuno

Tritium Engineering Laboratory
Japan Atomic Energy Research Institute

ABSTRUCT

Thermal desorption spectra were taken with isotropic graphite (EPT-10) tiles exposed to deuterium plasma for 1 hour or 5 hours. From the analysis of TDS, activation energies obtained are 1.90 ± 0.15 eV for the peak I around 800 K and 3.98 ± 0.32 eV for the peak II around 1200 K.

Diffuse reflectance measurements of plasma-exposed graphite powder sample by FT-IR were tried to find the evidence of the C-D bond in the bulk of graphite, which is considered to be related to the peak II in the thermal desorption spectra. There were two strong absorption bands observed at 3691 and 3652 cm^{-1} after the deuterium plasma exposure. The peaks remained after 800 K annealing in vacuo but disappeared after 1200 K annealing in vacuo. So those peaks seemed to be related of the C-D bond expected. But assuming they are absorption of C-D bonds, the force constants calculated (13.7 md Å for the 3691 cm^{-1} peak and 13.4 md Å for the 3652 cm^{-1} peak) are much larger than ones for normal C-H bonds of ordinary hydrocarbons.

Study for Estimation of Tritium Inventory in Plasma Facing Materials

Shigeru O'hira, Kusuo Ashibe, Yumi Yaita and Kenji Okuno

Tritium Engineering Laboratory
Japan Atomic Energy Research Institute

Activities for Plasma Surface Interaction Study in the Tritium Engineering Laboratory

1. Tritium Implantation/Permeation Experiment

-Measurement of tritium permeation rate by atomic ion implantation using a large current atomic ion source (up to 1 mA, uniform ion energy between 100 - 2000 eV)

Samples : 304ss, Inconel, Ni, Al, Mo, Al-Li alloy, Fe- Ti alloy, Ti, Fe, Pd, V, V alloy, Ti-Al alloy, 316ss and some coated materials
Parameters: temperature, ion beam flux, ion beam energy

Current status: Experiments using Deuterium are running.
Modification for tritium experiment is being carried out.

2. Tritium Thermal/Photo Desorption Experiment of Plasma-exposed Materials

-Thermal/photo desorption spectra measurement and chemical species analysis of hydrogen isotopes from plasma-exposed materials
-Chemical states analysis of hydrogen isotopes in plasma-exposed materials by means of spectroscopic methods

Samples: graphite (isotropic, c/c composite etc.), *beryllium and other metals including alloys*
Spectroscopes: AES, SIMS, ESCA, FT-IR, Laser Raman

Current Status: Thermal/photo desorption spectra measurements of D_2 are running.
ESCA has been set-up.
Diffuse reflectance spectra measurements by FT-IR are running.
Modification for tritium experiments is planned.

Mass Analyzed Thermal/Photo Desorption Spectroscopy of Hydrogen Isotopes from Plasma-exposed Materials

Specifications of apparatus
a) Plasma exposure system
- plasma chamber: Pyrex glass (25mmOD × 410mm L)
- plasma generation: RF-discharge with external electrodes (13.56 MHz, 0 - 500 W)
-gas pressure: 0.1 - 10 Torr of D_2, (T_2)

b)Desorption system
-heating: infrared furnace (1 kW infrared lamp with focusing mirror × 2, up to 1700 K)
-UV irradiation: 40 W low pressure Hg lamp, × 2
-gas analysis: quadrapole mass analyzer (1 - 400 amu)

Sample: EPT-10 (10mm × 10mm × 1mm, heated up to 1500 K before plasma exposure)

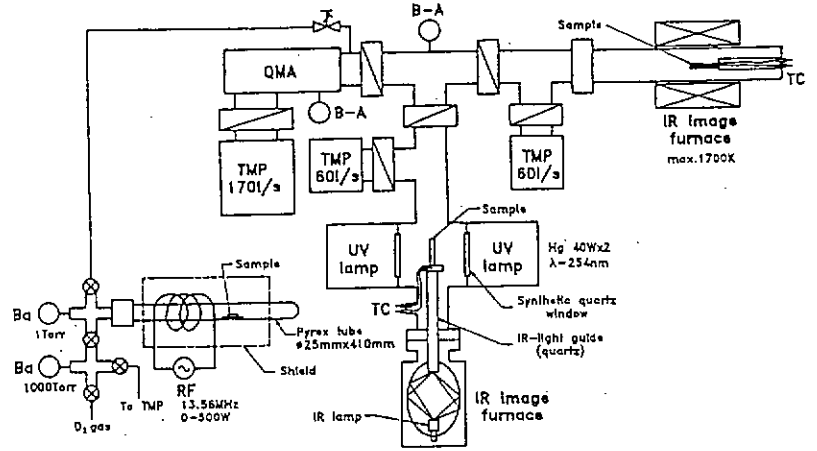

Figure 1. Schematic of apparatus for thermal/photo-desorption and retention research of hydrogen isotopes in plasma-exposed materials.

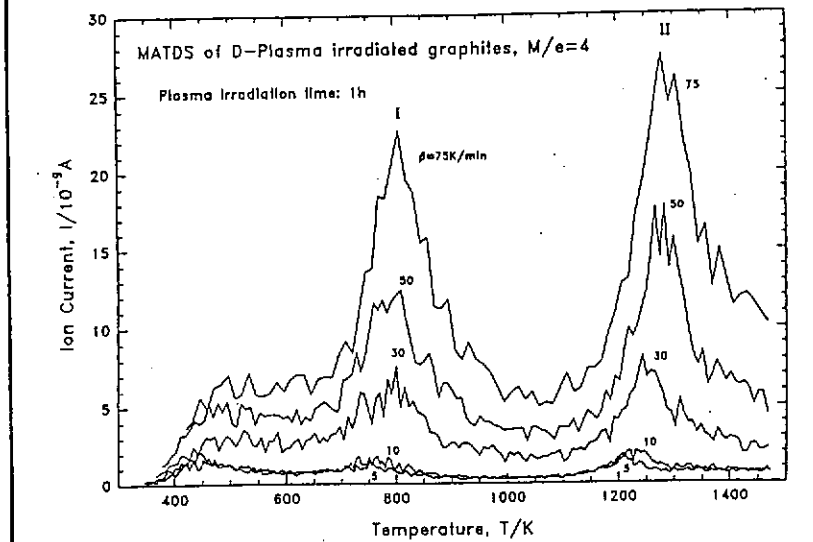

Figure 2. Mass analysis thermal desorption spectra (MATDS) of D plasma irradiated graphite samples. (M/e = 4, plasma irradiation for 1 hour)

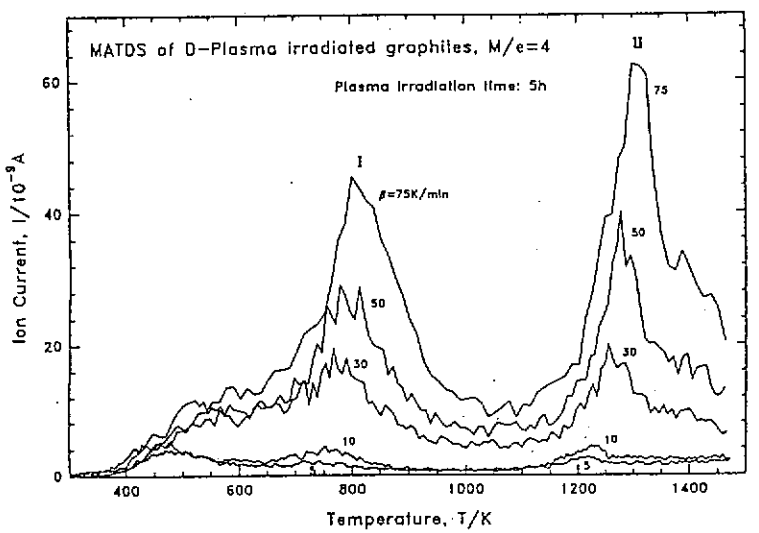

Figure 3. Mass analysis thermal desorption spectra (MATDS) of D plasma irradiated graphite samples. (M/e = 4, plasma irradiation for 5 hours)

Analysis of MATDS

Measurement of MATDS by heating sample at constant temperature ramp in a system evacuated with a large pump speed.

$$\ln(Tp^2/\beta) = (Ed/RTp) + \ln(Ed/nR\nu_d) - (n-1)\ln(\sigma) \quad \cdots (1)$$

$$\ln(\beta Ed/RTp^2) + (Ed/RTp) = \ln(n\nu_d) + (n-1)\ln(\sigma) \quad \cdots (2)$$

Tp : temperature at desorption rate maximum
β : temperature ramp
Ed : activation energy of desorption
n : order of surface reaction
ν_d : frequency factor
σ : hydrogen isotopes concentration on the sample surface

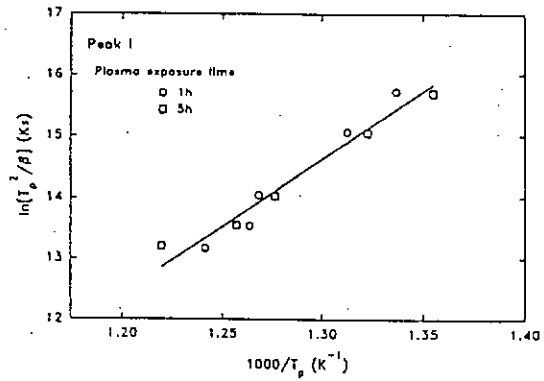

Ed = (1.90 ± 0.15) eV = (183 ± 14) kJ/mol = (43.8 ± 3.4) kcal/mol

Figure 4. Activation energy obtained from MATDS. (peak I around 800 K)

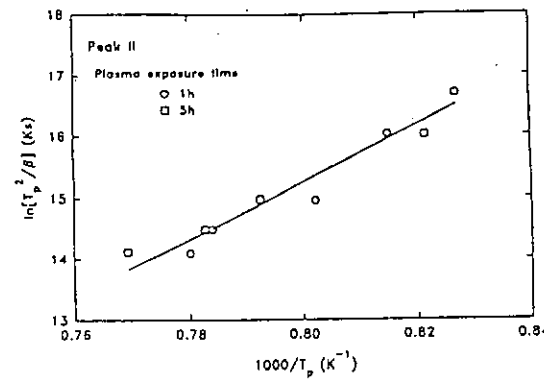

Ed = (3.98 ± 0.32) eV = (384 ± 31) kJ/mol = (91.8 ± 7.3) kcal/mol

Figure 5. Activation energy obtained from MATDS. (peak II around 1200 K)

Diffuse Reflectance Measurements of Plasma-exposed Material
by Infrared Fourier Transform Spectroscopy

Diffuse reflectance infrared spectrometry

Principle: When a ray of light is incident upon an inhomogeneous powder sample which consists of particles larger than the wavelength, the light is reflected by
(1) specular reflection on particle surface,
(2) diffuse reflection through the multiple process of refraction incidence into the particle, transmission inside the particle and reflection on the particle surface.

If (1) could be negligible, absorption spectra similar to the one by transmission method is obtained by transforming the ratio of incident and reflection light intensity by the following equation,

$$(1-R_\infty)^2/2R_\infty = K/S \equiv f(R_\infty)$$

R_∞ : relative reflection ratio (R/I) at a enough deep layer (no change of reflection ratio with layer depth increase)
K : absorbance coefficient
S : scattering coefficient
$f(R_\infty)$: Kubelka-Munk equation (approximation)
(cf. Lambert-Beer equation T = exp(-ad) for transmission)

Mechanism of diffuse reflection in powder sample

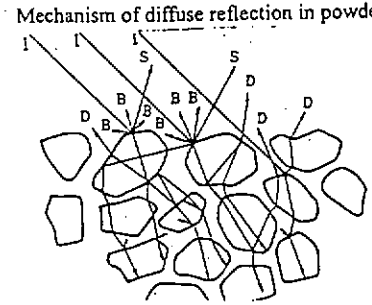

I: Incident ray
S: Specular reflection
B: Back scattering
D: Diffuse reflection
R = S + B + D

Features of Diffuse Reflectance Measurement by Infrared Fourier Transform Spectroscopy

1. No preparation is necessary for spectral measurement of powder sample. (cf. KBr disk, NUJOR)
2. Measurements of high sensitivity are possible with a sample of small amount. (~0.04 cc)
3. Adsorption/desorption phenomena can be observed by using a heating and gas flow/vacuum cell.
4. Not only powder sample but also porous or rough surface sample can be applied for measurement.

Infrared Diffuse Reflectance Spectra of Hydrogen Isotope Plasma-exposed Graphite

Apparatus:

Spectrometer :

JASCO FT-IR 7000

MCT(mercury cadmium telluride) detector

4,600 – 400 cm^{-1}

Diffuse reflectance cell:

Heating and gas flow cell (r.t. – 500℃)

(A: sample, B: KBr window, C: heater, D: gas flow pipe)

Optics

(A: cell, B: ellipsoid mirror, C, D, E: flat mirror)

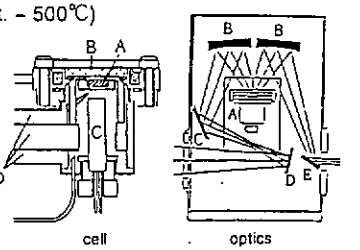

Samples:

Powdered graphite (EPT-10, < 32 μm, ~10 mg)

Sample A: blank (annealed at 1473 K for 30 min in vacuo)

Sample B: exposed sample A to deuterium plasma

Sample C: annealed sample B up to 900 K in vacuo

Sample D: annealed sample B up to 1200 K in vacuo

Plasma exposure:

(filling 0.5 Torr D_2 → plasma exposure) × 10 times

Absorbed deuterium concentration in the graphite powder sample is about 2×10^{-7} mol/mg (C/D ~ 2,400)

Spectra measured:

Background: Sample A

Spectrum 1: Sample B – Sample A

Spectrum 2: Sample C – Sample A

Spectrum 3: Sample D – Sample A

100 scans, resolution 2 cm^{-1}

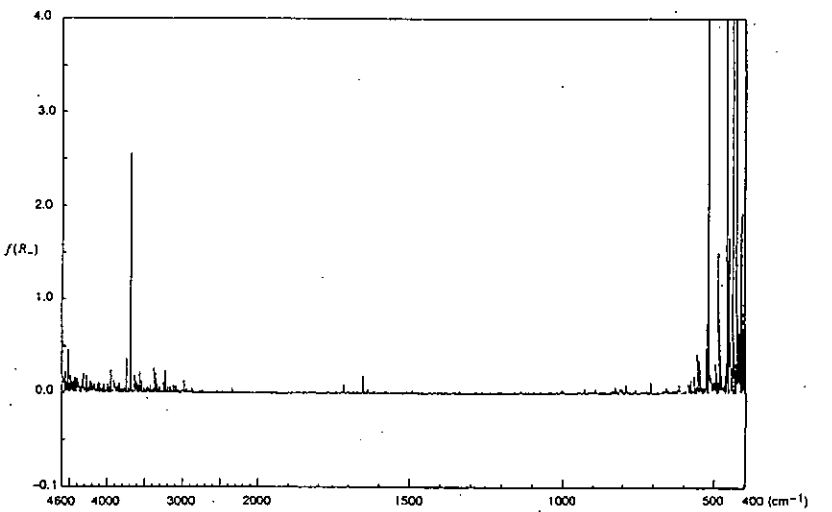

Figure 6. Spectrum 1 (Sample B – Sample A).

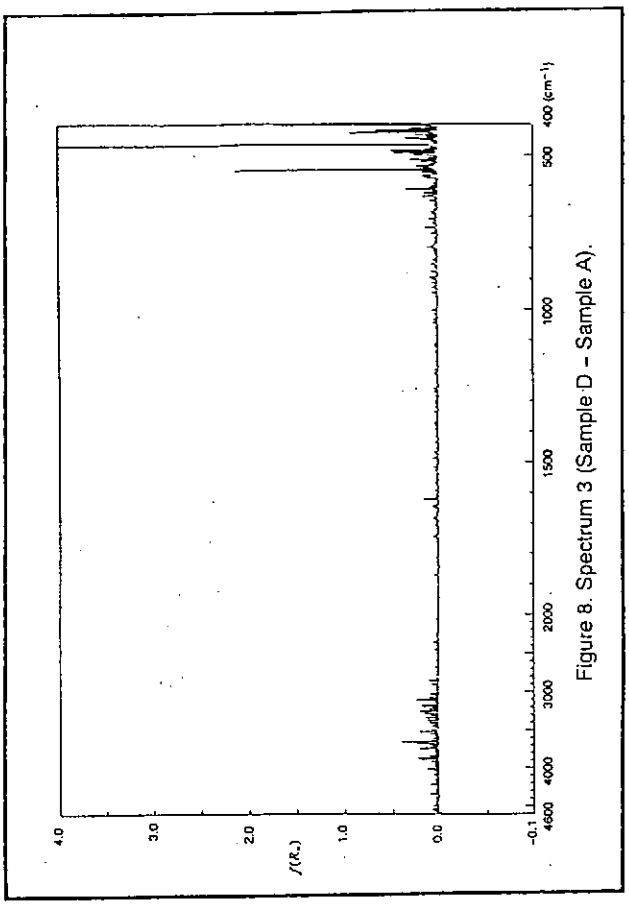

Figure 8. Spectrum 3 (Sample D – Sample A).

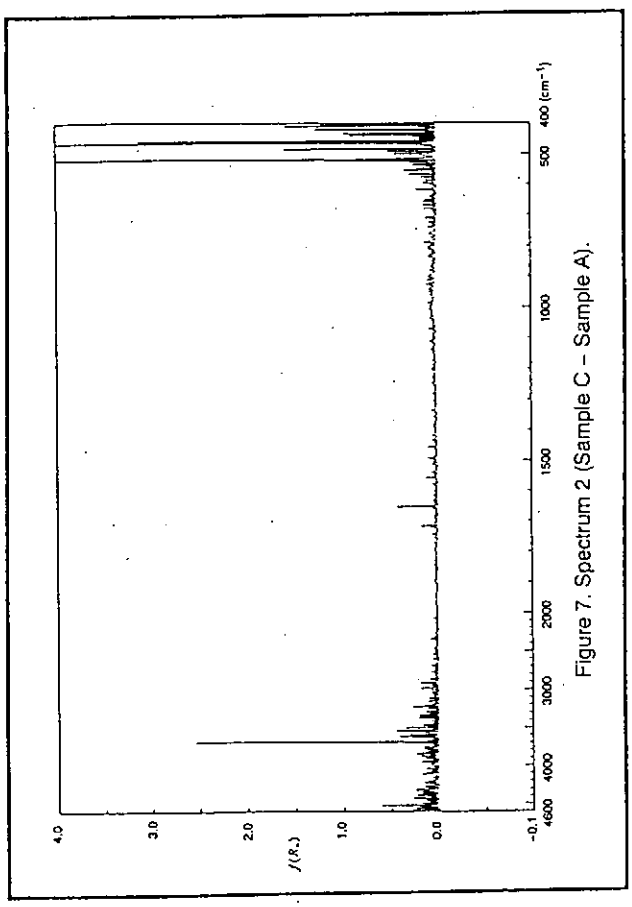

Figure 7. Spectrum 2 (Sample C – Sample A).

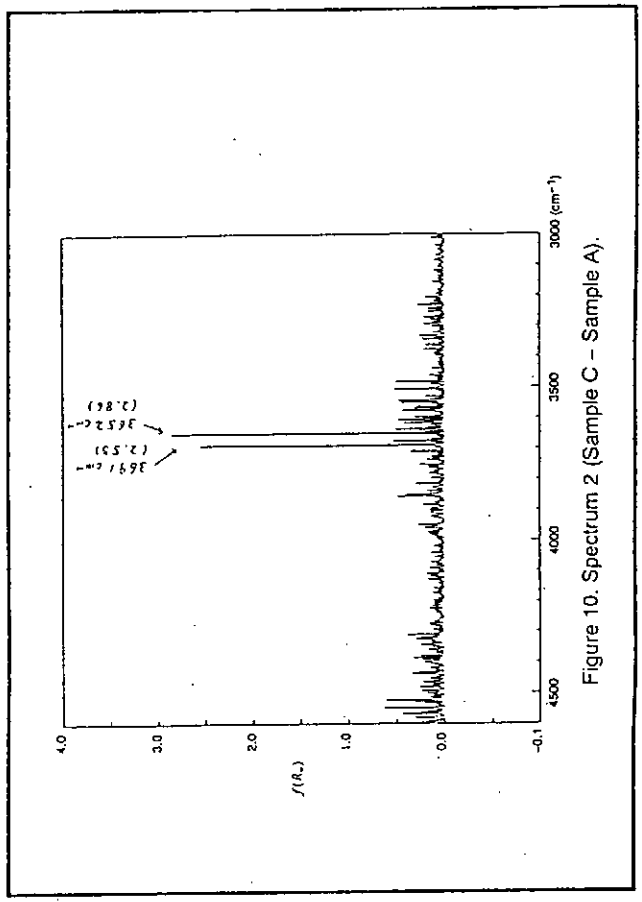

Figure 10. Spectrum 2 (Sample C – Sample A).

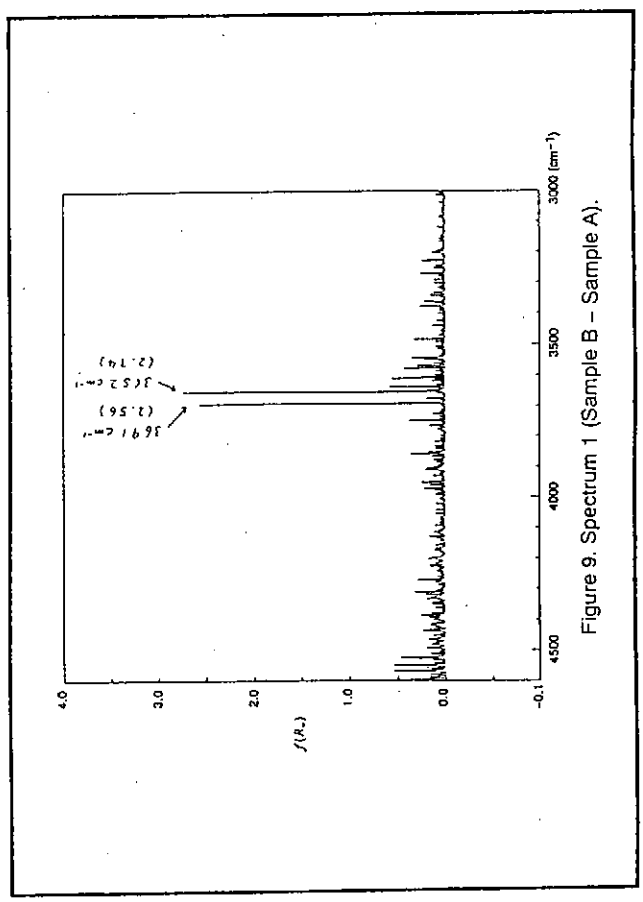

Figure 9. Spectrum 1 (Sample B – Sample A).

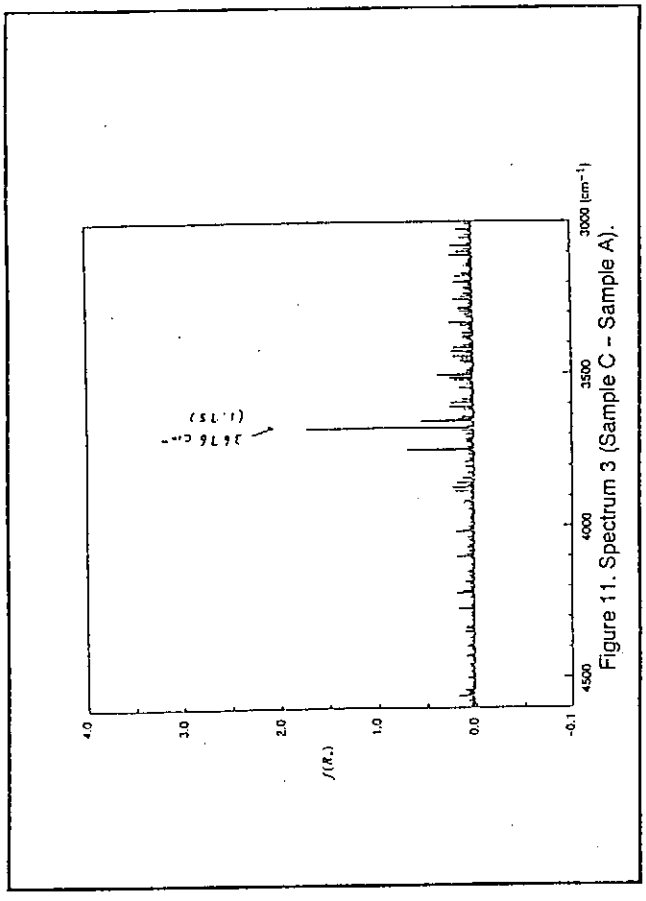

Figure 11. Spectrum 3 (Sample C – Sample A).

Force constant (md·Å)

		C-D?
CH_4 (C-H)	4.42	
C_2H_4 (C-H)	4.7	3691 cm⁻¹ 13.7
C_2H_2 (C-H)	5.0	3652 cm⁻¹ 13.4

C-D → C-H (?!)

3691 cm⁻¹ → 5038. cm⁻¹
3652 cm⁻¹ → 4977 cm⁻¹
} out of range 4600 cm⁻¹ – 400 cm⁻¹

Force constant represents energy potential steepness.

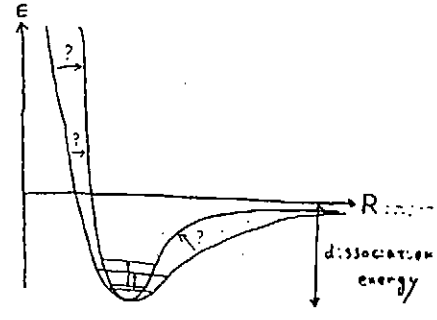

Hydrogen Adsorption on and Solubility in Graphites.

A.P.Zakharov, S.L.Kanashenko, A.E.Gorodetsky, V.N.Chernikov and A.V.Markin.

Institute of Physical Chemistry, Russian Academy of Sciences, Russian Federation.

B.Doyle and W.Wampler

Sandia National Laboratories, Albuquerque, NM, USA.

Abstract

The Langmuire type adsorption is proposed for the hydrogen isotopes - graphites interaction. The dangling sp^2-bonds relaxation was taken into account, the value of hydrogen adsorption enthalpy depends upon the nearest environment of carbon atom. The main variation of entropy under adsorption is caused by escaping of translation and rotation parts of gaseous hydrogen entropy and appearing of adsorbed hydrogen oscillation entropy.

Two kinds of traps are proposed:

Traps 1-carbon interstitial loops with the adsorption enthalpy of -4.4 eV/H_2 between the graphite planes;

Traps 2-carbon network edge atoms with the adsorption enthalpy of -2.3 eV/H_2;

Each type of graphite could be described with its own unique set of traps. For instance POCO AXF-5Q has the numbers of Traps 1 and Traps 2 of 20 and 200 appm respectively. The irradiation with neutrons or carbon atoms increases the Traps 1 and Traps 2 numbers. At damage level of ~1dpa under room temperature irradiation the numbers of Traps 1 and Traps 2 increased up to 1500 and 5000 appm respectively. Our adsorption experiments show that Traps 1 and Traps 2 are stable under high temperature annealing (1500K).

Experimental basis.

	Hydrogen-graphite energetic. (mean hydrogen concentration)	Temperature, K	Pressure, Pa	Reference
Binding energy	4.3 eV/H (17 ppm)	1400-1800	0.66-133	R.Causey [1]
Heat of adsorption	2.5 eV/H_2 (140ppm)	1173	1-100	E.Hoinkis [2]
Heat of solution	0.1- 0.2eV/H (200-300 ppm)	1123-1323	10^4	H.Atsumi et al.[3,4]

R.Causey et al. have proposed hydrogen trapping with binding energy of 4.3 eV/H.

E.Hoinkis suggested that the hydrogen - graphite interaction could be described in the terms of chemisorption. The Langmuire type isotherms for the dissociative adsorption was calculated with the assumption of $\Delta H = -2.5$eV/H_2 adsorption enthalpy.

H.Atsumi et al. have proposed a Sievert's law for the hydrogen solution in graphite with the following expression:

$S = S_0 p^{1/2}$, where

$S_0 = 6.44 \cdot 10^{-5} \exp(+0.2\text{eV}/kT)$ at.fraction/atm$^{1/2}$

Hydrogen-carbon interaction energetic.

To our opinion the relaxation process of carbon edge atoms of graphite network should be taken into account at hydrogen adsorption on graphites.

This relaxation might be as high as –1 eV/C.

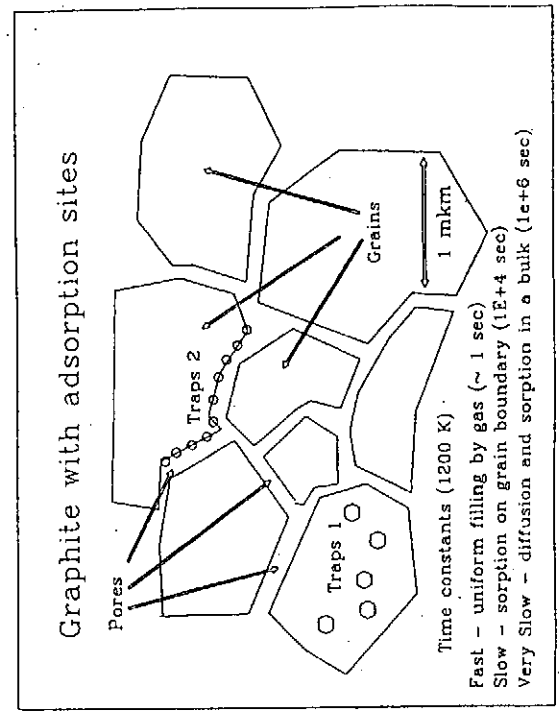

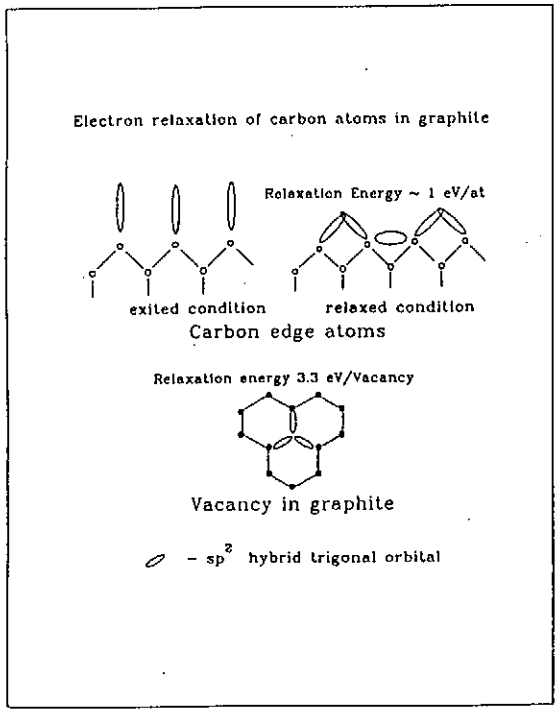

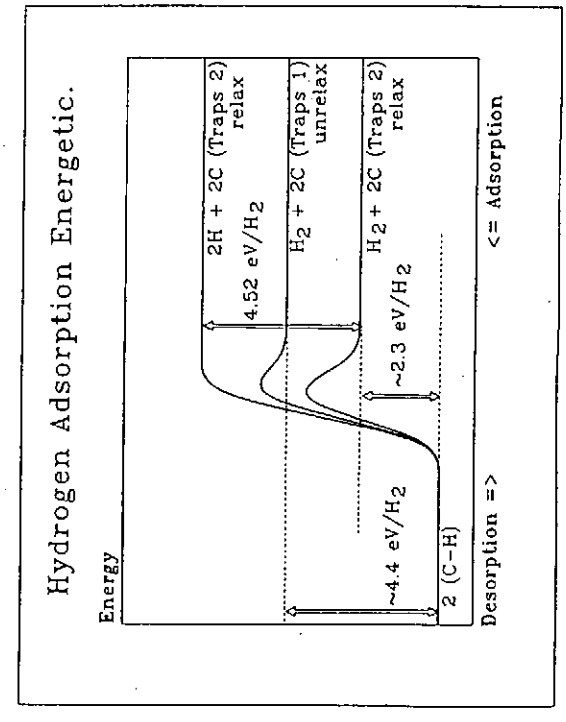

Adsorption Isotherms (Langmuir type isotherms)

$$\text{Inventory} = \frac{N_1\sqrt{k_1{}^A p}}{1+\sqrt{k_1{}^A p}} + \frac{N_2\sqrt{k_2{}^A p}}{1+\sqrt{k_2{}^A p}}$$

where $k^A = k^A_0 \cdot \exp(-\Delta H/RT)$, N_1 and N_2 -numbers of Traps 1 and Traps 2

Adsorption Enthalpy ΔH

$-\Delta H$=Heat of adsorption/H_2 = 2*$E_{C\text{-}H}$ - $E_{diss}(H2)$-E_{Relax}

(2.1 - 2.5) eV/H_2 (Experiment) = 2*4.45eV - 4.5eV - E_{Relax}

Traps 2 ΔH= - 2.3 eV/H_2

E_{Relax} ~1 eV/at.C for carbon edge atom of graphite network.

Traps 1 ΔH= - 4.4 eV/H_2

E_{Relax} = 0 In a case of interstitial loop.

Entropy factor k^A_0

We assume that the main variation of entropy is caused by escaping of translation and rotation parts of gaseous hydrogen entropy and appearing of adsorbed hydrogen oscillation entropy.

$$k^A_0 = \exp(-7/2)\cdot\left(\frac{2\pi mkT}{h^2}\right)^{-3/2}\cdot(kT)^{-1}\cdot(\theta_{rot}/T)^{*}$$

$$\exp\left(2\frac{h\nu}{kT}\frac{\exp(-\frac{h\nu}{kT})}{1-\exp(-\frac{h\nu}{kT})}\right)/\left(1-\exp(-\frac{h\nu}{kT})\right)^2$$

Isotope Exchange.

In a case of gas mixture (H_2 : 2 HD : D_2) sorption on graphite

$$\left(\frac{2P_{H_2}}{P_{HD}}\right)/(\theta_H/\theta_D) = \sqrt{\frac{k^0_H}{k^0_D}}$$, while $k^H > k^D > k^T$ = 5.65 : 1.96 : 1

ratio is weakly dependent upon temperature.

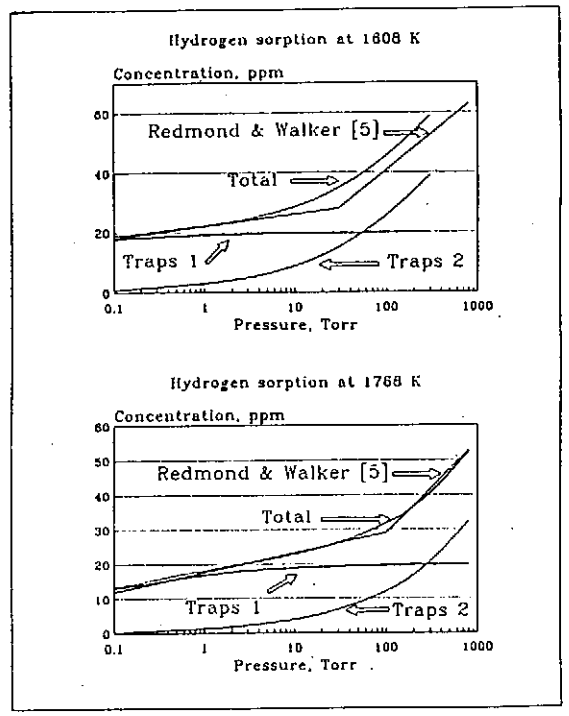

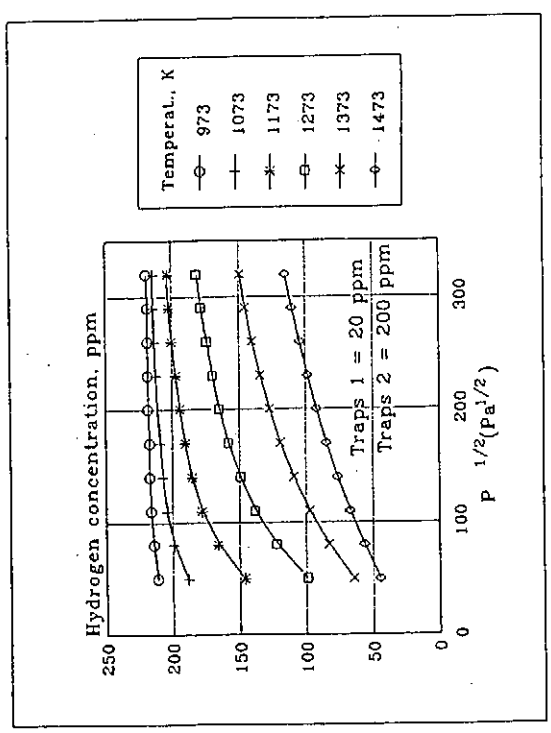

Irradiated graphites.

a) Damage was produced at room temperatures by ion irradiation of POCO AXF-5Q with 200 keV C^+ ions up to a damage dose of ~10 displacements per atom (dpa).

b) Following irradiation, the sample was soaked in deuterium gas at a temperature of 1473 K under pressure of 0.66 Pa for 1 hour. The concentration of D in the damaged region (0.5 mkm) was found as ~1400 appm.

c) Further this sample was soaked in deuterium gas at temperature of 1173 K under pressure of 133 Pa for 1 hour. The D concentration was found as ~2400 appm. It means that the number of Traps 2 filled with deuterium was ~1000 appm. The deuterium fraction coverage for the adsorption in graphite with enthalpy of 2.3 eV/H_2 is about 20%. The total number of Traps 2 should be estimated as ~5000 appm.

d) At last the sample was soaked in deuterium gas again at a temperature of 1473 K under pressure of 133 Pa for 24 hours. The D concentration was decreased and found as ~1500 appm.

Conclusion

1.The Langmuir type adsorption is proposed for the hydrogen isotopes - graphites interaction. Two kinds of traps are proposed:

Traps 1-carbon interstitial loops with the adsorption enthalpy of -4.4 eV/H_2 between the graphite planes;

Traps 2-carbon network edge atoms with the adsorption enthalpy of -2.3 eV/H_2;

Each type of graphite could be described with its own unique set of traps. For instance POCO AXF-5Q has the numbers of Traps 1 and Traps 2 of 20 and 200 appm respectively. The irradiation with neutrons or carbon atoms increases the Traps 1 and Traps 2 numbers. At damage level of ~1dpa under room temperature irradiation the numbers of Traps 1 and Traps 2 increased up to 1500 and 5000 appm respectively. Our adsorption experiments show that Traps 1 and Traps 2 are stable under high temperature annealing (1500K).

3. The proposed isotherms allow to describe the majority of experimental data on high temperature hydrogen inventory in initial and damaged graphites in a wide range of pressures.

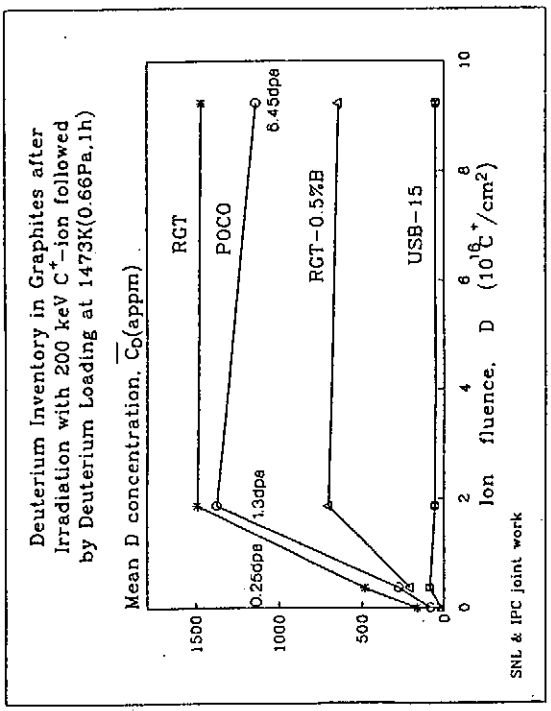

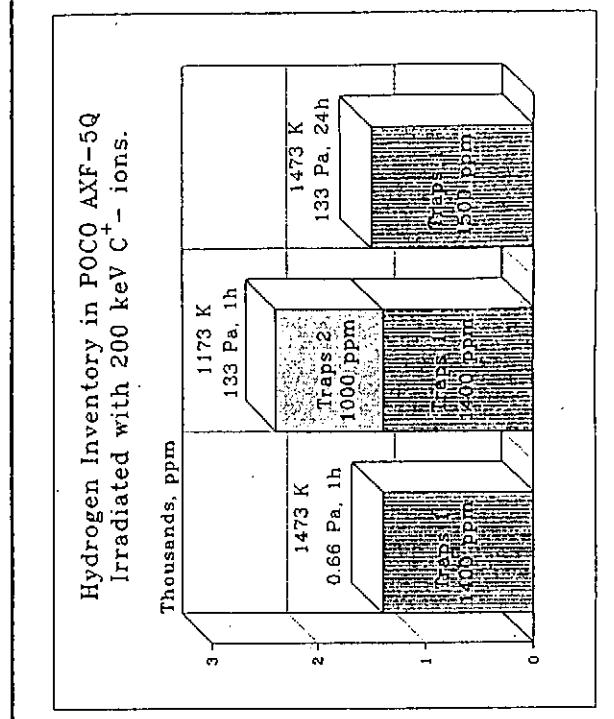

References

1. R.A.Causey Journ. Nucl. Mat. 162-164 (1989) 151
2. E.Hoinkis, Journ. Nucl. Mat. 182 (1991) 93; & 183 (1991) 9
3. H.Atsumi et al., JNM 155-157 (1988) 241
4. H.Atsumi, M.Iseki and T.Shikama, in: Proceedings of CIS-Japan Workshop on Interaction of Fuel Particles with Fusion Materials, Moscow, Oct. 1993 and ICFRM-6
5. J.P.Redmond and P.L.Walker , Jr., J.Phys.Chem., (1960) 1093

ON THE CHEMICAL FORM OF VOLATILE SPECIES RELEASED FROM CARBON-BASED MATERIALS

K. Yamaguchi, T. Nakaguma, S. Tanaka and M. Yamawaki

Nuclear Engineering Research Laboratory, University of Tokyo
Tokai-mura, Ibaraki-ken 319-11, Japan

One of the challenging problems in the field of plasma material interactions (PMI) involving graphite and its related materials is to clarify the factors which determine the chemical forms of hydrocarbon, C_xH_y, or carbon oxides, CO or CO_2, due to chemical sputtering or post-irradiation thermal release. In the present study, a thermochemical approach was employed to examine the extent to which the experimental results of chemical sputtering or thermal desorption may be explained from a point of view of thermochemistry.

To show an example of calculation, steady state chemical sputtering is assumed to be caused by continuous exposure to H(g) whose mass balance equation is expressed by

$$Z_H = 4R_{CH_4} + 4R_{C_2H_4} + 6R_{C_2H_6} + 6R_{C_3H_6} + 8R_{C_3H_8} + 2R_{H_2} + R_H \ , \qquad (1)$$

where Z_H is the impinging rate of H atoms, and R_i is the release rate of chemical species i. If one uses equilibrium constants for formation reaction which can be obtained form a thermochemical database, and assumes that solid-gas equilibrium is established, the R_i of species i can be calculated from its equilibrium partial pressure, P_i.

A quasi-equilibrium approach such as demonstrated in the present study enables to simplify complicated calculation as is often encountered in dealing with kinetic models. Although the validity of assumptions employed in the calculation is widely open to questions, as far as the experimental facts indicate the present approach may not be valid, so that the hydrocarbon formation is unlikely to be taking place in the gas phase.

Needless to say that both chemical sputtering and thermal desorption are kinetic processes, by no means in true equilibrium, where it is the activation energy instead of the free energy that controls the overall reaction rate. Furthermore, because of the simplicity, the present approach fails to explain some other important experimental observations; enhanced formation of heavier hydrocarbons at low incident energies, dependence of chemical forms on the ratio of incident H^+ to H fluxes, effect of initial graphite structure, etc.

ON THE CHEMICAL FORMS OF VOLATILE SPECIES RELEASED FROM CARBON-BASED MATERIALS

K. YAMAGUCHI, T. NAKAGUMA, S. TANAKA and M. YAMAWAKI

Nuclear Engineering Research Laboratory
University of Tokyo

presented at

2nd International Workshop
on
Tritium Effects in Plasma
Facing Components

May 19-20, 1994
Nagoya, Japan

CONTENTS

1. INTRODUCTION

1. Main Challenges in Plasma Material Interactions (PMI) Concerning Graphite
   - Hydrogen transport kinetics (discussed in the previous Workshop)
   - Clarification of the factors that determine the chemical form of hydrocarbons due to chemical sputtering and thermal desorption
2. Hydrocarbon Formation in Graphite
   - Experimentally, cracking of hydrocarbons occurs in a Quadrupole Mass Spectrometer.
   - Calculation is often complicated by the fact that there are various chemical reactions to be considered.
     $\Rightarrow$ is thermochemical database applicable ?
3. Scope of the Present Study
   - To apply a quasi-equilibrium calculation to study thermochemical aspects of hydrogen-graphite system.
   - To clarify the validity and limitation of such approach

2. THERMOCHEMICAL DATA AND CALCULATION OF RELEASE RATE OF C_xH_y

1. Basic Reactions ;

$$C(s) + 4H(g) = CH_4(g) , \quad (1)$$
$$2C(s) + 4H(g) = C_2H_4(g) , \quad (2)$$
$$2C(s) + 6H(g) = C_2H_6(g) , \quad (3)$$
$$3C(s) + 6H(g) = C_3H_6(g) , \quad (4)$$
$$3C(s) + 8H(g) = C_3H_8(g) , \quad (5)$$

2. Equilibrium Constants ;

$$K_{CH_4} = P_{CH_4}/P_H^4 , \quad (6)$$
$$K_{C_2H_4} = P_{C_2H_4}/P_H^4 , \quad (7)$$
$$K_{C_2H_6} = P_{C_2H_6}/P_H^6 , \quad (8)$$
$$K_{C_3H_6} = P_{C_3H_6}/P_H^6 , \quad (9)$$
$$K_{C_3H_8} = P_{C_3H_8}/P_H^8 , \quad (10)$$

3. Relation of Release Rate, R_i, and Equilibrium Pressure, P_i (In Molecular Flow Regime) ;

$$R_i = \frac{P_i}{\sqrt{2\pi M_i RT}} , \quad (11)$$

M_i; Molecular Weight of the Gas
R ; Gas Constant
T ; Temperature.

GIBBS ENERGY OF FORMATION
FOR C_xH_y
on the Basis of 1 mol H(g)

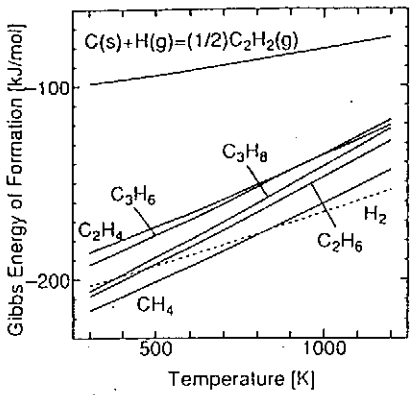

3. SIMULATION OF CHEMICAL SPUTTERING

1. Chemical sputtering may be simulated as being caused by continuous exposure to H(g).

2. In addition to eqs. (6) to (10), a mass balance of H atoms is required :

$$Z_H = 4R_{CH_4} + 4R_{C_2H_4} + 6R_{C_2H_6} + 6R_{C_3H_6} + 8R_{C_3H_8} + 2R_{H_2} + R_H , \quad (12)$$

Z_H ; impinging rate of H atoms.

3. Equilibrium of H(g) and H_2(g) is also required ;

$$P_{H_2} = K_{H_2} P_H^2 \ (2H(g) = H_2(g)) , \quad (13)$$

4. If $R_{H_2}, R_{CH_4} \gg R_{C_2H_x}, R_{C_3H_x}$,

$$P_H^1 + \frac{K_{H_2}}{2K_{CH_4}}\sqrt{\frac{M_{CH_4}}{M_{H_2}}}P_H^2 - \frac{\sqrt{2\pi M_{CH_4}RT}}{4K_{CH_4}}Z_H = 0 . \quad (14)$$

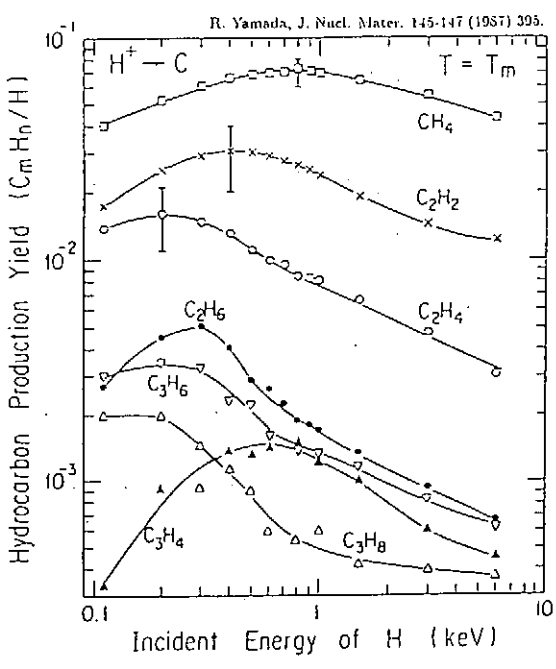

Fig. 5. Energy dependences of estimated C_2 and C_3 hydrocarbon production yields at the temperature of T_m. In order to obtain the chemical sputtering yields, the hydrocarbon production yields should be multiplied by the number of carbon atoms of the hydrocarbons. See text.

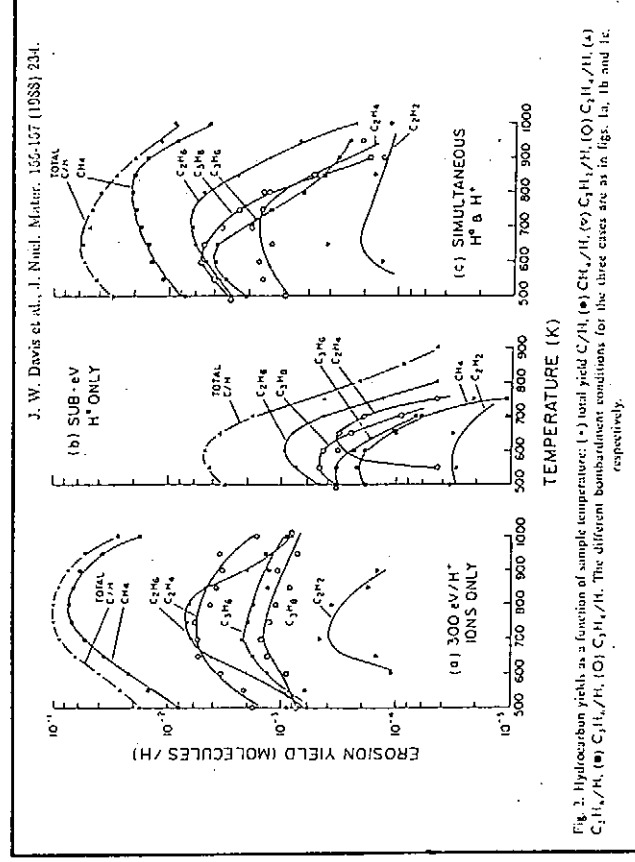

Fig. 2. Hydrocarbon yields as a function of sample temperature: (•) total yield C/H, (■) CH_4/H, (▽) C_2H_x/H, (○) C_3H_x/H, (▲) C_2H_x/H, (■) C_3H_x/H, (○) C_4H_x/H. The different bombardment conditions for the three cases are as in figs. 1a, 1b and 1c, respectively.

CALCULATION OF R_i OF C_xH_y AND H_2
($Z_H = 1.0\times10^{19}$ H m^{-2} s^{-1})

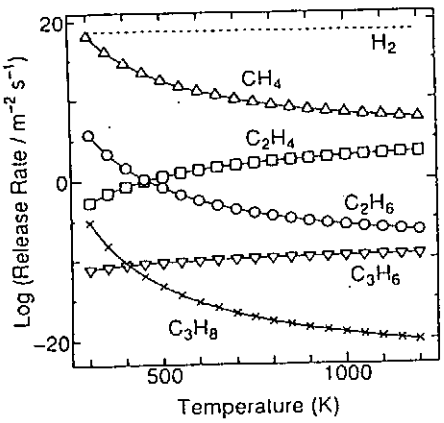

4. APPLICATION TO THERMAL DESORPTION

1. Summary of the Experimental Observation
   - $R_{CH_4} > R_{C_2H_6} > R_{C_2H_4} > R_{C_3H_6} > R_{C_3H_8}$
   - R_{CH_4} is more than an order of magnitude smaller than R_{H_2}.
   - R_i of C_3 hydrocarbons are about an order of magnitude smaller than that of C_2 hydrocarbons.
   - Results were essentially the same at different heating conditions.
   - The position of the desorption peak appeared at the same temperature, regardless of the chemical forms → same rate-determining step ?
2. Relation to Thermochemical Data
   - Gibbs energy of formation; $CH_4 < C_2H_6 < \cdots$
   - Gibbs energy of C_2H_2 is very large ⇔ No thermal desorption of C_2H_2 is observed.

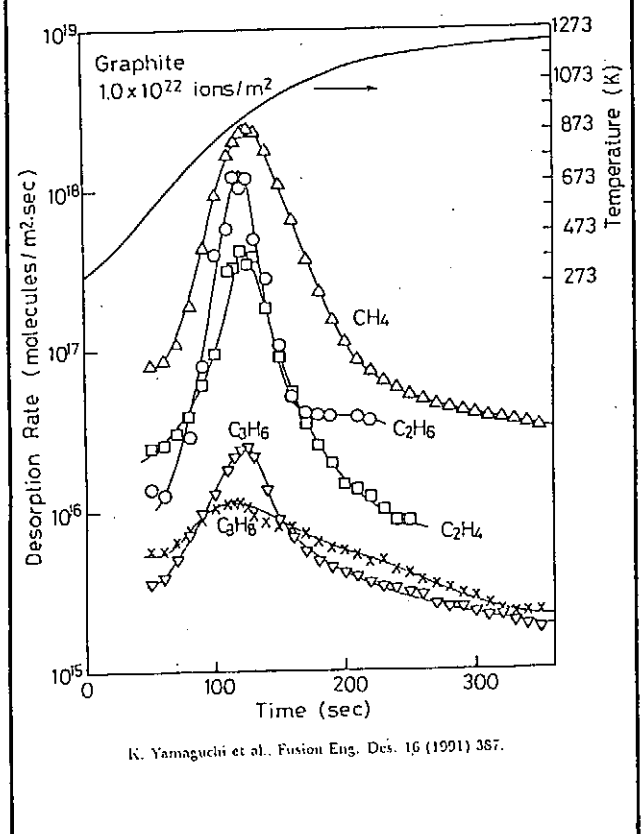

K. Yamaguchi et al., Fusion Eng. Des. 16 (1991) 387.

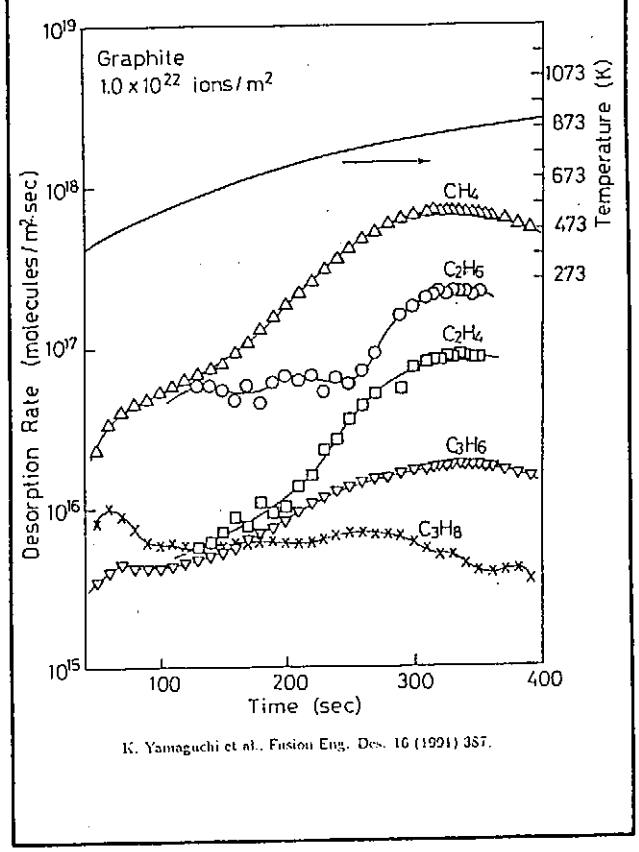

K. Yamaguchi et al., Fusion Eng. Des. 16 (1991) 387.

CALCULATION OF THERMAL DESORPTION RATE OF C_xH_y;

Basic Assumption :

- Reactions are so rapid that equilibrium is readily achieved at each temperature.
- Desorption rates are calculated relative to CH_4, where R_{CH_4} is taken from the experiment.

1. No precursor is assumed.
   - Same reaction equations used in the chemical sputtering simulation can be employed.
2. Precursor is assumed.
   - Hydrocarbons are assumed to be formed spontaneously upon forming the precursor
   - "Initial" state is the precursor state, C-H_3.
   - The precursor should be released from graphite and spontaneously become CH_3(g) in the gas phase (vacuum).

- Chemical reactions are expressed as follows;

$$CH_3(g) + H(g) = CH_4(g)\ , \quad (15)$$
$$2\,CH_3(g) = C_2H_4(g) + 2\,H(g)\ , \quad (16)$$
$$2\,CH_3(g) = C_2H_6(g)\ , \quad (17)$$
$$3\,CH_3(g) = C_3H_6(g) + 3\,H(g)\ , \quad (18)$$
$$3\,CH_3(g) = C_3H_8(g) + H(g)\ , \quad (19)$$

with the new equilibrium constants being:

$$K^*_{CH_4} = \frac{P_{CH_4}}{P_H P_{CH_3}}\ , \quad (20)$$
$$K^*_{C_2H_4} = \frac{P_{C_2H_4} P_H^2}{P_{CH_3}^2}\ , \quad (21)$$
$$K^*_{C_2H_6} = \frac{P_{C_2H_6}}{P_{CH_3}^2}\ , \quad (22)$$
$$K^*_{C_3H_6} = \frac{P_{C_3H_6} P_H^3}{P_{CH_3}^3}\ , \quad (23)$$
$$K^*_{C_3H_8} = \frac{P_{C_3H_8} P_H}{P_{CH_3}^3}\ , \quad (24)$$

respectively.

- Two unknown parameters; P_H are P_{CH_3}. $z = P_{CH_3}/P_H$ is taken as adjustable parameter (a) $z = 1$, (b) $z = 0.01$

RESULT OF CALCULATION
(1) No precursors are assumed

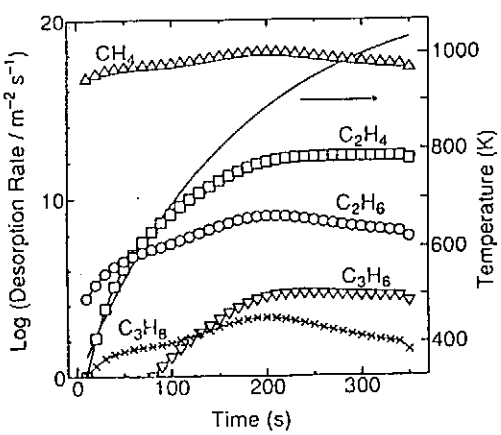

RESULT OF CALCULATION
(2a) Precursor, C-H_3, is assumed ; $z = 1$

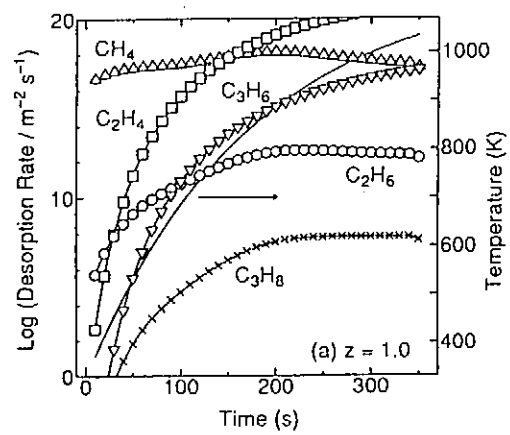

RESULT OF CALCULATION

(2b) Precursor, C-H_3, is assumed ; $z = 0.01$

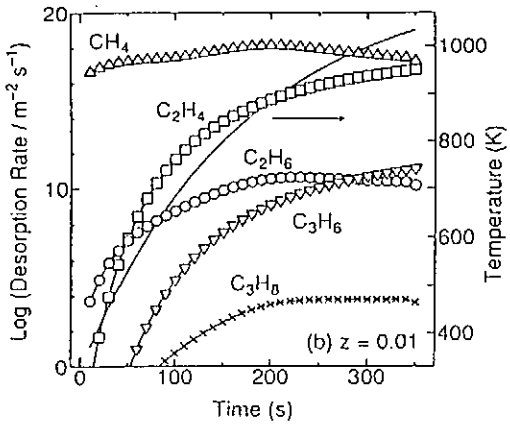

5. DISCUSSION

1. Calculation revealed that the ratios of R_i/R_{H_2} ($i = C_xH_y$) and R_j/R_{CH_4} ($j = C_xH_y$, $x \geq 2$) were considerably underestimated when they were compared with the experimental data.
2. In the case of chemical sputtering, the presence of precursor is required which is thermochemically stable at low temperatures.
3. In thermal desorption, R_i of heavier hydrocarbons increases with increasing $z = P_{CH_3}/P_H$.
4. In the calculation, $R_{C_2H_4} \geq R_{C_2H_6}$ is generally obtained. $\rightarrow R_{C_2H_6}/R_{C_2H_4}$ is determined by P_H.
   $P_{C_2H_6} \geq P_{C_2H_4} \Rightarrow P_H \geq \sqrt{K_{C_2H_4}/K_{C_2H_6}}$,
   $P_H \geq 1.7 \times 10^{-30} \sim 4.3 \times 10^{-4}$ Pa.
5. Under any condition, $R_{C_2H_6}$ was smaller than R_{CH_4} by many orders of magnitude.

In concluding, as far as the experimental facts indicate, the assumption of gas-solid equilibrium may not be valid.

6. SUMMARY

A quasi-equilibrium approach was applied to calculate chemical forms of hydrocarbon released from graphite.

1. Although the validity of assumptions employed in the calculation is widely open to questions, it enables to simplify complicated calculation.
2. Hydrocarbon formation is unlikely to be taking place in the gas phase.
3. It should be noted that chemical sputtering and thermal desorption are kinetic processes $\Rightarrow$ activation energy is important (not free energy).
4. Because of the simplicity the present calculation is not sufficient to explain some of the important experimental observations.
   (a) enhanced formation of heavier hydrocarbons at low incident energies (chemical sputtering),
   (b) dependence of chemical forms on the ratio of H^+ to H fluxes (chemical sputtering),
   (c) the effect of initial graphite structure.

Effects of Deuterium Ion Irradiation on Gas Emission and Sublimation of Graphite by Pulse High Heat Load

K. Tokunaga, Y, Yagi*, S.Fukuda, T. Muroga and N. Yoshida

Research Institute for Applied Mechanics,
Kyushu University, Kasuga, Fukuoka 816, Japan
*Interdisciplinary Graduate School Of Engineering Science,
Kyushu University, Kasuga, Fukuoka 816, Japan

Release of gases and particles of deuterium irradiated graphite by high heat load using a pulse laser beam has been investigated. Especially, gas and particle analyses using a high speed response quadupole mass spectrometer(QMS) made it possible to examine dynamic process of the release by pulse high heat load.

Isotropic graphite was irradiated with 4 keV deuterium ion to 3×10^{21} ions/m^2 at room temperature in a high vacuum chamber. Afterward, heat load experiment was carried out using a ruby laser with a pulse length of about 1.5 msec and a wavelength of 694.3 nm. Heat load power was 29 MW/m^2 to 830 MW/m^2. Gas/particle analyses and measurement of vacuum pressure were carried out with a QMS and a ionization vacuum gauge, respectively. Surface temperature was measured with a quick-response thermospot sensor. Surface morphology change was observed by a scanning electron microscope(SEM).

Maximum peak surface temperature during laser irradiation linearly increased with increasing heat load. The temperature of deuterium irradiated specimen was higher a few hundreds degree than that of un-irradiated specimen. This is expected to be caused by decrease of thermal conductivity due to change of structure of near surface of specimen by the deuterium ion irradiation.

Degradation of vacuum degree in the case of ion irradiated specimen during laser shot was larger than that of un-irradiated one. Particularly, the difference between the irradiated and un-irradiated specimen was large at low heat power, which influences surface layer mainly. This indicates that a large amount of gas release from deuterium ion irradiated layer of specimen.

The measurement using the QMS showed that many kind of gases and particles were emitted by pulse high heat load. The intensity of signal of C_1 and C_2 did not changed, but the that of C_2 decreased from the ion irradiated specimen in comparison with that of un-irradiated one at 830 MW/m^2. These results suggest that formation of C_2D_n increased in the case of deuterium ion irradiated specimen.

The present results show that hydrogen isotope irradiation from plasma enhanced materials degradation near surface and gases and particle emission for pulse high heat load(e.g. plasma disruption).

Effects of Deuterium Ion Irradiation on Gas Emission and Sublimation of Graphite by Pulse High Heat Load

K.Tokunaga, H. Yagi*, S. Fukuda, T. Muroga and N. Yoshida

Research Institute for Applied mechanics,
*Interdisciplinary Graduate School of Engineering Sciences,
Kyushu University,

2nd International Workshop
on Tritium Effects in Plasma Facing Components
19–20 May 1994, Nagoya University, Japan

Introduction

(a)Plasma-facing components
High heat load(e.g. plasma disruptions) : erosion, materials damage
Hydrogen isotope(<10 keV) : hydrogen retention, structural change

Synergistic effects of heat load and hydrogen influx

(b)Gas/particle emission experiment
Thermal desorption spectroscope
Sublimation measurement
(ramp heating or at constant elevated temperature)

Heat flux testing
Structure observation
Erosion measurement

(c)Present experiment
Gas/particle emission measurement during pulse high heat load with QMS etc.

Low energy deuterium irradiated graphite

Objectives

(1)To investigate dynamical information of gas and particle emission and surface morphological changes

(2)To investigate effects of deuterium ion irradiation on its properties

for an isotropic graphite by pulse high heat load.

Experimental

(1)Materials : Isotropic graphite IG-110U (Toyo Tanso Co. ltd)
(15 mm x 15 mm X 1mm)
(2)The condition of deuterium irradiation
Energy of deuterium ion (D^+) : 4 keV
Fluence : 3×10^{21} ions/m^2
Irradiation temperature : Room temperature
(3)The condition of pulse heat load
Pulse ruby laser beams
Heat flux : 29, 91, 164, 300, 500, 830 MW/m^2
Duration : 1 msec
Diameter : 3mmϕ
Specimen temperature before irradiation : room temperature
(4)Measurements : D_2, vacum pressure, surface temperature.

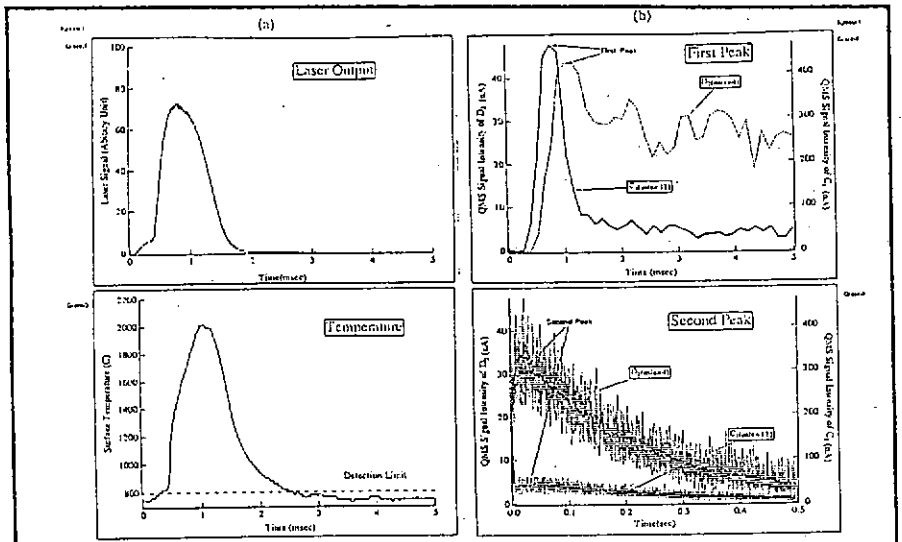

Typical examples of time evolution of (a)signal of laser output and temperature (b) QMS signal for C_1 (m/e=12) and D_2 (m/e=4).

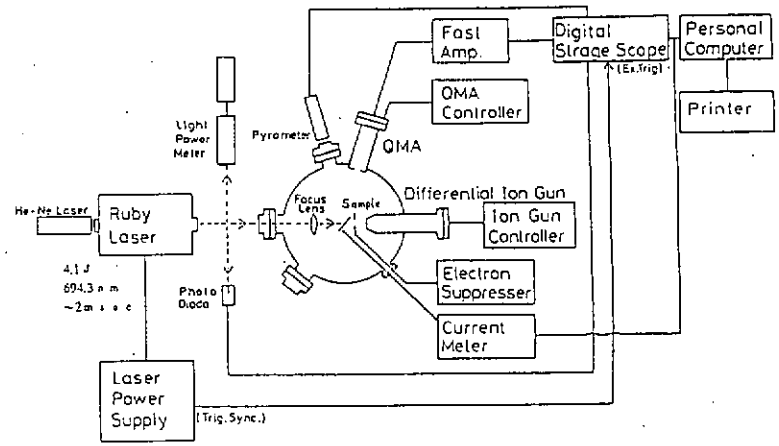

Schematic diagram of experimental device

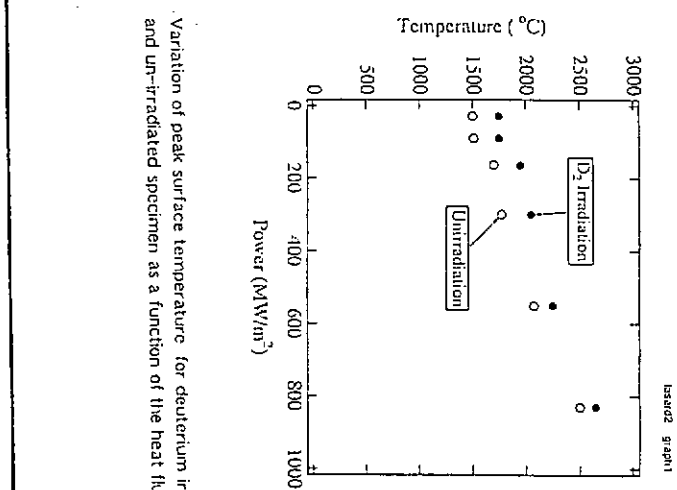

Variation of peak surface temperature for deuterium irradiated and un-irradiated specimen as a function of the heat flux.

SEM micrographs of isotropic graphite IG-110U

(a)Un-irradiated specimen (b)Deuterium irradiated specimen

(c)Laser irradiated(830MW/m^2) specimen (d)Laser irradiated(830 MW/m^2) specimen after deuterium irradiation

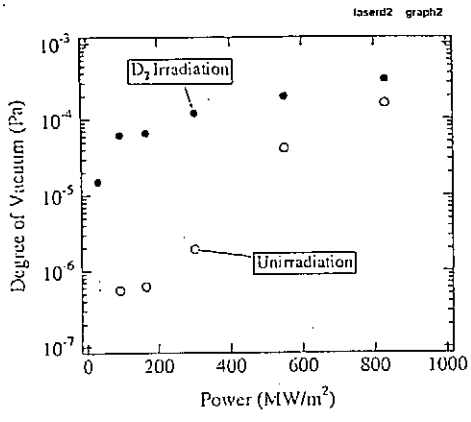

Variation of peak vacuum degradation of vacuum chamber for deuterium irradiated and un-irradiated specimen as a function of the heat flux.

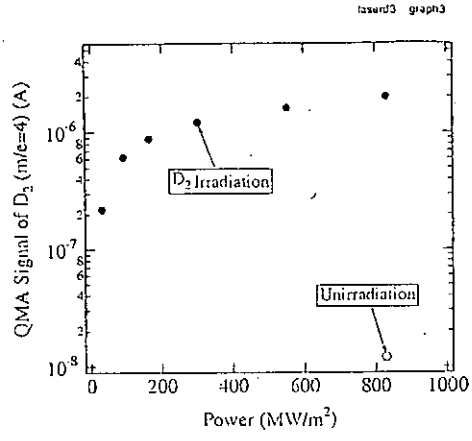

Variation of QMS peak signal of D_2(m/e=4) for deuterium irradiated and un-irradiated specimen as a function of the heat flux.

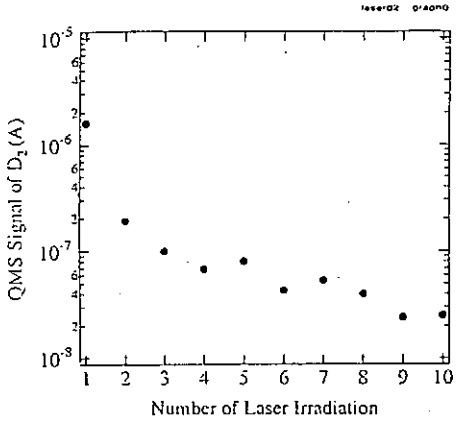

QMS peak signal intensity of D_2(m/e=4) for the same positions of deuterium irradiated specimen as a function of the number of laser irradiation. Heat load is 550 MW/m^2.

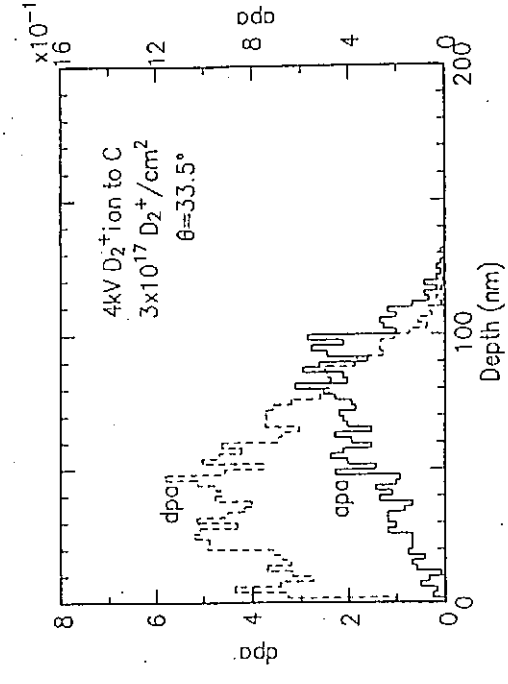

Displacement per atom (DPA) and deuterium atoms per atom (APA) for the present experiment condition.

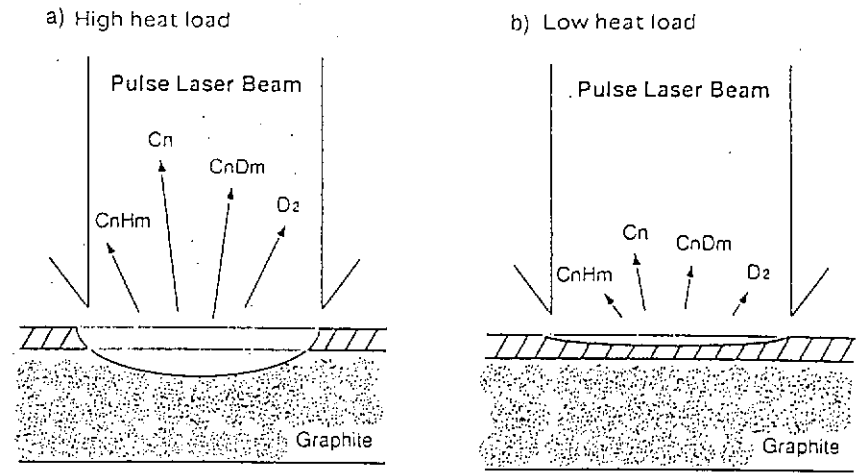

Schematic illustrations of erosion process by pulse heat load in the present experiment.

Summery

Pre-deuterium ion irradiated graphite was irradiated by pulse laser beams to examine influence of synergistic effects of hydrogen isotope irradiation and pulse high heat load on gases emission and materials damage of graphite materials.

(1)Surface temperature rise during laser beams irradiation increased due to decrease of thermal conductivity by amorphization which was caused by deuterium irradiation.

(2)By heat load at a few 10 MW/m^2 for 1ms, surface temperature reached at 1700 ℃～1800℃ and a part of deuterium trapped in the surface amorphous layer was released as deuterium gases.

(3)By heat load at 500～600 MW/m^2, surface temperature increased 2200℃. Emission by sublimation also increased. Deuterium and other gases were released.

(4)Production of graphite particles increased with increasing heat load (more than 600 MW/m^2) and most of deuterium implanted zone eroded.

Appendix A : Workshop Agenda

2nd International Workshop on Tritium Effects in Plasma Facing Components May 19-20 1994, Nagoya University, Japan

Workshop Agenda

Thursday May 19

8:30-9:00 Registration

9:00-9:10 Opening Prof. M. Hasatani
Prof. A. Iiyoshi

Session 1 (Chairman: Dr. Noda)

9:10-9:35 • Results of TFTR D-T Experiments
by D. Mueller, and TFTR Group

9:35-10:00 • Status of the Tritium Plasma Experiment
by R. Causey

10:00-10:25 • Fusion Research Programs of Russia - Its Principles and Future
by A. Sherbak

Coffee Break(20min)

10:45-11:10 • Transport of Hydrocarbon in the Laboratory Plasma MAP
by S. Tanaka, M. Matsuyama and M. Yamawaki

11:10-11:35 • Design of Carbon Sheet Pump for LHD and Demonstration of Hydrogen Pumping
by A. Sagara, H. Suzuki, N. Ohyabu and O. Motojima

Lunch

Session 2 (Chairman: Dr. E. Vietzke)

13:00-13:25 • Applications of Superpermeable Membranes in Fusion: Physico-Chemical Aspects of Reliability
by A. I. Livshits, M. E. Notkin, A. O. Busnyuk and V. I. Pistunovich

13:25-13:50 • Validation of Niobium as Superpermeable Membrane
by V. Bandurko, M. Yamawaki and K. Yamaguchi

13:50-14:15 • Isotopic Effects on Hydrogen Trapping, Release and Permeation in Plasma Facing Materials
by E. Abramov

14:15-14:40 • Tritium Migration in Group-V Metals under Thermal and Electric Potential Gradients
by M. Sugisaki and K. Hashizume

Coffee Break(20min)

15:00-15:25 • Interaction of Atomic Hydrogen with Metals
by T. Tanabe and T. Kiriyama

15:25-15:50 • Desorption of Hydrogen Isotopes from the Reactor First Wall
by V. I. Pistunovich

15:50-16:15 • Surface Effects on the Din 1.4914 Stainles Steel (MANET)
by A. Perujo, S. Alberici and E. Serra

16:15-16:40 • Measurements of D Concentration Profile in Metal Films during D Implantation
by S. Yamaguchi, S. Nagata, K. Takahiro and S. Yamamoto

16:40-17:05 • Deuterium Capture and Release during Low-Energy Ion Implantation in Beryllium
by V. A. Kurnaev, D. P. Luvchuk, A. A. Pisarev and O. V. Zabeida

17:05-17:30 • Hydrogen Permeation in Be
by T. Tanabe and K. Kizu

17:30-17:55 • Secondary Ion Emission from Beryllium Surface
• by K. Ashida, H. Kawamura and K. Watanabe

--- --- --- --- --- --- --- --- ---

18:00-20:00 Reception (Restaurant in Symposion Hall)

Friday May 20

Session 3 (Chairman: Prof. A. I. Livshits)

9:00-9:25 • A Critical Review of the Data Available for Tritium in Beryllium
by A. A. Pisarev

9:25-9:50 • Hydrogen Isotope Exchange in Boronization
by M. Yamage, T. Saito, H. Toyoda, M. Saidoh, N. Ogiwara and H. Sugai

9:50-10:15 • Effects of Alpha-Boron/C:H-film Porosity on the Diffusion and Erosion under Deuterium Plasma Irradiation
by V. Sharapov

Coffee Break(20min)

10:35-11:00 • Reflection of Low Energy Hydrogen from Carbon
by M. Mayer, W. Eckstein and B M. U. Scherzer

11:00-11:25 • Atomic Reemission of H from Pure and Boronized Graphites and Code Calculations for the Consequences in Tokamaks
by E. Vietzke, P. Franzen, D. Reiters *et al.*

11:25-11:50 • Deuterium Interaction with Carbon Fibre Composites Doped with SiC
by M. Rubel, B. Emmoth, H. Bergsaker and C. H. Wu

Lunch

Session 4 (Chairman: Dr. R. Causey)

13:00-13:25 • Hydrogen Retention in B4C Overlaid graphite
by T. Hino, Y. Yamauchi, Y. Hirohata and T. Yamashina

13:25-13:50 • Hydrogen Transport/ Retention/ Reemission in Graphite
by A. A. Haasz, J. W. Davis and S. Chiu

13:50-14:15 • Termal Re-emission of Hydrogen Isotopes from Graphite in the High Temperature Regime above 1000K

by B. Tsuchiya and K. Morita

14:15-14:40 • Hydrogen Trapping in Graphite at High Temperatures
by T. Tanabe, H. Atsumi, N. Kangai and K. Niwase

Coffee Break(20min)

15:00-15:25 • Study for Estimation of Tritium Inventory in Plasma Facing Materials
by S. Ohira, K. Ashibe and K. Okuno

15:25-15:50 • Hydrogen Adsorption on and Solubility in Graphite
by A. E. Gorodetsky, S. L. Kanashenko, V. N. Chernikov, A. V. Markin, B. L. Doyle, and W. R. Wampler (A. Zakharov)

15:50-16:15 • On the Chemical Form of Volatile Species released from Carbon-based Materials
by K. Yamaguchi, T. Nakaguma, S. Tanaka and M, Yamawaki

16:15-16:40 • Effects of Deuterium Ion Irradiation on Gas Emission and Sublimation of Graphite by Pulse High Heat Load
by K. Tokunaga, H. Yagi, S. Fukuda, T. Muroga and N. Yoshida

16:40 Closing Prof. M. Yamawaki

Appendix B : Participants List

* 2nd International Workshop Participants List

Abramov, Elhanan	Ben-Gurion University of the Negev	ISRAEL
Akaishi,Kenya	NIFS	JAPAN
Ashida, Kan	Toyama University	JAPAN
Bandurko, Vassili	University of Tokyo	JAPAN
Causey, Rion	Sandia National Laboratory	USA
Eckstein, Wolfgang	Max Planck Institut fuer Plasmaphysik	FRG
Emmoth, Birger	Frescati Royal Institute of Technology	SWEDEN
Esser, Hans Guntev	KFA Jülich	FRG
Haasz, Anthony A	University of Toronto	CANADA
Hino, Tomoaki	Hokkaido University	JAPAN
Kangai, Naoki	Osaka University	JAPAN
Kiriyama, Tadashi	Osaka University	JAPAN
Kizu, Kaname	Osaka University	JAPAN
Kurnaev, Valery	Moscow Engineering Physics Institute	RUSSIA
Livshits, Alexander	Bonch-Bruyevich University of Telecommunications	RUSSIA
Matsuyama, Seiji	University of Tokyo	JAPAN
Morita, Kenji	Nagoya University	JAPAN
Mueller, Dennis	Princeton Plasma Physics Laboratory	USA
Noda, Nobuaki	NIFS	JAPAN
Ohira,Shigeru	Japan Atomic Energy Research Institute	JAPAN
Pathak, H. A.	Institute for Plasma Research	INDIA
Perujo, Adolfo	Joint Research Centre	ITALY
Philipps, Volker	KFA Jülich	FRG
Pisarev, Alexander	Moscow Engineering Physics Institute	RUSSIA

Pistunovich, Vladimir	Russian Research Centre"Kurchatov Institute"	RUSSIA
Rubel, Marek	Frescati Royal Institute Of Technology	SWEDEN
Sagara, Akio	NIFS	JAPAN
Sharapov, Valery	Institute of Physical Chemistry of the Russian Academy of Sciences	RUSSIA
Sherbak, Anatoly	Ministry of Science and Technical Policy of Russian Federation	RUSSIA
Sugai, Hideo	Nagoya University	JAPAN
Sugisaki, Masayasu	Kyushu University	JAPAN
Suzuki, Hajime	NIFS	JAPAN
Tanabe, Teturou	Osaka University	JAPAN
Tanaka, Satoru	University of Tokyo	JAPAN
Tanaka, Shigeru	ITER Garching Co-center	JAPAN
Tokunaga, Kazutoshi	Kyushu University	JAPAN
Toyoda, Hirotaka	Nagoya University	JAPAN
Tsuchiya, Bun	Nagoya University	JAPAN
Tsuzuki, Kazuhiro	The Graduate University for Advanced Studies	JAPAN
Vietzke, Egon	KFA Jülich	FRG
Winter, J	KFA Jülich	FRG
Yamage, Masashi	Nagoya University	JAPAN
Yamaguchi, Kenji	University of Tokyo	JAPAN
Yamaguchi, Sadae	Tohoku University	JAPAN
Yamawaki, Michio	University of Tokyo	JAPAN
Zakharov, Andrei	Institute of Physical Chemistry of the Russian Academy of Sciences	RUSSIA

Publication List of NIFS-PROC Series

NIFS-PROC-1 *U.S.-Japan on Comparison of Theoretical and Experimental Transport in Toroidal Systems Oct. 23-27, 1989* Mar. 1990

NIFS-PROC-2 *Structures in Confined Plasmas –Proceedings of Workshop of US-Japan Joint Institute for Fusion Theory Program–* ; Mar. 1990

NIFS-PROC-3 *Proceedings of the First International Toki Conference on Plasma Physics and Controlled Nuclear Fusion –Next Generation Experiments in Helical Systems– Dec. 4-7, 1989* Mar. 1990

NIFS-PROC-4 *Plasma Spectroscopy and Atomic Processes –Proceedings of the Workshop at Data & Planning Center in NIFS–*; Sep. 1990

NIFS-PROC-5 *Symposium on Development of Intensed Pulsed Particle Beams and Its Applications February 20 1990*; Oct. 1990

NIFS-PROC-6 *Proceedings of the Second International TOKI Conference on Plasma Physics and Controlled Nuclear Fusion , Nonlinear Phenomena in Fusion Plasmas -Theory and Computer Simulation-;* Apr. 1991

NIFS-PROC-7 *Proceedings of Workshop on Emissions from Heavy Current Carrying High Density Plasma and Diagnostics;* May 1991

NIFS-PROC-8 *Symposium on Development and Applications of Intense Pulsed Particle Beams, December 6 - 7, 1990*; June 1991

NIFS-PROC-9 *X-ray Radiation from Hot Dense Plasmas and Atomic Processes*; Oct. 1991

NIFS-PROC-10 *U.S.-Japan Workshop on "RF Heating and Current Drive in Confinement Systems Tokamaks" Nov. 18-21, 1991*, Jan. 1992

NIFS-PROC-11 *Plasma-Based and Novel Accelerators (Proceedings of Workshop on Plasma-Based and Novel Accelerators) Nagoya, Japan, Dec. 1991*; May 1992

NIFS-PROC-12 *Proceedings of Japan-U.S. Workshop P-196 on High Heat Flux Components and Plasma Surface Interactions for Next Devices*; Mar. 1993

NIFS-PROC-13 『NIFS シンポジウム
「核燃焼プラズマの研究を考える－現状と今後の取り組み方」
1992年 7月 15日、核融合科学研究所』
1993年 7月
NIFS Symposium
"Toward the Research of Fusion Burning Plasmas -Present status and Future strategy-", 1992 July 15, National Institute for Fusion Science; July 1993
(in Japanese)

NIFS-PROC-14 *Physics and Application of High Density Z-pinches,*
July 1993

NIFS-PROC-15 岡本正雄、講義「プラズマ物理の基礎」
平成5年度 総合大学院大学
1994年 2月
M. Okamoto,
"Lecture Note on the Bases of Plasma Pysics"
Graduate University for Advanced Studies
Feb. 1994
(in Japanese)

NIFS-PROC-16 代表者 河合良信
平成5年度 核融合科学研究所共同研究
研究会報告書
「プラズマ中のカオス現象」
"Interdisciplinary Graduate School of Engineering Sciences"
Report of the meeting on Chaotic Phenomena in Plasma
Apr. 1994
(in Japanese)

NIFS-PROC-17 平成5年度NIFSシンオジウム報告書
「核融合炉開発研究のアセスメント」
平成5年11月29日-30日 於 核融合科学研究所
"Assessment of Fusion Reactor Development"
Proceedings of NIFS Symposium held on November 29-30, 1993 at National Insitute for Fusion Science"
Apr. 1994
(in Japanese)

NIFS-PROC-18 *"Physics of High Energy Density Plasmas Produced by Pulsed Power"*
June 1994